Norovirus Translation and Replication

by

Jia Lu

Wolfson College, University of Cambridge

September 2017

This dissertation is submitted for the degree of
Doctor of Philosophy

Division of Virology, Department of Pathology,
University of Cambridge, Addenbrooke's Hospital
Hills Road, Cambridge

Abstract

Human norovirus (HuNoV) is the leading cause of gastroenteritis worldwide. Despite the significant disease and economic burden, currently there are no licensed vaccines or antivirals. The understanding of norovirus biology has been hampered by the inability to cultivate HuNoV in cell culture. To establish a tissue culture system, infectious HuNoVs were purified from clinical stool samples. HuNoV replication was tested in different cell types. The B-cell and intestinal organoids culture systems were validated. In addition, using organoids culture a DNA-based reverse genetic system was shown to recover infectious HuNoV.

Due to the challenges associated with cultivating HuNoV, murine norovirus (MNV) was used as a surrogate system to understand the role of eIF4E phosphorylation in norovirus pathogenesis, and VP1-RdRp interaction in regulating viral genome replication.

MNV infection results in the phosphorylation of the translation initiation factor eIF4E, re-programming host-cell translation during infection. Inhibiting eIF4E phosphorylation reduces MNV replication in cell culture suggesting a role in viral replication. A mouse model with eIF4E S209A, a phosphor-ablative mutation, was established to understand the role of eIF4E phosphorylation in MNV pathogenesis. *In vitro* and *in vivo* characterisations demonstrated that eIF4E phosphorylation may have multiple roles in norovirus-host interactions, but overall has little impact on MNV pathogenesis.

The shell domain (SD) of norovirus major capsid protein VP1 interacts with viral RNA-dependent RNA polymerase (RdRp) in a genogroup-specific manner to enhance *de novo* initiation of RdRp, and to promote negative-strand RNA synthesis. To understand how VP1 regulates norovirus genome replication, chimeric MNVs with genogroup-specific residues mutagenised were characterised *in vitro* and *in vivo*. A single amino acid mutation was shown to destabilise viral capsid. SDs with reduced VP1-RdRp interaction showed less capacity to stimulate RdRp, resulting in delayed virus replication. *In vivo*, the replication of an MNV-3 with homologous mutations was abolished, highlighting the crucial role of this interaction.

Declaration

- This dissertation is the result of my own work and includes nothing which is the outcome of work done in collaboration except as declared here and specified in the text:
  - Differentiation of $\gamma\ \delta$ T cells by Marta Barisa (University College London)
  - Infection and passage of RGS GII.4 HuNoV by Ian Goodfellow and Myra Hosmillo (University of Cambridge).
  - LUMIER by Alexis de Rougemont (University of Cambridge).
  - RNA synthesis assay by Xiaoyan Lin (Indiana University)
- It is not substantially the same as any that I have submitted, or, is being concurrently submitted for a degree or diploma or other qualification at the University of Cambridge or any other University or similar institution except as declared in the Preface and specified in the text. I further state that no substantial part of my dissertation has already been submitted, or, is being concurrently submitted for any such degree, diploma or other qualification at the University of Cambridge or any other University or similar institution except as declared in the Preface and specified in the text
- It does not exceed the prescribed word limit for the relevant Degree Committee.

Acknowledgements

First, I would like to thank my supervisor Ian Goodfellow for giving me this opportunity to work and undertake my PhD in his lab, for his excellent support, guidance whilst still challenging my work and knowledge to be better. I am very grateful for the opportunities he has given me to not only work by the bench, but also help put an end to a devastating outbreak, for which I have learnt a lot. I would also like to extend my gratitude to my daily supervisors, Lucy Thorne, Frédéric Sorgeloos and Luke Meredith, for their brilliant ideas, help with problem-solving and writing, and for the encouragement and support I have received. I have sincerely enjoyed the time with all the present and previous members of the lab and the Sweeney lab, for this big thanks to Lucy Thorne, Frédéric Sorgeloos, Luke Meredith, Yasmin Goodfellow, Trevor Sweeney, Edward Emmott, Surender Vashist, Armando Arias, Alexis de Rougemont, Myra Hosmillo, Liliane Chung, Tina Christodoulou, Sarah Caddy, Shuqi Xiao, Bader Alhatlani, Rintaro Hiraide, James Eaglesham, Xinjie Wang, Aminu Jahun, Anna Smielewska, Thomas Sanford, Harriet Mears, Deok-Song Kim, Tim Fitzmaurice, Anna Yakovleva, Jessica van Loben Sels, Sebastine Arthur, and Mitsutaka Kitano. The same goes to friends within the Division of Virology at University of Cambridge.

I would also like to thank BBSRC for funding, and Wolfson College for funding and support. In particular, I would like to thank my college tutor Lesley MacVinish and college mentor Claudio Köser, for their advice and support.

Most importantly I would like to thank my family and friends, in particular my parents and parents-in-law, my wife, my daughter, Shu Zhu, Yanhua Li and Chen Gao for their constant support and encouragement throughout my study.

Table of Contents

Table of Figures

Tables

Abbreviations

ANOVA	analysis of variation
BHK	baby hamster kidney cells
BMDM	bone marrow-derived macrophage
BSR-T7	BHK-21 cell clone BSR-T7/5
BVDV	bovine viral diarrhoea virus
DAPI	4’,6-diamidino-2-phenylindole
DNA	deoxyribonucleic acid
dpi	days post infection
dsRNA	double stranded RNA
eIF4E	eukaryotic translation initiation factor 4E
FCV	feline calicivirus
FPV	fowl pox virus
gEq	genome equivalent
GFP	green fluorescent protein
HBGA	histo-blood group antigens
HCV	hepatitis C virus
HIE	human intestinal enteroids
HIEC	human intestinal epithelial crypt cells
hpi	hours post-infection
HuNoV	human norovirus
IFN	interferon
IP	immunoprecipitation
IRES	internal ribosomal entry site
IRF	interferon response factor
ISG	interferon-stimulated gene
JAK	janus kinase
kb	kilo bases
kDa	kilo Dalton
KI	knock in
LOD	limit of detection
LUMIER	LUminescence-based Mammalian IntERactome
min	minutes

MNV	murine norovirus
MOI	multiplicity of infection
mRNA	messenger RNA
NS	non-structural
ns	non-significant
ORF	open reading frame
PCR	polymerase chain reaction
PEG	polyethylene Glycol
PIV5	parainfluenza virus 5
qPCR	quantitative/real-time PCR
Raw/Raw264.7	mouse leukaemia monocyte macrophage cell line
RC	replication complex
RdRp	RNA-dependent RNA polymerase
RGS	reverse genetics
RHDV	rabbit haemorrhagic disease virus
RIG-I	retinoic inducible gene 1
RNA	ribonucleic acid
RNase	ribonuclease
RT	reverse transcription
SD	shell domain
SDS	sodium dodecyl sulhate
SDS-PAGE	SDS polyacrylamide gel electropheresis
SG	subgenomic
STAT1	signal transducer activator of transcription 1
$TCID_{50}$	50% tissue culture infectious dose
UTR	untranslated region
VF1	virulence factor 1
VLP	virus-like particle
VP1	major capsid protein
VP2	minor capsid protein
VPg	viral protein genome linked
vRNA	viral RNA
WT	wild type

Chapter 1

Introduction

1.1 Classification of the family *Caliciviridae*

The family *Caliciviridae* is named after the latin *calyx* for cup, with reference to the common cup-like virion morphology observed by electron microscopy. Caliciviruses are a group of human and animal pathogens, which are small, non-enveloped, positive-sense, single-strand RNA viruses. Caliciviruses are known for causing gastroenteritis as food-borne pathogens, other diseases also include respiratory infection and systemic haemorrhagic disease.

Since the first norovirus sequence became available, a new system has been used for classifying caliciviruses (Xi et al., 1990, Green et al., 2000). Based on the major capsid protein VP1 sequence, there are 5 genera in the family *Caliciviridae*, including *Lagovirus*, *Nebovirus*, *Norovirus*, *Sapovirus* and *Vesivirus*. The genus *Lagovirus* includes rabbit haemorrhagic disease virus (RHDV), which causes necrotic hepatitis and haemorrhage in lagomorphs (Parra and Prieto, 1990, Ohlinger et al., 1990). The genus *Nebovirus* is newly classified into the family, causing haemorrhages in calves (Bridger et al., 1984). The prototypic norovirus, Norwalk virus, was named after the city of Norwalk, Ohio where an acute gastroenteritis outbreak in a school occurred (Kapikian et al., 1972). The genus *Sapovirus*, together with the genus *Norovirus*, are common causative agents of gastroenteritis in humans (Madeley and Cosgrove, 1976). The prototype sapovirus is Saporovirus, which was isolated from an infant during a family outbreak of acute gastroenteritis (Chiba et al., 1979, Matson et al., 1995, Numata et al., 1997, Nakanishi et al., 2011). The genus *Vesivirus* includes feline calicivirus (FCV), which causes respiratory infection in cats (Kreutz et al., 1994).

There are 6 more genera of the family *Caliciviridae* tentatively named *Bavovirus*, *Nacovirus*, *Recovirus*, *Salovirus*, and *Valovirus* (International Committee on Taxonomy of Viruses. et al., 2012). *Bavovirus* and *Nacovirus* both infect poultry (Wolf et al., 2012, Wolf et al., 2011). The genus *Recovirus* includes Tulane virus, which was originally isolated from rhesus macaques (Farkas et al., 2008). The genus *Salovirus* is the latest genus proposed, including the Atlantic salmon calicivirus (Mikalsen et al., 2014). St-Valérien-like virus belongs to the genus *Valovirus* (L'Homme et al., 2009).

The genus *Norovirus* can be further divided into 7 genogroups, named GI to GVII (Vinje, 2015). The prototypic Norwalk virus belongs to GI and was isolated in 1968 (Kapikian et al., 1972). Human noroviruses cluster in GI, GII and GIV (Thorne and Goodfellow, 2014). Porcine noroviruses also belong to GII (Sugieda et al., 1998), whilst bovine and ovine noroviruses cluster in GIII (Oliver et al., 2003, Bridger et al., 1984). Canine noroviruses belong to GIV, GVI and GVII noroviruses (Roerink et al., 1999, San Gabriel et al., 1997, Caddy et al., 2014). Hosts of GV noroviruses are limited to rodents (Thackray et al., 2007, Smith et al., 2012, Tse et al., 2012).

Each genogroup can be further divided into genotypes, as summarised in Figure 1.1C. There are currently 9 genotypes in GI and 22 in GII (Kroneman et al., 2013). Of all the genotypes, GII.4 HuNoVs dominate the pandemics in the past two decades (Mikalsen et al., 2014).

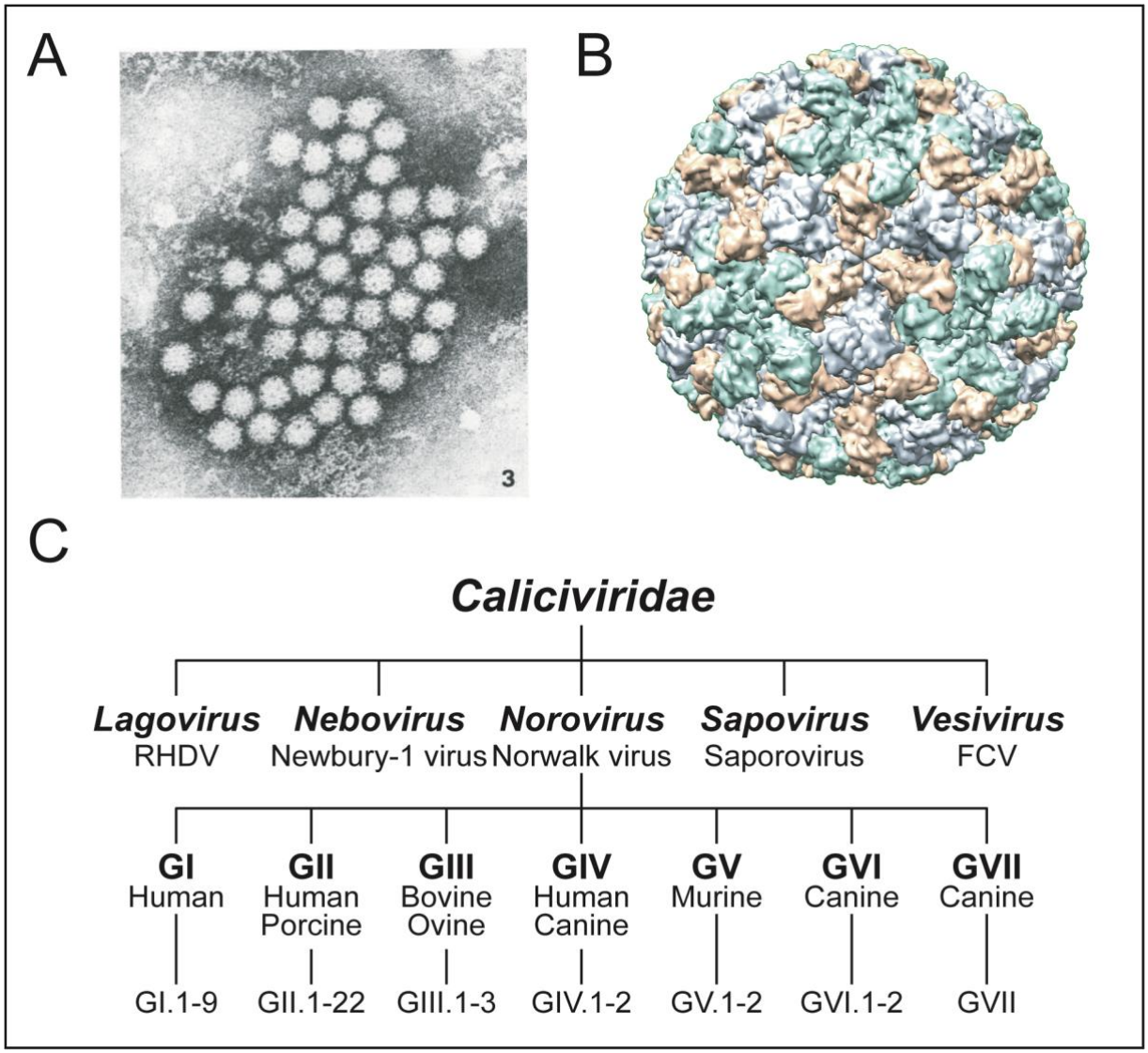

Figure 1.1 Morphology and classification of *Caliciviridae*. A) Norwalk virus particles under electron microscopy. Picture adapted from (Kapikian et al., 1972). B) Crystal structure of Norwalk virus particle (PDB ID: 1IHM). Different colours indicate quasi-equivalent subunits. Image adapted from (Prasad et al., 1999). C) Classification of *Caliciviridae*. Under each genus the prototype virus is listed. In the genus *Norovirus*, under each genogroup the host species and genotypes were listed.

1.2 Genome organisation

The genomes of all known caliciviruses are about 7.4 kb in length (Xi et al., 1990, Thorne and Goodfellow, 2014). A subgenomic RNA (about 2.6 kb) encoding the structural genes is also found in infected cells and in purified viral particles (Neill, 2002, Herbert et al., 1997, Herbert et al., 1996, Meyers et al., 1991a). Both genomic and

subgenomic RNA are linked to the viral protein VPg at the 5’ end and polyadenylated at the 3’ end (Schaffer et al., 1980, Burroughs and Brown, 1978). The 5’ and 3’ extremities of calicivirus RNA contain highly conserved RNA secondary structures, from the short untranslated regions (UTRs) extending into the coding region and are present throughout the genome (Lopez-Manriquez et al., 2013, Sandoval-Jaime and Gutierrez-Escolano, 2009, Gutierrez-Escolano et al., 2003, Gutierrez-Escolano et al., 2000, Vashist et al., 2012a). These structures are involved in binding viral and host factors to regulate translation, replication and pathogenesis (McFadden et al., 2013, Bailey et al., 2010b, Simmonds et al., 2008).

The calicivirus genome comprises 3-4 open reading frames (ORFs) (Figure 1.2). For genera *Norovirus* (HuNoV and MNV), *Vesivirus* (FCV) and *Recovirus* (TV, not shown in Figure 1.2), ORF1 encodes 6-7 non-structural proteins, whereas ORF2 and ORF3 encode the major (VP1) and the minor (VP2) capsid proteins, respectively (Sosnovtsev et al., 2006, Belliot et al., 2003, Liu et al., 1996, Glass et al., 2000, Sosnovtsev et al., 2002, Farkas et al., 2008). In genera *Lagovirus* (RHDV), *Sapovirus* (SaV), *Nebovirus*, and many of the recently proposed genera (*Bavovirus*, *Nacovirus*, *Salovirus*, *Valovirus*), the major structural protein is translated and processed as part of the ORF1 polyprotein (Meyers et al., 2000, Liu et al., 1995, Smiley et al., 2002, L'Homme et al., 2009, Wolf et al., 2011, Wolf et al., 2012, Mikalsen et al., 2014). In addition, they can also be synthesised via translation of the subgenomic RNA (Meyers et al., 1991b). In MNV, an ORF4 was identified with coding region overlapping ORF2, which encodes virulence factor 1 (VF1) (McFadden et al., 2011). Sapovirus is the only other member of the family *Caliciviridae* known to possess an equivalent ORF (Liu et al., 1995). ORF1 encodes non-structural proteins including those important for replication complex formation (NS1/2, NS3, NS4), genome linkage (VPg), polyprotein processing (NS6), and genome replication (RdRp). Norovirus p48 or NS1/2 has no known homologue

from other viruses. The according picornavirus homologues of other non-structural proteins of norovirus ORF1 are 2C (NS3), 3A (NS4), 3B (VPg), 3C (NS6) and 3D (RdRp). FCV VP1 is translated as a precursor and proteolytically processed by the viral protease to generate mature VP1 and a small leader of capsid (LC) protein, which was shown to induce cytopathic effect in cells and promotes Norwalk virus replicon replication *in trans* (Abente et al., 2013, Chang et al., 2008).

A unified nomenclature for norovirus proteins is yet to be defined (Figure 1.2). Throughout this thesis the names related to MNV will be used primarily, unless they are virus specific or for comparison purposes. The functions of norovirus proteins will be discussed in the context of the virus life cycle in more details below.

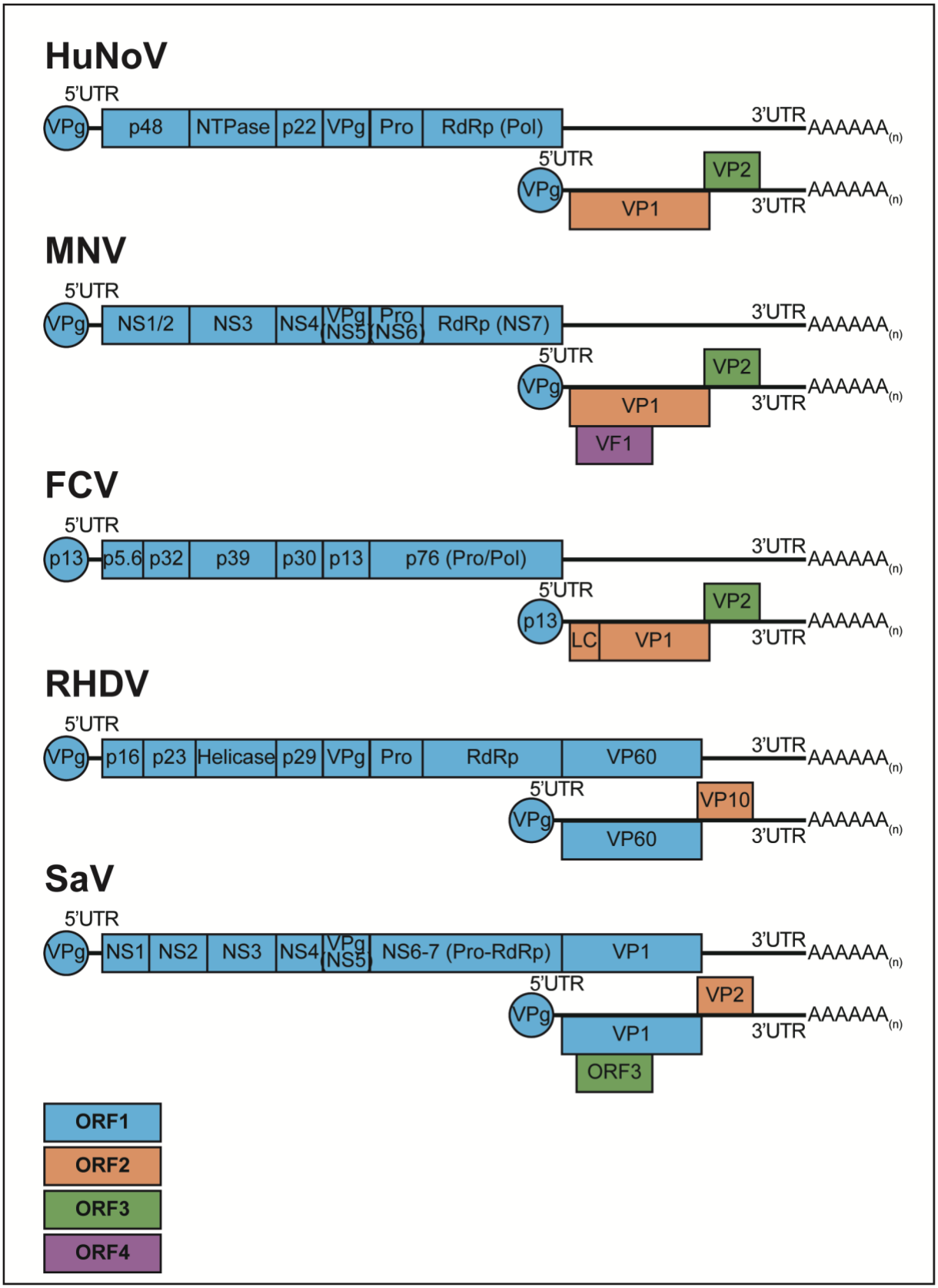

Figure 1.2 Genome organisation of caliciviruses. Open reading frames (ORFs) were coloured as indicated. The relevant genetic localisations of genes and their names were listed accordingly.

1.3 Epidemiology and transmission

Norovirus is the most common causative agent of acute gastroenteritis worldwide (Tam et al., 2012). Globally, HuNoV is estimated to cause 669 million illnesses, 219,000 deaths per year, in addition to $4.2 billion heath care cost and $60.3 billion societal cost (Bartsch et al., 2016). In the UK, it is estimated that the population burden of HuNoV infections is 59/1000 person year, equivalent to 3.7 million cases per year (Harris et al., 2017). The economic burden of HuNoV infections in the UK is estimated to be £81 million per year, which is more than the cost of *Campylobacter* and rotavirus infections combined (Tam and O'Brien, 2016). In the United States, the annual estimated HuNoV infections are 19-21 million illnesses per year, with 570-800 deaths (Hall et al., 2013), in addition to the associated cost of health care and loss of productivity of $2 billion (Bartsch et al., 2012).

The majority (55-85%) of HuNoV outbreaks are caused by the GII.4 variants. These are in conjunction with higher possibility of severe outcomes and deaths (Desai et al., 2012). The GII.4 variants are fast evolving, every two to three year a new circulating strain replaces the previous one due to the lack of cross protection. In the past two decades, at least seven GII.4 HuNoV variants caused pandemics: the US 1995/1996 variant in 1996, the Farmington Hills variant in 2002, the Hunter variant in 2004, the 2006a, 2006b variants in 2007-2008, the New Orleans variant from 2009 to 2012 and Sydney 2012 in late 2012 (Ramani et al., 2014, Lopman et al., 2004, Bull et al., 2006, Tu et al., 2008, Siebenga et al., 2009, van Beek et al., 2013). The latest dominant circulating strain is a GII.17 Kawasaki variant, however, which outcompeted the Sydney 2012 variant (Mori et al., 2017, Lu et al., 2016, Zhang et al., 2015, Chan et al., 2015). It is proposed that the GII.17 pandemic was caused by the lack of cross protection and the broad binding spectrum of the GII.17 capsid (Chan et al., 2015). In

terms of seasonality, HuNoV incidents peak during the winter seasons, which is why the media has named norovirus "the winter vomiting disease" (Lopman et al., 2009). The detailed mechanism of this seasonality is not fully understood, but it has been associated with the change of societal behaviour, more hospitalisations due to other infectious diseases, and yearly fading herd immunity (Lopman et al., 2009, Debbink et al., 2013).

Epidemiological studies of HuNoV infections mainly focus on the four categories: food-borne and water-borne gastroenteritis outbreaks, infections in the elderly or immunocompromised patients, sporadic acute gastroenteritis in young children under age of 5, and sporadic acute gastroenteritis in adults (Hoa Tran et al., 2013, Ramani et al., 2014).

There are many factors contributing to the large and fast outbreaks of HuNoV. First of all, HuNoV is resistant to environmental changes and survives through multiple inactivation procedures (Bohnker and Thornton, 2003, Vipond et al., 2002, Kuusi et al., 2002, Wu et al., 2005, Cheesbrough et al., 2000, Escudero-Abarca et al., 2014, Lou et al., 2012, Feng et al., 2011, Park et al., 2007, Hudson et al., 2007). Also, HuNoV can be bioconcentrated by animals (e.g. oysters) or biocontaminates vegetables (e.g. lettuce), posing challenges to traditional cleaning procedures in the food industry (Le Guyader et al., 2006, Gandhi et al., 2010, Urbanucci et al., 2009).

Secondly, HuNoV is highly infectious and can be transmitted by multiple routes. The 50% human infectious dose is estimated to be between 1320 and 2800 genome equivalent (Atmar et al., 2014). In comparison, peak faecal shedding of HuNoV is estimated to be about 10^{10} genome copies per gram faeces (Atmar et al., 2008). Vomiting has been shown to be not only a symptom but also a transmission risk of HuNoV (Kirby et al., 2016, Makison Booth, 2014). HuNoV can be transmitted by person-to-person contact or faecal-oral route (Verhoef et al., 2015). Together with its

environmental persistence, outbreaks of HuNoV infections usually happen in close-living environment, including hospitals, schools, care homes, and military bases (Sandmann et al., 2017, Godoy et al., 2016, Rajagopalan and Yoshikawa, 2016, Delacour et al., 2010). Repeated HuNoV outbreaks have also been reported in cruise ships (Vivancos et al., 2010).

The fast evolution of HuNoV also contributes to its constant presence (Zakikhany et al., 2012, Boon et al., 2011, Nilsson et al., 2003). In particular, the emergence of antigenically distinct GII.4 variants gave rise to pandemics due to the lack of cross protection from the previous circulating strains (de Graaf et al., 2016, White, 2014, Eden et al., 2014, Bull et al., 2010). Recombination at the ORF1/ORF2 junction also contributes to the failure of herd immunity against emerging variants (Lommer and Verstraete, 2003, Martella et al., 2013, Eden et al., 2013, Waters et al., 2007, Rohayem et al., 2005, Bull et al., 2005). In addition, zoonotic transmissions have been proposed to aid HuNoV evolution (Bank-Wolf et al., 2010) because GII noroviruses can infect both human, pigs and calves (Souza et al., 2008, Cheetham et al., 2006). Seroprevalence of HuNoV in pet dogs was also reported, yet currently there is no evidence of productive HuNoV replication in dogs (Di Martino et al., 2017, Caddy et al., 2015, Caddy et al., 2013, Summa et al., 2012).

1.4 Symptoms and diseases

The two major symptoms of HuNoV infections are watery diarrhoea and projectile vomiting, giving norovirus the name “the two-buckets disease”. Other symptoms include fever, stomach cramps, bloating and aching limbs. More severe symptoms have also been reported, in particular necrotising enterocolitis in neonates (Stuart et

al., 2010, Turcios-Ruiz et al., 2008), seizures in children (Hu et al., 2017, Ueda et al., 2015, Bartolini et al., 2011, Chen et al., 2009), and acute liver dysfunction in adults (Nakajima et al., 2012).

HuNoV infections have short incubation period of 12-48 hours. The onset of symptoms is fast and self-limiting, usually resolved in a few days. However, prolonged infections occur in the elderly (Harris et al., 2008) and in immunocompromised patients (van Beek et al., 2017, Jurgens et al., 2017, Westhoff et al., 2009, Lee et al., 2008, Gallimore et al., 2004). In particular, infections with HuNoV leads to complication of treatment (Engelen et al., 2011), rejection of transplant (Saif et al., 2011) or in severe cases the death of patients (Schwartz et al., 2011). Patients with persistent HuNoV infections were also thought as one of the reservoirs of HuNoV (Doerflinger et al., 2017, Schorn et al., 2010) but a recent analysis argued against it (Eden et al., 2017).

Although nosocomial transmissions are mainly caused by symptomatic infections (Sukhrie et al., 2012), there is no difference in shedding between symptomatic and asymptomatic infections (Newman et al., 2016, Teunis et al., 2015, Phillips et al., 2010, Okabayashi et al., 2008). This leads to a possible role of asymptomatic food handlers in causing food-borne norovirus outbreaks (Franck et al., 2015).

Not much is known about how norovirus infections cause vomiting and diarrhoea. A study characterising norovirus-infected duodenal biopsies showed disrupted epithelial barrier functions, reduced tight junctional sealing proteins and increased epithelial apoptosis, paralleled with increased intraepithelial cytotoxic lymphocytes and stimulated anion secretion. These are likely the cause of diarrhoea during norovirus infection (Troeger et al., 2009).

1.5 Challenges of cultivating HuNoV *in vitro*

1.5.1 Norovirus tropism

Despite its prevalence and impact, the understanding of noroivrus biology has lagged behind many RNA viruses, mainly because of the inability to propagate HuNoV in cell culture. There could be many factors contributing to this, one of which is the unknown tropism of HuNoV. It is unclear which cell type(s) HuNoV infects. However, because HuNoV is an enteric pathogen, the vast majority of reported attempts (and likely more unreported) at cultivating HuNoV have been focusing on human gastrointestinal tract epithelial cells, together with some common human and animal cell lines. Other possible factors such as virus strains, cellular differentiation status and cell culture additives have also been tested. These comprehensive efforts have led to no successful outcome as yet (Duizer et al., 2004). However, it was shown that transfection of VPg-linked Norwalk virus RNA into intestinal epithelial Caco-2 cells resulted in a single round of virus replication (Guix et al., 2007). This observation suggests that the restriction of HuNoV infection in epithelial cells is possibly viral entry. Since the discovery of MNV and its cell culture system, it has been long suspected HuNoV may share similar a haematopoietic tropism. MNV infects macrophages and dendritic cells, and virus replication is restricted by STAT1-dependent type I IFN responses (Wobus et al., 2004). However, infection of primary macrophages and dendritic cells isolated from peripheral blood showed no evidence of HuNoV replication, nor did the inhibition of innate immune responses with IFN cocktails promoted replication (Lay et al., 2010). The development of B cell culture system in 2014 by Jones et al. showed that both HuNoV and MNV infect B cells, and an enteric bacterium *Enterobacter cloacae* (*E. cloacae*) potentially bridges HuNoV to B cells ((Jones et al.,

2015, Jones et al., 2014) will be discussed in Chapter 3). However, HuNoV replication in B cells is very limited, highlighting the need to identify host proviral and antiviral factors in this system.

Besides cell types, it is also possible that established cell lines do not phenotypically represent fully differentiated cells as found *in vivo*, for example the polarised intestinal epithelial cells. In agreement with this, an *ex vivo* cell culture system reported HuNoV replication in duodenal biopsies (Leung et al., 2010). HuNoV replication was observed in glandular epithelial cells by evidence of increased viral RNA, the expression of viral structural and non-structural genes, and the presence of negative-sense replication intermediate. However, due to the limited supply and the inherent variations of *ex vivo* biopsies its application is limited. Attempts were also made to differentiate enteric epithelial cell lines to mimic primary intestinal epithelial cells. A three-dimensional culture system was first developed using rotating wall vessels (RWV) to maintain and differentiate INT-407 or Caco-2 cells, and the initial attempts showed increase of HuNoV viral RNA in infected cells (Straub et al., 2007, Straub et al., 2011). However, the extensive following attempts to repeat these results failed to reproduce the initial observations (Herbst-Kralovetz et al., 2013, Takanashi et al., 2014, Papafragkou et al., 2014). In 2016, Ettayebi et al. established a primary intestinal organoids (or enteroids) culture system for HuNoV, which demonstrated an enterocytic tropism of HuNoV and virus strain-dependent requirement of bile for infection ((Ettayebi et al., 2016) will be discussed in Chapter 3).

Without an *in vitro* infection system, the details of HuNoV life cycle are either inferred by surrogate viruses (will be discussed in later sections) or by studying certain stages of infection outside the context of infection. A Norwalk virus RNA replicon system was developed to study norovirus genome replication, showing antiviral effects of type I IFN responses and ribavirin (Chang et al., 2006). This system has been mainly used for

screening potential antiviral compounds (Bok et al., 2008, Chang, 2009, Chang and George, 2007). The RNA replicon system is complemented with recombinant virus-like particle (VLP) system. The major capsid proteins VP1 is the only protein on the outside of norovirus virion, and using various expression systems recombinant VP1 can self-assemble into VLPs morphologically and antigenically indifferent to native HuNoV virions (Huang et al., 2005, Baric et al., 2002, Green et al., 1997, Jiang et al., 1992, Taube et al., 2005). Therefore, they are useful tools to study virion physical properties, antibody responses, and interactions with attachment factors (Tresset et al., 2013a, da Silva et al., 2011, Hutson et al., 2003, Harrington et al., 2002).

1.5.2 *In vivo* model systems for HuNoV

Volunteer challenge was the main method to understand HuNoV pathogenesis and immunity. Typically, volunteers are challenged with stool filtrates from infected individuals and the disease outcome, duration of infection, immunogenicity (also compared with individuals challenged with VLPs), and protective immune response from previous exposures were monitored (Lindesmith et al., 2015, Ramirez et al., 2012, Tacket et al., 2003, Harrington et al., 2002, Gray et al., 1994, Gary et al., 1987, Thornhill et al., 1975, Lindesmith et al., 2005, Bernstein et al., 2015, Johnson et al., 1990). The duration and magnitude of shedding were also investigated, including the median duration of illness (1-2 days), median duration of faecal shedding (28 days), and median peak amount of faecal shedding (9.5×10^{10} genomic copies per gram of stool), which are useful for disease control during outbreaks (Atmar et al., 2008). This *in vivo* model of HuNoV in its natural host also revealed a genetic factor (*FUT2*) that confer susceptibility to HuNoV infection (Hutson et al., 2005, Hutson et al., 2002, Chan et al., 2008, Marionneau et al., 2005, Lindesmith et al., 2003). However, the interpretation of results from the early volunteer studies are complicated by the limited

sample size, the variations in individual susceptibility to infection, and the lack of previous history of exposure. The use of faecal filtrates as a source of infectious HuNoV also poses safety concern of the potential inclusion of other pathogens.

Because of the difficulties of volunteer studies, a robust animal model of HuNoV is long needed. Various non-human primates have been tested due to the genetic similarities. First of all, the presence of calicivirus in non-human primates was observed (Jiang et al., 2004, Smith et al., 1985). The infection of rhesus macaques with Norwalk virus was subclinical, but faecal shedding was detected, together with the induction of adaptive immune response (Rockx et al., 2005). Inoculation of a GII Toronto P2-A virus to new born pigtail macaques resulted in transmittable sporadic clinical symptoms (Subekti et al., 2002). Moreover, chimpanzees were demonstrated to be susceptible to asymptomatic Norwalk virus infection, and recently evaluated as a model system for vaccine development (Bok et al., 2011, Wyatt et al., 1978). Immunohistochemistry analysis of duodenal biopsies showed capsid expression in cells of the lamina propria positive for DC-SIGN (dendritic cells) or CD20 (B cells), supporting the proposed haematopoietic tropism of HuNoV (Bok et al., 2011). Although Norwalk virus does not replicate in PBDC, it is still possible that tissue-specific lineages of DCs and B cells are permissive for HuNoV infection (Lay et al., 2010).

Gnotobiotic pigs are more widely used as a model system for HuNoV (Lei et al., 2016b, Lei et al., 2016a, Lou et al., 2015, Kocher et al., 2014, Bui et al., 2013, Jung et al., 2012, Souza et al., 2008, Souza et al., 2007a, Cheetham et al., 2007, Cheetham et al., 2006). This is supported by the presence of HBGA-like receptors in buccal and intestinal tissues enabling norovirus VLP binding, and that GII noroviruses have been isolated from healthy pigs (Cheetham et al., 2007, Sugieda and Nakajima, 2002, Sugieda et al., 1998). Infection of gnotobiotic pigs by a GII HuNoV caused mild diarrhoea, paralleled with faecal shedding of viral genomic RNA, expression of viral

structural and non-structural genes in intestinal enterocytes, and virus-specific innate and mucosal immunity (Souza et al., 2007a, Cheetham et al., 2006). Follow-up studies revealed the proviral effect of the cholesterol management drug simvastatin, and that pre-treatment of IFN-α prior to infection is inhibitory to virus replication (Bui et al., 2013, Jung et al., 2012). In a severe combined immunodeficiency (SCID) phenotype gnotobiotic pig model where RAC/IL2R deficiency was generated by CRISPR knock out, increased HuNoV replication, dissemination and prolonged infections were observed (Lei et al., 2016a). This agrees with the observation of chronic HuNoV infections in immunocompromised patients (Echenique et al., 2016, Lemes et al., 2014, Saif et al., 2011, Siebenga et al., 2008, Woodward et al., 2017, Avery et al., 2017, Lambregts et al., 2010, Westhoff et al., 2009). However, in this model the enteric bacterium *E. cloacae* was found to inhibit HuNoV infection, where in the B cell culture model *E. cloacae* promotes infection (Lei et al., 2016b, Jones et al., 2014). Due to the large animal size gnotobiotic calves are not widely used, although calves are naturally susceptible to bovine norovirus infection (GIII Norovirus) and can be infected by HuNoV (Souza et al., 2008, Woode and Bridger, 1978). A mouse model for HuNoV was also developed (Taube et al., 2013). However, HuNoV replication in humanised mice is independent of the presence of human immune cells but depends on the immunocompromised status of mice.

1.5.3 Surrogate systems to study norovirus biology

In addition to *in vivo* models of HuNoV, surrogate systems are also important tools to study norovirus biology (reviewed in (Vashist et al., 2009)). Cell culture systems have been developed for the following caliciviruses: porcine sapovirus (PoSaV), Tulane virus (TV), RHDV, FCV, MNV (Parwani et al., 1991, Flynn and Saif, 1988, Farkas et al., 2008, Liu et al., 2007, Kreutz et al., 1994, Karst et al., 2003). PoSaV, previously known as

porcine enteric calicivirus, is one of the few cultivatable caliciviruses which causes diarrhoea, and the prototypic Cowden strain was first isolated by serially propagating the virus isolated from gnotobiotic pigs in tissue culture (LLCPK cells) (Flynn et al., 1988, Flynn and Saif, 1988). Bile acid or GCDCA is required for infection, and subsequent studies showed their roles in inhibiting STAT1, which is one of the key factors in type I IFN response (Parwani et al., 1991, Chang et al., 2004, Chang et al., 2002). However, our recent development of a reverse genetics system for PoSaV argues against it, because in the presence of bile acids, PoSav replication is still restricted by STAT-1-mediated type I IFN responses (Chang et al., 2005, Hosmillo et al., 2015). TV infects rhesus macaques and causes diarrhoea, and a reverse genetics system has also been developed (Sestak et al., 2012, Wei et al., 2008). Although RHDV was discovered in 1990, a cell culture and reverse genetics system was only available since a decade ago (Parra and Prieto, 1990, Ohlinger et al., 1990, Meyers et al., 1991b, Liu et al., 2008). In addition, RHDV infections in lagomorphs are systemic and usually lethal, therefore it is not a good model to study HuNoV pathogenesis, which mainly causes gastroenteritis (Meyers et al., 1991b, Forrester et al., 2007). FCV was the most frequently used surrogate system to study norovirus biology due to the early development of cell culture, reverse genetics system, and shared similarities with norovirus in protein functions and virus life cycle (Kreutz et al., 1994, Sosnovtsev and Green, 1995). However, FCV is not a suitable model system to study norovirus pathogenesis, as it causes lower respiratory tract or systemic infections.

MNV was the only cultivatable norovirus prior to the development of HuNoV culture system (Karst et al., 2003, Thackray et al., 2007). MNV infects macrophages, dendritic cells and B cells *in vitro* and *in vivo* (Wobus et al., 2004, Jones et al., 2014). The first MNV was isolated from the brain of immunocompromised (STAT1/RAG$^{-/-}$) mice. The lethal and systemic infection was caused by the loss of innate immune response. In

STAT1$^{-/-}$ mice MNV-1 causes lethal infection, whereas homologous RAG1/2 deficiency leads to systemic persistence (Karst et al., 2003). In immunocompetent mice, sub-clinical MNV-1 infection is restricted by STAT1-mediated innate immune responses (Mumphrey et al., 2007). Mice are natural hosts of MNV, and the majority of MNVs isolated from immunocompetent mice cause persistent infections (Hsu et al., 2007, Hsu et al., 2006). MNVs were found in mice from both laboratory and the field, indicating their wide distribution (Ohsugi et al., 2013, Farkas et al., 2012, Kitajima et al., 2009). In terms of genome similarity, MNV shares more than 50% nucleotide sequence identities with HuNoV, and structurally and functionally conserved nucleotide sequences and genes were reported (Vashist et al., 2009, Bull et al., 2011, Lin et al., 2015, Subba-Reddy et al., 2012). Both DNA-based and RNA-based reverse genetics have been developed for MNV, allowing virus manipulation to study virus replication and virus-host cell interactions (Chaudhry et al., 2007, Ward et al., 2007, Arias et al., 2012). Both HuNoV and MNV are enteric pathogens, but unlike HuNoV, MNV infections in mice are usually asymptomatic (Mumphrey et al., 2007). Despite its biological diversity, MNV comprises a single genogroup and a single serogroup, limiting its applications as a model system for vaccine development (Thackray et al., 2007, Hsu et al., 2006).

1.6 Norovirus life cycle

Compared to other small RNA viruses, relatively little is known about the life cycle of HuNoV, primarily due to the lack of a cell culture system. Studies using surrogate viruses, especially MNV and FCV, started to review details of each stage of the

calicivirus life cycle. PSaV, RHDV and BoNoV are also used. Figure 1.3 is an overview of the calicivirus replication cycle and each stage will be discussed in detail, primarily using MNV as the model system.

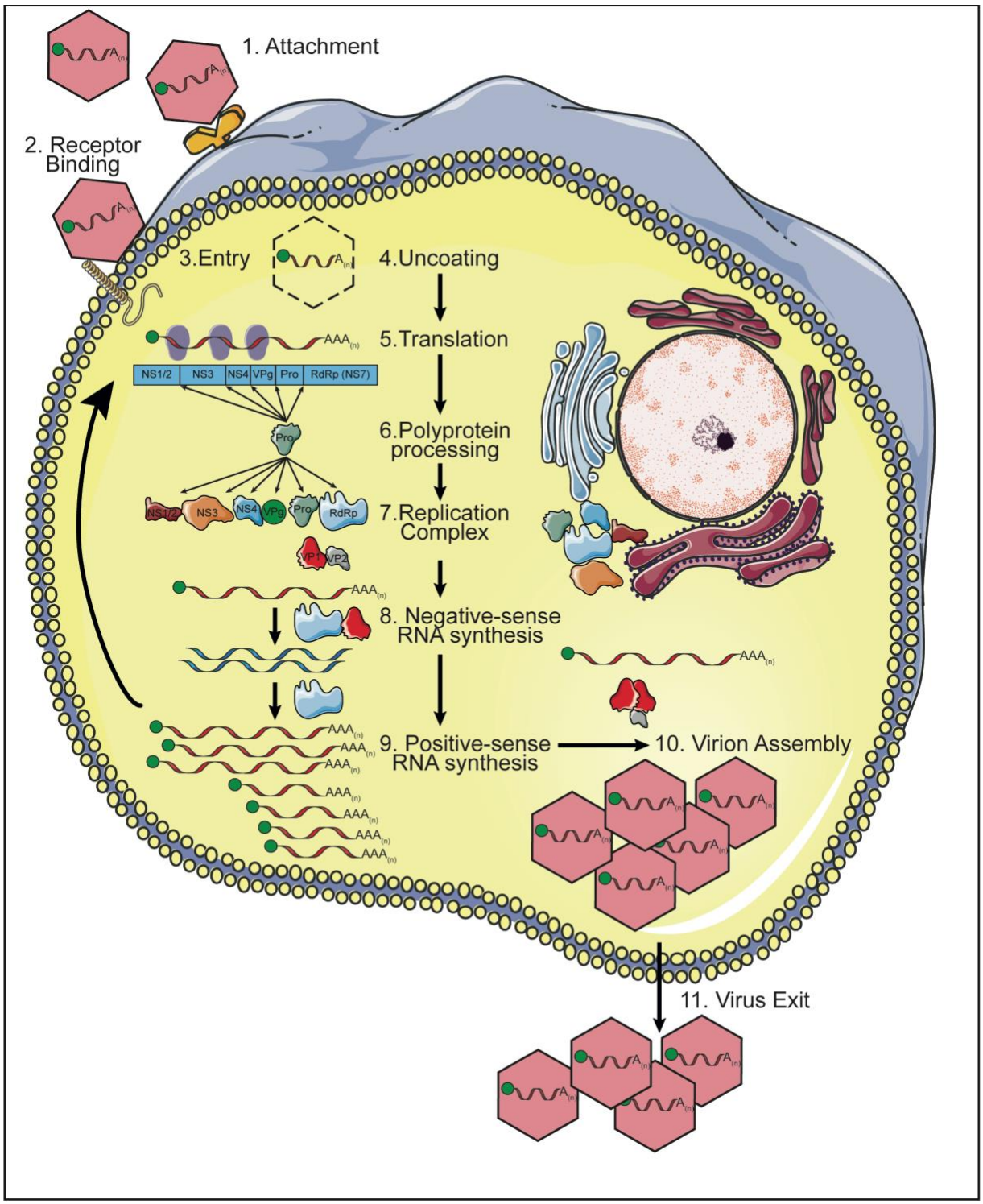

Figure 1.3 Overview of the calicivirus life cycle. 1) Viral binding to attachment factors and 2) translocation to receptors. 3) Viral entry and 4) uncoating through unknown mechanisms. 5) Pioneer round of translation and 6) polyprotein processing by viral and cellular proteases to 7) establish viral replication complex (RC). 8) Synthesis of negative-sense replication intermediate by *de novo* initiation

of RdRp, followed by 9) VPg-dependent initiation to produce genomic and subgenomic RNA. 10) Virion assembly by VP1 and VP2 11) Exit by cell lysis.

1.6.1 Attachment and entry

The norovirus capsid (*T* = 3 icosahedral) comprises 180 copies of the major capsid protein VP1, and the capsid is stabilised by 2 copies of minor capsid protein VP2 associated with VP1 shell domain (Glass et al., 2000, Vongpunsawad et al., 2013). Therefore, VP1 is thought to bind cellular receptors and mediate viral entry.

The norovirus major capsid protein VP1 can be divided into three domains, Figure 1.4A and (Prasad et al., 1999). The functions of the N-terminal domain is unknown, the shell domain is sufficient to assemble capsid, whilst the P domain stabilises the capsid (Bertolotti-Ciarlet et al., 2002). The P domain can be further divided into two subdomains. The P1 domain forms the basis of the arch and is heavily involved in dimerisation of P particle formation (Tan and Jiang, 2005b). The P2 domain is the least conserved region of VP1 and is thought to contain the receptor binding site, Figure 1.4B and (Chakravarty et al., 2005). Analysis of the capsids of MNV and other caliciviruses revealed a similar structural arrangement (Katpally et al., 2010, Laurent et al., 2002, Yu et al., 2013, Wang et al., 2013).

The molecular details of how human norovirus enters susceptible cells are not fully understood, mainly due to the lack of known tropism. There is increasing evidence suggesting that norovirus entry is a multi-step process coordinated by an attachment factor and a proteinaceous receptor.

The correlation between secretor status and resistance to infection of certain HuNoV strains has been long observed. In one volunteer study, certain individuals are completely resistant to Norwalk virus infections, and pre-existing antibodies does not correlate with protection (Parrino et al., 1977). In norovirus outbreaks, the resistant individuals cluster in families, despite similar exposure as did the infected, suggesting

a genetic factor possibly contributes to norovirus resistance (Koopman et al., 1982). Histo-blood group antigens (HBGAs) are carbohydrates present on the cell surface. They were first identified as the receptor of RHDV, followed by showing the prototype Norwalk virus binds the HBGAs on the surface of intestinal epithelial cells (Ruvoen-Clouet et al., 2000, Marionneau et al., 2002). This observation was then supported by an investigation of a norovirus outbreak, where fucosyltransferase 2 (*FUT2*) non-secretor genotype was associated with the resistance to norovirus infections (Thorven et al., 2005). Secretor-negative individuals do not express HBGAs on the epithelial cell surface due to non-functional *FUT2* genes (usually homozygous G428A non-sense or A385T missense mutations), which is required for synthesising H1 antigen (blood type O) and subsequently A and B antigens (blood types A and B) (Thorven et al., 2005). Between secretor-positive individuals and HuNoV strains, blood group-dependent binding patterns were observed (Marionneau et al., 2002, Huang et al., 2003, Tan et al., 2008). However, secretor status-independent outbreaks and the binding of intestinal epithelial cells were also observed (Nordgren et al., 2010, Murakami et al., 2013). GII.4 HuNoV can also infect non-secretor individuals, suggesting alternative entry mechanisms (Tamura et al., 2004, Carlsson et al., 2009, Rydell et al., 2009). Importantly, there is early evidence suggesting a proteinaceous receptor for Norwalk virus entry, where most studies of norovirus-HBGA interactions focus on binding (White et al., 1996). Therefore, it is possible that norovirus binds to an attachment factor, followed by entry via a proteinaceous receptor.

For other caliciviruses, bovine norovirus binds carbohydrate Gal α epitope which is not present on human cell surface (Vildevall et al., 2010, Zakhour et al., 2010, Mauroy et al., 2011). MNV binds to glycolipid and glycoprotein in a strain-dependent manner (Taube et al., 2009, Taube et al., 2012). However, a recent study identified CD300ld and CD300lf as proteinaceous receptors of MNV (Orchard et al., 2016, Haga et al.,

2016). Permissive BV-2 cells depleted of CD300lf showed complete resistance to MNV infection. Therefore, for MNV there are attachment factors glycolipid and glycoprotein, and cellular receptors CD300ld and CD300lf. FCV is the only other calicivirus with an identified functional receptor. FCV binds α2,6-linked sialic acid then enters cells via junctional adhesion molecule 1 (JAM-1) (Stuart and Brown, 2007, Makino et al., 2006). Porcine sapovirus also binds α2,6-linked sialic acid in addition to α2,3-linked sialic acid, and bile acid is crucial for viral entry (Shivanna et al., 2014, Kim et al., 2014).

The details of which entry pathway(s) norovirus utilise are unknown. For MNV, endocytosis is dynamin and cholesterol dependent, but independent of pH, clathrin, and caveolae, which excluded most of the major pathways (Perry et al., 2009, Perry and Wobus, 2010, Gerondopoulos et al., 2010). The cellular entry of FCV is by clathrin-mediated endocytosis and is dependent on acidification of endosomes (Stuart and Brown, 2006).

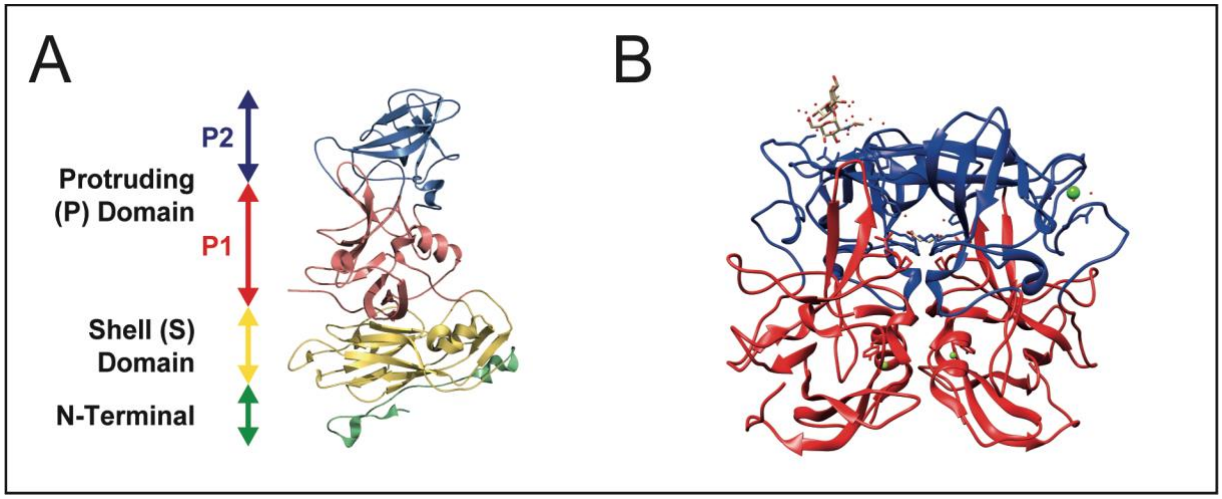

Figure 1.4 Norovirus interaction with HBGA. A) Crystal structure of Norwalk virus VP1, PDB ID: 1IHM, adapted from (Prasad et al., 1999). VP1 is divided into N-terminus, shell domain and P domain. The P domain can be further divided into P1 and P2 subdomains. B) Norwalk virus P domain interaction with H type 1 antigen (PDB ID: 2ZL7, adapted from (Choi et al., 2008)).

1.6.2 Translation and polyprotein processing

Norovirus genomic RNA is covalently linked to a cap-substitute viral protein VPg and polyadenylated at the 3’ end, thus functionally mimicking cellular mRNAs (Figure 1.5). Following viral entry and uncoating, the incoming genomic RNA is translated to establish viral replication complex (RC). To initiate translation, norovirus VPg functions as cap-substitute to recruit translation initiation factors (Daughenbaugh et al., 2006, Goodfellow et al., 2005, Daughenbaugh et al., 2003). This translation initiation mechanism is different from many small positive-sense RNA viruses, where a highly structured internal ribosome entry site (IRES) at the 5’ end of genomic RNA recruits translation initiation factors (Belsham, 2009). In addition, picornavirus VPg is mainly used as a protein primer for viral genome replication (Pathak et al., 2008). Prior to norovirus, VPg-dependent translation initiation was not observed in other animal viruses, instead this mechanism is used by some plant RNA viruses such as those within the family *Potyviridae* (Leonard et al., 2004).

Both the HuNoV and MNV VPgs interact with eIF4F components. In particular, both VPgs interact with the cap-binding protein eIF4E and the scaffold protein eIF4G (Chaudhry et al., 2006, Daughenbaugh et al., 2003). However, VPg-dependent translation initiation is insensitive to eIF4E depletion (Chaudhry et al., 2006), and a followup study showed that a conserved C-terminus of VPg interacts with the HEAT-1 domain of eIF4G to direct translation initiation (Leen et al., 2016). Together, it appears that VPg can recruit translation initiation factors independent of eIF4E, and there may be additional functions of the VPg-eIF4E interaction in norovirus life cycle. As the norovirus RNA is highly structured, the RNA helicase eIF4A, which is another component of the eIF4F ternary complex (eIF4A/eIF4E/eIF4G), was thought to help unwinding the RNA secondary structure to promote translation. Accordingly, the translation of MNV VPg-linked RNA is sensitive to a dominant-negative eIF4A

(Chaudhry et al., 2006). In addition to the eIF4F components, the norovirus VPg also interacts with eIF3, which may help recruiting the 43S pre-initiation complex (Daughenbaugh et al., 2006, Daughenbaugh et al., 2003). To date, with all the initiation factors, eIF3, eIF4E and eIF4G directly bind VPg (Leen et al., 2016, Goodfellow et al., 2005, Daughenbaugh et al., 2003), co-immunoprecipitation of eIF4A with VPg likely occur via the eIF4G-eIF4A interaction, as the VPg-eIF4A complex was not observed (Leen et al., 2016). For porcine sapovirus and FCV, VPg interaction with eIF4E is essential for translation initiation, as a eIF4E inhibitor 4E-BP1 reduces the translation of VPg-linked RNA (Chaudhry et al., 2006, Goodfellow et al., 2005).

The translation of the norovirus ORF1 polyprotein is processed primarily by viral protease NS6 or its precursor forms, some of which have been shown to be enzymatically active *in vitro* (Emmott et al., 2015, Scheffler et al., 2007, Sosnovtsev et al., 2006, Blakeney et al., 2003, Belliot et al., 2003, Liu et al., 1999, Liu et al., 1996). For MNV, the cleavage of NS1/2 by cellular protease caspase 3 was observed at late stage of infection, the significance of which is unknown (Sosnovtsev et al., 2006). Viral proteins VP1 and VP2 (and VF1 in MNV) are thought to translate from the subgenomic RNA. Given the presence of the larger abundance of subgenomic RNA, this could provide a mechanism by which more structural proteins are synthesised for capsid assembly (Yunus et al., 2015). The translation of VP2 occurs via a termination-reinitiation mechanism, as demonstrated in MNV, FCV and RHDV (Napthine et al., 2009, Luttermann and Meyers, 2007, Meyers, 2003). Upon termination of ORF2 (VP1) translation, a proportion of ribosomes are thought to remain associated with the subgenomic RNA and initiate ORF3 (VP2) translation via a start codon overlapping with the ORF2 stop codon. A termination upstream of ribosomal binding site (TURBS) sequence which is partially complementary to the 18S rRNA was also observed in MNV, which also contributes to the efficient translation of VP2 (Napthine et al., 2009). The

translation of VP1 via a similar termination-reinitiation mechanism at the ORF1/ORF2 junction was only observed in bovine norovirus (McCormick et al., 2008).

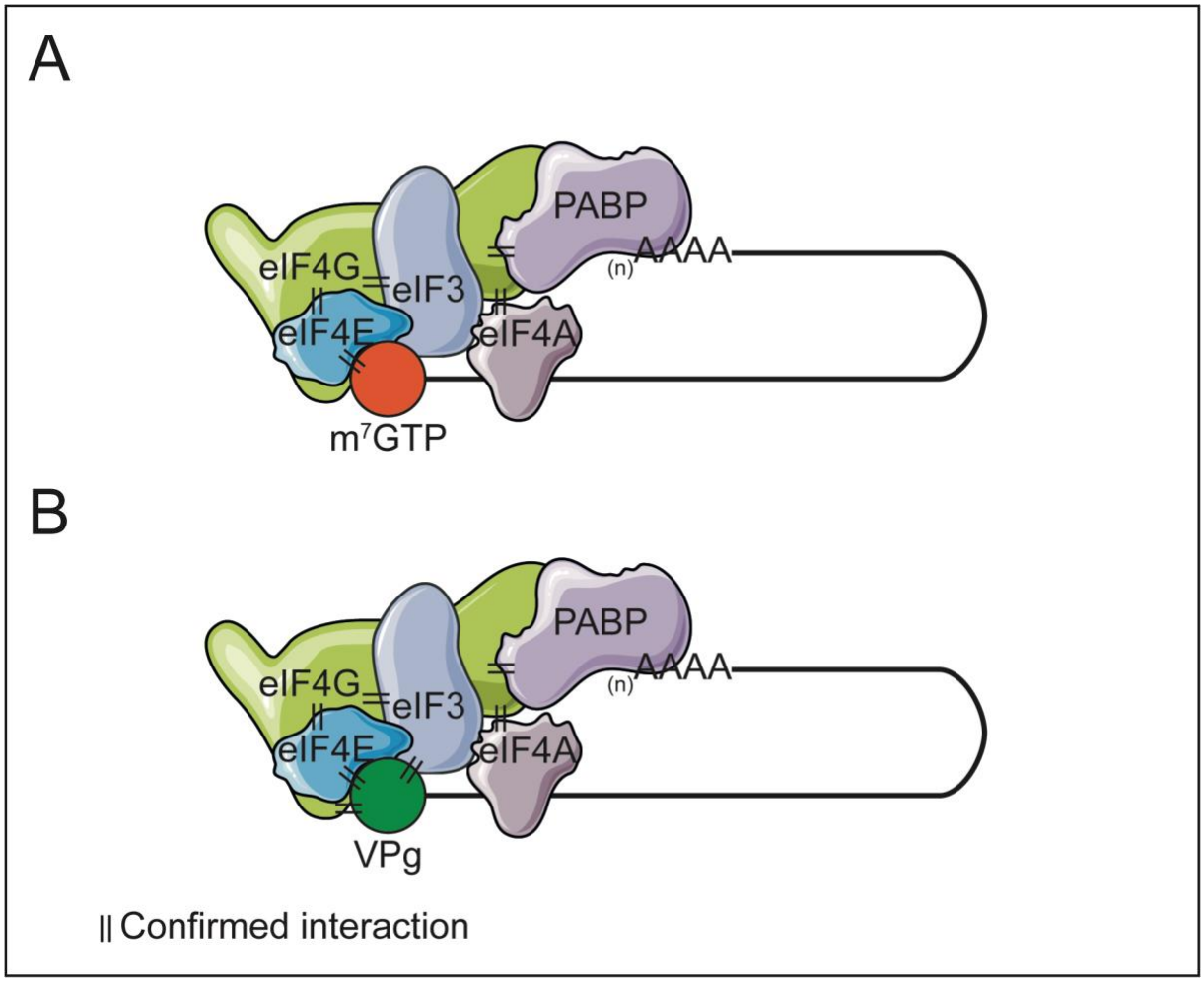

Figure 1.5 Cap- and VPg-dependent translation initiation. A) eIF4F complex is first assembled (eIF4A, eIF4E and eIF4G), then cap-binding protein eIF4E binds to m^7GTP at 5' end of mRNA. PABP binds poly(A) tail at 3' end of mRNA, then interacts with eIF4G to circularise mRNA. Helicase eIF4A scans mRNA to locate the start codon. eIF3 then binds eIF4G and recruits the 40S ribosomal subunit. B) VPg-dependent translation initiation. Most of the processes are the same except that VPg replaces m^7GTP. Also VPg interacts with eIF4G and eIF3. Adapted from (Thorne and Goodfellow, 2014).

1.6.3 Viral genome replication

1.6.3.1 Assembly of viral replication complex

Following initial translation of viral proteins, norovirus establishes viral replication complex (RC) to facilitate viral genome replication (Figure 1.6). Like many other small,

positive-strand RNA viruses, the norovirus RC is cytoplasmic and originates from re-arrangement of cellular membranes.

Early studies of the HuNoV N-terminal nonstructural protein p48 (NS1/2 in MNV) suggested possible roles in re-organising cellular membranes to establish viral RC (Fernandez-Vega et al., 2004, Ettayebi and Hardy, 2003). Another nonstructural protein p22 (NS4 in MNV), was shown to inhibit cellular secretory pathways (Sharp et al., 2012, Sharp et al., 2010). When expressed in cells, MNV NS1/2 co-localises with the ER marker calnexin, whilst NS4 co-localises with Golgi apparatus and endosomes (Hyde and Mackenzie, 2010). Recently, together with others we showed that norovirus NS1/2 contains a mimic of phenylalanine-phenylalanine-acidic-tract (FFAT) motif that co-opts the cellular proteins VAMP-associated protein A (VAP-A) and VAP-B to establish RC (McCune et al., 2017). The membrane-redistribution function was also observed in picornaviruses (Dorobantu et al., 2015). Although initial investigation showed no clear co-localisation of MNV NS3 with ER, Golgi apparatus or endosomes (Hyde and Mackenzie, 2010). HuNoV NTPase and MNV NS3 were then shown to associate with lipid and microtubule to form replication complex-like structure when expressed in cells (Cotton et al., 2017). MNV VP1 was shown to redistribute the microtubules during infection. Although morphological changes of microtubules were observed at later stages of infection, the disruption of microtubules prior to infection or at early stages post infection inhibited MNV replication, indicating that the VP1-microtubule interaction is also important for RC formation (Hyde et al., 2012). Together, norovirus proteins rearrange cellular membranes and utilise cytoskeleton networks to establish the viral RC. For other caliciviruses, FCV viral proteins p32 (NS1/2 in MNV), p39 (NS3 in MNV) and p30 (NS4 in MNV) initiate RC formation via rearranging ER membranes, which is different to norovirus (Bailey et al., 2010a).

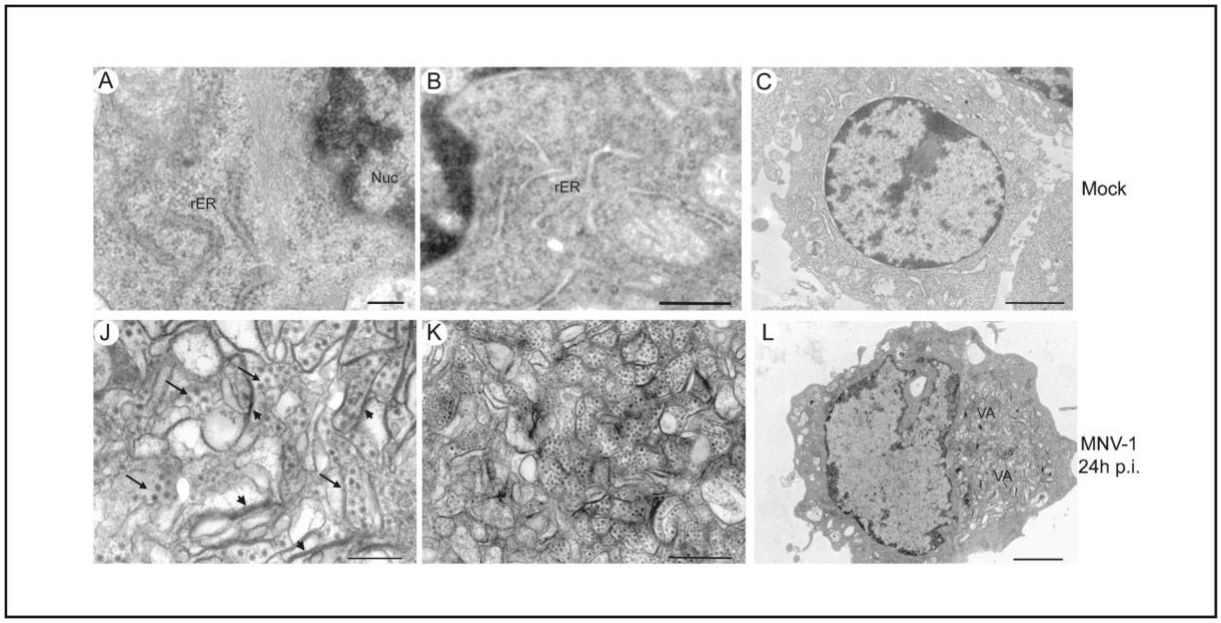

Figure 1.6 Norovirus replication complex. Raw264.7 cells were infected with MNV-1, the arrows indicate MNV-containing membraneous RCs. Figures adapted from (Wobus et al., 2004).

1.6.3.2 Two modes of initiation by the norovirus RdRp

Like other small positive-strand RNA viruses, the norovirus genome replication begins by the synthesis of negative-sense replication intermediates. The negative-sense genomic and subgenomic RNAs are then used as the template to synthesise the positive-sense genomic and subgenomic RNA.

The norovirus RdRp plays a central role in the viral genome replication. To date several crystal structures are available, including those of the prototypic GI.1 Norwalk virus and the GII.4 HuNoV, which account for the majority of norovirus outbreaks since 2000 (Ng et al., 2004, Zamyatkin et al., 2008, Zamyatkin et al., 2009, Hogbom et al., 2009, Mastrangelo et al., 2012, Croci et al., 2014b, Croci et al., 2014a). In addition to HuNoV, the crystal structures of other calicivirus RdRps were also determined (Ng et al., 2002, Fullerton et al., 2007, Lee et al., 2011, Alam et al., 2012). All of the characterised calicivirus RdRps display a partially closed right hand-like structure with fingers, palm and thumb subdomains (Figure 1.7), which is highly conserved among positive-strand

RNA viruses (Ng et al., 2004, Zamyatkin et al., 2008, Hogbom et al., 2009, Alam et al., 2012).

Detailed structural information reveals a 5-step RNA synthesis reaction of the norovirus RdRp which is common among viral RdRps. The apo-enzyme has its C-terminus bound to the active site, Figure 1.7A and (Ng et al., 2004). The RNA synthesis is initiated by a template-bound RdRp recruiting an NTP complementary to the template base. Then conformational changes of the thumb subdomain of RdRp are induced to accommodate the RNA primer and form a closed ternary complex, Figure 1.7B and (Zamyatkin et al., 2008). The active site of RdRp is located within the palm subdomain and coordinates two divalent metal ions to mediate the catalysis of nucleotide linkage (Ng et al., 2004, Ng et al., 2002, Vazquez et al., 2000). Following catalysis the RdRp remains in a closed complex, but the thumb subdomain returns to a similar conformation as in the apo-enzyme. Conformational changes of the thumb subdomain then release the pyrophosphate and translocates the RNA duplex to the next position. In addition to structural similarity, norovirus RdRps are functionally similar (Bull et al., 2011). This supports the use of the MNV RdRp to study norovirus replication.

The norovirus RdRp can initiate RNA synthesis by two distinct mechanisms, named *de novo* initiation and VPg-dependent initiation (Rohayem et al., 2006b). *De novo* initiation is primer-independent with the first nucleotide providing the ribose 3’ OH for the subsequent nucleotide linkage and the synthesis of the full length RNA (Beerens et al., 2007, Kao et al., 2001). Recombinant norovirus RdRps can initiate RNA synthesis *in vitro* using homopolymeric and heteropolymeric templates (Belliot et al., 2005, Fukushi et al., 2004, Rohayem et al., 2006a).

The norovirus RdRp can also initiate RNA synthesis using VPg as a protein primer (Rohayem et al., 2006a). Structural and functional analyses suggest a compact helical core structure of VPg is central for mediating the VPg-RdRp interaction, but further

conformational changes of the RdRp are likely required to accommodate VPg at the primer binding pocket (Leen et al., 2013). How the norovirus RdRp interacts with VPg is unknown, because a crystal structure of the RdRp-VPg complex is not yet available. As the norovirus genomic and subgenomic RNAs are covalently linked to VPg (Schaffer et al., 1980), it is believed that the nucleotidylylation of VPg is the first step of VPg-primed RNA synthesis. A recombinant norovirus RdRp can catalyse nucleotidylylation of VPg *in vitro* (Rohayem et al., 2006b, Belliot et al., 2005). Interestingly, despite the first nucleotide of both genomic and subgenomic RNA of all noroviruses is invariably guanosine, both guanylylation and uridylylation were observed in an *in vitro* nucleotidylylation assay. It is therefore possible that VPg also primes negative-sense RNA synthesis by generating VPg-poly(U) which is complementary to the poly(A) tails at 3’ ends of positive-sense genomic and subgenomic RNAs. However, using a mass spectrometry-based approach guanylylated VPg was detected from both MNV- and FCV-infected cell lysates, and there was no evidence of uridylylation of VPg (Olspert et al., 2016). Although the absence of uridylylated VPg may be due to the quantity difference between the positive- and negative-sense RNAs in infected cells (Vashist et al., 2012b), it is also possible that the biochemical nucleotidylylation assay of the norovirus RdRp does not confer the functional specificity of VPg nucleotidylylation *in vivo*. For example, in one study the tyrosine 117 was identified as the uridylylation site of MNV VPg (Han et al., 2010), yet multiple evidence suggest the conserved tyrosine 26 (27 in HuNoV, 24 in FCV) is important for nucleotidylylation, genome linkage and infectivity (Medvedev et al., 2017, Belliot et al., 2008, Leen et al., 2013, Subba-Reddy et al., 2011). Together, it is generally accepted that the norovirus RdRp synthesises the negative-sense genomic RNA via *de novo* initiation, and VPg-primed initiation is required for the synthesis of the positive-sense genomic and subgenomic RNAs.

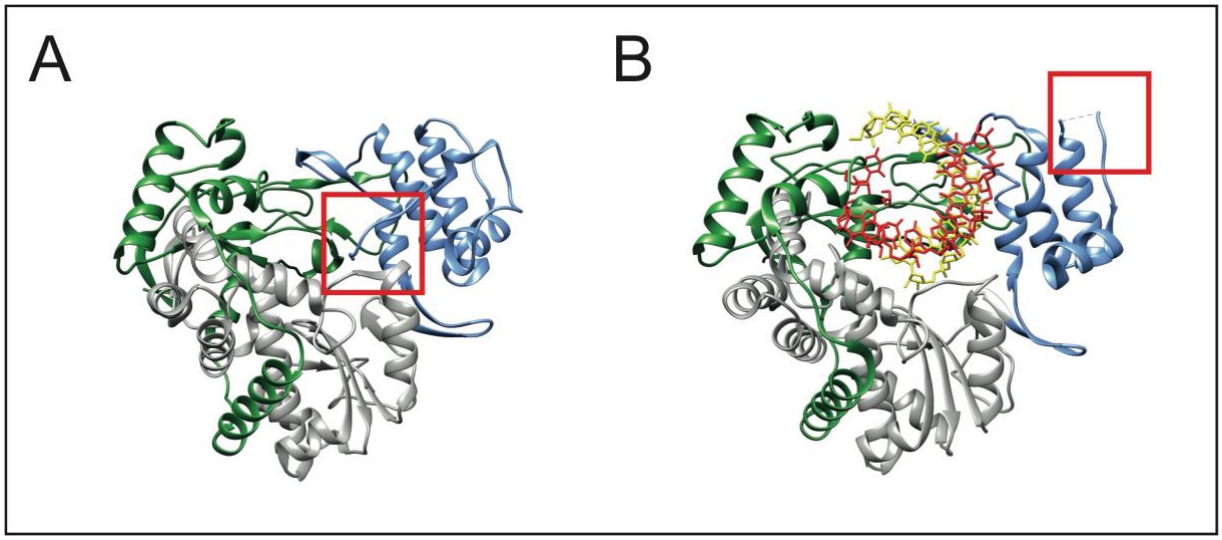

Figure 1.7 RNA-dependent RNA polymerase. Crystal structures of the A) Apo-enzyme (PDB ID: 1SH0) and B) Replicative form (PDB ID: 3BSN) of the Norwalk virus RdRp (fingers: green, palm: grey, thumb: blue, template: red, RNA primer: yellow). Note the different locations of the C-terminus of the thumb subdomain (red square) in the replicative form, exposing the active site during RNA synthesis.

1.6.3.3 Directed initiation of replication

In addition to the different modes of initiation, it is crucial that the norovirus RdRp initiate the RNA synthesis at an accurate site to preserve viral genetic information. Not much is known about how norovirus directs an accurate initiation of the positive-sense genomic RNA. However, due to the similarity of RNA sequence at both extremities, the positive-sense subgenomic RNA is usually used as a surrogate to understand the molecular details of norovirus genome replication.

Two models have been proposed for the initial synthesis of norovirus subgenomic RNA (Figure 1.8). The pre-mature termination model proposed an unidentified termination signal leading to the synthesis of negative-sense subgenomic RNA, which is then used as the template to synthesise the positive-sense subgenomic RNA. Evidence supporting this model includes the identification of the negative-sense subgenomic RNA in Norwalk virus replicon-bearing HG23 cells (Chang et al., 2006), in RNA synthesis assay using enzymatically active replication complex purified from FCV-infected cells (Green et al., 2002), and also in MNV-infected cells (Yunus et al., 2015).

Another model of initiation, named the internal initiation model, suggests that a highly conserved RNA stem loop upstream of the subgenomic start site binds to the norovirus RdRp and directs an accurate initiation. Bioinformatic and functional analyses suggested the presence of a highly conserved stem loop structure in the negative-sense genomic RNA upstream of the subgenomic start (Simmonds et al., 2008). The following structural and biochemical investigation showed the norovirus RdRp binds to the conserved stem loop to direct the subgenomic RNA synthesis (Yunus et al., 2015, Lin et al., 2015). The presence of the negative-sense subgenomic RNA can be argued as the products of additional rounds of replication using the newly synthesised positive-sense subgenomic RNA as templates. The presence of both templates, together with its smaller size, can contribute to the larger abundance of the subgenomic RNA compared with the full length genomic RNA (Vashist et al., 2012b, Yunus et al., 2015).

1.6.3.4 Regulation of genome replication by viral factors

Besides the RdRp, other norovirus proteins are also involved in regulating the viral genome replication. Together with the Kao lab (Indiana University), we previously developed a cell-based reporter assay (NoV-5BR assay) to indirectly measure the norovirus RdRp activity. In addition to the norovirus RdRp, firefly luciferase is expressed under an IFN-β promoter, which is activated upon the expression of the norovirus RdRp. In the NoV-5BR assay, VPg can stimulate the RdRp activity (Ranjith-Kumar et al., 2011). This stimulation is independent of the mode of initiation, i.e. VPg interacts with RdRp to promote a state where RdRp is more competent in RNA synthesis. In addition to VPg, three more norovirus proteins were shown to modulate RdRp activity. NS1/2 (p48 in HuNoV) and VP1 enhance the RdRp activity, whereas the RdRp interaction with the minor capsid protein VP2 is inhibitory. Additive enhancement on the RdRp activity was not observed when VP1 and NS1/2 were co-expressed,

indicating a possible functional redundancy. Moreover, all of these interactions are genogroup-specific, indicating a functional conservation of these interactions through the differed residues.

In a follow-up study, the norovirus VP1-RdRp interaction was further characterised (Subba-Reddy et al., 2012). Both HuNoV and MNV VP1 interact with their cognate RdRp and enhance the RdRp activity in a VPg-free NoV-5BR assay. The shell domain (SD) of VP1 is sufficient and necessary to stimulate the RdRp activity. Further mapping using chimeric SDs showed genogroup-specific residues of the flexible loops 1, 3, 5 and 7 confer the specificity of the enhancement. The biological significance of the VP1-RdRp interaction in the norovirus life cycle was demonstrated by complementing the expression of the SD *in trans* to stimulate norovirus RNA replication using an otherwise replication-deficient MNV replicon system. Because this stimulation is also concentration-dependent, it is thought to be important for promoting the synthesis of the negative-sense genomic RNA at the early stages of infection, where VP1 is present at low concentration, either from incoming capsid or translated from the subgenomic RNA *de novo*. The VPg-linked subgenomic RNA has been observed in FCV and RHDV viral particles (Meyers et al., 1991a, Neill, 2002). Therefore, it is possible that the translation of ORF2 from the incoming subgenomic RNA produces a small amount of VP1 sufficient to stimulate the RdRp activity. Moreover, in bovine norovirus (GIII *Norovirus*), VP1 can be synthesised from the genomic RNA via termination-reinitiation between the ORF1 and the ORF2, suggesting an alternative mechanism to synthesise VP1 via a less efficient means (McCormick et al., 2008). Together, these results demonstrate a non-structural role of a viral structural protein, supporting the hypothesis that small, positive-sense, single-stranded RNA viruses encode multifunctional proteins to compensate for the limited coding capacity of the small genomes. In fact, characterisation of the non-encapsidation functions of viral structural proteins have

become an increasingly important subject in RNA virology (reviewed in (Bol, 2008) and (Ni and Cheng Kao, 2013)).

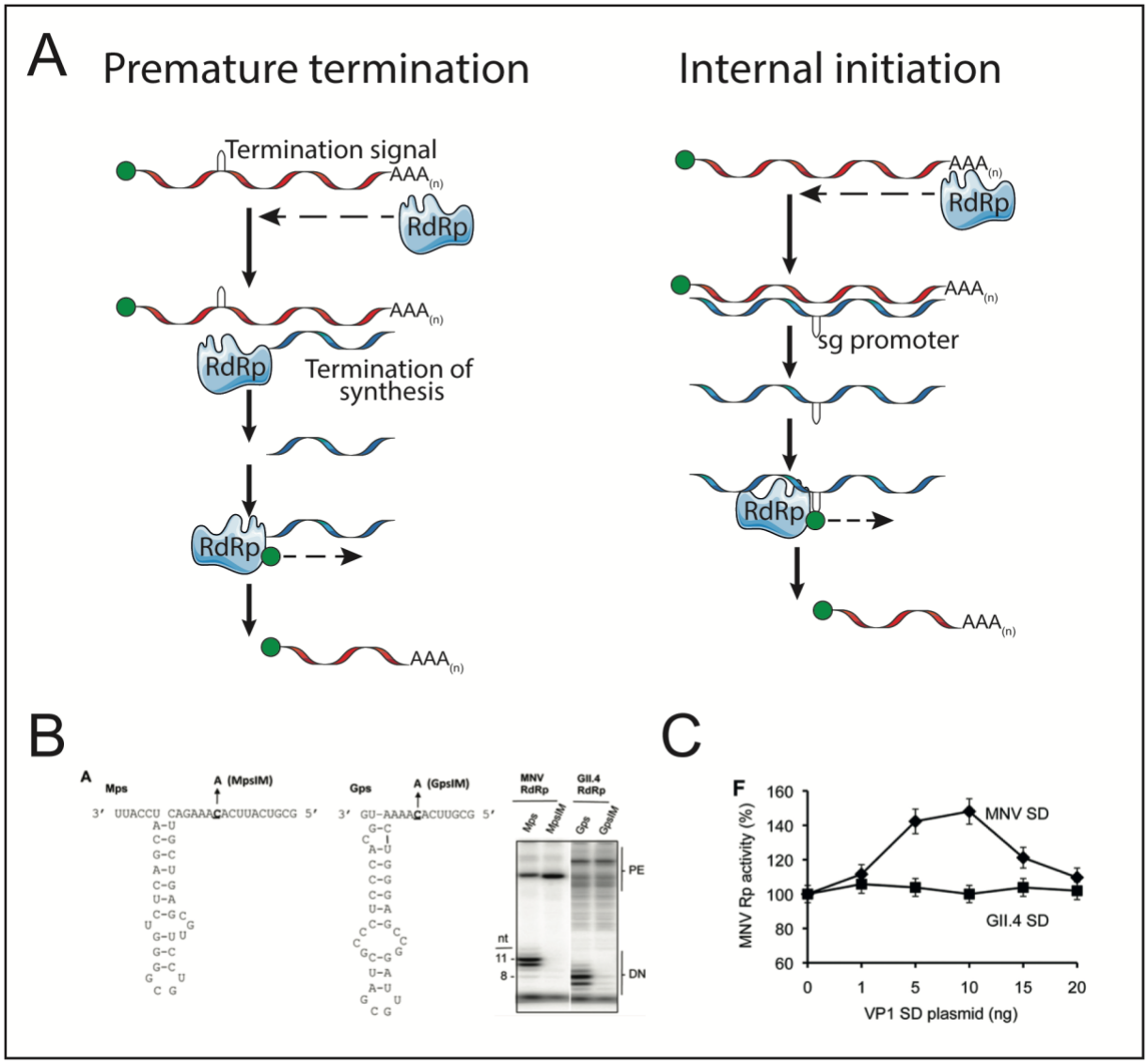

Figure 1.8 Regulation of genome replication. A) Two models of initiation of the norovirus subgenomic RNA. The premature termination model requires a termination signal on the positive-sense genomic RNA. RNA synthesis is terminated by this signal and the positive-sense subgenomic RNA is synthesised from the negative-sense, subgenomic RNA. The internal initiation model suggests a subgenomic promoter in the negative-sense genomic RNA. The positive-sense subgenomic RNA is synthesised through the RdRp recognising the sg promoter. B) Directed initiation of the synthesis of subgenomic RNA. Artificial RNA templates (proscripts) containing the conserved stem loops on the negative-sense genomic RNA of MNV-1 (Mps, left panel) and a GII.4 HuNoV (Gps, middle panel) can direct accurate initiations at the highlighted nucleotide, generating RNA products with defined length (Mps and Gps on right panel). C to A mutations of the initiation site nucleotide abolished the synthesis of DN products (MpsIM and GpsIM). This is adapted from (Lin et al., 2015). C) The norovirus capsid shell domain can enhance the RdRp activity in a genogroup-specific manner. The activity of the MNV RdRp can be

enhanced by the MNV SD in a concentration-dependent manner, but not by the GII.4 HuNoV SD, *vice versa*. This is adapted from (Subba-Reddy et al., 2012).

1.6.4 Assembly and exit

Not much is known about the details of the norovirus viral particle assembly and exit. Using different expression systems, recombinant norovirus virus and other caliciviruses VP1 can self-assemble into virus-like particles (VLPs) morphologically indifferent to the infectious viral particles, suggesting that VP1 is sufficient for virus assembly (Tresset et al., 2013a, Souza et al., 2013, Oka et al., 2009, Almanza et al., 2008, Yan et al., 2005, Han et al., 2005, Nicollier-Jamot et al., 2003, Lochridge and Hardy, 2003, Baric et al., 2002, Guo et al., 2001, Geissler et al., 1999, Green et al., 1997, Sibilia et al., 1995, Nagesha et al., 1995, Jiang et al., 1995, Jiang et al., 1992, Prasad et al., 1999, Prasad et al., 1994). The crystallisation of the Norwalk virus VP1 proposed a virus assembly model initiated by the subunits A, B and C forming A/B and C/C dimers. The pentameric A/B dimers then recruited C/C dimers around the 5-fold symmetry centre. The resulting intermediates assemble into capsids via binding at the 3-fold symmetry centres (Prasad et al., 1999). This model is supported by a biophysical characterisation of self-assembly kinetics which identified three main species: dimers, intermediates comprising of some 11 dimers, and icosahedral $T = 3$ capsids containing 90 dimers (Tresset et al., 2013b). Although the shell domain is sufficient for assembly, the P domain enhances the stability of viral particles (Bertolotti-Ciarlet et al., 2002). The minor capsid protein VP2 is not required for VLP self-assembly but can also enhance the capsid stability, and the 3’ UTR of the Norwalk subgenomic RNA can stimulate VP1 expression *in cis* (Bertolotti-Ciarlet et al., 2003). In norovirus capsid, a highly conserved Isoleucine (Ile52 of the Norwalk virus) at the N terminus of the shell domain is essential for the VP2 association (Vongpunsawad et al., 2013). Only a few copies of VP2 were packaged into capsids, although 90 icosahedrally equivalent Ile-

52 pairs are present in the capsids. The reason for this substoichiometry distribution is still unknown (Glass et al., 2000, Sosnovtsev and Green, 2000). Another unanswered question is the packaging mechanism of norovirus genome. Due to the absence of appropriate sized holes in the capsid structure, the viral genomic RNA is unlikely encapsidated after capsid assembly (Prasad et al., 1999). The norovirus VP2 is long-speculated to be involved in viral genomic RNA packaging due to its highly basic nature, yet it was only shown in FCV that VP2 is required for the production of infectious virions (Sosnovtsev et al., 2005).

The mechanistic details about norovirus exit is not fully understood, but MNV, together with RHDV and FCV, induces apoptosis during infection (Herod et al., 2014, Furman et al., 2009, Roberts et al., 2003, Alonso et al., 1998). Three putative caspase 3 cleavage sites were identified in MNV NS1/2, and two were found to be cleaved during MNV infection (Sosnovtsev et al., 2006). These cleavages separate NS1 from NS2. MNV infection is paralleled with down regulation of apoptosis inhibitor survivin (Bok et al., 2009), and VF1 was shown to delay apoptosis during MNV infection (McFadden et al., 2011). But it could be argued as extending the window for replication before the final apoptosis and exit stages.

1.6.5 Interactions with cellular factors and pathways

1.6.5.1 Translation control

Many small RNA viruses interact with cellular factors and pathways to facilitate productive virus replications (Nagy and Pogany, 2011). Several previous studies have started to fill in the knowledge gaps of host factors of norovirus replication.

The structured extremities of the norovirus genome provide binding sites for cellular proteins to regulate translation and/or to regulate between translation and viral genome

replication. Poly(A)-binding protein (PABP) was shown to bind the 3’ extremities of mammalian mRNA and can stimulate translation (Kahvejian et al., 2005). PABP also binds the 3’ UTR of Norwalk virus RNA, suggesting a possible role in norovirus translation or replication (Gutierrez-Escolano et al., 2003). Other RNA-binding proteins identified to bind the norovirus genome include but are not limited to poly(rC)-binding protein 2 (PCBP2), La, polypyrimidine tract-binding protein (PTB), heterogeneous nuclear ribonucleoprotein L (hnRNP L), hnRNP A1, and DDX3 (will be discussed in the next section). The functions of these factors in norovirus translation remain to be determined. RNA-binding factors also regulate translation and replication of other caliciviruses. For example, nucleolin promotes FCV viral RNA translation (Hernandez et al., 2016). Polypyrimidine tract binding protein (PTB) is a negative regulator of FCV translation but is required for efficient FCV replication. It is possible that PTB clears ribosomes from viral RNA at later stages of infection to stimulate viral genome replication (Karakasiliotis et al., 2010).

Because of the different requirements for translation initiation factors, norovirus can alter host cell translation without impacting viral translation. Our latest study of host cell proteome changes during MNV infection showed that MNV infection decouples host translation from transcription (Emmott et al., 2017). Transcripts of interferon-stimulated genes (ISGs) were induced during MNV infection, yet defects were observed in expression of the corresponding genes. The protease NS6 cleaves PABP, contributing to a global translation shut down (Figure 1.9A). In addition, apoptosis paralleled with MNV infection cleaves eIF4G, disassociating the 43S initiation complex from the eIF4F complex (Herod et al., 2014, Bok et al., 2009, Emmott et al., 2017). However, norovirus translation is not impacted, as VPg binds eIF3 directly to recruit the 43S preinitiation complex (Daughenbaugh et al., 2006, Daughenbaugh et al., 2003).

This distinct mechanism allows MNV to efficiently translate viral proteins, to suppress host cell translation and to subvert innate immune response at the same time.

Norovirus VPg also binds the cap-binding protein eIF4E, but eIF4E depletion has no impact on MNV translation (Chaudhry et al., 2006). Therefore, the functional significance of this interaction remains unknown. eIF4E binds the m7G cap at the 5' termini of eukaryotic mRNAs. Due to the limiting amount of functionally-available proteins, eIF4E is considered as the rate limiting step of cap-dependent translation initiation (Rau et al., 1996). The activity of eIF4E can be regulated by eIF4E binding proteins (4EBPs), or by phosphorylation at serine 209 position (Ueda et al., 2004).

It is still debatable whether eIF4E phosphorylation promotes or inhibits translation. Early biochemical studies showed that eIF4E phosphorylation increases the electrostatic repulsion against 5' cap which should inhibit cap-dependent translation initiation (Zuberek et al., 2004, Zuberek et al., 2003). However, the global translation efficiency is not altered in MEF cells with homozygous eIF4E S209A mutations, which abolish the phosphorylation. Instead, the translation of a subset of mRNAs is altered (Furic et al., 2010). Biochemical analysis of the pathways modified in these cells showed the mRNAs sensitive to eIF4E phosphorylation contain cap and a 5'-terminal hairpin structure (Korneeva et al., 2016). Therefore, it appears that eIF4E phosphorylation specifically regulate the translation of mRNAs with structured 5' UTR.

A previous study of our laboratory showed that MNV infection reprogrammes global translation by phosphorylating eIF4E, Figure 1.9B and (Royall et al., 2015). MNV infection activates the p38-MNK pathways to phosphorylate eIF4E, which alters the translation states (TS) of several cellular mRNAs. Also, MAP-interacting serine/threonine kinases (Mnks) also binds eIF4G to phosphorylate eIF4E (Shveygert et al., 2010). Together with the direct interaction between VPg and eIF4G, and the

cleavage of eIF4G at the late stage of MNV infection (Emmott et al., 2017), it is possible that VPg with cleaved eIF4G mediates translation control by bringing eIF4E and Mnk to a physical proximity.

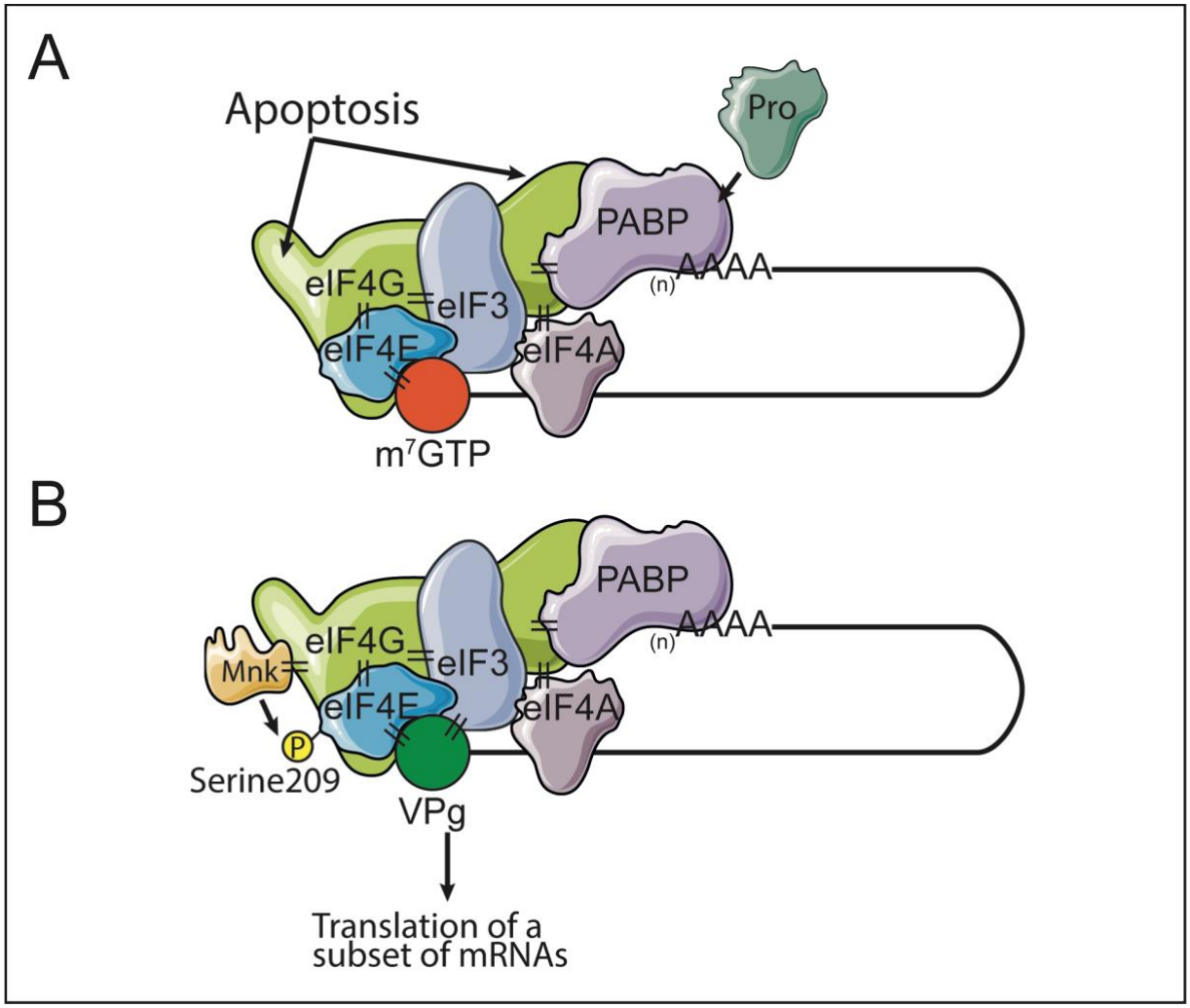

Figure 1.9 Translation control. A) The cleavage of eIF4G during MNV infection induced-apoptosis separates the N-terminus and the PABP-binding domain of eIF4G from the middle domain, which contains the binding sites for eIF3, eIF4A and eIF4E. Also, norovirus protease cleaves PABP. Adapted from (Emmott et al., 2017). B) Phosphorylation of eIF4E at Serine 209 by Mnk to facilitate the translation of a subset of mRNAs. Mnk binds eIF4G and phosphorylates eIF4E at serine 209, leading to enhanced translation of a subset of mRNAs, including NF-κB inhibitor IκBα.

1.6.5.2 Host factors for virus replication

The norovirus genome is known to be highly structured at both extremities, and studies have identified several host proteins binding to these regions (Vashist et al., 2012a, Bailey et al., 2010b, Sandoval-Jaime and Gutierrez-Escolano, 2009, Gutierrez-

Escolano et al., 2000). PCBP2, La, PTB, and hnRNP L interact with the Norwalk virus genome (Gutierrez-Escolano et al., 2003, Gutierrez-Escolano et al., 2000). Using riboproteomics, PCBP2, La, and PTB were also identified to bind to MNV genomic RNAs (Lopez-Manriquez et al., 2013, Vashist et al., 2012a, Bailey et al., 2010b). Additionally, RNA-binding proteins (RBPs) like DDX3 and hnRNP A1 are proviral host factors for MNV. PCBP2 and hnRNP A1 are required for circularisation and replication of the MNV genomic RNA (Lopez-Manriquez et al., 2013). RNA-inhibition (RNAi)-mediated knock down of the RBPs La, PTB and DDX3 negatively impacted MNV replication (Vashist et al., 2012a). MNV replication *in vivo* is attenuated when the polypyrimidine tract stem loop at the 3’ end of MNV genome is mutated, suggesting viral RNA-host protein interaction is important for norovirus pathogenesis (Bailey et al., 2010b). As for norovirus, PTB is also important for FCV replication, where PTB negatively regulates FCV translation to promote virus genome replication (Karakasiliotis et al., 2010, Karakasiliotis et al., 2006).

Interactions with cholesterol pathways have also been implicated in norovirus replication. In Norwalk virus RNA replicon-bearing cells cholesterol biosynthesis is down-regulated (Chang, 2009). Lowering cholesterol with simvastatin promotes HuNoV replication in a gnotobiotic pig model (Bui et al., 2013, Jung et al., 2012). The epidemiological correlation between the severity of HuNoV infections and the use of anti-cholesterol drugs suggests statins may be a risk factor for norovirus patients (Rondy et al., 2011). Although the gnotobiotic pig model of HuNoV infection suggested simvastatin antagonises innate immunity, the molecular details of how cholesterol biosynthesis affects norovirus replication is still unknown (Jung et al., 2012).

1.6.5.3 Interactions with host immune pathways

Subverting host cell immune responses is another important function of norovirus-host cell interactions. Innate immune responses are the first line of defence against acute norovirus infections. Norwalk virus RNA replication is sensitive to type I IFNs (Chang et al., 2006, Chang and George, 2007). Treating infected gnotobiotic pigs with IFN-α reduces HuNoV faecal shedding (Jung et al., 2012). Because of the established tissue culture system and the mouse model, there are more details of how MNV interacts with type I IFN responses. First of all, MNV replication is sensed by helicase melanoma differentiation-associated protein 5 (MDA-5), which recognises double stranded RNA (dsRNA) produced during replication (McCartney et al., 2008). The activation of MDA-5 leads to signalling cascades mediated by mitochondrial antiviral signalling protein (MAVS), followed by the activation of transcription factors IRF-3, IRF-7 and NF-κB (Seth et al., 2005). Accordingly, MDA-5-, IRF-3/IRF-7 double-, and IRF-3/IRF-5/IRF-7 triple knock-out enhance MNV replication *in vivo* (Lazear et al., 2013, Thackray et al., 2012, McCartney et al., 2008). The expression of interferon-stimulated genes (ISGs) are initiated by IFN-α and IFN-β binding to the type I IFN receptor IFNAR and signalled through the JAK-STAT pathways (Ivashkiv and Donlin, 2014). Genetic knock-out of the type I IFN receptor IFNAR promotes MNV pathogenesis in mice (Wobus et al., 2004, Karst et al., 2003). Similarly, STAT1 has been well documented to be crucial for controlling MNV infection (Niendorf et al., 2016, Karst et al., 2003, Wobus et al., 2004).

In response, MNV can antagonise innate immunity via virulence factor 1 (VF1), which is encoded by the MNV-specific ORF4 overlapping the ORF2 coding region (Thackray et al., 2007, Simmonds et al., 2008). VF1 localises to mitochondria and our preliminary results suggest that VF1 does not interact with any other MNV proteins (A. de

Rougemont, unpublished data). This observation supports an accessory role of VF1 to regulate host cellular innate immunity. Ectopic expression of VF1 reduces RIG-I-mediated immune sensing (Zhu et al., 2013). *In vitro*, the loss of VF1 expression enhances type I IFN induction, paralleled with a fitness cost for MNV replication. *In vivo*, MNV lacking VF1 (MNV-1^{VF1-}) is less virulent and the viral replication is attenuated (McFadden et al., 2011). However, this was observed in STAT1$^{-/-}$ mice, suggesting VF1 also interacts with cellular pathways other than STAT1 to promote MNV replication. To date a VF1 homologue protein is not found in HuNoV, at present it is unknown how HuNoV replication regulates host cell immunity. For other caliciviruses, the FCV p39 (NS3 in MNV) prevents IRF-3 activation (Yumiketa et al., 2016). Recently, MDA-5 and RIG-I show important roles in innate immune sensing in the early and the late stages of Tulane virus infection, respectively (Chhabra et al., 2017).

Between type I and type III innate immune responses, it is believed that type I IFN responses are important for preventing systemic infections while type III IFN responses have more significant roles in controlling epithelial cell infections (Pott et al., 2011, Pervolaraki et al., 2017). The interactions between MNV and type III IFN responses have also been investigated. IFN-λ is important for controlling faecal shedding and enteric viral titre during persistent MNV infections. IFN-λ treatment can cure persistent MNV infections in the absence of adaptive immune response, highlighting its potential as an antiviral drug (Baldridge et al., 2015). Moreover, a recent study confirmed the expression of IFN-λ receptor *Ifnlr1* on intestinal epithelial cells are critical for its antiviral functions, suggesting a possible role of intestinal epithelial cells in persistent MNV infection (Baldridge et al., 2017).

The norovirus interactions with adaptive immune responses have been characterised with attempts to understand the mechanisms of protective immunity against norovirus infections. Volunteer challenge studies of the early days have already noticed that mucosal immune responses do not protect individuals against re-challenge of HuNoV (Parrino et al., 1977, Johnson et al., 1990, Okhuysen et al., 1995). As in HuNoV, primary high dose infection of an acute MNV does not provide protection against homotypic re-challenge (Liu et al., 2009). Antibody, B cell, CD4 and CD8 T cells are important for the clearance of MNV infection (Chachu et al., 2008b, Chachu et al., 2008a) and the suboptimal CD8 T cell response contributes to MNV persistence (Tomov et al., 2013). However, the interaction between dendritic cells (DCs) and MNV is more complicated. DCs are permissive to MNV infection (Wobus et al., 2004). The depletion of DCs lead to increased intestinal replication of MNV, reduced viral dissemination and impaired antibody production (Elftman et al., 2013). Moreover, the depletion of IFNAR expression in DCs leads to a systemic MNV persistence despite enhanced adaptive immune responses, indicating that DCs may bridge the innate and adaptive immune responses (Nice et al., 2016).

In addition to host factors, two viral genes have been shown to contribute to norovirus persistence. First of all, a single amino acid mutation on NS1/2 of an acute MNV results in persistent infections and alteration of viral tropism (Nice et al., 2013). Secondly, the minor capsid protein VP2 regulates antigen presentation cell maturation and protective immune response induction (Zhu et al., 2013). The VP2 of a persistent MNV-3 antagonises B cell antigen presentation, leading to the impaired control of acute infections (Zhu et al., 2016). Together, immunity to control MNV infections require both mucosal and cellular immunity, and MNV antagonises both pathways to facilitate viral pathogenesis.

1.7 Antivirals and vaccines

1.7.1 Antivirals

Understanding the molecular details of norovirus life cycle has begun the intervention of norovirus antivirals.

Interferons (type I/II/III) have shown various antiviral activities against norovirus replication (Chang and George, 2007, Maloney et al., 2012, Nice et al., 2015). Compared with type I IFNs, IFN-λ treatment may have greater specificity and less adverse effects because its receptor is largely restricted to epithelial cells. Although it has not yet been used for treating chronic HuNoV infections, IFN-λ treatment cures persistent MNV infection without the need of adaptive immune response, highlighting the antiviral potential in treating chronic HuNoV infection in the immunocompromised (Nice et al., 2015).

Norovirus relies on efficient viral entry to initiate infection. Genetic knock-out of MNV receptor CD300 from MNV permissive cell line BV-2 confers resistance to infection (Orchard et al., 2016, Haga et al., 2016). Although HuNoV entry is not studied using a native virus, it is well known that HuNoV VLPs bind HBGAs (Marionneau et al., 2002). Porcine gastric mucin competitively inhibits the HuNoV VLP binding to intestinal epithelial cells (Tian et al., 2005), so as some small molecule inhibitors (Feng and Jiang, 2007). This has been proposed as a prophylactic means for outbreak control, but the utility is likely limited.

Due to its central role in norovirus replication, there is more information on the inhibitors of norovirus RdRp than that of any other norovirus proteins. Ribavirin is a nucleoside analogue widely used to treat RNA virus infections, including HCV (Te et al., 2007), RSV (Marcelin et al., 2014) and Lassa fever virus (Hadi et al., 2010). Ribavirin

efficiently inhibits MNV RdRp and increases quasispecies diversity (Arias et al., 2014, Julian et al., 2016, Alam et al., 2012). In a Norwalk virus RNA replicon, ribavirin inhibits the viral RNA replication and gene expression (Chang and George, 2007). Favipirivir is a nucleoside analogue which induces lethal mutagenesis during MNV replication *in vivo* (Jin et al., 2015, Arias et al., 2014, Rocha-Pereira et al., 2012b). Another potent RdRp inhibitor is 2'-C-Methyl-Cytidine (2CMC) (Rocha-Pereira et al., 2012a). In both MNV and Norwalk virus RNA replicon, 2CMC effectively inhibits the viral genome replication (Jin et al., 2015). The antiviral potential of 2CMC was further demonstrated by protecting the immunocompromised mice from lethal MNV infections, and preventing MNV transmission when used as a prophylactic treatment (Rocha-Pereira et al., 2015, Rocha-Pereira et al., 2013).

An increasingly important target of antiviral intervention is the viral protease NS6. Polyprotein processing is important for the functions of ORF1 non-structural proteins (Emmott et al., 2015). Inferred from the crystal structures NS6 is a highly conserved cysteine protease (Oka et al., 2007, Zeitler et al., 2006). Structure-guided inhibitors design and biochemical characterisation have yielded some candidate drugs (Galasiti Kankanamalage et al., 2017b, Galasiti Kankanamalage et al., 2017a, Weerawarna et al., 2016, Galasiti Kankanamalage et al., 2015, Deng et al., 2013, Tiew et al., 2011), however more *in vitro* and *in vivo* functional studies are needed to evaluate the efficacy of these inhibitors (Kim et al., 2015, Emmott et al., 2015, Qu et al., 2014).

1.7.2 Vaccines

The development of a HuNoV vaccine will particularly benefit the high-risk groups, including health care workers, military personnel, the young, the elderly and the immunocompromised. Also, food-borne outbreaks can be potentially reduced by vaccinating food handlers. During norovirus outbreaks, rapid ring vaccination can

establish herd immunity to aid disease control, especially when outbreaks occur in medical wards or in cruise ships. Currently there are no licensed vaccines for HuNoV. And due to the lack of a robust tissue culture system for HuNoV, vaccine designs are limited to inducing immunity against viral structural proteins with VLPs or P particles.

There are several other challenges for developing a HuNoV vaccine. First, immunity against HuNoV infections is short-lived and the immune correlates of HuNoV infections remain unknown. It was speculated that primary HuNoV challenges elicit short-term protection against homotypic re-challenge, yet the results were complicated by the lack of pre-challenge exposure history and the screening of genetic susceptible factors (Johnson et al., 1990, Atmar et al., 2008). Second, HuNoV sequences are very diverse, with nucleotide sequence identity as little as 50% (Vashist et al., 2009). Different HuNoV strains or variants display distinct antigenicity, resulting in difficulties for both antigen-based diagnostics and the development of a vaccine providing broad protection (Lindesmith et al., 2005). Therefore, a multivalent vaccine may be needed (LoBue et al., 2006, Malm et al., 2015). Moreover, as previously discussed, HuNoV especially the GII.4 variants evolve quickly. Therefore it is important and challenging to antigenically characterise a new variant whilst to produce a reformulated vaccine in due course (Ramani et al., 2014).

Several vaccine candidates are under clinical trials, all of which are based on either VLPs or P particles (Lucero et al., 2017). Recombinant HuNoV VLPs induce robust immune responses in mice, gnotobiotic pigs, chimpanzees, and human (Ball et al., 1998, Bok et al., 2011, Souza et al., 2007b, Ball et al., 1999). In a previous study volunteers were vaccinated using monovalent Norwalk virus VLPs and challenged with homotypic virus. Immunisation reduces the severity of symptoms and provides partial protection, yet 37% of the immunised group developed gastroenteritis (Atmar et al.,

2011). This study at least demonstrates the possibility of inducing protective immune responses with HuNoV VLPs.

1.7.3 Rational attenuation of norovirus

Live attenuated vaccines have been successfully developed for influenza virus (FluMist®) and other RNA viruses, including polio (OPV), measles, rotavirus, and yellow fever virus. Compared to inactivated or VLP-based vaccines, live attenuated vaccines induce more robust immunity because of multiple targets for immunisation (Lauring et al., 2010).

Empirically attenuated viruses were obtained by blind passage in different cell lines. Virus attenuation is mediated by adapting to new cellular environment (Lauring et al., 2010). However, the mechanism of attenuation is unknown, and immunisation in the natural host of the virus risks the reversion to a virulent strain. For example, oral polio vaccine (OPV) is known to accumulate mutations (Sahoo et al., 2017). Although OPV is more cost effective, inactivated polio vaccine (IPV) was chosen to eradicate poliomyelitis. Tissue culture adaptation was observed in MNV infection (Bailey et al., 2008, Zhu et al., 2015), the mechanism of which is unknown. Without a cell culture system it is not yet possible to produce a live attenuated HuNoV.

One possible strategy of rational attenuation is by generating replication defective viruses. This is achieved by targeting the viral genes or processes important for infection. This has been demonstrated in MNV that a genetic knock-out of VF1 attenuates MNV replication *in vivo* (McFadden et al., 2011). However, as there is no VF1 homologue in the HuNoV genome this approach cannot be applied for the attenuation of HuNoV. Therefore, targeting the processes of infection which are functionally conserved between HuNoV and MNV not only enables the identification of

important viral and host factors but also lay the basis for the development of a live attenuated HuNoV.

1.8 Project aims

The rational attenuation of norovirus depends on the establishment of a cell culture system for HuNoV and characterising the host and viral factors important for norovirus replication. Therefore, the first part of this thesis focused on establishing a cell culture system of HuNoV. Based on previous results, different cell lines were screened to identify permissive cells. Also, the inhibition of innate immune responses was applied to promote HuNoV replication in the tested cells.

Using MNV as the model system, the second and third parts of this thesis were focused on two aspects of norovirus life cycle: the role of eIF4E phosphorylation in norovirus translation control, and the role of the shell domain of the major capsid protein VP1 in regulating norovirus genome replication. Specifically, MNV elicits translational reprogramming by inducing eIF4E phosphorylation, which regulates innate immune response during virus infections (Royall et al., 2015, Herdy et al., 2012). This chapter aimed to determine whether eIF4E phosphorylation was involved in norovirus subverting the innate immune responses, and the impact on norovirus pathogenesis when eIF4E phosphorylation was inhibited.

The biological significance of the structural protein VP1 in regulating norovirus genome replication was also investigated. The norovirus VP1 modulates the RdRp activity in a genogroup-specific manner (Subba-Reddy et al., 2012). Mutagenesis was applied to identify the residues in VP1 important in mediating the VP1-RdRp interaction. The attenuation of MNV has been achieved by mutating the VP1 with an unknown

mechanism (Bailey et al., 2008). By understanding the VP1-RdRp interaction in norovirus pathogenesis rational attenuation could be achieved by targeting the non-structural function of this structural protein.

Chapter 2

Materials and methods

2.1 Cells and bacteria

Caco-2 cells were purchased from ECACC and maintained in Dulbecco's-modified Eagles Medium (DMEM, Sigma-Aldrich) with 10% heat-inactivated foetal bovine serum (FBS), 2 mM L-glutamine (L-Gln, Gibco), 1× MEM non-essential amino acids (NEAA, Gibco), and 100 SI units/ml penicillin and 100 μg/ml streptomycin (P/S). LS174T (WT and dominant negative TCF4) cells were kindly provided by Hans Clevers (Hubrecht Institute, Utrecht, Netherland). Cells were maintained in DMEM with 10% FBS, 2 mM L-Gln, and P/S. Every month cells were selected with blasticidine (10 μg/ml) for 1 week. In addition to blasticidin, the LS174T dnTCF4 were also selected with zeocin (500 μg/ml).

Human intestinal epithelial crypt (HIEC) cells were obtained from ECACC and maintained in OptiMEM with 5% Cellect Fetal Bovine Serum (MP Biomedicals), 0.01 M HEPES (Gibco), 1× Glutamax (Gibco), and 5 ng/ml epidermal growth factor (EGF).

BJAB cells were kindly provided by Paul Farrell (Imperial College London) and Stephanie Karst (University of Florida, Gainesville, USA). Cells were grown in RPMI1640 (Sigma-Aldrich) with 10% FBS, P/S and 2 mM L-Gln. The cell density was maintained between 2.5 × 10^5 and 2 × 10^6 /ml in 6-well plates.

Primary tonsillar cells were isolated based on previously published protocol (Cameron and Stent, 2001). Approximately 1 g tonsil tissues obtained from tonsillectomy was maintained in cold RPMI1640 media until use. The tissue was first divided into small pieces using scalpel and forceps, then digested with 25 μg/ml DNaseI and 2 mg/ml collagenase II at 37 ℃ using water bath. The digestion was stopped with 10 mM final

concentration of EDTA and ice-cold tissue culture media (RPMI1640 with 10% FBS, P/S and 2 mM L-Gln). Cells were filtered with 40 μm cell strainer and centrifuged at 300 × g for 10 minutes at 4 ℃. Cells were then counted and infected with HuNoV.

KBM7 cells were maintained in DMEM with 10% FBS, 2 mM L-Gln, and P/S. Cell density was maintained between 2.5 × 10^5 and 2 × 10^6 /ml.

Differentiation of peripheral blood-derived γδ T cells was performed and kindly provided by Marta Barisa (J. Anderson lab, University College London). 5 to 10 ml peripheral blood was obtained from two healthy donors with consent. Inactivated *E.coli* was used to expand γδ T cell population. Two to three weeks post differentiation cells were phenotyped and transported to Cambridge. On the same day cells were infected by HuNoV.

Primary duodenal organoids D196 and D353 were kindly provided by Matthias Zilbauer (University of Cambridge) and maintained by M. Hosmillo and Y. Goodfellow. Protocols for maintaining and differentiating intestinal organoids were based on previous publications with modifications (Sato et al., 2011). Organoids were maintained in 20 - 40 μl per well of Matrigel® Matrix (BD Bioscience) adherent to the bottom of 48-well or 24-well plates, with 250 μl proliferation media consisting of 50% v:v WNT-conditioned media (M. Hosmillo and Y. Goodfellow), 100 ng/ml mouse recombinant noggin (Peprotech), 1× B-27 supplement minus vitamin A (Gibco), 1.25 mM N-Acetyl-L-cysteine (Sigma-Aldrich), 10 mM Nicotinamide (Sigma-Aldrich), 50 ng/ml mouse recombinant EGF (Sigma-Aldrich), 2 μM A 83-01 (Tocris Bioscience), 3 μM SB 202190 (Sigma-Aldrich), 1 mg/ml Primocin (InvivoGen), and ADF+++ (advanced DMEM/F-12 containing 0.01 M HEPES, 1× Glutamax and P/S) to make up the volume. Every 48 hours 50% of the media was replaced by carefully removing the media without disturbing the Matrigel drops. Every 6-7 days the organoids were split

1:2 to 1:3. On the day of splitting, Matrigel stocks were kept on ice to remain in liquid phase, whilst cell culture plates were maintained at 37 ℃. Matrigel drops containing organoids were mixed with proliferation media and organoids were sheared into smaller clumps of 3 to 10 cells by pipetting up and down about 15 times with a crushed tip. Organoids suspension was then centrifuged at 800 × g for 5 minutes at 4 ℃. Proliferation media containing liquified Matrigel was removed by gentling pipetting without disturbing the organoids pellet. Tubes containing organoids were chilled on ice for 5 minutes before cold Matrigel was added and mixed. Matrigel containing organoids was then added at the bottom of cell culture plates without proliferation media. Plates were then returned to 37 ℃ upside-down for solidification of Matrigel, before adding fresh proliferation media and maintained at upright position. For differentiation of organoids, plates were coated with 40 μg/ml collagen (Sigma-Aldrich) in H_2O at 37 ℃ for 2 hours. Proliferation media was removed and organoids were washed twice with cold EDTA in PBS, trypsinised for 3.5 minutes and stopped with ADF+++ media containing 10% FBS. Organoids were pipetted up and down and passed through a 40 μm cell strainer. Cells were centrifuged at 800 × g for 5 minutes at 4 ℃ and resuspended in proliferation media with 10 μM Y-27632 (Sigma-Aldrich), and seeded at 1.7 × 10^4 cells per well of 48-well plates. On the second day, cell culture media was carefully removed and replaced with differentiation media containing ADF+++ with 100 ng/ml mouse recombinant noggin (Peprotech), 1× B-27 supplement minus vitamin A (Gibco), 1.25 mM N-Acetyl-L-cysteine (Sigma-Aldrich), 50 ng/ml mouse recombinant EGF (Sigma-Aldrich), 2 μM A 83-01 (Tocris Bioscience), and 1 mg/ml Primocin (InvivoGen). 10 μM Y-27632 (Sigma-Aldrich) was initially added in addition to differentiation media, and was removed as soon as a confluent monolayer was

observed. Differentiation media was replaced every 48 hours until infection (usually 5 days post seeding). After infection cells were maintained in differentiation media.

Baby Hamster Kidney (BHK) cells engineered to express T7 RNA polymerase (BSR-T7 cells) were obtained from Karl-Klaus Conzelmann (Ludwid Maximillians University, Munich, Germany) and maintained in DMEM containing 10% FBS, 2 mM L-Gln, P/S, and 0.5 mg/ml G418 (InvivoGen). HEK293T and Raw264.7 cells were maintained in DMEM supplemented with 10% FBS, 2 mM L-Gln and P/S. Murine microglial BV-2 cell line was provided by Jennifer Pocock (University College London), maintained in DMEM with 10% FBS, 2 mM L-Gln, and P/S.

Enteric bacteria *Enterobacter cloacae* was obtained from ECACC. The bacteria were revived in LB media and grown overnight at 37 ℃. Bacteria was then pelleted, washed with PBS, followed by heating at 70 ℃ for 40 minutes and mixed every 10 minutes. Serially diluted, pre-inactivated bacteria culture was plated and incubated at 37 ℃ overnight. Live bacterial density of the inactivated stock was calculated by counting the colonies and extrapolating to undiluted stock.

2.2 Plasmids

The second-generation lentiviral packaging plasmids psPAX2, pMD2.G, and lentiviral plasmids pdl-MCS, pdl-BVDV NPro, and pdl-PIV5 V were all provided by F. Sorgeloos. For cloning of FUT2 lentiviral plasmid, cDNA was synthesised from total RNA (digested with DNaseI and purified) from the following cell lines: Caco-2, HT-29 and BJAB. FUT2 cDNA was sub-cloned into a pTM900 plasmid (provided by F. Sorgeloos). A secretor and a non-secretor FUT2 clones were selected.

HuNoV plasmids, pUC57: GII.4-flc, pUC57: GII.4-F/S and pUC57: GII.6-flc were previously generated (I. Goodfellow and L. Thorne, unpublished data). Plasmid pUC57: GII.6-F/S was generated by introducing a +2 frame shift at the active site of the RdRp coding sequence.

The full-length cDNA clones of MNV-1 (pT7: MNV 3’ Rz) and MNV-3 (pT7: MNV-3 3’ Rz) were reported previously with accession numbers of DQ285629.1 and JQ658375.1, respectively (Chaudhry et al., 2007, Arias et al., 2012). Derivative mutants of these two constructs were generated by overlap-extension PCR and restriction digestion. Specifically, chimeric MNV-1s or MNV-3s with combinations of SD flexible loops mutated to HuNoV VP1 sequences were named after the according loops mutated. For example, MNV-1 L1 indicates the loop 1 of SD was mutated to HuNoV sequence by mutating Threonine 74 into Alanine (Table 5.1).

To generate expression constructs for LUMIER assay, first of all, VP1 cDNA sequences were amplified by PCR from chimeric MNV-1 infectious clones. A second round of PCR was performed to add recombination sites to PCR products. BP reactions were then performed using purified PCR product and pDONR227 entry clone plasmid following manufacturer’s instructions (ThermoFisher). Following recombination, plasmids were transformed into *ccd*B survival competent cells. Positive clones were selected and VP1 coding regions were sequence verified. LR reactions were then performed to generate VP1 expression constructs in pcDNA3-GW-RL and pT-Rex-Dest30-PA backbones. Expression constructs of RdRp, positive controls (pcDNA3-RL-jun and pT-Rex-Dest30-PA) and negative control pT-Rex-Dest30-PA-PA were provided by A. de Rougemont. pEGFP-RdRp was provided by S. Vashist.

MNV shell domain expression constructs were generated by PCR amplifying WT and L1,7 SD cDNA from infectious clones into pTriEx 1.1 plasmid. Positive clones after ligation and transformation were sequence verified.

2.3 Reverse genetics

DNA-based reverse genetics was reported previously (Chaudhry et al., 2007, Arias et al., 2012). Briefly, BSR-T7 cells were seeded the day before transfection to be more than 90% confluent on the day of transfection. Then cells were infected by fowlpox virus expressing T7 RNA polymerase (FPV-T7) at an MOI of 0.5-1 PFU per cell for 2 hours at 37 ℃. 1 μg of plasmids containing MNV cDNA clones were mixed with 4 μl of Lipofectamine®2000 (ThermoFisher Scientific) in 200 μl OptiMEM (Gibco) for 15 minutes at room temperature. After incubation, cells were washed once and replaced with 3 ml antibiotic-free media. Then transfection mix was added to the cells drop-wise. After 24-48 hours post transfection, cells were freeze-thawed at -80 ℃ and titrated by 50% tissue culture infectious dose ($TCID_{50}$). Total cellular protein was also harvested by lysing cells using radio immunoprecipitation assay (RIPA) buffer with 1 × protease inhibitors cocktail (Merck). 10 μg total cellular protein or 5 μl eluate from immunoprecipitation was analysed for SDS-polyacrylamide gel electrophoresis (SDS-PAGE) analysis.

2.4 Immunofluorescence microscopy

For immunostaining of differentiated organoids, cells were seeded in 24-well trans-well plates (Corning), harvested by fixing with 4% paraformaldehyde (PFA) in PBS at room temperature for 15 minutes. Then cells were washed once with PBS, quenched using 100 mM glycine at room temperature for 5 minutes and permeabilised with 0.2% Triton ™ X-100 in PBS at room temperature for 5 minutes. Cells were then blocked with 0.1% Tween 20 in PBS (PBST) containing 1% normal goat serum (Sigma-Aldrich), 1%

bovine serum albumin (BSA) at room temperature for 1 hour before primary antibody was added. After 1 hour incubation, cells were washed 3 times with PBST before 1 hour incubation with secondary antibody. Following another 3 washes with PBST and once with 15mM Sodium Azide in PBS, trans-well membranes were carefully removed by a scalpel and mounted on coverslips with DAPI/MOWIOL. The apical sides of membrane should be in contact with coverslips. The coverslips were then mounted on glass slides and dried overnight at 4 ℃. Imaging of BMDM, Raw264.7 and BV-2 cells were performed similarly as of organoids, except that cells were seeded on coverslips instead of in trans-wells. All microscopy images were obtained using a Leica TCS SP5 confocal microscopy at NIHR Cambridge BRC Cell Phenotyping Hub.

2.5 Total RNA extraction

Total RNA from cells or viruses was extracted following manufacturer’s instruction (GenElute Mammalian total RNA mini-prep kit, Sigma-Aldrich) and eluted in 50 μl MilliQ H_2O. For RT-qPCR of *Ifnb*, total RNA was digested with DNaseI for 15 minutes, purified and eluted in 50 μl MilliQ H_2O before RT. For faecal samples, stool pellets were weighted and resuspended in PBS to a final concentration of 100 mg faeces per ml PBS. After homogenisation and a 5-minute centrifugation using a table top centrifuge, 100 μl of supernatant was used for RNA extraction. Animal tissue samples were retrieved from -80 ℃ and thawed on ice, about 200 mg of tissues were added to 500 μl RNA lysis buffer with 500 μl silicon beads. Tissues were homogenised and 250 μl lysate was used for RNA extraction.

2.6 Statistical analysis

Unless indicated, all experiments were performed with at least three biological replicates, and representative experimental data was shown. Statistical analysis was performed using GraphPad Prism7.0.

2.7 HuNoV-specific methods

2.7.1 Purification of HuNoV

HuNoV-positive faecal samples (about 1 g per sample) were resuspended in PBS at 1:10 w:v. After vortex, the insolubles were centrifuged at 4000 RPM for 10 minutes at 4 ℃. Polyethylene Glyco (PEG) 3000 and NaCl were then added to the supernatant at 10% w:v and 150mM, respectively. After overnight incubation at 4 ℃, precipitated HuNoV was centrifuged using a high-speed centrifuge at 15000 RPM for 10 minutes at 4 ℃. The pellet was resuspended using cold PBS and slowly overlaid onto 30% w:v sucrose cushion in PBS. The virus was then centrifuged using Beckman ultracentrifuge with SW55Ti rotor at 45 000 RPM for 18 hours at 4 ℃. The pellet was then resuspended in PBS overnight at 4 ℃ with gentle swirling every a few hours. Insolubles were removed by centrifuge at maximum speed for 5 minutes at 4 ℃. The purified HuNoV was then aliquoted and stored at -80 ℃.

HuNoV CDC4 and CDC14 were kindly provided by Stephanie Karst (University of Florida, Gainesville, USA). HuNoV A42DD was purified and provided by M. Hosmillo.

To generate concentrated virus stocks from reverse genetics, 48 hours post transfection BSR-T7 cells were freeze-thawed to release viruses. Cell debris was removed by centrifuging the lysates at 4 000 RPM for 5 minutes at 4 ℃. The supernatant (about 30 ml in total for each virus) was then gently overlaid on top of 5 ml 30% sucrose in PBS. Ultracentrifugation was performed at 25 000 RPM for 2 hours at 4 ℃. The supernatant was then removed and 200 μl PBS was added to each tube with gentle swirl overnight at 4 ℃. The insolubles were removed by centrifugation at maximal speed for 5 minutes at 4 ℃. The pellet was washed once more with 100 μl ice-cold PBS and the supernatant was combined with the first extraction. Together, 300 μl of 100× concentrated virus was generated per construct. Viruses were then aliquoted and stored at -80 ℃ until use.

2.7.2 Genotyping PCR for HuNoV

The norovirus genotyping PCR was performed as published (Kojima et al., 2002). Total RNA was extracted from 1 aliquot of purified HuNoV sample using GenElute™ mammalian total RNA miniprep kit and eluted in 50 μl RNase-free water. 2.5 μl RNA was used in a total volume of 25 μl reverse transcription (RT) reaction using M-MLV RT (Promega) following manufacturer's instruction. The RT reaction was performed at 42 ℃ for 1 hour and stopped by 85 ℃ for 5 minutes. RT reactions without the reverse transcriptase were used as the negative controls.

After the RT reaction, genotyping PCRs were set up using 5 μl of cDNA in a total volume of 50 μl reaction. G1SKF/G1SKR and G2SKF/G2SKR were used as the primers for PCR reactions of genogroups 1 and 2, respectively (Kojima et al., 2002). After PCR, samples were run on 2% agarose gel using TBE buffer. Samples with clear

PCR products at correct sizes were column purified and sequenced using corresponding PCR primers. The genotype was then assigned using the norovirus genotyping tool (http://www.rivm.nl/mpf/typingtool/norovirus/).

2.7.3 HuNoV RT-qPCR

The reverse transcription - real time quantitative PCR (RT-qPCR) of HuNoV was performed as previously published (Kageyama et al., 2003). Briefly, 2.5 μl RNA or 1:10 serially-diluted *in vitro*-transcribed RNA standard was used in a total volume of 20 μl RT reaction using M-MLV RT (Promega) following manufacturer's instruction. The RT reaction was performed at 42 ℃ for 1 hour and stopped by 85 ℃ for 5 minutes. 5 μl of 1:2 diluted cDNA was used in a 20 μl Real time PCR (qPCR) reaction in conjunction with 400 nM each primer, 100 nM Taqman probe and 1× PrecisionPLUS qPCR master mix (PrimerDesign). Thermal conditions for qPCR were as followed: 95 ℃ for 8 minutes, 50 cycles of 95 ℃ for 10 seconds and 60 ℃ for 1 minute. Signals were detected at the end of each 60 ℃ incubation.

Relative qPCR was performed with 5 μl 1:2 diluted cDNA, 100 nM of each primer and 1× SYBR Green I qPCR Core kit (Eurogentec). Thermal conditions were as followed: 55 ℃ for 2 minutes, 95 ℃ for 10 minutes, 40 cycles of 95 ℃ for 15 seconds and 60 ℃ for 1 minute. A melt curve analysis was performed immediately after PCR cycles. Gene expression was calculated using the ΔΔCt method (Rao et al., 2013).

2.7.4 Lentivirus production and transduction

The production of recombinant lentivirus encoding innate immune antagonists was performed following the second-generation lentivirus packaging protocol (Naldini et al.,

1996). HEK293T cells were seeded at 5 × 10^6 cells per 10 cm dish in antibiotic-free media. The following plasmids were first mixed in 500 µl OptiMEM media: 6 µg of pxPAX2 packaging plasmid, 6 µg of lentiviral vector, 3 µg of pMD2.G VSV-G envelop plasmid. Then 45 µl of Lipofectamine®2000 in 500 µl OptiMEM was added and mixed. After a 10-minute incubation at room temperature, the transfection mix was added to 293T cells drop-wise. In addition to lentiviruses encoding BVDV NPro and PIV5 V, empty vector (MCS) and EGFP lentiviruses were also produced in parallel. At 24 and 48 hours post transfection, supernatants were carefully harvested and replaced with 10 ml of warm media. Cell debris from the combined supernatant was removed by centrifugation at 4000 RPM for 5 minutes at 4 ℃. Then the supernatant was slowly overlaid on top of 5 ml of 30% sucrose in PBS. Lentivirus was centrifuged at 25 000 RPM for 2 hours at 4 ℃. The pellet was resuspended in 200 µl PBS at 4 ℃ overnight. The insolubles were removed by centrifugation at maximal speed for 5 minutes at 4 ℃. The pellet was washed once with 100 µl PBS and the supernatant was combined. The concentrated lentivirus was aliquoted and stored at -80 ℃.

To titrate lentivirus, 1:5 serially diluted, unconcentrated (1×) and concentrated (100×) lentiviruses were added to 5 × 10^4 HEK293T cells and incubated at 37 ℃ for 3 days. Cells were then fixed and analysed by FACS analysis. The infectious unit (IU) was calculated as published (Kutner et al., 2009).

For transduction of cell lines, adherent cells were seeded at 5 x 10^4 cells per well of 24-well plate and infected with 5 µl of concentrated lentiviruses. Three days post transduction, the green fluorescence was confirmed in the LV-EGFP-transduced cells. Then the cell media was replaced by puromycin-containing media. After 3 passages of

selection, no live cells were observed in the non-transduced well and selected, transduced cells were expanded used for experiments

2.7.5 HuNoV infection of adherent cells

For infection of adherent cells, 0.5-1 × 10^5 cells were seeded per well of 24-well plate. HuNoV were added to cells in a total volume of 250 - 300 µl. The cells were incubated at 37 ℃ for 1 hour. The cells were then washed twice and replaced with 500 µl complete media. At each time post infection, the cells were scraped off the plate and mixed by pipetting up and down. Then 100 µl of cell/media mixture was used for RNA extraction. HuNoV RNA was then determined by RT-qPCR.

2.7.6 HuNoV infection of suspension cells

The infection of suspension cells was adapted from previously published protocols (Jones et al., 2015, Jones et al., 2014). Briefly, in 100 µl of total volume, 1.3 × 10^5 cells were incubated with 10 µl of 1:10 diluted HuNoV at 37 ℃ for 2 hours. In experiments using binding factors (HBGA or enteric bacteria), HuNoV was pre-incubated with stimulating factors at 37 ℃ for 1 hour before cells were added to the virus mix. After incubation, cells were centrifuged at 750 × g for 7.5 minutes and resuspended in 100 µl media. The cell suspension was then divided evenly and added to 48-well plates containing 950 µl media. At each time point, 500 µl cell suspension was used for RNA extraction by Trizol reagent (Invitrogen).

2.7.7 Differentiation of LS174T cells

The differentiation of LS174T dnTCF4 cells into goblet cell-like phenotype was previously published (van de Wetering et al., 2002). LS174T cells (wild type or dnTCF4)

were first selected with zlasticidin with or without zeocin for 1 week. Then cells were seeded at 5 × 10^5 cells/well for 6-well plate and 5 × 10^4 for 24-well plate. In addition to blasticidin and zeocin, doxycycline was added at 5 μg/ml for induction of dnTCF4. For cell growth analysis, cells were fixed on day 5 post differentiation and stained with toluidine blue. Total cellular RNA was extracted from samples of days 0, 1 and 5 post differentiation and gene expression was determined by RT-qPCR. Expression of *MUC2* was normalised to housekeeping gene *ACTB*. For HuNoV infection, cells were infected on day 1 post differentiation and samples were harvested at the indicated time points.

2.8 MNV-specific methods

2.8.1 MNV RT-qPCR

5 μl eluted total RNA was used for RT reaction using MMLV-RT following manufacturer's instruction. After RT, cDNA was diluted 1:2 using RNase-free H_2O and 5 μl diluted cDNA was used for qPCR as previously reported (Kitajima et al., 2010). Relative qPCR was performed as for human gene qPCR.

2.8.2 $TCID_{50}$

Viral 50% tissue culture infectious dose ($TCID_{50}$) was performed as published (Hwang et al., 2014). $TCID_{50}$ by antigen were performed as follows: standard $TCID_{50}$ assays were set up using Raw264.7 cells and were incubated at 37 ℃ for 5 days. Wells displaying cytopathic effect (CPE) were recorded and $TCID_{50}$ by CPE were calculated. The tissue culture media was then carefully removed by multichannel pipette and

remaining cells were washed once with PBS, fixed using 4% PFA, quenched using 100 mM Glycine (pH3) and permeabilised with 0.2% Triton X-100. Cells were then blocked with blocking buffer for 1 hour before primary antibody (rabbit anti-NS3 1:1000 diluted in blocking buffer) was added. Cells were washed 3 times with 0.1% PBST after 1 hour incubation, before another 1 hour incubation with secondary antibody (Alexa Fluor 568 goat anti rabbit, ThermoFisher). 3 washes with 0.1% PBST were performed before keeping cells in 15mM sodium azide for visualisation. Wells with cells only and processed the same way as wells containing diluted viruses were first visualised under fluorescent microscope for evaluation of background staining. Then the wells with positive staining were recorded and the $TCID_{50}$ by antigen was calculated the same way as $TCID_{50}$ by CPE.

2.8.3 Virus stock generation

10 ml of virus from recovery was added to one T150 BV-2 cells and incubated at 37 ℃ for 1 hour. After infection, the inoculum was replaced with fresh media and cells were maintained at 37 ℃ until CPE was observed. Progeny viruses were released by freeze-thawing lysates and cell debris was removed by centrifugation at 4000 RPM for 10 minutes at 4 ℃. Virus was passed through 0.2 μm filter and aliquoted. Titres of virus stocks were determined by $TCID_{50}$.

2.8.4 Viral growth kinetics analysis

For growth kinetics analysis, BV-2 cells were infected by MNV-1 or MNV-3 at an MOI of 0.05 or 5 $TCID_{50}$ per cell at 37 ℃ for 1 hour. The end of incubation was determined as 0 hour post infection (hpi). Then cells were washed twice with warm tissue culture media, resuspended to 5 x 10^5 cells/ml and plated in 96-well plates for titration and in

24-well plates for RNA extraction. At each time point, titration plates were frozen at -80 ℃ to release viruses from cells, tissue culture media was removed from RNA plates and the total cellular RNA was extracted.

2.8.5 Ethics

Tonsil tissue was donated anonymously with consent. All HuNoV stool samples were obtained as leftover from diagnosis.

Studies with mice were performed in the Department of Pathology Biological Support Unit (PCD 80/2802) after ethical review by the University of Cambridge Review Panel and subsequent approval by the UK Home Office (PPL70/7689). All animal procedures and care conformed strictly to the UK Home Office Guidelines under The Animals (Scientific Procedures) Act 1986.

2.8.6 Animal experiment

A breeding colony of mice containing heterozygous eIF4E S209A mutation (KI) was provided by Christos Gkogkas (University of Edinburgh). Sex and age-matched littermate were used for infections. Before challenge, tail blood was sampled and the body weight of each animal was recorded. 1000 $TCID_{50}$ (low dose) or 100 000 $TCID_{50}$ (high dose) was inoculated peroral per mouse. Body weight changes were recorded and faecal samples were collected on the days indicated in each figure. At the end of experiment, mice were sacrificed and the organs were preserved in RNAlater solution at -80 ℃ until use.

For primary challenge, 5-week old C57BL6/J mice were allocated 5 mice per group and inoculated peroral with 2.4 x 10^4 $TCID_{50}$ by antigen (equivalent to 10000 $TCID_{50}$ determined by CPE) of MNV-3 viruses in a total volume of 100 μl. On the days

indicated faecal samples were directly collected from each mouse. In order to measure production of MNV-specific serum IgG, peripheral blood samples were collected by tail bleeding. Serum samples were obtained by spinning down the blood samples at maximal speed for 5 minutes using a table top centrifuge. Re-challenge experiment was performed by inoculating mice with 1000 $TCID_{50}$ MNV-3. Faecal and serum samples were collected as above.

2.8.7 eIF4E genotyping PCR

The eIF4E genotyping PCR was reported previously (Furic et al., 2010). Ear biopsies were obtained from 2 to 4 week-old pups. 50 μl of solution 1 (25 mM NaOH, 0.2 mM EDTA) were added to the biopsies and boiled at 99 ℃ for 20 minutes. The reaction was neutralised by adding 50 μl of solution 2 (40 mM Tris-HCl), then vortex for 15 seconds. 2 μl of the supernatant DNA was used for a genotyping PCR of 25 μl in volume, consisting of 1× Taq buffer, 1.5 mM $MgCl_2$, 0.2 mM dNTPs, 1 μM of each primer, and 1.25 U Taq polymerase (Invitrogen). The thermal cycling conditions are as followed: 1) 94 ℃ for 4 minutes. 2) 35 cycles of 94 ℃ for 45 seconds, 58 ℃ for 45 seconds, and 72 ℃ for 1 minute and 15 seconds. 3) 72 ℃ for 4 minutes. 5 μl of the PCR product was resolved on 2% agarose gel using TBE buffer. The PCR product from the ear biopsies of the first heterozygous breeding cage were used as the genotype markers.

2.8.8 Primary BMDM differentiation

Differentiation of BMDMs from primary bone marrow cells was reported previously (Trouplin et al., 2013). Briefly, mice were sacrificed using a schedule 1 method, and the femur bones were isolated from both thighs. The bones were kept in macrophage

complete media DMEM on ice during transport. The remaining tissues associated with the bones were removed using clean tissue paper. The bones were then washed once with 1× PBS, sterilised with 70% ethanol, and washed once more with 1× PBS. Scalpels were then used to cut open the bones and cells were flushed out with cold DMEM. Cells were passed through 40 μm cell strainer and centrifuged at 500 × g for 5 minutes at 4 ℃. Cells were then seeded at 0.5 - 1 × 10^7 cells per 150 mm untreated dishes, in BMDM differentiation media (macrophage complete media with 10% CMG-14 conditioned media). Cell culture media was replaced every other day and cells were used on day 7 post differentiation.

2.8.9 Purification of MNV

10 T150 flasks of BV-2 cells were infected by MNV at MOI = 0.01 $TCID_{50}$/cell until CPE was observed. Cells were freeze-thawed and cell debris was removed by centrifugation at 4000 RPM for 10 minutes at 4 ℃. Supernatant was then overlaid on 5 ml of 30% sucrose in PBS and centrifuged using a ST32Ti rotor at 25 000 RPM for 2 hours at 4 ℃. Pellets were resuspended in PBS and stored at -80 ℃. The titres of concentrated virus stocks were determined by thawing one aliquot of each virus and titrated by $TCID_{50}$.

2.8.10 Cell stimulation

BMDM or Raw264.7 cells were seeded at 1 × 10^5 cells/well of 48-well plates and were transfected with different amounts of poly (I:C) using FuGENE® HD following manufacturer’s recommendation. IFN-β was pre-mixed with cell culture media and replaced the seeding media. At 12 hours post transfection, cell media was removed and total RNA was extracted. RNA was then digested with DNaseI and purified.

Relative gene expressions were determined by RT-qPCR and calculated by the ΔΔCt method (Rao et al., 2013).

2.8.11 ELISA

ELISA for detecting MNV-specific serum IgG in peripheral blood from mouse was reported previously (Hwang et al., 2014, Wobus et al., 2004). Briefly, MNV3 VLP, kindly provided by Stephanie Karst (University of Florida, Gainsville, USA) was diluted 1:100 using carbonate buffer at pH 9.6 and 50 μl VLP was used per well to coat the Nunc MaxiSorp™ 96-well plate overnight at 4 ℃. Serum collected from mice were used at 1:100 dilution in 50 μl total volume. The reactions were developed by adding 100 μl 1-Step™ Turbo TMB-ELISA Substrate Solution (Life Technologies) or 50 μl 1× TMB solution (eBioscience) and stopped by adding equal volume of 1N sulphuric acid solution. The absorbance at 450nm were read and normalised absorbance were calculated by subtracting the mean absorbance of wells without primary antibody. The cutoff of positive results was determined as the mean + 3 × standard deviation of mock serum absorbance.

2.8.12 Thermal inactivation assay

MNV virus stocks were diluted 1:10 in PBS and kept on ice until the beginning of incubation. 100 μl diluted virus was added to 96-well PCR plate (Axygen) and incubated at 60 ℃ for 3 minutes before keeping on ice immediately. Then 25 μl enzyme mix with or without RNaseA (final concentration 1 mg/ml) diluted in PBS was added to each well. The reaction mix was then incubated at 37 ℃ for 15 minutes before keeping on ice again. 25 μl reaction mix was used for $TCID_{50}$ and the rest was used for RNA extraction. For control of RNaseA digestion, 10^8 genome equivalent (gEq)

of *in vitro* transcribed MNV3 RNA was diluted with PBS and processed the same way as other viruses. The unprocessed samples maintained on ice were used as the initial titres or vRNA. For each virus and each treatment, the experiment was repeated 3 times and one-way ANOVA was used for statistical analysis.

2.8.13 Immunoprecipitation assay

The immunoprecipitation protocol was published previously (Emmott and Goodfellow, 2014). Briefly, 293T cells were co-transfected with pEGFP-RdRp and pCDNA3-RL-VP1 plasmids. Cells were harvested at 24 hours post transfection and lysed with GFP lysis buffer. After lysis on ice for 30 minutes, total lysates were centrifuged at maximal speed for 10 minutes at 4 ℃, and the protein concentration of the total soluble fraction was measured by BCA assay (Pierce). The input was then normalised using GFP dilution buffer. The anti-GFP agarose was prepared by washing 25 μl agarose per reaction 3 times with 1 ml GFP dilution buffer. Then the anti-GFP agarose was mixed with roughly 1:5-diluted total cell lysate at 4 ℃ rotating overnight. After binding, the agarose was centrifuged at 2500 x g for 5 minutes at 4 ℃ and the unbound fraction was carefully removed. The agarose was further washed 3 times with GFP dilution buffer before elution with 50 μl 2X loading buffer by heating at 95 ℃ for 5 minutes. 10 μl input and 5 μl eluate were analysed on 12.5% polyacrylamide gel for SDS-PAGE and western blot analysis.

2.8.14 RNA synthesis analysis

RdRp assays were performed as previously described (Yunus et al., 2015, Lin et al., 2015) with minor modifications. All RNAs used in this study were chemically synthesized (Thermo Scientific). The MNV proscript was designed based on MNV

CW1 isolate (DQ285629) nucleotides 5012 to 5059. The RNA contains three non-viral nucleotides (GCG) at their 5′ termini to allow the incorporation of radiolabelled [α-^{32}P]CTP during RNA synthesis *in vitro*. The RNA synthesis reactions were of 20 μl containing 20 mM sodium glutamate (pH 8.2), 12.5 mM dithiothreitol (DTT), 4 mM $MgCl_2$, 1 mM $MnCl_2$, 0.5% Triton X-100 (v/v), 0.05 mM GTP, 0.05 mM ATP and 0.01 mM UTP, 33.3 nM [α-^{32}P]CTP (MP Biomedicals), 50 nM of template RNA and 250 nM of recombinant RdRp. The reactions were incubated at 30 ℃ for 2 hours, and then stopped by the addition of EDTA (pH 8.0) to a final concentration of 10 mM. RNA products were directly analysed with a 24% polyacrylamide gel containing 7.5 M urea. The radiolabelled RNA products were visualized and quantified by using a PhosphoImager (Typhoon 9210; Amersham Biosciences) and ImageQuant software. Statistical analysis was performed using excel *t*-test.

2.8.15 Bioinformatic analysis

Protein sequence comparison between GII.4 HuNoV and MNV VP1 was performed by searching the BLAST server for full length VP1 sequence using the reference sequences of GII.4 HuNoV VP1 (GenBank accession number ABG49509.1) and MNV VP1 (GenBank accession number ABB90154.1)(Johnson et al., 2008). For HuNoV and MNV, the organisms were restricted to norovirus GII.4 (taxid:489821) and norovirus GV (taxid:1246677), respectively. Default parameters were used except that the entries length searched were restricted to between 500 to 600 residues, and maximal target sequences were limited to 1000. Sequences were aligned using ClustalOmega and redundant sequences were removed using the CD-HIT server (Sievers et al., 2011, Fu et al., 2012). Conservations were represented by the WebLogo server (Crooks et al., 2004).

2.8.16 LUMIER

LUMIER analysis was performed as previously described (Vashist et al., 2015). Briefly, 293T cells were seeded in 96-well plates. 80-90% confluent cells were transfected with 60ng of each of pcDNA3-GW-RL and pT-Rex-Dest30-PA plasmids with 0.3 μl Lipofectamine®2000 and 30 μl OptiMEM (LifeTechnologies). Experiments were performed in quadruplicate. Plasmids encoding c-jun and fos were used as positive control. Co-transfection of pcDNA3-GW-RL with pT-Rex-Dest30-PA empty vector was used as negative control, which was performed in octuplicate. Cells were harvested at 24 hours post transfection with lysis buffer (PBS with 1% Triton X-100, 0.1% BSA, 1× Halt protease and phosphatase inhibitors cocktail (Novagen), 1mM DTT and 1:100 benzonase). Soluble cell lysates were bound with sheep anti-rabbit IgG-coated magnetic beads (Invitrogen, Dynabeads M280) and luciferase reading of 10% total lysate was used as the expression control.

2.8.17 Expression and purification of MNV SD

SD expression plasmids were transformed into Rosetta™ 2 competent cells and grown in 500 ml LB media with ampicillin and chloramphenicol at 37 ℃ until OD_{600} reached between 0.5 and 0.6. SD expression was induced by 1mM IPTG at 37 ℃ for 24 hours. Cells were lysed by sonication in 0.5 mg/ml lysozyme with resuspension buffer (50 mM Tris-HCl pH8.0, 150 mM NaCl, 0.1 mM EDTA). Soluble proteins were purified by centrifugation at 20 000 × g for 15 minutes at 4 ℃ and passed through 0.45 μm filter. 1 ml 50% Ni-NTA resin was equilibrated with 10 column volume (CV) of resuspension buffer before soluble proteins were loaded. Bound resin was then washed sequentially with 10 CV of resuspension buffer with: 1) no imidazole, 2) 5 mM Imidazole, 3) 10 mM Imidazole, and 4) 40 mM Imidazole. Bound protein was eluted

with resuspension buffer containing 200 mM Imidazole in 1 ml aliquots. Eluates were analysed by SDS-PAGE and stained with commassie blue. Fractions with protein size matching theoretical molecular weight of SD (25 kDa) were pooled and dialysed overnight at 4 ℃ twice in 1 L resuspension buffer with 5% glycerol. Protein concentrations were determined by OD_{280} and flash frozen in liquid nitrogen at -80 ℃ until use.

Chapter 3

Establishment of a cell culture system for HuNoV

3.1 Background

The understanding of HuNoV biology has been hampered by the inability to cultivate HuNoV in cell culture. Many previous attempts, using different combinations of viruses, cell lines and additives (reviewed in (Duizer et al., 2004)) indicate that some fundamental requirements essential for virus replication are absent in most immortalised cells.

There are numerous factors that could contribute to the lack of norovirus replication *in vitro*. First, a cell culture-permissive virus strain is needed, like the development of hepatitis C cell culture system by isolating the JFH-1 strain (Wakita, 2009). Therefore, to maximise the sequence diversity for screening, HuNoVs isolated from both acute and chronic patients should be tested.

One inevitable drawback of using stool-purified HuNoV is biocontamination. In comparison, reverse genetics facilitate recovery of genetically defined HuNoV free of faecal contaminants. Several reverse genetics systems of HuNoV have been published to date, but due to the inability to culture HuNoV, indirect methods were used to validate the efficacy (Asanaka et al., 2005, Guix et al., 2007, Katayama et al., 2014). The development of reverse genetics systems for two MNV strains (MNV-1 and MNV-3) raised the potential by adopting a similar rationale (Ward et al., 2007, Chaudhry et al., 2007, Yunus et al., 2010). The transcription driven by a vaccinia virus expressing T7 RNA polymerase (MVA-T7) inhibits MNV replication, yet T7 RNA polymerase expressed by a similar fowlpox virus (FPV-T7) enables the recovery of infectious MNV (Chaudhry et al., 2007).

The possible lack of a functional receptor also contributes to the inability of HuNoV to establish infection in various cell lines. The identification of attachment factors and a proteinaceous receptor for MNV suggest a possible multi-step entry process of norovirus (Taube et al., 2012, Perry and Wobus, 2010, Taube et al., 2009, Perry et al., 2009, Orchard et al., 2016, Haga et al., 2016). Norwalk virus VLP can be internalised into Caco-2 cells (White et al., 1996), and a 105 kDa membrane protein was proposed to be the proteinaceous receptor (Tamura et al., 2000). However, apart from this it is generally recognised that HBGA is the cellular receptor for HuNoV, mainly due to the correlation between the secretor status and the resistance to HuNoV infection (Ruvoen-Clouet et al., 2013, Han et al., 2015, Tan and Jiang, 2014, Tan and Jiang, 2011, Tan and Jiang, 2008, Tian et al., 2007, Tan and Jiang, 2005a, Tan et al., 2004). It is possible that whilst HBGA is important as an attachment factor for HuNoV, a proteinaceous receptor required for viral entry is missing in most cell lines.

Moreover, the limited HuNoV replication in cells indicates the possible presence of intracellular restriction factors, or the possible absence of essential cellular factors. Norwalk virus RNA replicon replicates in Huh7 cells, and the viral genome replication is sensitive to type I IFNs (Chang and George, 2007, Chang et al., 2006). However, the establishment of infection is relatively inefficient and antibiotic selection is required to maintain the viral genome (I. Goodfellow, personal communication). Purified HuNoV genomic RNA can be transfected into cells, but the replication is only observable with abundant input RNAs (Asanaka et al., 2005, Guix et al., 2007, Qu et al., 2016). Together, these results indicate the replication of HuNoV in cells is inefficient and the cellular or viral factors required for replication may be missing.

Two important papers were published during the development of this project. The first one is a B cell culture system (Jones et al., 2014). In this paper, Jones et al. showed that both MNV and HuNoV can infect B cells. However, instead of a purified virus,

unfiltered stool samples were required for productive infections (about 30-fold increase of viral RNA over five days). In addition to the increase of viral RNA, the expression of non-structural protein was observed, and a subsequent passage of infected cell lysate resulted in productive infection. Of the purified virus, pre-incubation with the enteric bacteria *Enterobacter cloacae* (*E. cloacae*) or soluble H antigen rescued the negative impact of sample purification on replication, suggesting a proviral role of enteric bacteria or HBGA to promote replication. Supporting this idea, certain enteric bacteria, including *E. cloacae*, express HBGA-like molecules on the cell surface (Miura et al., 2013). Clinically, B cell deficient patients display less HuNoV faecal shedding, indicating a proviral role of B cells in a natural HuNoV infection (Brown et al., 2016). Together, this is the first direct evidence of a professional antigen presenting cell line permissive for HuNoV infection.

In 2016, Ettayabi et al. established a primary *ex vivo* cell culture system for HuNoV (Ettayebi et al., 2016). This system, called human intestinal organoids (or enteroids), utilises the Lgr5+ stem cells derived from intestinal crypts of endoscopic biopsy samples to mimic the *in vivo* propagation and differentiation of intestinal epithelial cells (Sato et al., 2011). Intestinal organoids can be maintained continuously as three-dimensional culture, and the differentiation can be achieved by modifying the culture conditions. The differentiation of intestinal organoids produces the following cell types: enterocytes, goblet cells, Paneth cells and enteroendocrine cells (Sato et al., 2011). The inoculation of HuNoV to differentiated intestinal organoids (duodenum, jejunum and ileum) resulted in robust HuNoV replication (1.5 to 2.5 $\log_{10}$ increase in viral RNA over four days) (Ettayebi et al., 2016). Different HuNoV strains were also tested and certain strains require bile for productive infection. Importantly, in this model enterocytes were found to be permissive for HuNoV. Compared with the B cell system,

HuNoV infection in primary intestinal organoids appear to be more robust. In addition to HuNoV, human rotavirus can infect intestinal organoids (Saxena et al., 2015).
Both culture systems were established in our laboratory along with the screening of other cells for HuNoV replication. Attempts were made to validate the previous observation and to improve these methods if possible.

3.2 Aims

The aim of this chapter was to establish an *in vitro* culture system for HuNoV, using the following rationale:

1. Previous attempt did not utilise sufficient sequence coverage. Therefore, HuNoVs from faecal samples of acute and persistent infections were both be tested for infection to increase the possibility of isolating a replication-competent HuNoV. If replication was observed, the according isolate was characterised.
2. Intestinal epithelial cells and immune cells were tested for infection.
3. To promote HuNoV replication, recombinant lentiviruses encoding innate immune antagonists was used to prevent innate immune activation during infection.

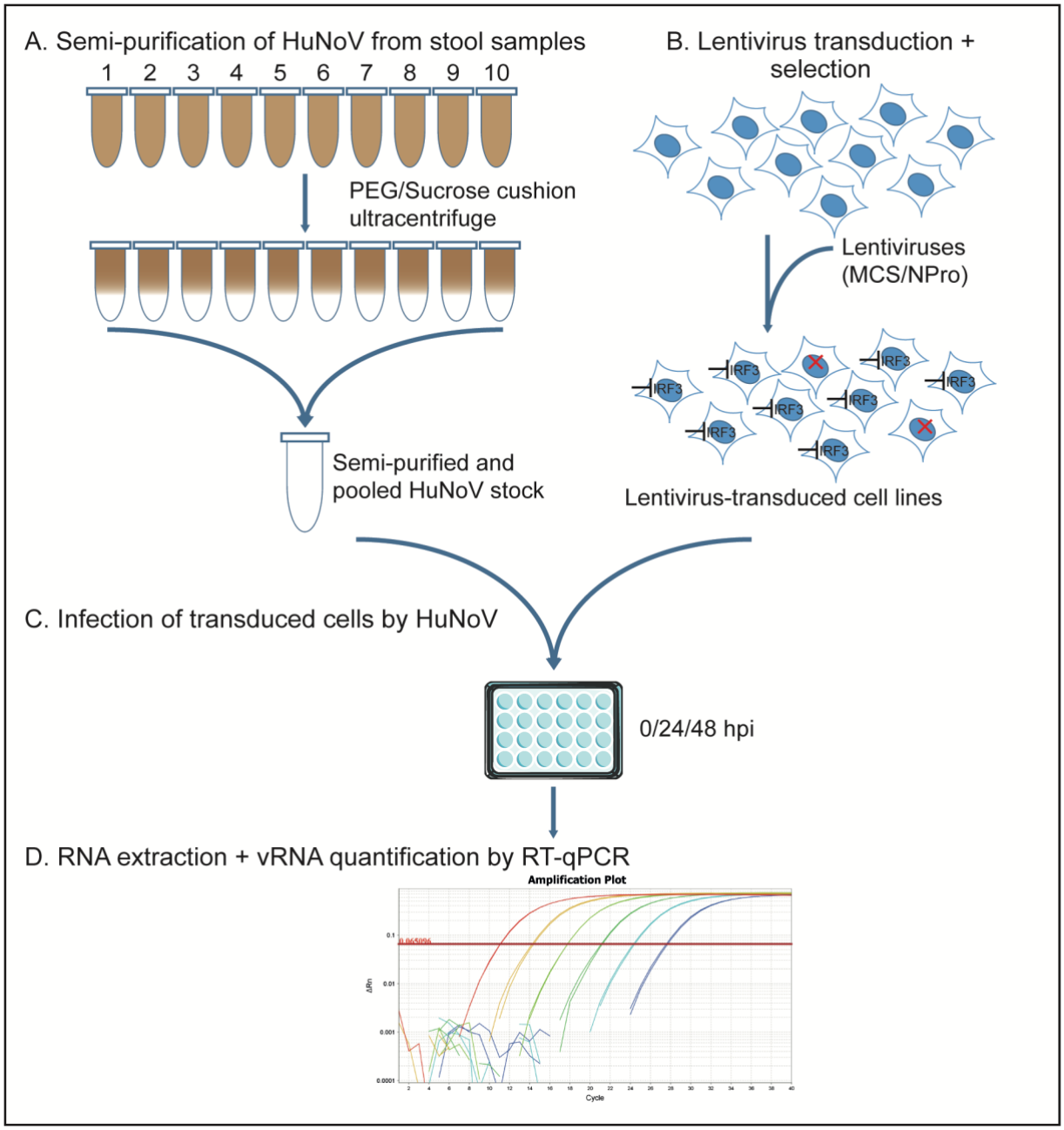

Figure 3.1 General procedure overview. A) HuNoV-positive stool samples were resuspended in PBS, HuNoV was precipitated by polyethylene glycol (PEG) and concentrated by ultracentrifugation. The samples from acute and persistent infections were combined separately as the acute and persistent pool, accordingly. B) Recombinant lentiviruses encoding empty vector (MCS) or BVDV NPro were generated and purified. Cell lines were transduced and positive cells were selected with puromycin. C) HuNoV was inoculated to lentivirus-transduced cells. The cells were then washed and incubated at 37 ℃. At different time points post infection the cells were harvested in RNA lysis buffer. D) The total RNA was extracted from each sample and RT-qPCR was used to determine total HuNoV RNA in each sample.

3.3 Results

3.3.1 Purification of HuNoV from faecal samples

The primary source of HuNoV is clinical stool samples. To establish virus stocks for screening, 10 norovirus-positive faecal samples from acute infections and 6 from persistent infections were purified by PEG precipitation and ultracentrifugation. The genotype of each isolate was determined by RT-PCR of the ORF1/ORF2 junction and the genotypes were assigned using the norovirus typing tool (http://www.rivm.nl/mpf/typingtool/norovirus/), summarised in Table 3.1. Semi-purified viruses from patient samples of acute or persistent infections were then combined into two pools. The HuNoVs provided by others are: a42dd (M. Hosmillo), CDC4 and CDC14 (Stephanie Karst, University of Florida).

Sample Name	Acute/Persistent	Genotype	Titre (gEq/µl)	Virus name
11	Acute	GII.4 Sydney_2012	2.61×10^{7}	A_{pool}
12	Acute	GII.4 Sydney_2012	6.46×10^{7}	
13	Acute	GII.4 Sydney_2012	1.05×10^{7}	
14	Acute	GII.4 Sydney_2012	5.19×10^{8}	
15	Acute	GII.4 New_Orleans_2009	1.63×10^{4}	
16	Acute	GII.4	5.75×10^{4}	
17	Acute	GII.4 Sydney_2012	3.34×10^{6}	
18	Acute	GII.4 Sydney_2012	5.71×10^{8}	
19	Acute	GII.4 Sydney_2012	2.81×10^{8}	
20	Acute	GII.4 Sydney_2012	1.38×10^{6}	
AD17/04/13	Persistent	GII.21	2.16×10^{7}	P_{pool}
DF19/04/13	Persistent	GII.4	1.40×10^{4}	
RT18/04/13	Persistent	GII.4	1.77×10^{4}	
RT03/05/13	Persistent	GII.4	3.00×10^{3}	
MD01/05/13	Persistent	GII.3	9.00×10^{5}	

MD27/06/13	Persistent	GII.3	1.19×10^4	
AD17/04/13	Persistent	GII.21	3.28×10^7	GII.21
01-15-0359	Persistent	GII.1	3.24×10^7	GII.1
a42dd	Acute	GII.4	ND	a42dd
CDC4	Acute	GII.4	ND	CDC4
CDC14	Acute	GII.4	ND	CDC14

Table 3.1 Genotypes of HuNoV samples

3.3.2 Ribonuclease sensitivity of purified HuNoV

After the acute and the persistent pools were produced, the viral RNA was determined. As shown in Figure 3.2A, the viral RNA of the acute pool is about ~1000 fold higher than that of the persistent pool with GII.4-Sydney 2012 being the dominant genotype. Purified HuNoVs were also diluted 1:10 and extracted, and the detection of similar viral RNA after extrapolation indicates minimal interference of HuNoV quantification by potential PCR inhibitors co-purified from the faecal samples.

In order to assess the capsid integrity of the purified HuNoV pools, the sensitivity of the viral RNA to RNase was tested. This was used as a surrogate indicator based on the hypothesis that encapsidated RNA is resistant to ribonuclease (Arthur and Gibson, 2015). Acute pool HuNoV was incubated with RNase A at 37 ℃ for various time (Figure 3.2B). Over 5 days little reduction of viral RNA was observed, indicating purified HuNoV RNA is protected from ribonuclease degradation. In contrast, three-hour incubation of *in vitro* transcribed MNV RNA with RNase A reduced vRNA to the limit of detection, indicating the efficient degradation of unprotected RNA.

3.3.3 Recovery of infectious HuNoV by reverse genetics

In addition to purification of HuNoV from faecal samples, previously developed DNA-based reverse genetics for MNV was applied to recover contaminant-free HuNoV. Two

HuNoV cDNAs were cloned into a vector containing 5’ T7 promoter and 3’ ribozyme, allowing similar transcription and processing of mRNAs as the MNV reverse genetic system. BSR-T7 cells were infected with FPV-T7, followed by transfection of the GII.4 or GII.6 HuNoV cDNAs. Progeny viruses were released from cell lysates by freeze-thawing and concentrated by ultracentrifugation. As negative controls, HuNoV cDNAs with deleterious frame-shift (F/S) mutations in the RdRp were included. The synthesis of viral proteins was predominantly mediated by a FPV-T7 transcribing cDNA, therefore not affected by the mutations. However, the virus genome replications are abolished in the F/S mutants because of the truncated RdRps. The mature and precursor forms of HuNoV VPg were observed in all lanes except for the mock, indicating the successful translation of viral non-structural proteins (Figure 3.2C top panel). After ribonuclease digestion of cell lysates from recovery, viral RNA of infectious and non-infectious clones was compared. HuNoV RNAs from infectious clones were significantly more abundant than those of F/S, indicating infectious HuNoV cDNAs produce more nuclease-resistant HuNoV RNAs (Figure 3.2C bottom panel). Because BSR-T7 cells are not permissive for HuNoV infection, FPV-mediated reverse genetics results in a single round of replication.

The viral protein synthesis in the transfected cells was also compared between two reverse genetics systems (Figure 3.2D). FPV-T7-based reverse genetics generated significantly more VPg mature and precursor forms than EF-1α-driven recovery did, suggesting that FPV-T7 may be better for recovering infectious HuNoV.

Together, the FPV-based reverse genetics appear to have generated encapsidated HuNoV RNA. However, as there was no direct evidence of infectivity of these viruses, HuNoV purified from faecal samples were used primarily to evaluate cell line permissiveness for HuNoV.

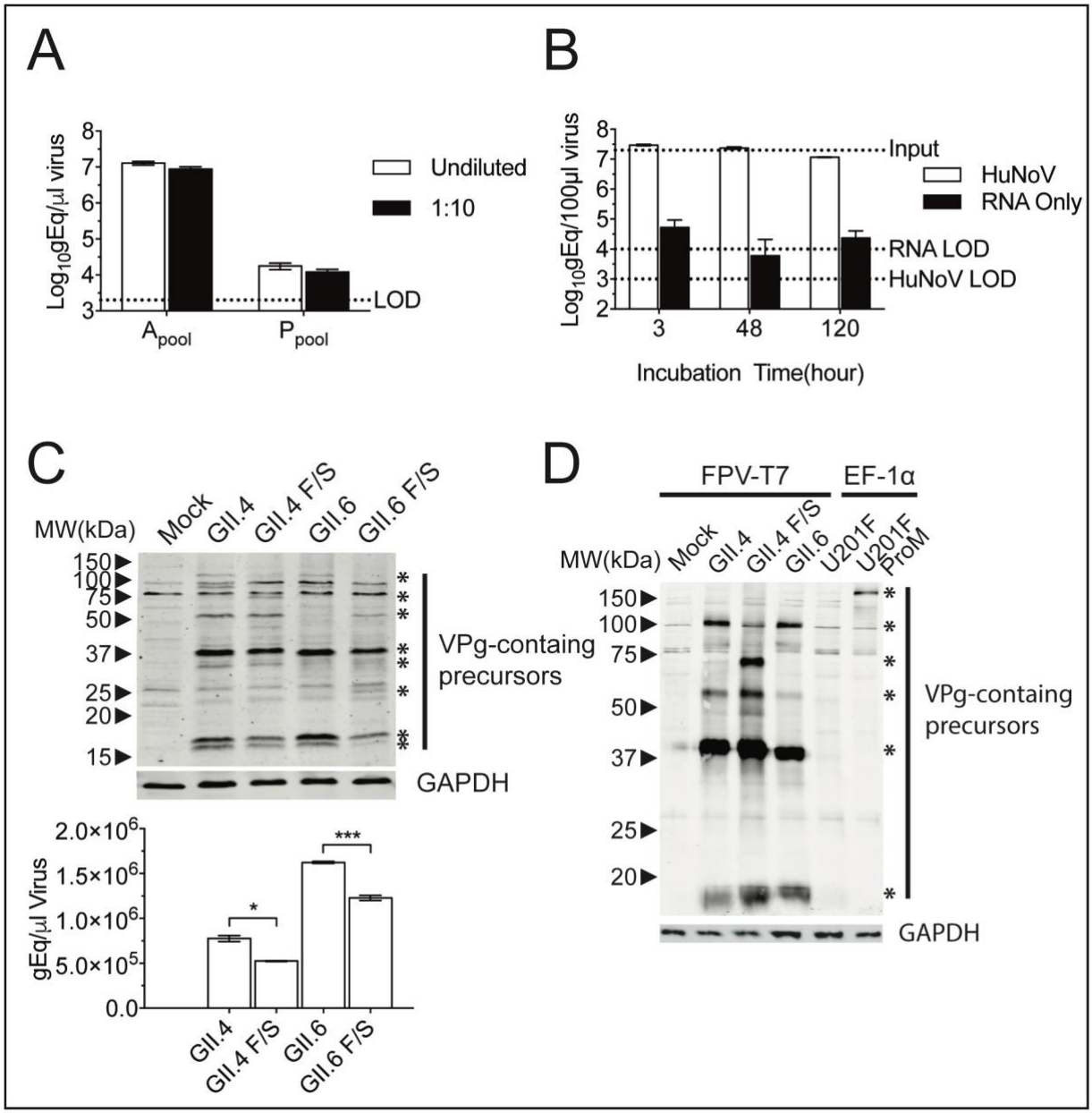

Figure 3.2 Recovery of HuNoV. A) Viral RNA of pooled HuNoV stocks. Individual HuNoV isolates were purified and combined into two pools. The viral RNA of each pool was measured by RT-qPCR. Purified HuNoVs were also diluted 1:10 and processed similarly to determine if PCR inhibitor was present in virus stocks B) Nuclease-sensitivity of purified HuNoV. HuNoV was treated with RNase A to examine RNase-protected HuNoV RNA. MNV RNA was used to evaluate the efficacy of RNase treatment. C) Recovery of HuNoV from BSR-T7 cells by DNA-based reverse genetics. HuNoV cDNA clones were transfected into FPV-T7-infected BSR-T7 cells. The expression of VPg indicate similar transfection efficiency and GAPDH was used as the loading control. * indicates the presence of mature and precursor forms of VPg. For nuclease treatment (bottom panel), viruses were released by freeze-thawing the cell lysates. After nuclease treatment and purification, RT-qPCR was used to determine the viral RNA of viable and non-viable (F/S) viruses. Statistical analysis was performed using one-way ANOVA and Dunnett test (*, $p<0.05$, **, $p<0.01$, ***, $p<0.001$) D) Comparison of helper virus-based (FPV-T7) and plasmid-based (EF-1 α) reverse genetics (Katayama et al., 2014). HuNoV cDNA clones were

transfected into BSR-T7 cells and the expression of VPg was used as the indication of translation. * indicates the presence of VPg-containing precursors. GAPDH was used as the loading control. ProM is the protease mutant of the GII.3 U201F.

3.3.4 Antagonism of cellular innate immune responses

Because norovirus replication is sensitive to type I IFN responses (Chang and George, 2007), it is possible that the contaminants co-purified with HuNoV may activate the candidate cell lines and restrict replication. Accordingly, it was proposed that inhibiting type I IFN responses may promote HuNoV replication. Two innate immune antagonists were selected. The N-terminal protease fragment of bovine viral diarrhoea virus (BVDV NPro) degrades IRF-3 (Hilton et al., 2006). Our work showed that BVDV NPro enhances porcine sapovirus replication *in vitro* by inhibiting IRF-3-dependent type I IFN signalling (Hosmillo et al., 2015). The accessory V protein of parainfluenza virus 5 (PIV5 V) inhibits both the sensing and the signalling pathways of type I IFN. PIV5 V binds to MDA-5 preventing the activation of IFN β promoter (Childs et al., 2007, Andrejeva et al., 2004). In addition, type I IFN signalling pathways are targeted via the degradation of STAT1 (Gitlin et al., 2010). Therefore, the stable expression of these proteins using lentiviral expression systems may potentially promote HuNoV replication by preventing the type I IFN responses.

Recombinant lentiviruses encoding BVDV NPro or PIV5 V were produced using a second-generation lentivirus packaging system (psPAX2 + pMD2.G (Zufferey et al., 1997)). Lentiviruses were indirectly titrated by producing and titrating a lentivirus encoding EGFP in parallel. The EGFP lentivirus was also used to determine the transduction efficiency.

Two representative cell lines were chosen to demonstrate the transduction and validation procedures. First of all, both Caco-2 and BJAB cells were efficiently transduced to express EGFP (Figure 3.3A and B, left panels). After selection with

puromycin, the expressions of BVDV NPro and PIV5 V were functionally validated by examining the levels of endogenous IRF-3 and STAT1. BVDV NPro expression significantly reduced IRF-3 levels in both Caco-2 and BJAB cells (Figure 3.3A and B, right panels), whilst PIV5 V expression in BJAB cells abolished STAT1 expression. The reduction was not due to the lentivirus transduction, as a lentivirus encoding empty vector (MCS) showed no impact on the endogenous IRF-3 and STAT1 levels. Successfully transduced cell lines were then tested for HuNoV replication.

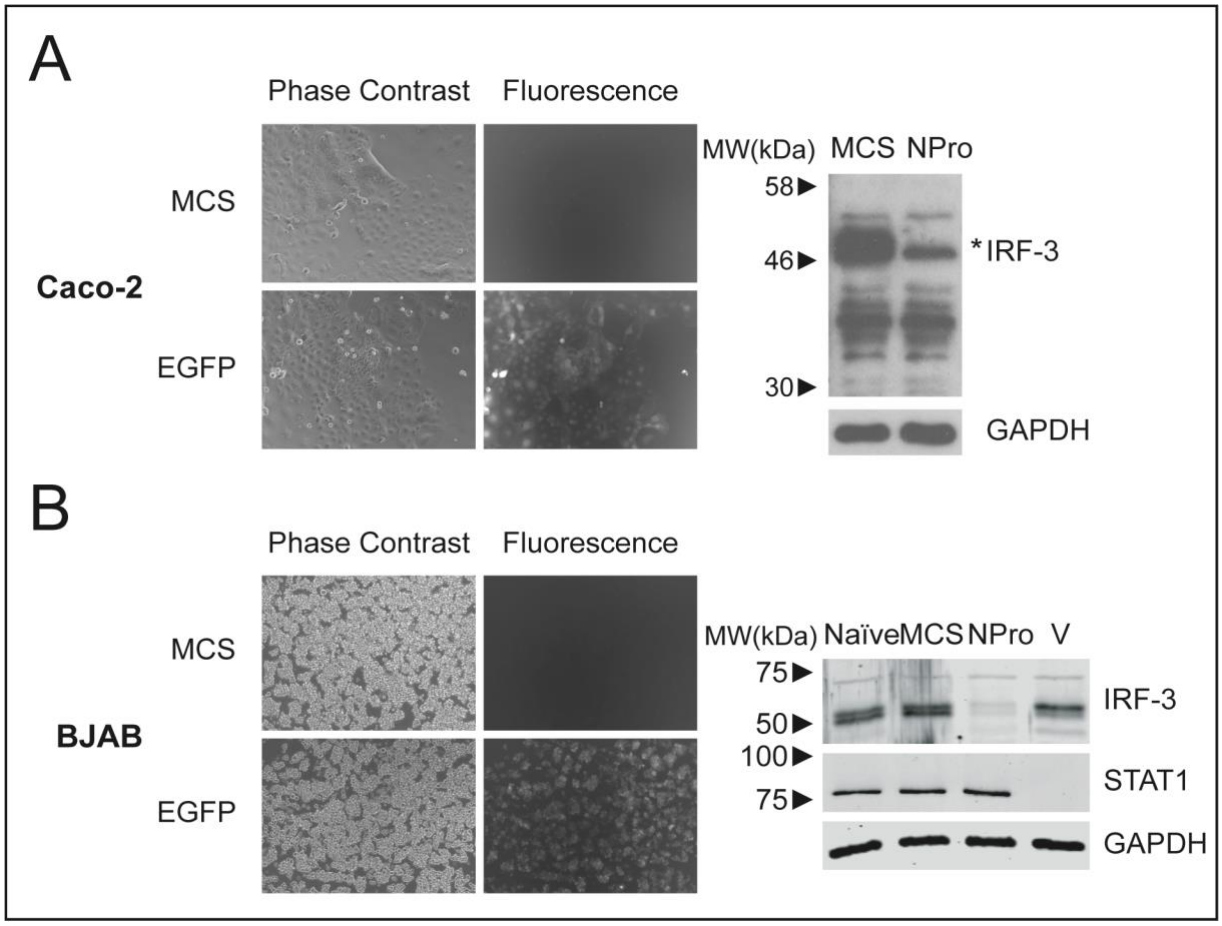

Figure 3.3 Lentiviral transduction of cell lines. A) Caco-2 cells were transduced with concentrated lentiviruses produced from 293T cells, containing either empty vector (MCS), EGFP, or BVDV NPro. Microscopy pictures were taken 3 days post transduction. The right panel showed functional validation of lentivirus encoding BVDV NPro, which degrades IRF-3. B) The same batch of lentiviruses from panel A was used to transduce BJAB cells, and the left panel showed transduction efficiency of the lentivirus encoding EGFP. The right panel showed functional validation of lentiviruses encoding BVDV NPro and PIV5 V, which degrade IRF-3 and STAT1, respectively.

3.3.5 HuNoV infection in intestinal epithelial cells

Based on the hypothesis that HuNoV likely infects intestinal epithelial cells or immune cells, first of all, several intestinal epithelial cell lines were selected and tested. Enterocytes and goblet cells are the most prevalent cell types of intestinal epithelia, constituting more than 80% and 4% of the total population, respectively (van der Flier and Clevers, 2009). Therefore, it was logical to determine if HuNoV can infect these cell types.

Enterocyte-like cell line Caco-2 has been tested extensively previously with no success (Duizer et al., 2004). However, a low level of HuNoV replication was observed when VPg-linked HuNoV RNA was transfected into Caco-2 cells (Guix et al., 2007).

To determine if the restricted HuNoV replication can be improved by suppressing innate immune sensing, Caco-2/BVDV NPro cells were inoculated with both the acute and the persistent pools HuNoVs and viral RNA was monitored over the course of 4 days. However, no significant increase was observed in either cells infected by either virus (Figure 3.4A).

To determine if goblet cells are susceptible to HuNoV infections, intestinal epithelial cell line LS174T expressing a dominant negative TCF4 (dnTCF4) was utilised. TCF4 is involved in intestinal epithelial cell differentiation, and the expression of dnTCF4 in LS174 cells results in a goblet cell-like phenotype characterised by the elevated expression of *MUC2* (van de Wetering et al., 2002).

The expression of dnTCF4 in LS174T cells was induced by doxycycline resulting in cell cycle arrest. In a growth assay (Figure 3.4B, left panel), differentiated LS174T dnTCF4 showed less cell replication compared with LS174T WT or uninduced (-Dox) cells. The differentiation of LS174T dnTCF4 was also characterised by the increased expression of *MUC2* (Figure 3.4B, right panel). It appeared that *MUC2* was induced

24 hours post induction. Together, LS174T dnTCF4 can be differentiated, paralleled by the expression of goblet cell signature gene *MUC2*.

The infection of HuNoV in goblet cells was then tested. The differentiation of LS174T did not result in increased viral binding at the beginning of infection, nor was an increase of HuNoV RNA observed over 5 days (Figure 3.4C). Therefore, under these experimental conditions, goblet cells are not permissive for HuNoV infection.

Transformation of cell lines often results in modified gene expression, possibly including the host factors important for HuNoV replication. HuNoV binds to a related primary human intestinal epithelial crypt (HIEC) cells (HIEC-6) in a PCR-based neutralisation assay (Fan et al., 2015). Also, HIEC-6 was previously tested for HuNoV replication with only a low level of viral genome replication (less than 100 fold) observed (Leung et al., 2010).

To test if HIEC cells can be infected by HuNoV and whether the inhibition of type I IFN responses can enhance this low-level replication, transduced HIEC cells were infected with the acute pool HuNoV (Figure 3.4D). The preliminary results showed significant variations. However, compared with viral RNA at 3hpi, there was no significant increase of HuNoV RNA at 48hpi. Together, HuNoV infection of primary or continuous intestinal epithelial cell lines showed no evidence of robust replication.

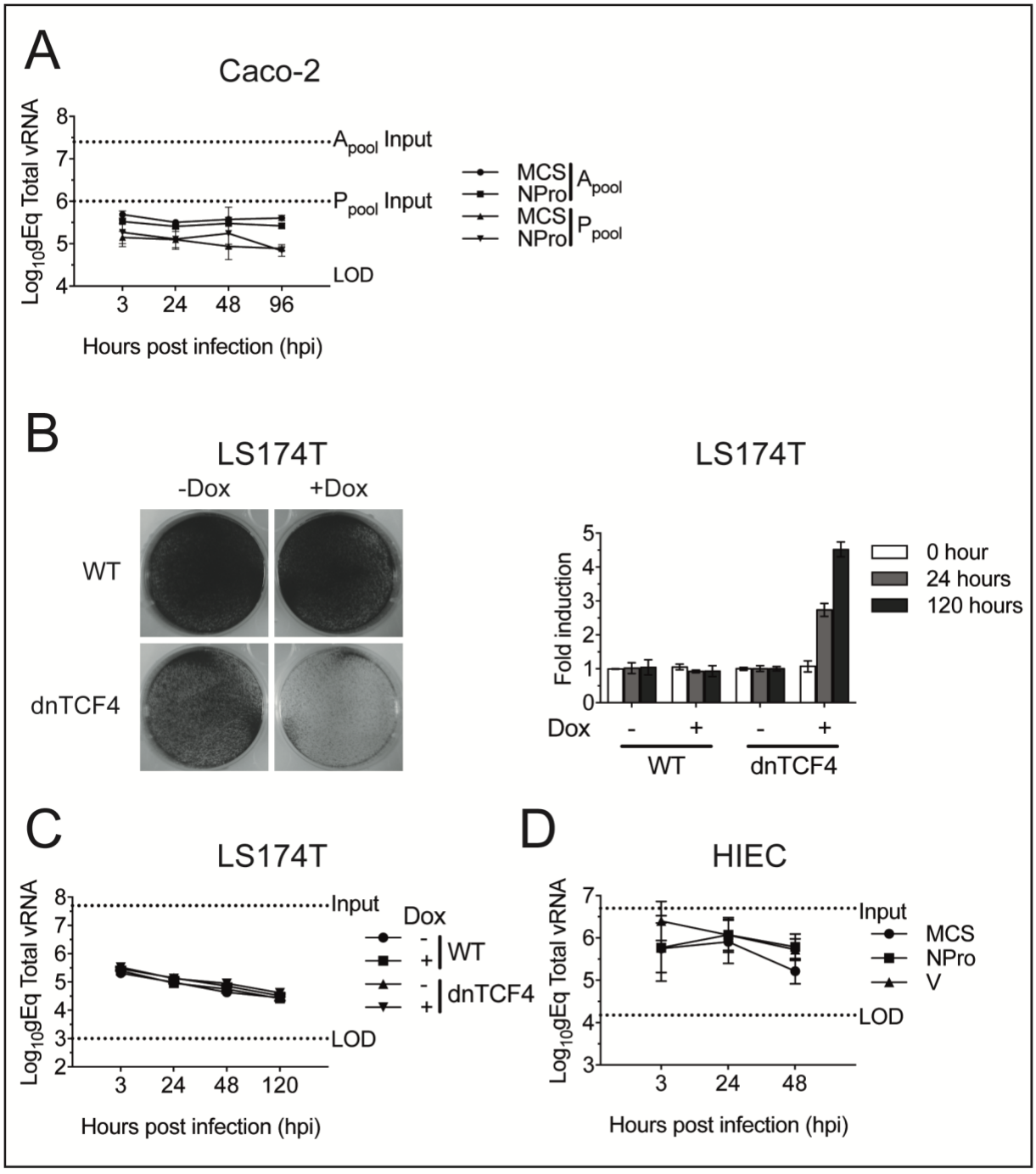

Figure 3.4 Infection of intestinal epithelial cells. A) Infection of Caco-2 cells by HuNoV. The acute and the persistent pool HuNoVs were inoculated to transduced, undifferentiated Caco-2 cells, and HuNoV RNA at indicated time points was determined by RT-qPCR. B) Differentiation of LS174T cells into goblet-cell like phenotype. WT LS174T or LS174T dnTCF4 were treated with or without doxycycline, and the picture on the left panel showed the growth of cells on day 5 post treatment. On the right panel showed the induction of goblet cell marker *MUC2* in LS174T cells following doxycline induction. The fold induction was calculated by $\Delta\Delta$Ct method. C) Infection of LS174T cells by HuNoV. 1 day post doxycycline treatment the cells were infected by acute pool HuNoV. Viral RNA was determined by RT-qPCR. D) Infection of primary human intestinal epithelial crypt (HIEC) cells by HuNoV. The acute pool

HuNoV was inoculated to transduced HIEC cells, and at different time points the HuNoV RNA was determined by RT-qPCR.

3.3.6 HuNoV infection in immune cells

In addition to intestinal epithelial cells, HuNoV infection in human immune cells was also investigated. This is because in an *in vivo* chimpanzee model of HuNoV infection, HuNoV antigens were detected in cells positive for DC-SIGN (dendritic cells) or CD20 (B cells). Although, macrophages and dendritic cells (DCs) derived from peripheral blood were previously shown not to support Norwalk virus replication (Lay et al., 2010), the intestinal immune cells possess different phenotypes compared to circulating immune cells (Smythies et al., 2005, Lee et al., 1985, Liu and Nussenzweig, 2010). Therefore, immune cells from different sources should be tested for HuNoV replication. Tonsils are lymphoid tissues with enriched immune cell populations, and tonsillectomy is a possible source of obtaining a mixture of primary immune cells (mainly dendritic cells).There is evidence showing the heterogeneity of DC populations (Stent et al., 2002, Summers et al., 2001). Therefore, primary tonsillar cells represent a heterologous primary immune cell model to examine HuNoV replication. Tonsillar cells were isolated from an anonymous donation of tonsillar tissues following elective tonsillectomy. The acute or the persistent pool HuNoVs were inoculated directly to the purified cells. A slight decrease, followed by a small increase in viral RNA was observed over 4 days (Figure 3.5A). Although the increase of HuNoV RNA was not statistically significant, it is possible that tonsils contain immune cells susceptible to HuNoV infection.

Chronic human myelogenous leukaemia cell line KBM7 was also tested for HuNoV replication using an unpurified GII.1 HuNoV (Figure 3.5B). Through communication with the Karst laboratory (Jones et al., 2014) we learned that a pre-incubation with soluble HBGA enhances HuNoV replication in B cells. Since then, HBGA was included

as an additive during the screening of KBM7 and the primary γδ T cells for HuNoV replication. GCDCA is one of the components of bile. Porcine sapovirus requires bile acid for viral entry (Chang et al., 2004). To examine whether bile can also promote HuNoV entry and replication, HuNoV was mixed with GCDCA before inoculated to KBM7 cells. Compared to inoculation without additives, pre-incubation with HBGA slightly increased the bound vRNA (0hpi, HBGA). However, the increased binding did not increase HuNoV replication significantly. Although the difference is statistically significant, the fold increase on 72hpi is less than 10-fold in all experiments.

A recent case of HuNoV infection in a paediatric patient following a bone marrow transplant showed that through the course of infection a particular strain of GII.6 HuNoV became the dominant variant (J. Lockwood, University College London, unpublished data). This observation coincided with the enrichment of γδ T cells after the transplant (data not shown), raising the possibility of γδ T cells being infected by HuNoV. To test this hypothesis, γδ T cells were expanded from peripheral blood of two healthy donors by Marta Barisa (J. Anderson lab, University College London), and were inoculated with the purified acute pool or an unpurified GII.1 HuNoV. Initially, a less than 10-fold increase of viral RNA was observed in the infected cells from the second donor (Figure 3.5C, left panel). In order to validate this observation, primary γδ T cells were expanded from donor 2 and infected by the acute pool and the GII.1 HuNoVs alongside concentrated HuNoVs from reverse genetics (Figure 3.5C, right panel). However, in this experiment no increase of vRNA was observed over 3 days.

HuNoV RNA was readily detected on day 0 samples of immune cells, indicating the presence of an attachment factor on the surface of these cells. However, a robust

increase of viral RNA was not observed in cells, suggesting that HuNoV does not establish efficient infection in the tested immune cells.

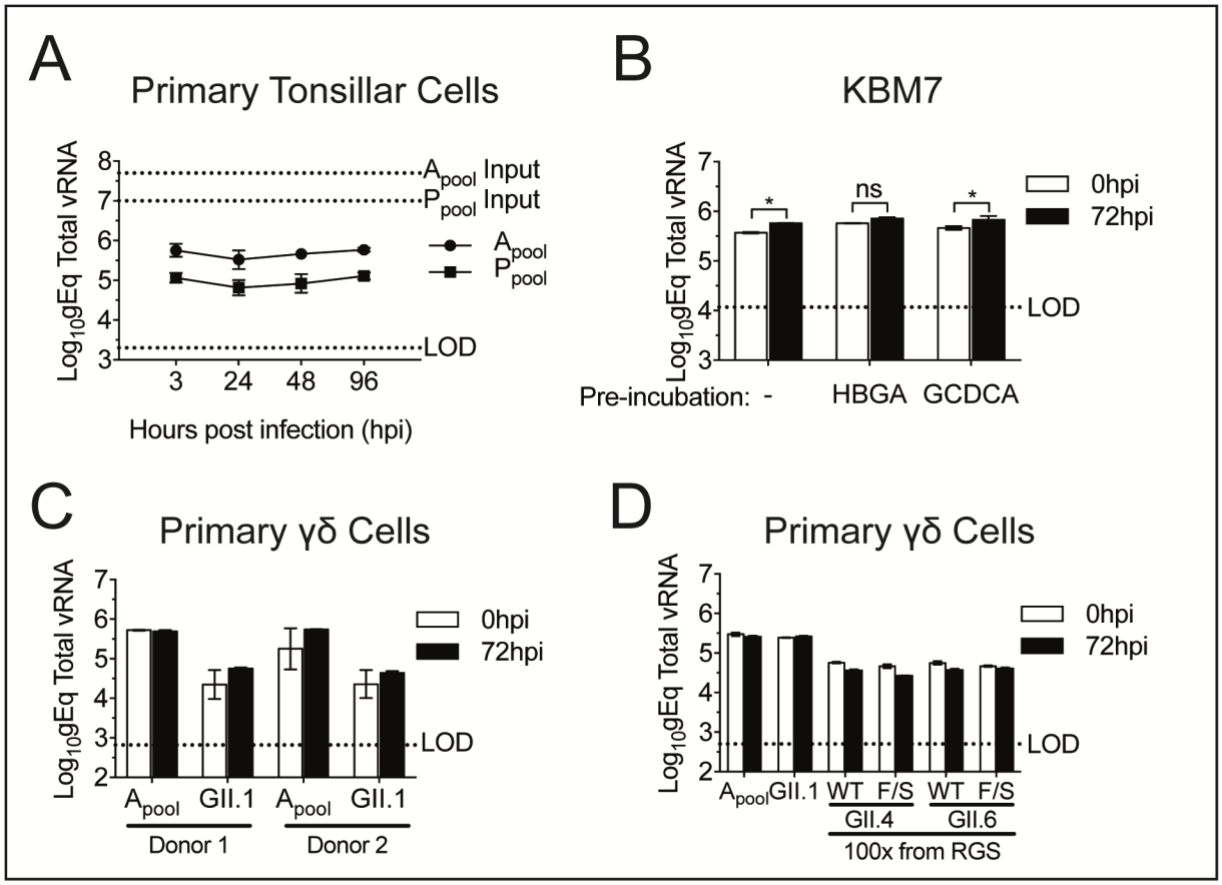

Figure 3.5 Infection of immune cells. A) HuNoV infection of primary tonsillar cells. Cells were isolated and were inoculated with the acute and the persistent pool HuNoVs. HuNoV vRNA from different samples was determined by RT-qPCR. B) HuNoV infection of near-haploid cell line KBM7. Unpurified HuNoV GII.1 was either directly incubated with KBM7 cells, or pre-incubated with HBGA or GCDCA before being added to the cells. The HuNoV RNA was determined by RT-qPCR. Two-way ANOVA analysis was performed using Dunnett test (* p<0.05, ** p<0.01, *** p<0.001) C) HuNoV infection of peripheral blood-derived γ δ T cells. 10ml peripheral blood was obtained from two anonymous donors following expansion of γ δ T cells. Differentiated cells were infected with purified acute pool HuNoV or unpurified GII.1 HuNoV. At 0 and 72 hpi, total RNA was extracted and the total HuNoV RNA was determined by RT-qPCR. D) Donor 2 γ δ T cells infection by HuNoVs. After C), peripheral blood was again obtained from donor 2 and expanded. The two HuNoVs tested together with 100×-concentrated HuNoVs from reverse genetics were tested. At 0 and 72 hpi, the HuNoV RNA was determined.

3.3.7 Validation of HuNoV infection in B cells

Since the discovery of a B cell culture for HuNoV, efforts have been made to validate and improve this culture system (Jones et al., 2014, Jones et al., 2015). Initially, the acute pool or a persistent GII.21 HuNoV (the main isolate in the persistent pool) were inoculated into BJAB cells. However, over the course of five days no significant increase of HuNoV RNA was observed (Figure 3.6A).

Lentivirus encoding BVDV NPro was used to test if the induction of innate immunity inhibited HuNoV replication in BJAB cells (Figure 3.6B) Also, pre-incubation with heat inactivated enteric bacteria *E.cloacae* or HBGA was used to help HuNoV binding. In spite of these measures, no increase of HuNoV RNA was observed over 5 days.

As suggested in the initial publication by Jones et al., HuNoV replication in BJAB cells is inefficient and subject to the stringent experimental set up of both cells and viruses (Jones et al., 2015, Jones et al., 2014). Therefore, HuNoV infection of BJAB cells was also tested during the visit of the Karst lab (University of Florida). Different HuNoVs were inoculated to BJAB cells from both laboratories. An average 10-fold increase of RNA was observed in an unpurified GII.4 HuNoV (CDC4)-infected samples (Figure 3.6C). However, because this result was not yet available when the following experiment was performed (Figure 3.6D), instead of the CDC4, the HuNoV CDC14 was chosen to test HuNoV replication in BJAB from the Karst lab (University of Florida), or from the Farrell lab (MCS and NPro). In this experiment, only CDC14 infection in transduced BJAB NPro showed statistically significant increase of vRNA 3 days post infection. However, this observation was confounded by significantly less vRNA on 0hpi. Therefore, it is possible that CDC14 replicates at low level in BJAB NPro, but a conclusion can only be drawn after independent validation.

After establishing the BJAB propagation and HuNoV infection protocols in our laboratory, the effect of inoculation dose on HuNoV replication was tested (Figure 3.6E).

Inoculation of 10 µl unpurified GII.1 HuNoV showed slight increase of HuNoV RNA 3 days post infection. Interestingly, similar to the infection in BJAB NPro (Figure 3.6D), this experiment also displayed more variations of day 0 vRNA. Further biological and technical repeats indicated that there was up to 9-fold increase in viral RNA, but 6 out of the 9 experiments showed limited viral genome replication (Figure 3.6F).

These results together show some evidence of HuNoV replication in BJAB cells, but the consistency of the system needs to be improved, and more evidence of a productive infection (e.g. *de novo* translation of viral proteins, successive propagation of HuNoV from infected BJAB) is required to make this system viable.

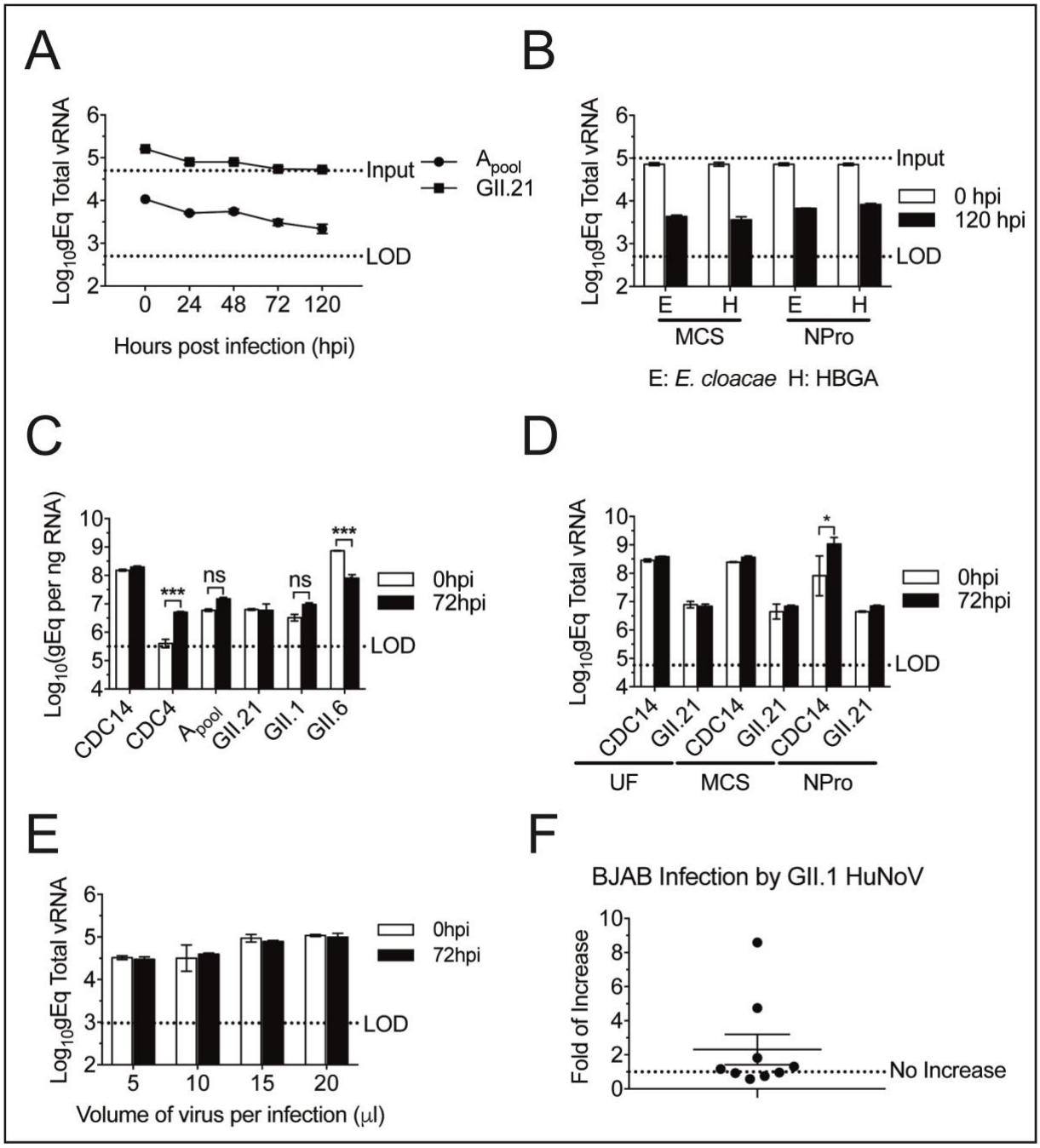

Figure 3.6 Infection of BJAB. A) BJAB cells infection by the acute pool or the persistent GII.21 HuNoVs. BJAB cells were infected and HuNoV RNA was determined at the indicated time points post infection. B) BJAB infection with pre-incubation of *E. cloacae* or HBGA. Transduced BJABs were infected with the persistent GII.21 HuNoV. The total RNA was harvested on days 0 and 5, followed by detection of vRNA by RT-qPCR. C) Effect of viruses on BJAB infection. Different HuNoV were tested for HuNoV infection following the published protocol (Jones et al., 2015, Jones et al., 2014). Samples were harvested and HuNoV RNA determined by RT-qPCR. Two-way ANOVA was performed using Bonferroni test, ***, $p<0.001$ D) Effect of cells on BJAB infection. BJAB from the Karst lab and transduced BJABs from IG lab were infected by CDC14 and GII.21 HuNoV and the total RNA was extracted on 0 and 3 dpi. E) Titration of HuNoV. BJAB cells were infected with unpurified GII.1 HuNoV following published protocol with different volumes of virus. Total RNA extraction and RT-qPCR were performed on samples of 0 and

3 dpi. F) Summary of 9 biological experiments on BJAB infections using the published protocol. BJABs were infected with 10 µl unpurified GII.1 HuNoV and harvested on 0 and 3 dpi. In 3 biological triplicate experiments (total 9 repeats), the fold of increase was plotted.

3.3.8 Maintenance and differentiation of intestinal organoids

HuNoV replication in primary human intestinal organoids (or enteroids) was recently described (Ettayebi et al., 2016). Several genotypes of HuNoVs were shown to replicate in this system, and bile was identified as a host factor for certain HuNoV strains. Importantly, the replication of GII.4 but not GII.3 HuNoV depends on the secretor status of organoids.

Following this, the primary intestinal organoids culture was established in our laboratory (M. Hosmillo, Y. Goodfellow, I. Goodfellow, unpublished results). Duodenal organoids D196 were maintained in proliferation media with Matrigel. The culture was propagated every week, and typically organoids started to appear one day after splitting (Figure 3.7A). There are between 50-100 cells per organoid, displaying multi-lobulated or spherical structures.

HuNoV effectively infects enterocytes obtained from differentiated intestinal organoids (Ettayebi et al., 2016). Therefore, the differentiation of organoids D196 was first characterised. Upon differentiation (n of 1 experiment), a reduction of stem cell marker *LGR5*, and an increase of enterocyte marker *ALPI* were observed (Figure 3.7B). This is consistent with previously published data (Saxena et al., 2015).

Differentiation markers were also visualised by fluorescent microscopy. The expression of goblet cell marker *MUC1* throughout differentiation was determined (Figure 3.7C). MUC1 was readily observable one day post differentiation. Starting from day 2, a change of sub-cellular expression patterns was observed. Cytoplasmic MUC1 decreased while cell surface distribution of MUC1 increased. Five days post

differentiation, ubiquitous apical surface expression of MUC1 was observed. Because MUC1 is a recognised as a goblet cell marker, the significant proportion of MUC1 positive cells may indirectly suggest that the number of enterocytes in this batch of differentiated organoids is suboptimal. However, it is important to mention that the differentiation of organoids is readily reproducible (M. Hosmillo and Y. Goodfellow, unpublished data).

3.3.9 Replication of HuNoV in intestinal organoids

The supply of organoids was limited, primarily due to the difficulty in maintaining the culture and slow replication kinetics. The initial test of HuNoV infection was performed using another duodenal organoids D353. Both D196 and D353 are secretor positive (M. Hosmillo, personal communication), therefore both organoids are less restricted to HuNoV genotypes. A GII.4 HuNoV a42dd (kindly provided by M. Hosmillo) was used to demonstrate HuNoV replication in organoids D353 and an 8.5-fold increase in viral RNA was observed over the course of 2 days (Figure 3.7D). It is important to mention that this is a n of 1 experiment, and increases in viral RNA more than 1000-fold are now routine but highly dependent on the state of monolayer differentiation (M. Hosmillo and Y. Goodfellow, unpublished data).

GII.4 HuNoV recovered by reverse genetics was also tested for replication in intestinal organoids (Figure 3.7E). The first passage of the GII.4 HuNoV in duodenal organoids D196 showed a modest level of replication (Passage 1). Passaging was performed by inoculating cell lysates from passage 1 to differentiated organoids and HuNoV RNA levels on day 0 and day 3 were determined. Compared to passage 1, there was much less cell-associated HuNoV RNA on day 0, whereas comparable viral RNA was observed on day 3, resulting in an average of more than 2000-fold increase of vRNA. The variation of this experiment was significantly lower than that seen in the BJAB

infections, and the significant increase of HuNoV RNA indicates that FPV-mediated reverse genetics recovers infectious GII.4 HuNoV.

In summary, primary intestinal organoids may be the most robust method for cultivating HuNoV. Using this system, FPV-mediated reverse genetic system showed recovery of infectious GII.4 HuNoV, which opens new avenues for infectious virus generation, rather than using faecal samples.

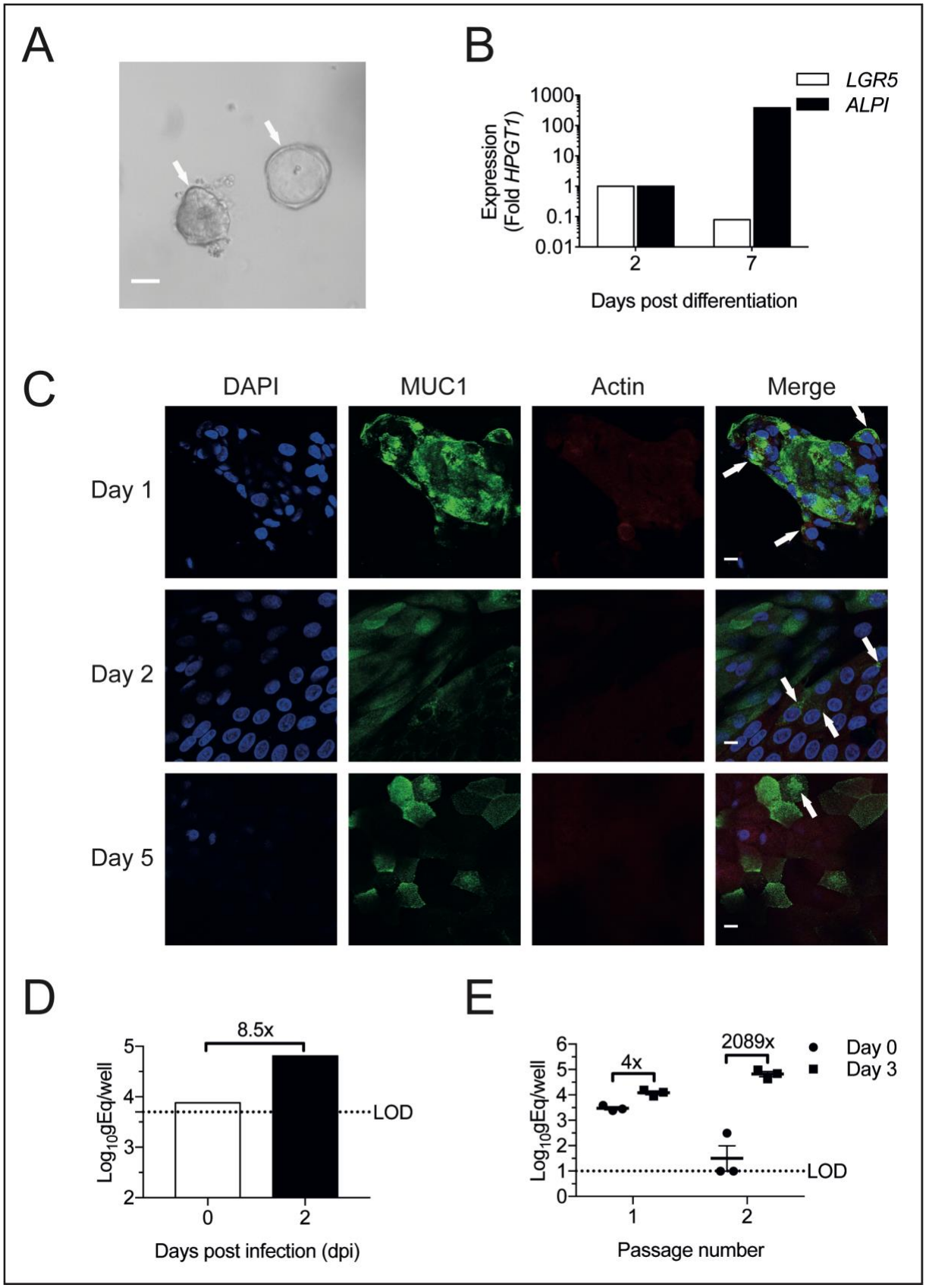

Figure 3.7 Infection of intestinal organoids. A) Proliferating organoids. Picture was taken on day 3 after splitting, the arrows indicated individual organoids. Scale bar represent 50 µm. B) Differentiation of organoids (n=1). Duodenum organoids D196 was differentiated and on days 2 and 7 post differentiation, the expression of stem cell marker LGR5 and enterocyte marker ALPI were determined

by qRT-PCR. C) Differentiation of goblet cells. Duodenum organoids D196 was differentiated, and on days 1, 2 and 5 post differentiation, cells were fixed and stained with the goblet cell marker MUC1. Arrows indicate a typical cytoplasmic distribution of MUC1 and a goblet cell morphology. Scale bar represents 10 μm. As differentiation progressed, surface expression of MUC1 was observed. D) Infection of differentiated organoids with HuNoV. Duodenum organoids D353 was differentiated and HuNoV a42dd inoculated (n=1). On days 0 and 2 post infection, HuNoV RNA was determined by RT-qPCR. E) Infection of differentiated organoids with HuNoV recovered from reverse genetics. RGS GII.4 HuNoV was inoculated to differentiated duodenal organoids D196. On days 0 and 3 post infection, HuNoV RNA was determined by RT-qPCR. Following passage 1, cell lysates was used for infection of passage 2. And the samples were processed accordingly. HuNoV infections and RT-qPCR in E) was performed by M. Hosmillo.

3.4 Discussion

In this chapter, extensive efforts have been attempted to establish an *in vitro* culture system for HuNoV. HuNoV was either purified from clinical specimen or generated *de novo* using reverse genetics. Recombinant lentiviruses encoding innate immune antagonists were used to prevent potential activation of innate immune responses during infection to enhance HuNoV replication. Different cell types, mainly the intestinal epithelial cells and immune cells, were tested for HuNoV replication. Following two recent publications, HuNoV infections were tested in the B cell and primary enteroids systems. Some of the presented evidence agreed with the published results, whilst the caveats of others indicate that more efforts are required to develop a robust culture system to study HuNoV biology.

3.4.1 HuNoV can be recovered from different sources

One clinical characteristic of HuNoV is robust faecal shedding of viral RNA. In fact, most of the acute infection faecal samples possessed high viral load even after semi-purification (Table 3.1). RNase sensitivity assay showed that the purified acute virus pool is highly RNase-resistent (Figure 3.2B).

Compared to faecal samples from acute infections, samples of persistent infections showed diverse genotypes and variations in viral RNA. The majority of the acute pool samples were genotyped as GII.4_Sydney_2012. As these samples were collected during similar time (2013), it was not surprising that Sydney 2012 dominated the genotypes of the acute pool stock. In comparison, in the persistent viruses there was a chronic patient with high viral RNA but non-diarrhoea sample (GII.21). Sequential samples collected from this patient had lower titres but likely great genetic diversity than the acute infections (Debbink et al., 2014, Doerflinger et al., 2017, Hasing et al., 2016). The development of hepatitis C virus tissue culture system highlights the importance of a cell culture-adaptive virus isolate (Wakita, 2009). Therefore, although persistent pool was of lower titre, it increased the diversity of HuNoV strains being screened. It is important to mention that the GII.21 sample has more than 100 times higher titres than the rest of the persistent samples. Therefore, in the persistent pool over-represented GII.21 was the dominating genotype. The development of the primary intestinal organoids as HuNoV cell culture system enabled culturing different HuNoVs (Ettayebi et al., 2016). GII.3 and GII.4 HuNoVs, together with GII.1 and GII.21 HuNoVs were purified in this study. The replication of these isolates in organoids was yet to be characterised.

DNA-based reverse genetics system was also tested as an alternative method to generate infectious HuNoV. The success of this method will facilitate the production of genetically defined HuNoV, with the potential of genetically manipulating HuNoV to study the details of HuNoV replication and virus-host interactions. HuNoV recovered by reverse genetics will also be free of contaminants from faecal matter, which preventing activation of cells during infection. The transfection of two HuNoV cDNA clones (GI.4 and GII.6) using FPV-T7 reverse genetics system showed robust production of viral proteins (Figure 3.2C). A previous study showed a similar MVA-T7

inhibits MNV replication, whereas FPV-T7 enabled recovery of infectious MNV (Chaudhry et al., 2007). It remains to determine whether the similar constraint applies to the recovery of HuNoV.

3.4.2 Antagonism of innate immunity

The development of the Norwalk virus RNA replicon started to reveal details of the intracellular life cycle of HuNoV, one of which is the sensitivity of norovirus replication to type I IFN responses (Chang et al., 2006). The characterisation of norovirus RdRp using a cell-based NoV-5BR assay also showed that active norovirus RdRp triggers type I IFN responses. In one study a lack of IFN responses was observed in norovirus RNA replication (Qu et al., 2016). However, the number of replicating cells was low and this conclusion should only be drawn when similar observations were obtained in a more robust replication system, e.g. the primary intestinal organoids.

BVDV NPro and PIV5 V were used to antagonise innate immune sensing during infection. Lentiviruses encoding BVDV NPro and PIV5 V effectively degrade IRF-3 and STAT1, respectively (Figure 3.3). However, the only direct evidence of recombinant lentivirus aiding HuNoV replication was that in BJAB NPro infected with HuNoV CDC14 showed significant replication compared to BJAB MCS (Figure 3.6D). This finding was also confounded by significantly less viral RNA on day 0, despite that vRNA on day 3 was slightly higher. In all the other cell lines tested, it can only be concluded that neither IRF-3 or STAT1 is the key restriction host factor for HuNoV replication in the tested cells.

HuNoV infection in primary intestinal organoids show promising results. It will be interesting to determine if BVDV NPro or PIV5 V improves HuNoV replication in these cells. HuNoV infection in organoids was performed with ruxolitinib, which is a JAK inhibitor (Mesa, 2010) as our preliminary results showed that ruxolitinib enhances

HuNoV replication (M. Hosmillo, unpublished data). Therefore, it is possible that PIV5 V can functionally replace ruxolitinib due to the similarly targeted JAK/STAT pathways.

3.4.3 Roles of B cells in HuNoV pathogenesis

Since the publication of the B cell culture system for HuNoV, extensive efforts were invested to establish this model in our laboratory. It was proposed that HuNoV can replicate in BJAB at low level, and a robust HuNoV cell culture system can be established by improving this system. It was observed that patients with congenital B cells deficiency showed reduced HuNoV infection (Brown et al., 2016). Also, B cells were found in intestinal lamina propria, suggesting that HuNoV can be in close physical proximity to B cells during infection (Schlissel, 2013). Moreover, in a chimpanzee infection model system, B cells and dendritic cells were found to co-localise with Norwalk virus capsid signals (Bok et al., 2011). MNV was also found to infect B cells (Jones et al., 2014), supporting the idea that B cells are a possible tropism of HuNoV. However, histopathological analysis of biopsies from immunocompromised patients with chronic norovirus infection showed no evidence of HuNoV-infected B cells present in the samples screened (Karandikar et al., 2016). This study supported the hypothesis that HuNoV mainly replicated in enterocytes, while macrophages, T cells and dendritic cells can also be infected.

Our investigation of HuNoV infection of BJAB cells showed some evidence of virus replication (Figure 3.6C, D and F). However, in agreement with the previous data (Jones et al., 2015, Jones et al., 2014), significant variations were observed. This variable, low level replication unlikely facilitates the robust HuNoV infections clinically. However, in MNV the antigen presentation function of B cells is antagonised by viral protein VP2 (Zhu et al., 2016), highlighting the multiple functions of B cells in norovirus

pathogenesis. Therefore, it is still important to understand the roles of B cells in HuNoV life cycle.

3.4.4 Host factors for HuNoV infection remain to be studied

The development of a cell culture systems for HuNoV is the first step towards filling the knowledge gaps in understanding the molecular details of HuNoV replication. Now that a permissive cell type is identified, the next obvious question is what makes these cells susceptible to HuNoV infections, i.e. what host factor(s) are essential for B cells or organoids to support HuNoV infections?

First of all, both B cells and organoids may express sufficient cellular receptors for HuNoV entry. From screening of intestinal epithelial cells and professional antigen presenting cells, it became clear that HuNoV binds to all cells tested to different degrees. These results indicated the presence of attachment factors on cell surface, likely the HBGAs. However, it was unclear whether the inoculated HuNoV is internalised in these cells. In BJAB and organoids HuNoV replication was observed, which must be accompanied with successful viral entry. These two systems can therefore potentially be used to identify entry factors of HuNoV.

In BJAB, pre-incubation with enteric bacteria or HBGA enhances viral replication (Jones et al., 2014). Therefore, it is logical to propose that the limiting factor for viral entry in BJAB is cell surface HBGA expression. One enzyme recognised to be important for HBGA synthesis is FUT2, which adds a fucose group to the HBGA precursors, generating H antigens (de Graaf et al., 2016). Individuals with non-functional FUT2 genes, known as non-secretors, confer a certain degree to innate resistance to norovirus infections (Le Pendu et al., 2006). To test the hypothesis whether H antigen was the limiting factor for HuNoV entry in BJAB cells, the *FUT2* gene was cloned from enterocyte HT-29 cells into lentivirus expression construct.

Preliminary experiments using a norovirus pseudovirus particle entry assay showed that the overexpression of FUT2 in BJAB led to significant increase of HuNoV entry (L. Meredith, unpublished data), indicating that BJAB is a potential model to identify HuNoV entry factors.

In addition to viral entry, other host factors required for HuNoV replication remain to be characterised. Despite the possible lack of receptor expression on the cell surface, HuNoV replication in cell culture was not robust, as a low level of replication was observed in 293T cells transfected with HuNoV VPg-linked RNA (Qu et al., 2016). During the screening of cell lines for HuNoV infection, the replication of HuNoV genomic RNA in cell culture was also tested. The total RNA was purified from the acute pool stock or from Norwalk virus replicon-bearing BHK cells (clone G6). Transfection of both RNAs into BV-2, BHK and BJAB cells led to no increase in viral RNA (data not shown), indicating that HuNoV RNA does not replicate in cell lines efficiently. The primary intestinal organoids so far showed the most promising evidence of HuNoV replication. Therefore, by comparing gene expression profiling of differentiated organoids with BJAB or immortalised intestinal epithelial cell lines (e.g. Caco-2, HT-29, LS174T), genes up-regulated in organoids may be the factors important for HuNoV replication.

3.4.5 Improving the intestinal organoids system

With the development of the two cell culture systems, for the first time there is hope in understanding all the mystery of the ‘uncultivatable’ HuNoV. As discussed previously, BJAB may be useful to identify cellular receptor, whereas organoids are useful to understand the intracellular life cycle of HuNoV.

Despite all the exciting findings, there is room to improve the cost effectiveness and efficiency of the primary intestinal organoids system. In the current system, some

reagents are not commercially available, and the cost and efforts to maintain organoids are significant. All primary organoids were originally obtained from biopsies, with inevitable individual variations and the lack of a ‘gold standard’. Given that organoids double every six to seven days, and the large number of cells required per experiment, even simple experiments like the titration of HuNoV require significant input and advance planning. Therefore, in addition to using organoids to identify factors required for HuNoV replication, it is important to translate this knowledge to establish a more robust and cost-effective cell culture system for HuNoV. For example, differentiated organoids could potentially be immortalised and experiments performed to determine if they maintain susceptibility to HuNoV infection. Also, the differentiation of organoids can be directed to generate a higher proportion of enterocytes, which are infected by HuNoV in organoids (Ettayebi et al., 2016). Moreover, established intestinal epithelial cell lines like Caco-2, HT-29, LS174 or T84 could be modified so that they phenotypically mimic primary enterocytes. The development of any of these approaches could significantly lower the technical barrier of HuNoV culture and facilitate more studies of HuNoV using this system.

In summary, in this chapter attempts were made to establish an *in vitro* culture system for HuNoV. First of all, infectious HuNoV was obtained from either norovirus-positive faecal samples or from DNA-based reverse genetic system. Recombinant lentiviruses were applied to promote HuNoV replication by antagonising cellular innate immunity. Intestinal epithelial cells and immune cells were tested for HuNoV infection with little evidence of robust virus replication. Two HuNoV cell culture systems, the B cell and the primary intestinal organoids were tested and showed that the FPV-mediated reverse genetic system recovered infectious HuNoV. Although further efforts are needed to optimise the organoids system, the results demonstrate great potential of

engineering HuNoV to interrogate the details of HuNoV replication and dissect the norovirus-host cell interactions.

Chapter 4

Translation control of norovirus infection

4.1 Background

In the previous chapter, attempts were made to cultivate HuNoV *in vitro*. Because the two culture systems are in the early stages of development, surrogate systems remain invaluable tools to understand norovirus biology.

Viruses are intracellular obligate parasites. During infection, host cellular pathways are hijacked by viruses to facilitate the replication of viral genes and to overcome the cellular defence mechanisms. Compared to transcriptional control, translation control is an effective mechanism for viruses to antagonise and subvert host responses at the protein level, resulting in direct modulation host proteome during infection (Roth et al., 2017).

The majority of eukaryotic translation initiation is cap-dependent, for which the interaction between the cap-binding protein eIF4E and the 5’ cap of mRNAs is essential for recruiting the eIF4F complex (eIF4A, eIF4E and eIF4G). eIF4E is recognised as the rate-limiting step for cap-dependent translation initiation and its activity can be regulated by both host cellular and viral pathways. The main regulator of eIF4E is the eIF4E-binding proteins (4E-BPs) which binds eIF4E on its dorsal surface, sharing the binding site with eIF4G (Marcotrigiano et al., 1999, Peter et al., 2015). These mutually exclusive interactions are thought to regulate the eIF4G:eIF4E interaction. Besides binding to 4B-BPs, the activity of eIF4E can also be regulated by phosphorylation at Serine 209 by the MAP kinase-interacting serine/threonine-protein kinase 1/2 (Mnk1/2) (Shveygert et al., 2010). Whilst 4E-BPs regulate cap-dependent translation initiation by competing with eIF4G to bind eIF4E, phosphorylation of eIF4E is thought to modulate the translation of a subset of mRNAs with long, structured 5’

UTRs, including genes encoding growth regulatory proteins (Feoktistova et al., 2013). Besides in cancer progression, phosphorylation of eIF4E has also been observed during several infections of several DNA viruses (Zaborowska and Walsh, 2009, Walsh et al., 2005, Walsh and Mohr, 2004, Furic et al., 2010). Later, it was proposed that both DNA and RNA viruses hijack the phosphorylation of eIF4E to translationally regulate type I IFN responses during infection (Herdy et al., 2012).

MNV infection induces phosphorylation of eIF4E via the p38-Mnk1 signalling pathway (Royall et al., 2015). Inhibition of this pathway using pharmaceutical drugs reduces MNV replication in immortalised cells. In addition, the phosphorylated eIF4E relocates to polysome and changes the translation state of several mRNAs during MNV infection. One of the mRNAs with increased translation state is *Nfkbia*, which encodes NF-κB inhibitor IκBα. Increased translation of IκBα inhibits NF-κB activity, resulting in impaired innate immunity and enhanced virus replication. As norovirus replication is sensitive to type I IFN responses (Thackray et al., 2012, Chang et al., 2006), the phosphorylation of eIF4E induced by MNV infection may be a viral mechanism to induce translational bias during infection.

Several questions remain to be answered with the hypothesis. Can the initial observations be reproduced in a more biologically relevant, *in vivo* model? Is MNV replication impacted by genetically inhibiting phosphorylation of eIF4E? In addition to modulating type I IFN responses, how does norovirus infection elicit translation control through the phosphorylation of eIF4E?

To understand the translational bias induced by eIF4E phosphorylation during MNV infection, the phosphorylation site of eIF4E (Serine 209) was genetically engineered into a non-phosphorylatable alanine (S209A) (Furic et al., 2010). eIF4E S209A knock-in mice (referred as the KI mice hereafter), showed reduced tumorigenesis and cancer progression (Furic et al., 2010). In MEF cells derived from KI mice, the global

translation is not impacted. However, the reduced translation of IκBα results in enhanced type I IFN responses, inhibiting both RNA and DNA virus replications (Herdy et al., 2012). This observation highlights the potential of the KI mice as a model system to study the antiviral role of eIF4E phosphorylation during MNV infection.

4.2 Aims

The aim of this chapter was to understand the translational bias by norovirus to subvert host immune pathways. Based on the previous observations, it was proposed that the loss of eIF4E phosphorylation due to the S209A mutation should lead to enhanced type I IFN responses, attenuating MNV replication *in vivo*.

4.3 Results

4.3.1 Introduction of the eIF4E S209A mouse model

Mice were bred from parents carrying heterozygous S209A mutation of eIF4E, to exclude interference of host-microbiome interactions in the study (Stappenbeck and Virgin, 2016). Sex- and age-matched littermates were used for *in vitro* and *in vivo* studies. Two heterozygous breeding trios were introduced to establish a breeding colony. Ear biopsies taken from the initial breeding trios and WT C57BL/6 mice were used for establishing and validating the genotyping PCR (data not shown).

For all experiments, mice were genotyped and WT or KI mice were used for bone marrow differentiation or MNV infections per oral. Throughout this project, the total numbers of each genotype were as follow:

	WT (WT/WT)	Het (WT/S209A)	KI (S209A/S209A)
Male	41	73	38
Female	37	80	47

Table 4.1 Number of pups of each genotype.

4.3.2 Type I IFN signalling in KI BMDM

MEF cells from the KI mice show stronger type I IFN response due to increased NF-κB activity (Herdy et al., 2012). In order to validate this activation, primary bone marrow-derived macrophages (BMDMs) were differentiated from femur bones of KI and WT mice. On day 7 post differentiation, the cells were stimulated by poly I:C transfection (Figure 4.1).

Upon stimulation, BMDMs from KI mice showed more than 2 times higher induction levels of *Ifnb* compared WT BMDMs (Figure 4.1A), nevertheless both of which were significantly lower than that of the Raw264.7 cells. The significantly higher induction of *Ifnb* in KI BMDMs is consistent with previously published results, which is thought to due to the increased NF-κB activity (Herdy et al., 2012). Therefore, it is possible that other genes whose expression are controlled by NF-κB activity would have elevated induction upon poly (I:C) transfection. *Il6* is one of the NF-κB target genes (Libermann and Baltimore, 1990, Son et al., 2008). When BMDMs or Raw264.7 cells were stimulated with poly (I:C), significant inductions of *Il6* were observed in all cells (Figure 4.1B). However, there was no difference between WT and KI BMDMs. Significantly higher induction was again observed in Raw264.7 cells. These results indicate that although phosphor-ablative mutation of eIF4E induces stronger *Ifnb* induction upon stimulation possibly via elevated NF-κB activity, the enhancement does not apply to all NF-κB target genes.

The type I IFN responses through poly (I:C) stimulation were also assessed. The transfection of poly (I:C) did not induce transcription of *Rsad2* mRNA in either BMDM, suggesting the production of IFN β is the major effect of poly (I:C) stimulation of BMDMs. However, a significant induction was observed in Raw264.7 cells, suggesting the poly (I:C) concentrations used in the experiment can induce transcription of ISGs. In order to exclude the possibility of gene-specific effects, the induction of *Isg15* was also determined (Figure 4.1D). In agreement with the observed induction of *Rsad2*, no significant induction was observed in WT or KI BMDMs, while in Raw264.7 cells significant *Isg15* induction was observed.

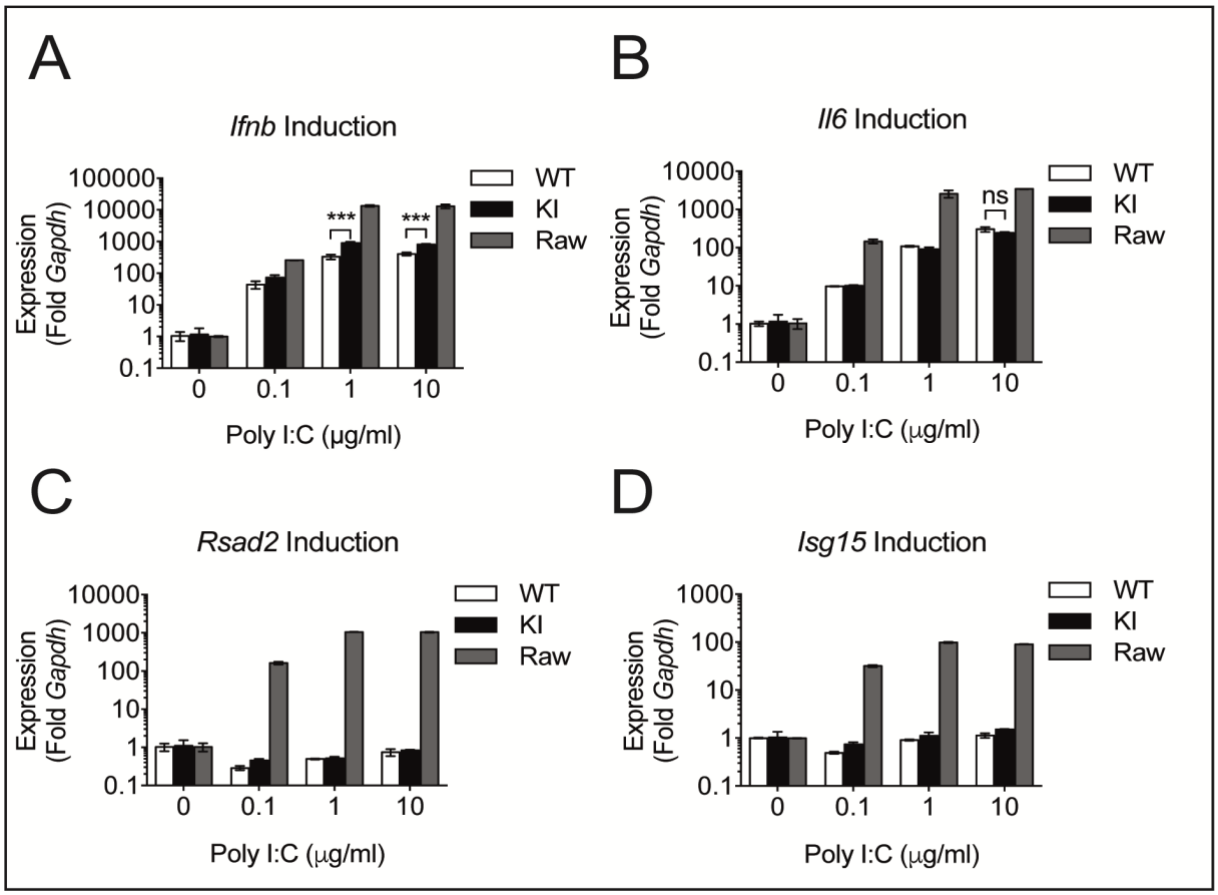

Figure 4.1 Type I IFN signalling of BMDM. Bone marrow cells were isolated from WT or KI littermates (n=2 of each genotype) and differentiated using conditioned CMG14-12 supernatant (Takeshita et al., 2000). Differentiated BMDMs were transfected with different concentrations of poly (I:C). Raw264.7 cells were used as the positive control for transfection. Cells were harvested at 12 hours post-transfection and the total cellular RNA was extracted. RT-qPCR was performed to assess the induction of A) *Ifnb*, B) *Il6*, C) *Rsad2*, and D) *Isg15*. The expression level of each gene was normalised to that of *Gapdh*, and

the fold of induction was calculated using the $\Delta\Delta$Ct method (Livak and Schmittgen, 2001). Two-way ANOVA was performed using Bonferroni test (* p<0.05, ** p<0.01, *** p<0.001).

4.3.3 Production of ISGs in BMDM

To compare the type I IFN responses between differentiated BMDMs, different concentrations of recombinant IFNβ were added to the differentiated BMDMs and Raw264.7 cells, and the total cellular RNA was harvested at 12 hours post treatment. Figures 4.2A and B showed the induction of *Rsad2* and *Isg15*, respectively. IFNβ treatment induced significant expression of *Rsad2* and *Isg15*. Together with Figure 4.1C and D, these results indicate that the low level of ISG induction in BMDMs upon poly (I:C) transfection was not due to the inability of BMDM to respond to IFN-β. In fact, BMDMs from both KI and WT mice responded better to IFNβ by producing more *Rsad2* mRNAs than Raw264.7 cells did.

In summary, *in vitro* characterisation of BMDMs from WT and KI mice showed observations consistent with data from others, yet it is possible that the effect of eIF4E S209A mutation on type I IFN pathways is more complicated than simply enhancing NF-κB-mediated signalling.

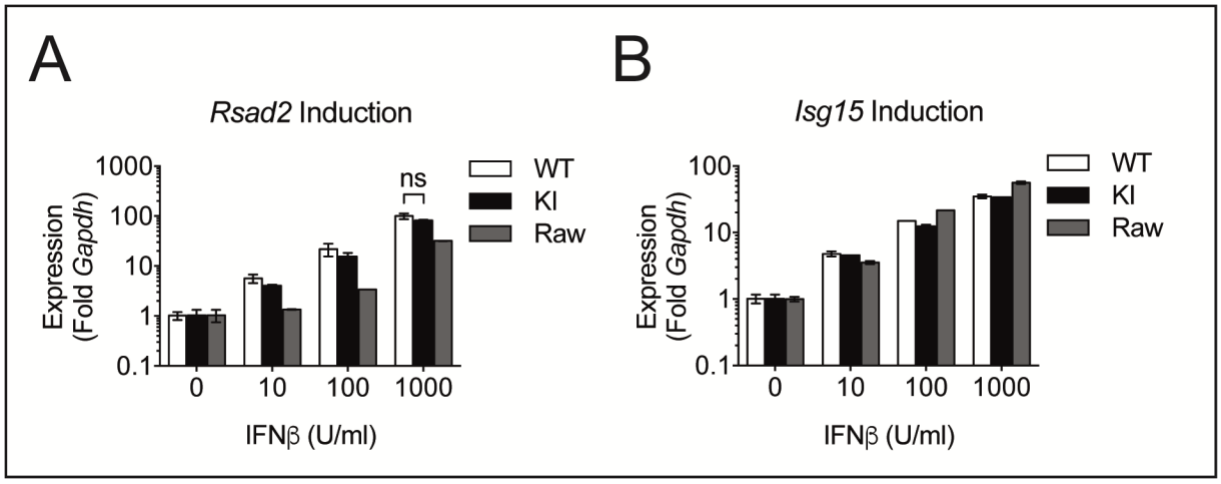

Figure 4.2 ISG production of BMDM. BMDMs from WT or KI littermate were differentiated as in Figure 4.1 (n=2 of each genotype) and different concentrations of IFNβ were added to cells. 12 hours post treatment the total cellular RNA was isolated and relative RT-qPCR was used to determine the induction

of two representative ISGs: A) *Rsad2*, and B) *Isg15*. The relative gene expressions were normalised to the housekeeping gene *Gapdh* and the fold of induction was calculated using the $\Delta\Delta$Ct method (Livak and Schmittgen, 2001). Two-way ANOVA was performed using Bonferroni test (* $p<0.05$, ** $p<0.01$, *** $p<0.001$).

4.3.4 Infection of BMDM

To assess the effect of phosphor-ablative eIF4E mutation on MNV replication, *in vitro* infection model was first established using the well-characterised MNV-1. MNV-1 causes acute infection in immunocompetent mice without significant pathology. In cell culture, MNV-1 readily infects permissive macrophage (Raw264.7) and microglial (BV-2) cell lines (Cox et al., 2009). In primary dendritic cells and macrophages, MNV-1 can still establish infection, though with a lower infection rate and virus yield (Wobus et al., 2004).

MNV infection of BMDM was assessed by staining for two markers of infection, NS3 and dsRNA. As shown in Figure 4.3, BMDM and Raw264.7 cells were infected by MNV-1 at the same MOI (10 $TCID_{50}$ per cell). At 12hpi, there are more NS3 and dsRNA positive cells in Raw264.7 cells than in BMDM, suggesting BMDM are less susceptible to MNV infection.

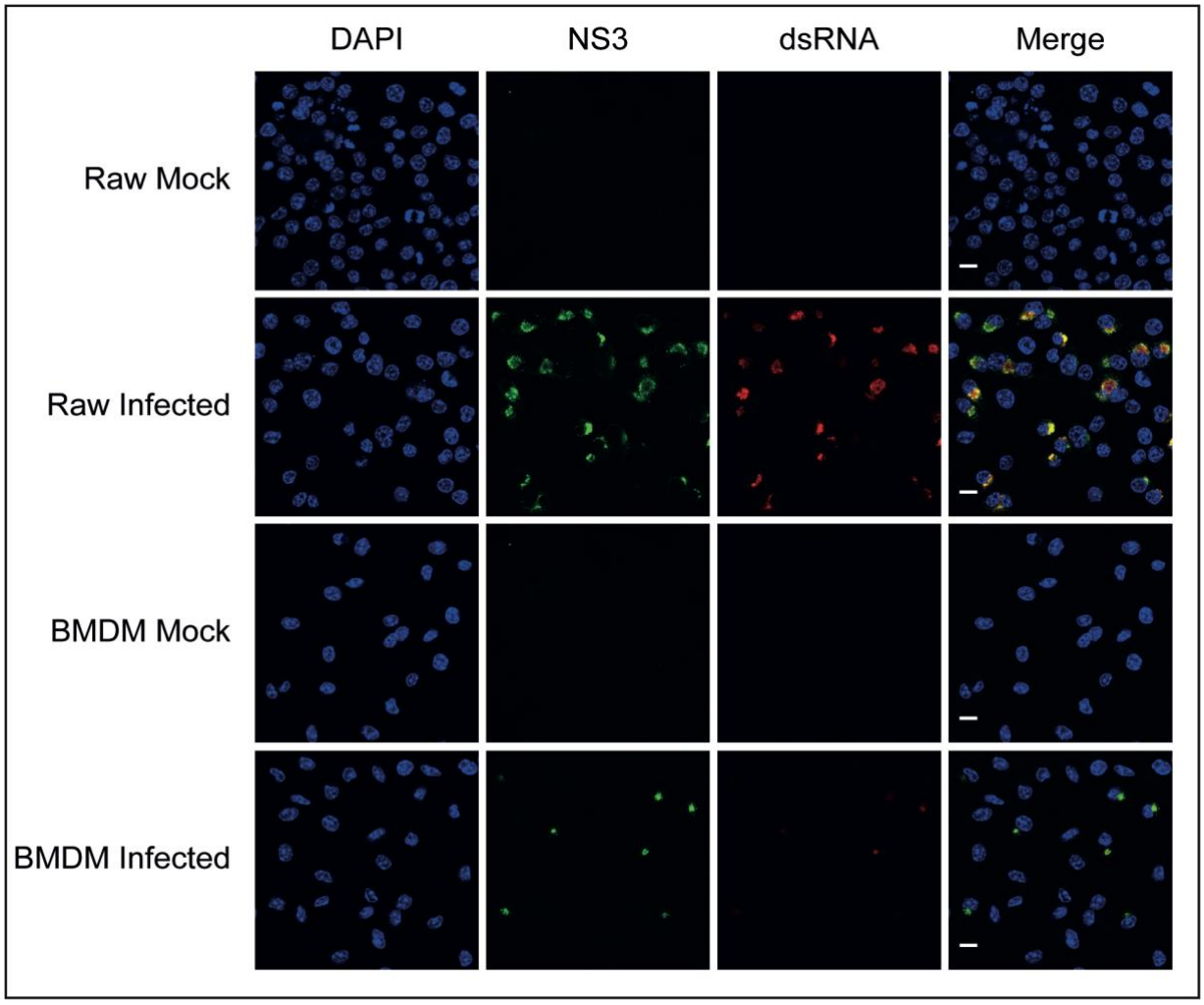

Figure 4.3 BMDM infection. Bone marrow cells were isolated and differentiated according to previously published protocols (Takeshita et al., 2000). On day 7 post differentiation, BMDMs or Raw264.7 cells were infected with purified MNV-1 at an MOI of 10 TCID50/cell. At 12hpi, cells were fixed and stained for dsRNA and NS3. The nuclei were stained with DAPI. Both dsRNA and NS3 co-localised in the perinuclear foci. Scale bar represents 10 μm.

4.3.5 Infection of KI BMDM by MNV-1

The ISG inductions following infection were determined by infecting BMDM with purified MNV-1. Productive infection of BMDM was seen from different MOIs (Figure 4.4A to C). All inoculations led to increases in viral titres over time, peaking between 10^4 to 10^5 $TCID_{50}$/ml. Even at different MOIs, no significant difference in virus yield between WT and KI BMDMs was observed.

MNV-1 infection of both BMDMs significantly induced transcription of *Ifnb* (Figure 4.4D). At MOI 0.5 and 5 $TCID_{50}$/cell, the induction of *Ifnb* was significantly higher in KI BMDMs.

Increased *Ifnb* induction was paralleled with significantly higher induction of *Rsad2* (Figure 4.4E). MNV is known to uncouple host translation from transcription during infection (Emmott et al., 2017). To determine the production of ISGs in infected BMDMs, total protein from infected cells (MOI 0.5) were harvested at 12hpi. Cellular RNA from all MOIs was also extracted. The phosphor-ablative mutation in KI BMDMs was confirmed by the absence of p-eIF4E (Figure 4.4F). MNV-1 infection of both BMDMs induced significant expression of viperin compared to Raw264.7 cells, yet the production of viral protein NS3 was barely observable. In contrast, in Raw264.7 cells the NS3 signal was very significant. The significantly higher expression of both eIF4E and p-eIF4E was observed in Raw264.7 cells, but in this experiment MNV-1 infection did not increase the level of p-eIF4E in Raw264.7 cells. Together, these results suggest that a stronger type I IFN response was observed in MNV-1 infected KI BMDMs, but this had little effect on MNV replication.

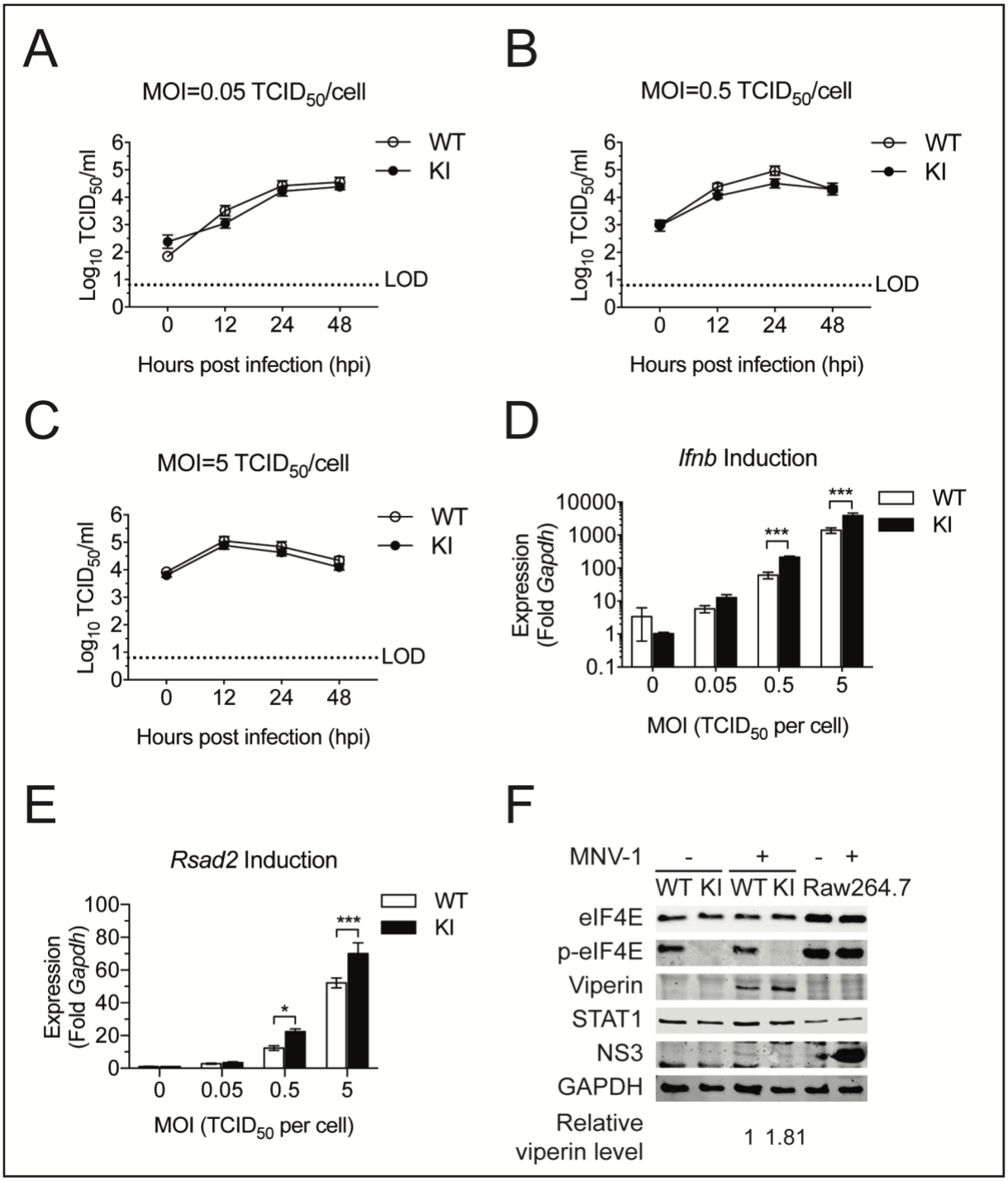

Figure 4.4 Infection of KI BMDM by MNV-1. WT or KI BMDMs from littermates (n=6 of each genotype) were differentiated and infected by MNV-1 at different MOIs. Virus yield was determined at the indicated time points post infection (A to C). At 12hpi, the total RNA was extracted from each sample and the inductions of *Ifnb* and *Rsad2* were determined by RT-qPCR (D and E). Two-way ANOVA was performed using Bonferroni test (* p<0.05, ** p<0.01, *** p<0.001). F) showed the production of viral protein NS3 and induction of ISGs upon infection.

4.3.6 Infection of KI BMDM by MNV-3

The initial characterisation of KI BMDMs showed a higher *Ifnb* induction upon poly (I:C) transfection and during MNV-1 infection, yet there was no impact on virus yield. MNV-1 causes acute infection and was isolated from the brain of a IFN$\alpha\ \beta\ \gamma$R$^{-/-}$ mouse (Karst et al., 2003). Compared with MNV-3, MNV-1 CW1 p3 is a relatively attenuated virus (Zhu et al., 2013). Also, BMDM is one of the cell types infected by MNV *in vivo* (Wobus et al., 2004). Previous work has shown that MNV can be attenuated *in vivo* with no significant defect in replication in cell culture (Bailey et al., 2008). Therefore, it is possible that the effect of eIF4E phosphorylation on MNV replication was not shown in the acute infection model.

MNV-3 was chosen as the model system to study the effect of phosphor-ablative eIF4E on norovirus pathogenesis *in vivo*. A mutant of MNV-3 was also used, MNV-3^{VF1-}, containing stop codons at the N-terminus of VF1 coding region. The production of functional VF1 is consequently abolished without codon changes of the overlapping VP1 shell domain coding region. *In vitro* characterisation showed MNV-3^{VF1-} replication to be comparable to WT MNV-3, but a stronger induction of type I IFN response was observed. *In vivo* replication of MNV-3^{VF1-} in immunocompetent mice is attenuated (T. Christoudoulo, manuscript in preparation). Therefore, in KI mice MNV-3^{VF1-} replication should be further restricted because of the enhanced type I IFN responses.

Initially, BMDMs from WT or KI mice were differentiated for 7 days before infection with either WT or mutant virus at different MOIs to determine the *in vitro* replication kinetics of MNV-3 and MNV-3^{VF1-} (Figure 4.5). MNV-3 infection in WT BMDMs resulted in slightly higher viral titres compared with in KI BMDMs (Figure 4.5A, C and E). This result is most obvious at the early stages of infection at low MOI (Figure 4.5A). As

infection progressed, virus replication in both BMDMs reached comparable titres. At MOI=0.5 and 5 $TCID_{50}$ per cell (Figure 4.5C and E), the infection kinetics are slower and the overall folds of replication are smaller compared with low MOI, possibly indicating that the infection has yielded the maximal virus. At all MOIs, titres at 48hpi are comparable to titres at 0hpi, possibly indicate the decaying of excessive input viruses and progeny viruses.

The replication kinetics of MNV-3^{VF1-} is slower in general than that of the MNV-3 WT (Figure 4.5 B, D and F). Gradually increasing virus titres were observed at different MOIs, except for MNV-3 at MOI = 0.5 $TCID_{50}$ per cell at 48hpi (Figure 4.5D). This also resulted in the only data point with statistically significant differences in virus yield between WT and KI BMDMs. Apart from WT BMDM infected at MOI 0.5, virus yield of MNV-3^{VF1-} at 48hpi was higher than that of MNV-3 WT. Overall, no significant difference was observed in the *in vitro* replication kinetics of two MNV-3s between WT and KI BMDMs.

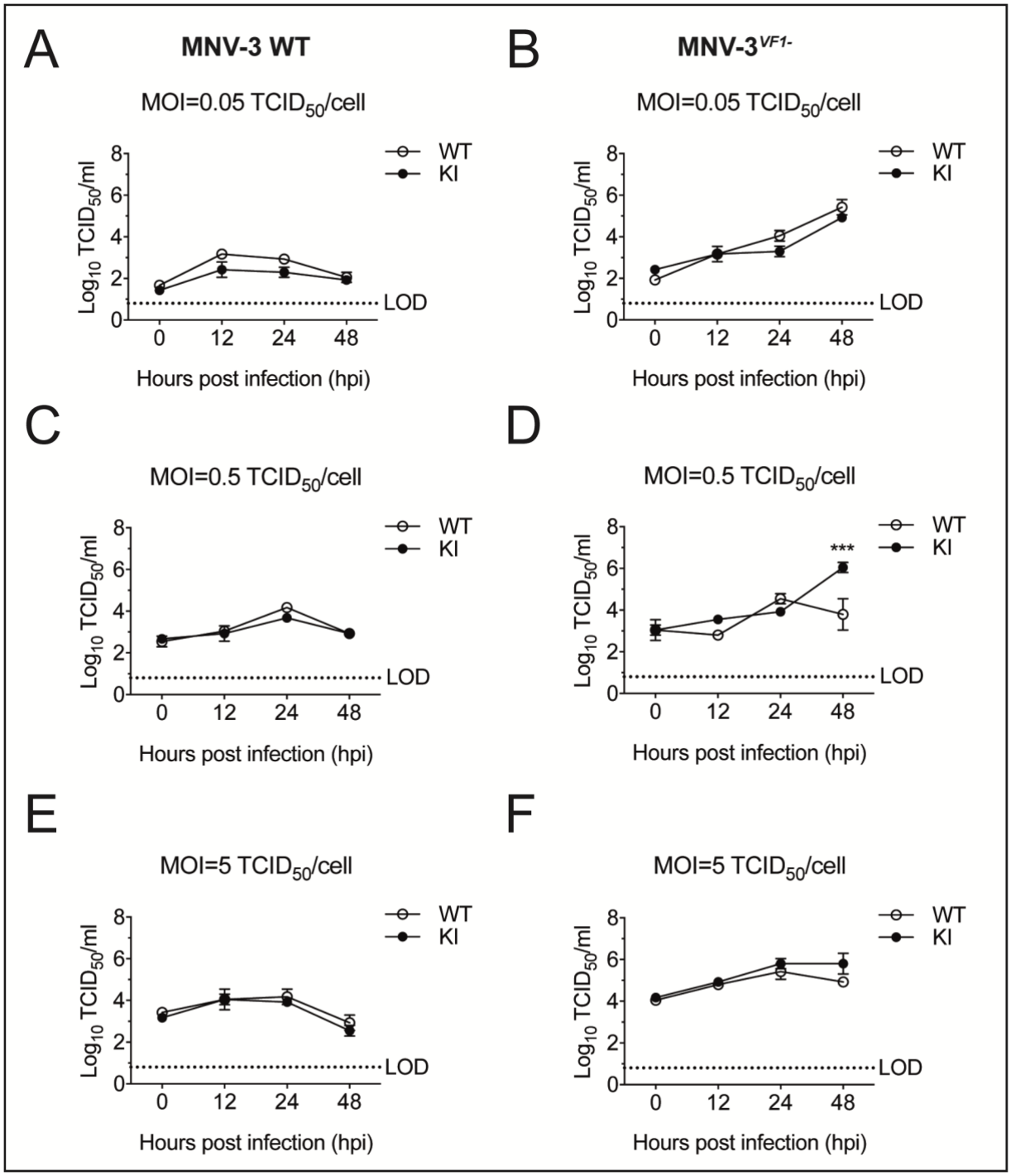

Figure 4.5 Infection of KI BMDM by MNV-3. Differentiated BMDMs (n=2 of each genotype) were infected by MNV-3 WT (A, C and E) or MNV-3^{VF1-} (B, D and F) at the indicated MOIs. The virus yields at different time points post infection were determined by $TCID_{50}$. Statistical analysis was performed using two-way ANOVA with Bonferroni test (* p<0.05, ** p<0.01, *** p<0.001).

4.3.7 Infection of KI mice by MNV-3

To characterise the effect of eIF4E phosphor-ablative mutations on MNV pathogenesis, MNV-3 was inoculated into WT or KI littermates per oral. Both male and female mice were tested for MNV-3 replication (Figure 4.6A). Prior to infection, no faecal shedding was detected in any mice. During acute infection (days 1 to 7), faecal shedding was detected from day 1 and peaked on 3 days post inoculation, resulting in more than 10^5 gEq/mg faeces. The faecal shedding continued to decrease during the persistent infections, but remained readily detectable on 56 days post infection. However, no significant differences in faecal shedding were observed at any time points post infection.

The body weight changes were compared to pre-infection and showed no evidence of significant pathology (Figure 4.6B), consistent with prior observations that the pathology of MNV-3 infections in immunocompetent mice is sub-clinical (Zhu et al., 2013, Arias et al., 2012, Kahan et al., 2011). The production of MNV-specific serum IgG increased significantly starting from day 7 post infection and on day 14 reached levels comparable to 4 weeks post infection (Figure 4.6C). On day 56 post infection, high levels of serum IgG in both WT and KI mice were observed. In summary, MNV-3 established persistent infections in WT and KI mice, but there was no difference in viral replication, pathogenesis and induction of mucosal immunity.

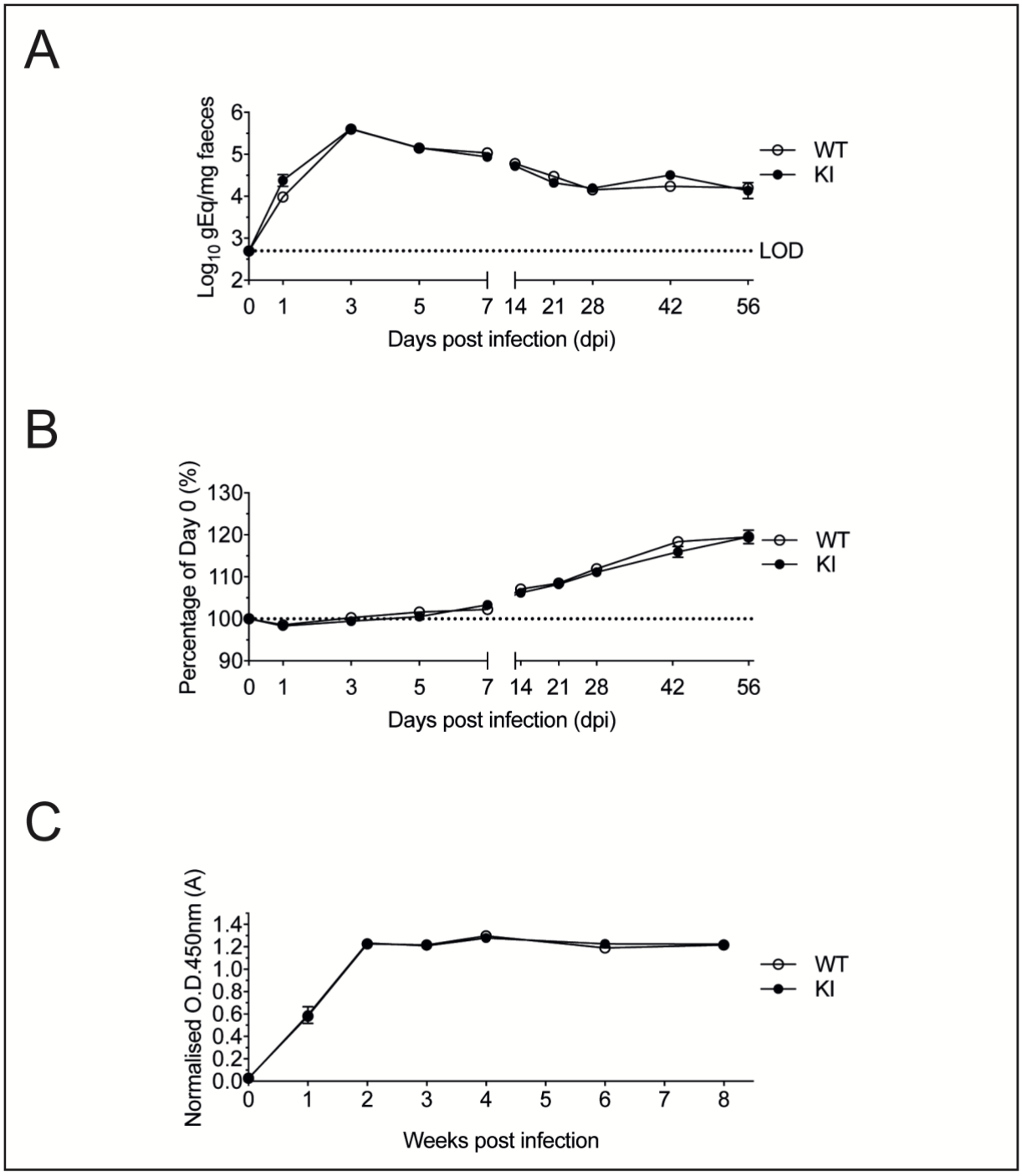

Figure 4.6 MNV-3 pathogenesis in KI mice. 4-6-week WT (n=9) or KI (n=10) littermates were infected by MNV-3 WT at 1000 $TCID_{50}$ per animal and A) faecal shedding, B) weight change, and C) production of MNV-specific antibody were determined. No difference in MNV-3 replication, pathogenesis or mucosal immune response was observed between WT and KI mice. Two-way ANOVA was performed using Bonferroni test (* p<0.05, * p<0.01, *** p<0.001).

4.3.8 Low dose MNV-3^{VF1-} challenge in KI mice

In vivo replication of MNV-3^{VF1-} in WT and KI mice is shown in Figure 4.7. During the acute infections, faecal shedding of MNV-3^{VF1-} in WT and KI mice was significantly lower compared to MNV-3 WT. This is consistent with the previous observations that MNV-3^{VF1-} is attenuated *in vivo* (manuscript in preparation). However, at 3 and 5 days post infection, faecal shedding of the KI mice infected with MNV-3^{VF1-} is significantly higher than those of WT mice. This observation differs from the original hypothesis that eIF4E phosphor-ablative mutations led to more restriction in virus replication. No significant difference was observed during the persistent infections. The slight growth advantage of MNV-3^{VF1-} in KI mice did not lead to more changes in body weight (Figure 4.7B).

The better infection of MNV-3^{VF1-} in KI mice was also supported by the production of more MNV-specific serum IgG on 14 and 21 days post infection. (Figure 4.7C). This difference was not significant from 21 days post infection. Together, during the acute phase of infection, the phosphor-ablative mutations in the KI mice partially rescued the replication of an attenuated MNV-3^{VF1-}, but the effect is marginal and does not restore the replication back to the level of MNV-3 WT.

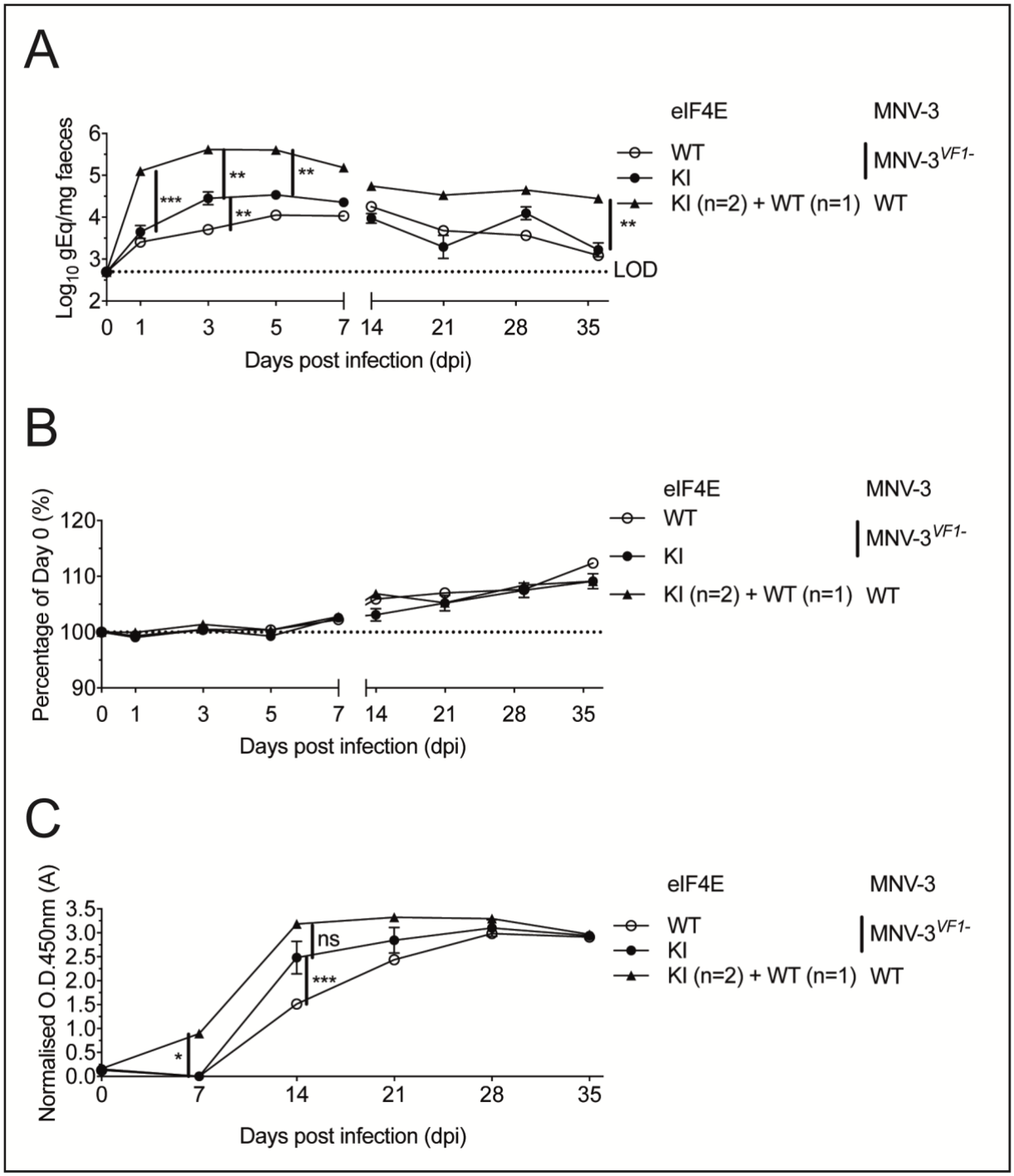

Figure 4.7 MNV-3^{VF1-} pathogenesis in KI mice. 4-6-week old WT (n=10) or KI (n=9) littermates were infected with 1000 $TCID_{50}$ of MNV-3^{VF1-} and A) faecal shedding, B) weight change and C) production of MNV-specific antibody was measured through 5-week period. For comparison in this experiment, KI (n=2) and WT (n=1) mice were infected with 1000 $TCID_{50}$ of MNV-3 WT and the according data was collected together. Two-way ANOVA was performed using Bonferroni test (* p<0.05, * p<0.01, *** p<0.001). Note that a different TMB substrate was used in C)

4.3.9 Tissue tropism of MNV-3^{VF1-} during persistent infection

At 35 days post infection, the mice were sacrificed and the tissues harvested. The total RNA was extracted from colon (Figure 4.8A), caecum (Figure 4.8B) and MLN (Figure 4.8C), which were previously reported to be the tropism of persistent MNV-3 infections (Arias et al., 2012). No significant difference was found in viral RNA between infected WT and KI mice. The colon and caecum viral RNA in mice infected with MNV-3^{VF1-} is significantly lower than those infected with MNV-3 WT. Therefore, during the persistent infections the marginal growth advantage of MNV-3^{VF1-} in the KI mice during acute infections was not reflected in the tissue tropism.

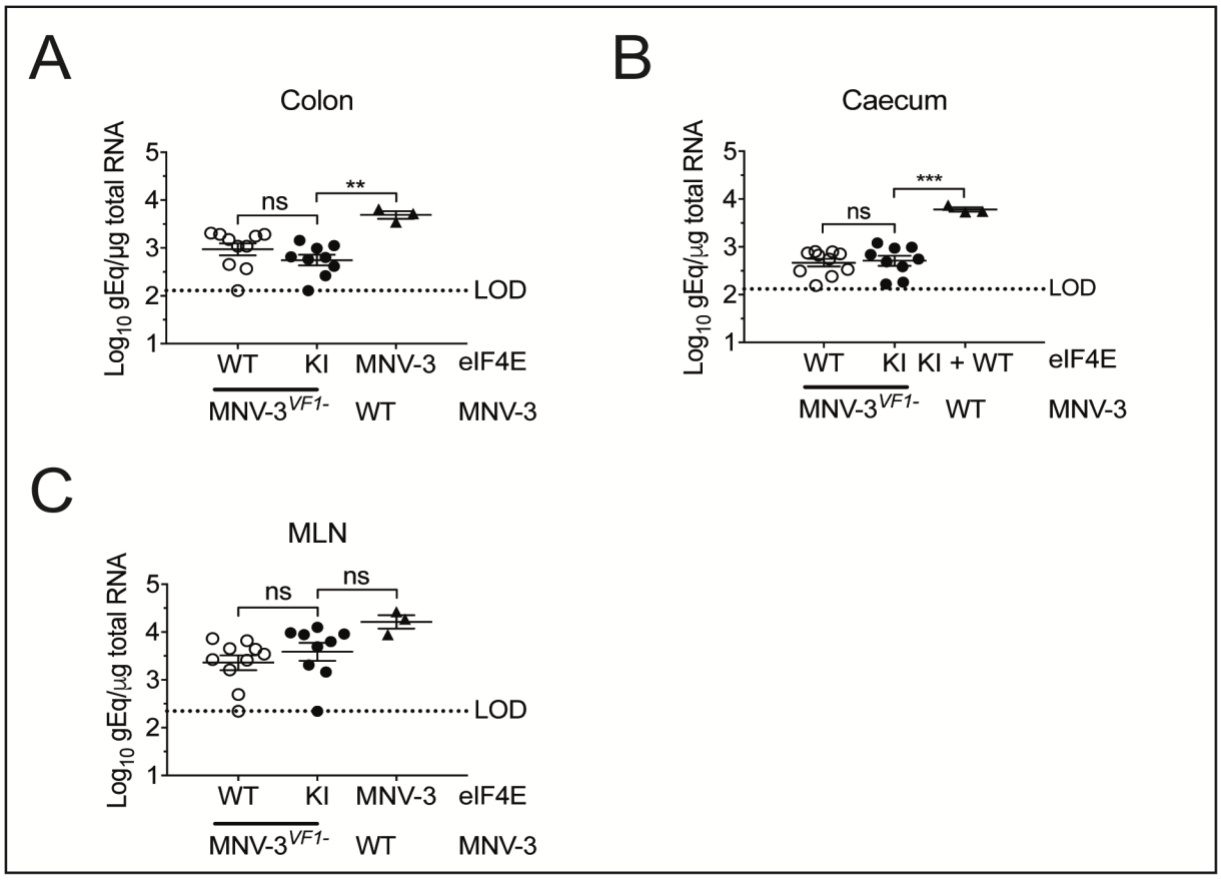

Figure 4.8 Tissue tropism of MNV-3^{VF1-} during persistent infection. On day 35 of the experiment in Figure 4.7, the according tissues were harvested and the viral RNA was determined by RT-qPCR: A) Colon B) Caecum and C) MLN. One-way ANOVA was performed using Dunnett test (* p<0.05, * p<0.01, *** p<0.001).

4.3.10 Tissue tropism of MNV-3^{VF1-} during acute infection

It was possible that the phosphorylation of eIF4E is more important for the replication of MNV-3^{VF1-} during the acute infection. Therefore, WT or KI littermates were challenged with high dose of MNV-3^{VF1-} (10^5 $TCID_{50}$ per mouse by oral gavage), based on the hypothesis that a robust MNV-3^{VF1-} replication may display more growth advantage in the KI mice over the WT mice. The mice were sacrificed on 3 days post infection and tissues were harvested to determine the viral RNA (Figure 4.9). The total RNA was extracted from faeces, duodenum, colon and mesenteric lymph nodes and the viral RNA was determined by RT-qPCR. No significant difference in faecal shedding was observed between WT and KI mice (Figure 4.9A). Faecal shedding of mice from high dose challenge is lower than that of mice challenged with low dose of MNV-3^{VF1-} (Figure 4.8A). MNV RNA was barely detectable in duodenum (Figure 4.9B). In tissues where MNV-3 establishes persistent infection (large intestine and MLN), MNV RNA was readily detected and there was no significant difference between WT and KI mice (Figures 4.9 C and D). The production of IFN β in serum was also determined in uninfected and in infected mice. Although the faecal shedding was shown to be the highest on 3 days post infection (Figures 4.6A and 4.7A), no significant level of serum IFN β was detected compared to uninfected mice. In summary, high dose challenge of an attenuated MNV-3^{VF1-} reduced the peak titre of faecal shedding, and there is no difference in tropism of MNV-3^{VF1-} in between WT and KI mice. No significant production IFN β was observed on day 3 post infection. Together, the S209A mutation in eIF4E only appears to enhance replication of an attenuated MNV-3^{VF1-} during acute infection in a dose-dependent manner.

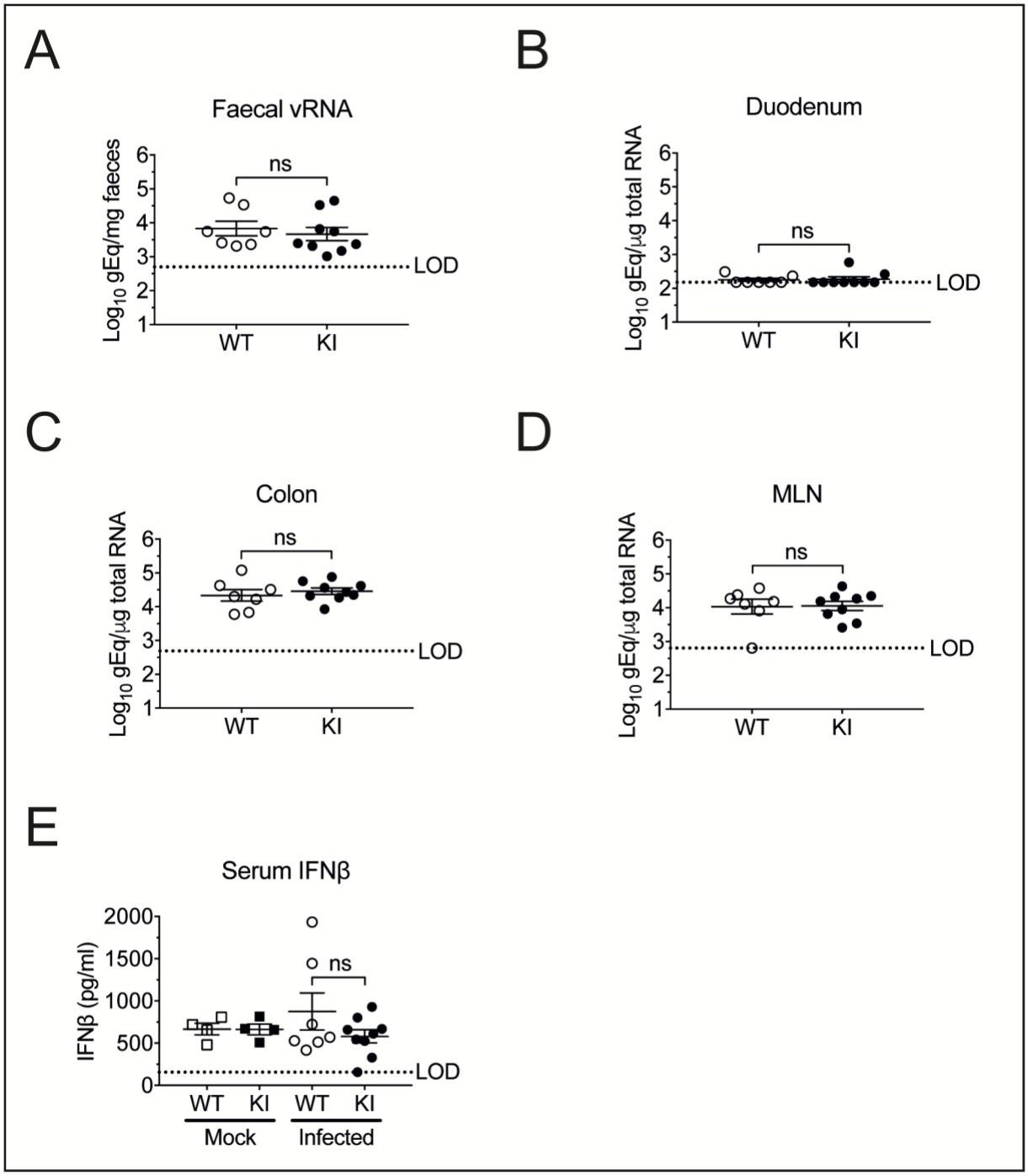

Figure 4.9 Tissue tropism of MNV-3^{VF1-} during acute infection. WT (n=7) or KI (n=9) littermates were infected with 10^5 $TCID_{50}$ of MNV-3^{VF1-} and the mice were sacrificed 3 days post challenge. A) Faecal shedding, and viral RNA of the following tissues were determined by RT-qPCR: B) Duodenum, C) Colon, and D) MLN. Serum IFN β was determined by ELISA (E). For all experiments, one-way ANOVA was performed using Dunnett test (* p<0.05, ** p<0.01, *** p<0.001).

4.4 Discussion

Our previous study of MNV translation control revealed a mechanism by which MNV activates the p38-Mnk1 pathways and re-programmes host translation via regulating eIF4E activity (Royall et al., 2015). This provides a possible explanation why norovirus VPg interacts with eIF4E *in vitro* and *in vivo*, but eIF4E is dispensable for MNV translation and infectivity (Chaudhry et al., 2006). Similarly, dengue virus replication is sensitive to the inhibition of the p38-Mnk1 pathway (Roth et al., 2017). In addition to re-programming host-cell translation, phosphorylation of eIF4E also enhances viral protein translation during infection. During Chikungunya virus (CHIKV) infection, phosphorylation of eIF4E at early stage of infection leads to enhanced translation of viral proteins (Joubert et al., 2015). Instead of activating the p38-Mnk1 pathway, the cross talk between the PI3K and the Mnks signalling pathways is responsible for phosphorylating eIF4E. In addition to using pharmaceutical drugs, the importance of eIF4E phosphorylation in virus-host cell interaction was also demonstrated by genetically mutating the phosphorylation site (Serine 209) into a non-phosphorylatable Alanine. In the KI cells, higher NF-κB activity leads to enhanced type I IFN responses, thereby restricts the replication of two positive-strand RNA viruses (Sindbis virus, EMCV), one negative-strand RNA virus (VSV), and one DNA virus (Vaccinia virus) (Herdy et al., 2012). Together, eIF4E phosphorylation is important in viral replication and in viral-host cell interaction.

In this chapter, the hypothesis that norovirus infection induced translational bias by phosphorylating eIF4E was tested. It was thought that in the KI mouse model, MNV replication should be restricted, possibly due to the enhanced type I IFN responses. To determine the importance of eIF4E phosphorylation in MNV pathogenesis, the KI mice breeding colony was established, and type I IFN signalling pathways in KI BMDMs

were characterised. The induction of *Ifnb* upon stimulation was enhanced compared with WT, which is consistent with previous observation (Herdy et al., 2012). The same study also proposed that increased NF-κB activity is responsible for the increased IFNβ production. However, while poly (I:C) stimulation significantly induced *Il6* expression, there was no difference between WT and KI BMDM, indicating that this enhancement does not apply to all genes regulated by NF-κB activity. Therefore, more evidence is required to understand the induction of type I IFN in KI BMDM.

Another observation is that with a significant induction of *Ifnb*, no ISG induction was observed in poly (I:C)-stimulated BMDMs (Figure 4.1C and D). Both WT and KI BMDM were able to produce ISGs when treated with IFNβ (Figure 4.2). Therefore, in BMDM the inability to express ISGs is possibly caused by poly (I:C)-induced translation shut down (Clavarino et al., 2012). In Raw264.7 cells significant *Rsad2* and *Isg15* inductions were observed, possibly due to better tolerance to translation shut down compared to BMDM.

To determine if WT and KI BMDM have the same capacity to responded to IFNβ, expressions of ISGs were compared following IFNβ treatment. Induction of *Rsad2* and *Isg15* were observed in both WT and KI BMDM, and there was no difference in the magnitude of responses (Figure 4.2A and B). Therefore, the enhanced type I IFN responses are likely due to more IFNβ produced in KI BMDM.

A previous study showed that due to the increased production of IFNβ, VSV-infected KI mice have enhanced survival rates compared to WT mice (Herdy et al., 2012). MNV-1 infection is sensitive to type I IFN responses, and in immunocompetent mice the induction of type I IFNs in intestinal homogenates and serum were observed starting from 1 day post infection (Wobus et al., 2004, Mumphrey et al., 2007). Therefore, it was thought that due to increased production of IFNβ, MNV replication should be

attenuated in KI BMDMs. In MNV-1-infected KI BMDM, the *Ifnb* induction was more significant than in WT BMDMs, resulting in higher induction of *Rsad2* (Figure 4.4E). Also, more viperin was produced (Figure 4.4F). However, even at different MOIs, the impact of phosphor-ablative mutations on MNV-1 replication was trivial (Figure 4.4A to C). This indicates that at least in the current experiment set up, MNV-1 replication is not sensitive to enhanced *Ifnb* production in BMDM. In addition to the acute infection model, *in vitro* replication kinetics of persistent MNV-3 was compared between WT and KI BMDM. With different MOIs and viruses, there was minimal effect of eIF4E S209A mutation on MNV replication, with the only exception of MNV-3^{VF1-}, MOI 0.5 at 48hpi (Figure 4.5D). Together, with the enhanced production of IFN β, MNV replication in BMDM is minimally impacted by phosphor-ablative mutations of eIF4E.

One of the possible explanations of the different observations between in Raw264.7 cells and in BMDM is that the translation re-programming via phosphorylation of eIF4E is cell type-specific. It was observed that compared with BMDM, Raw264.7 cells have higher expression of both eIF4E and p-eIF4E (Figure 4.4F). Because of this, it is possible that the effect of eIF4E phosphorylation on MNV replication is different between the two cell lines.

MNV infects macrophages, dendritic cells and B-cells both *in vitro* and *in vivo* (Wobus et al., 2004, Jones et al., 2015, Jones et al., 2014). It is possible that S209A KI may have more significant effect on MNV replication in other susceptible cell types, or on MNV pathogenesis systemically. MNV-3 was chosen as the *in vivo* infection model, as it causes persistent infection in immunocompetent mice, thereby mimicking a natural infection model (Perdue et al., 2007, Arias et al., 2012). Our previous study of MNV VF1 generated a mutant MNV-3^{VF1-}. VF1 expression in MNV-3^{VF1-} was abolished by introducing pre-mature termination of VF1 translation without changes in the VP1 protein sequence. Like MNV-1^{VF1-}, MNV-3^{VF1-} is replication competent *in vitro* but

attenuated *in vivo* (McFadden et al., 2011). In addition, MNV-1^{VF1-} showed increased type I IFN responses during infection. Therefore, infection of KI mice with MNV-3^{VF1-} may amplify any type I IFN responses-related observations during infection.

For MNV-3, there is no difference in faecal shedding, body weight change or production of MNV-specific serum IgG between WT and KI mice (Figure 4.6). However, for MNV-3^{VF1-} in the low-dose challenge experiment, KI mutation partially rescued the faecal shedding of MNV-3^{VF1-} during acute infection (Figure 4.7). This observation is different to the hypothesis that enhanced type I IFN responses during MNV-3^{VF1-} infection should suppress viral replication in KI mice, indicating the possibility of eIF4E phosphorylation having multiple roles on MNV replication.

The multiple roles of dendritic cells in MNV pathogenesis is an example of multifunctional host factors. Dendritic cells (DCs) are a class of important antigen presenting cells, therefore they have a critical role in priming the type I IFN responses during MNV infection (Thackray et al., 2012). Nevertheless, MNV infects DCs *in vivo*, so the overall effect of DC depletion *in vivo* was unknown (Wobus et al., 2004). Depletion of DCs results in higher viral shedding, but viral dissemination into secondary lymphoid tissues is inhibited (Elftman et al., 2013). As eIF4E is also involved in host cell translation, genetically modified eIF4E S209A may have other unknown effect on host cell translation during MNV infection. Also, tissue-specific expression of eIF4E and phospho-eIF4E may also differentially impact MNV replication and host antiviral responses.

During the persistent infections, there was no difference in faecal shedding of MNV-3 or MNV-3^{VF1-} between WT and KI mice, and no difference was observed in faecal shedding, tissue tropism or serum IFNβ when the mice were challenged with high dose MNV-3^{VF1-} (Figure 4.9). Together, these results indicate that although

phosphorylation of eIF4E may have multiple functions in MNV pathogenesis, the overall effect of eIF4E S209A mutation is minimal.

Previously microarray study has identified changes in steady state gene expression in S209A MEF cells (Furic et al., 2010). However, to reveal the global effect of S209A mutation on MNV pathogenesis, a gene expression profile during MNV infection or upon activation of type I IFN signallings is needed. MNV infection is known to inhibit cellular translation and uncouple transcription from translation (Emmott et al., 2017). Although whole cell proteomics changes during MNV infection has been reported before, it remains interesting to study the changes of mRNAs and newly synthesised proteins during MNV infection.

Chapter 5

Replication control by the norovirus capsid shell domain

5.1 Background

In the previous chapter, the role of eIF4E phosphorylation in regulating type I IFN responses during MNV infection was investigated. MNV pathogenesis in a mouse model with a phosphor-ablative mutation of eIF4E showed different observations compared with findings obtained from a previous *in vitro* study. These results suggest that eIF4E phosphorylation is likely to play multiple roles in norovirus pathogenesis.

During virus replication, both host factors and viral factors are important for successful replication. Both HuNoV and MNV are known for the fast establishment of infection (Okhuysen et al., 1995, Gonzalez-Hernandez et al., 2014), which contribute to the rapid transmission during outbreaks. Avoiding host detection and subverting innate immune responses can contribute to this characteristic, but more likely this is due to efficient virus replication. Therefore, it would be important to understanding the molecular biology of norovirus replication.

Norovirus encodes an RNA-dependent RNA polymerase (RdRp), which plays a central role during norovirus genome replication. The norovirus RdRp can initiate RNA synthesis in both primer-dependent and independent manners (Rohayem et al., 2006b). The primer-dependent initiation utilises a viral protein VPg as a protein primer, whilst the *de novo* initiation of norovirus RdRp is primer-independent (Rohayem et al., 2006a). The mechanistic details of how and when the norovirus RdRp switches between the two modes of initiation are unclear. In a cell-based assay, the norovirus RdRp activity was measured indirectly by ectopic expression of firefly luciferase under the control of IFN-β promoter, which was activated by retinoic acid-inducible gene I (RIG-I) sensing the production of double-strand RNA (dsRNA) replication

intermediates (Subba-Reddy et al., 2011). This assay, termed the NoV-5BR assay, showed genogroup-specific interactions between the norovirus RdRp and VPg, and that VPg can enhance the RdRp activity. The VPg-primed initiation of RNA synthesis in the NoV-5BR assay utilises cellular RNA as templates, while RNaseL processing is involved in sensing the VPg-linked RNA. In addition to VPg, other viral proteins also modulate the RdRp activity. NS1/2 (p48 in HuNoV) specifically promotes the HuNoV RdRp activity, whereas the effect of VP2 is inhibitory. The major capsid protein VP1 showed the most significant enhancement on the RdRp activity. A following study showed that the capsid shell domain (SD) is necessary and sufficient for VP1 to interact with the RdRp and enhance the RdRp activity (Subba-Reddy et al., 2012). The biological relevance of this interaction was demonstrated by trans-complimenting the VP1 expression in an MNV replicon system to enhance viral genome replication, yet the importance of this interaction was not shown in an infectious virus system.

Because in the latter NoV-5BR assay design, only VP1 was co-expressed with RdRp, thus the RNA synthesis is independent of VPg, it is thought that VP1 SD enhances the *de novo* initiation activity of RdRp. The function of this interaction in norovirus life cycle is unclear, but the dependence on a narrow range of VP1 concentrations suggests that it may be important at early stages of infection. After viral entry and uncoating, VP1 from either incoming virions or the initial rounds of translation can stimulate the synthesis of negative-sense, genomic and subgenomic RNAs, coinciding with the most significant stimulatory effect at lower VP1 concentrations. The negative-sense RNAs then serve as the template for the synthesis of VPg-linked genomic and subgenomic RNAs. With the accelerated translation of VP1 from the subgenomic RNAs, the VP1-VP1 interaction is preferred over the VP1-RdRp interaction, therefore the stimulatory effect on the RdRp is lost in favour of viral genome replication (Subba-Reddy et al., 2012). The preferential synthesis of the negative-sense replication intermediate was

also demonstrated by studying temporal changes of genomic positive/genomic negative ratios during MNV infection using a strand specific real-time RT-qPCR (Vashist et al., 2012b).

Both HuNoV and MNV SDs can only enhance their cognate RdRp activity. A subsequent mutagenesis study has mapped the domains of SD responsible for this species-selectivity to the flexible loops 1, 3, 5 and 7, which are all on one side of the capsid shell domain (Figure 5.1C).

5.2 Aims

The aims of this chapter were to understand the importance of temporal regulation of norovirus replication, the roles of VP1-RdRp interactions, and whether this functionally-conserved interaction can be targeted for rational attenuation of norovirus.

Based on the previous observations, the following hypotheses were proposed:

1. Genogroup-specific residues on loops 1, 3, 5 and 7 of SD are responsible for the species-specific enhancement on the *de novo* initiation activity of the norovirus RdRp;

2. Mutating these residues should affect the VP1-RdRp interaction, resulting in changes in the temporal regulation of norovirus genome replication.

3. The altered norovirus genome replication should lead to a reduced norovirus pathogenesis *in vivo*.

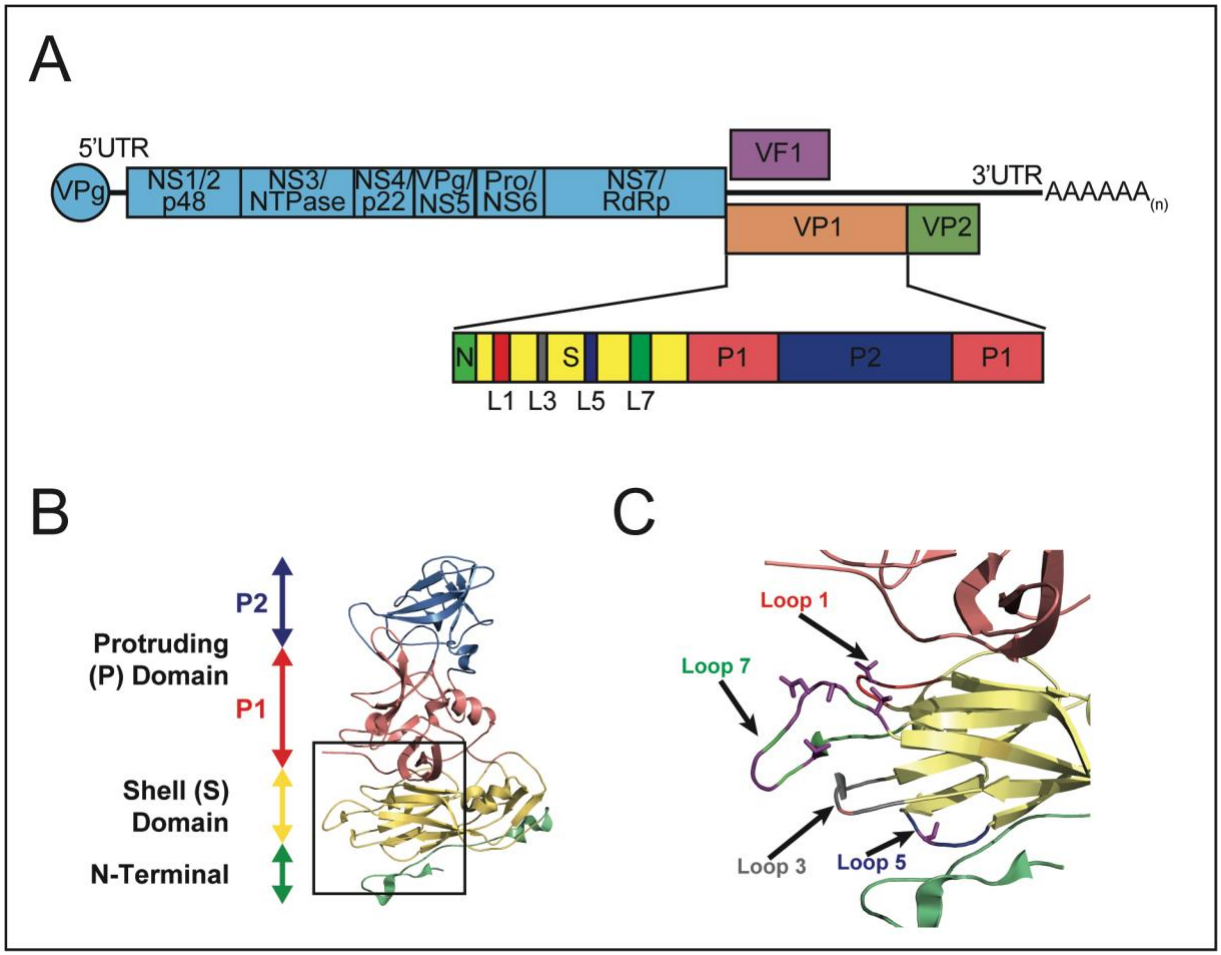

Figure 5.1 Illustration of norovirus capsid shell domain. A) Genome organisation of MNV. Subdomains of VP1 and the relative positions of the SD flexible loops are indicated. B) Crystal structure of Norwalk virus capsid protein VP1 (PDB ID: 1IHM). This is adapted from (Prasad et al., 1999). C) A zoomed-in view of the highlighted region in B). The locations of flexible loops were indicated and the side chains of genogroup-specific residues were displayed.

5.3 Results

5.3.1 VP1-RdRp interaction is functionally conserved in norovirus

To determine the sequence conservation of the odd-numbered flexible loops 1, 3, 5 and 7, 509 GII.4 HuNoV and 91 MNV non-redundant VP1 amino acid sequences were analysed by ClustalOmega (Figure 5.2). The SD sequences were generally highly conserved separately in HuNoV and in MNV. This is consistent with the previously

published results (Chakravarty et al., 2005, Hutson et al., 2004, Cotten et al., 2014). Except for loop 7, loops 1, 3, and 5 are highly conserved between GII.4 HuNoVs and GV MNVs. Therefore, it is likely that the genogroup specificity for the norovirus SD to enhance the RdRp activity is conferred by these differing residues, as the chimeric MNV SD carrying HuNoV odd-numbered flexible loop sequences failed to enhance its cognate RdRp activity, and *vice versa* (Subba-Reddy et al., 2012).

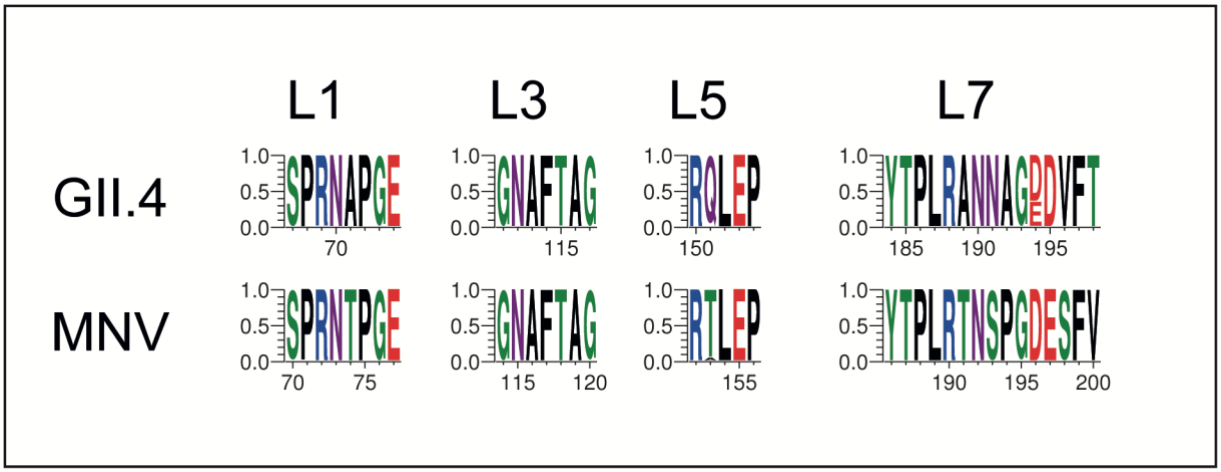

Figure 5.2 Sequence conservation of SD flexible loops. 509 GII.4 HuNoV and 91 MNV VP1 sequences were aligned and the sequence conservation of the odd-numbered flexible loops of SD was demonstrated.

5.3.2 Genogroup-specific residues are important for MNV replication

The sequence conservation analysis indicate that the genogroup-specific residues are likely important for the specificity of VP1-RdRp interaction. It was then thought that swapping the residues of MNV SD with the corresponding HuNoV SD residues should negatively impact the VP1-RdRp interaction and allow the identification of functionally important domains. Combinations of HuNoV VP1 SD loop sequences were cloned into an infectious MNV-1 cDNA clone (GenBank accession number DQ285629.1) by overlap extension PCR. All mutant cDNA clones were verified by sequencing the VP1 region. Chimeric MNVs were named after the according loop(s) replaced with GII.4 HuNoV sequences (Table 5.1). For example, mutant L1 indicates the loop 1 of MNV

VP1 SD replaced by the loop 1 of GII.4 HuNoV VP1 SD, corresponding to a Threonine74 to Alanine mutation. Because the loop 3 is conserved between MNV and HuNoV (Figure 5.2), the mutant L1,5,7 represents a complete swap of the odd-number flexible loops.

The production of infectious viruses was determined using an end-point titration assay ($TCID_{50}$) following DNA-based reverse genetics (Figure 5.3A). The complete replacement of the flexible loops (mutant L1,5,7) was lethal for MNV replication (Figure 5.3A). Two more passages were performed for the mutant L1,5,7. No infectious virus was detected using $TCID_{50}$, nor was the viral genomic RNA detected using RT-PCR (data not shown), indicating mutant L1,5,7 is non-viable. While the virus yield of mutant L5,7 from recovery was under the detection limit, subsequent passage showed production of infectious virus (Figure 5.3B). These results showed that the mutated residues in loops 5 and 7 are important for MNV infectivity.

All infectious chimeric MNVs were passaged twice more, then the VP1 and the RdRp regions were sequenced. Results showed no reversion of the mutated residues in VP1 and no complimentary mutation in RdRp (data not shown). These results suggest that though some chimeric MNVs were attenuated *in vitro*, the mutations introduced are stable.

Name	Mutations (L1/L3/L5/L7)
WT	N/A
L1	T74A
L5	T153Q
L7	T191A S193N P194A D196E E197D S198V V200T
L1,5	T74A T153Q
L5,7	T153Q T191A S193N P194A D196E E197D S198V V200T
L1,7	T74A T191A S193N P194A D196E E197D S198V V200T
L1,5,7	T74A T153Q T191A S193N P194A D196E E197D S198V V200T

Table 5.1 Chimeric MNVs and the corresponding mutations All the numbers correspond to VP1 from MNV-1 CW1 (GenBank accession number DQ285629.1).

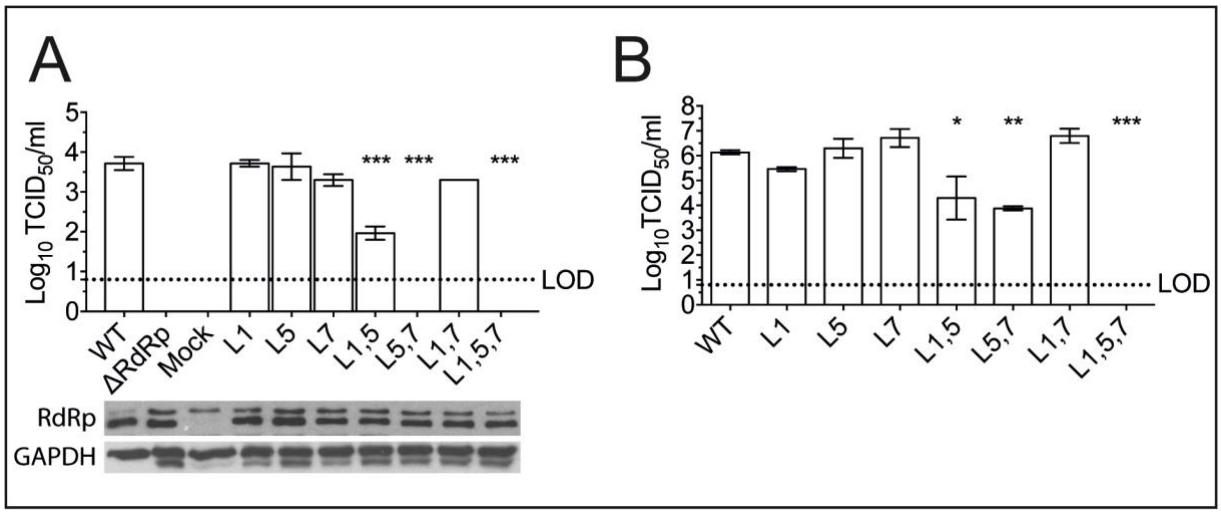

Figure 5.3 Recovery and propagation of chimeric MNV-1s. A) Virus yield of chimeric MNV-1s by DNA-based reverse genetics, where the active site of RdRp of mutant ΔRdRp was mutated to YGGG. The bottom panels showed the similar production of viral RdRp in all transfections and GAPDH was used as loading control. B) Passage of recovered chimeric MNVs. 250 μl of viruses from DNA-based reverse genetics were inoculated to BV-2 cells, virus yield was determined at 72 hpi. One-way ANOVA was performed using Dunnett test (* $p<0.05$, ** $p<0.01$, *** $p<0.001$).

5.3.3 A point mutation in the SD reduces virus stability

In addition to modulating the RdRp activity, the main known role of VP1 during the norovirus life cycle is encapsidation of viral genomic RNAs (Bertolotti-Ciarlet et al., 2002). As the chimeric MNVs containing mutation in L5 were either attenuated or non-viable (Figure 5.3), with the exception of L5, it was logical to access the capsid stability of these viruses.

Capsid stability can be studied by assessing the infectivity of virus at high temperatures and the susceptibility of encapsidated viral RNA to degradation with RNase. Thermal inactivation conditions were determined based on previous literature and preliminary results (Arthur and Gibson, 2015). Replicative WT and chimeric MNVs (including mutant L5) were tested for thermal inactivation (Figure 5.4) and the results showed the mutant L5 lost significantly more infectivity and viral genomic RNA after heat treatment than did WT (-RNase groups in Figure 5.4). Together with RNase treatment (+RNase

group), no infectious mutant L5 was detected after 3 minutes thermal inactivation at 60 ℃. This result clearly indicates that the VP1 T153Q mutation significantly increases the susceptibility of mutant L5 to thermal inactivation. Also, mutant L1 (T74A) showed slightly improved thermal stability compared to WT, demonstrating that the viral capsid is slightly more stable than the native virus.

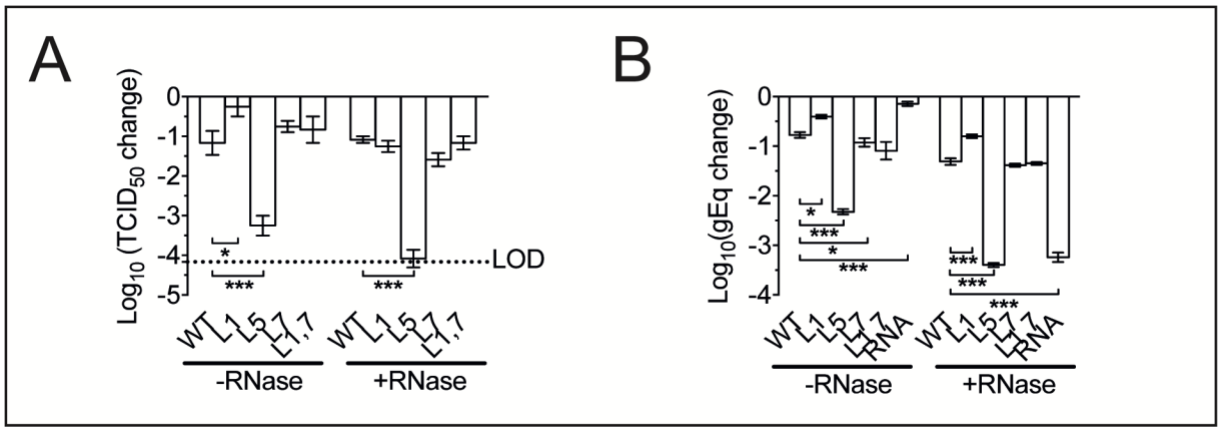

Figure 5.4 Thermal stability of chimeric MNV-1s. Similar amount of infectious MNVs were subjected to thermal inactivation (60 ℃ for 3 minutes) followed by RNase treatment (with or without 1 mg/ml RNaseA at 37 ℃ for 15 minutes). The reduction between initial and remaining A) infectivity was determined by $TCID_{50}$, whilst B) genomic RNA changes were determined by RT-qPCR. One-way ANOVA was performed using Dunnett test (* p<0.05, ** p<0.01, *** p<0.001).

5.3.4 Identification of domains important for MNV replication

The replication kinetics of the various clones were assessed using a single-step growth kinetics analyses (Figure 5.5), The results showed the replication of mutant L5 was comparable to WT during the early stages of infection (Figure 5.5A and B). However, after 12 hours, a consistent 1 log_{10} difference of infectious titre compared to WT was observed, whilst the cellular vRNA of mutant L5 was comparable to that of WT MNV-1. This observation indicates that mutant L5 is replication competent, but likely in the later stages of infection, the destabilised viral capsids result in faster decay of progeny viruses.

The mutants L1, L7 and L1,7 showed no clear defect in virion stability, however, the replication of all three mutants were significantly slower than that of WT (Figure 5.5). Generally, at the early stages of infection (6-12hpi), all three mutants showed significantly reduced infectivity (Figure 5.5A and C) and viral genomic RNA (Figure 5.5B and D), indicating both the synthesis of infectious virus and the genome replication were impaired. These results suggest that the loops 1 and 7 are likely involved in the genogroup-specific enhancement of the norovirus RdRp activity at the early stages of MNV infection, when the *de novo* initiation of RdRp is needed to synthesise the negative-strand replication intermediate.

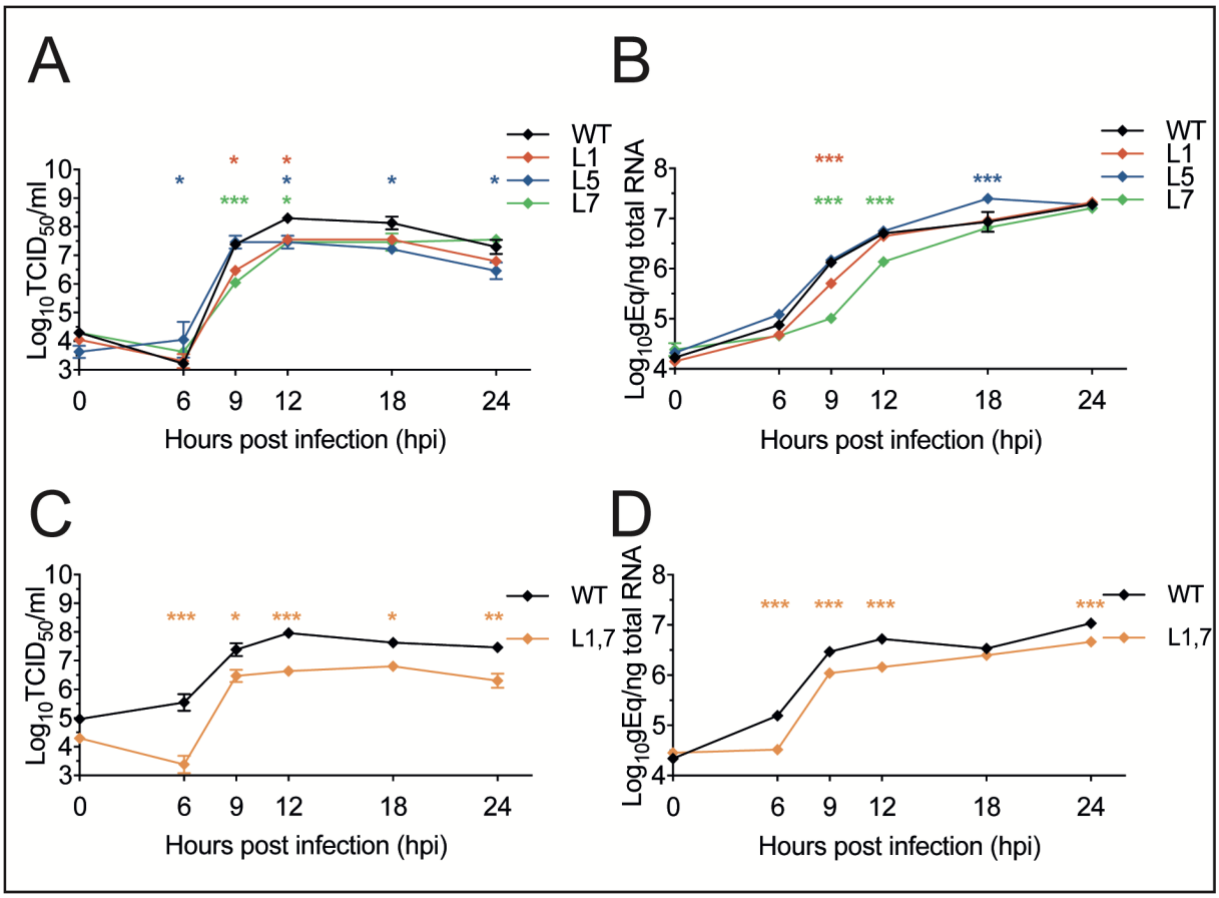

Figure 5.5 *In vitro* growth kinetics of chimeric MNV-1s. BV-2 cells were infected by MNV-1 WT or mutants L1, L5, L7 or L1,7 (MOI = 5 $TCID_{50}$/cell), where A) and C) showed virus yield at each time point, B) and D) showed cellular vRNA determined by RT-qPCR. Two-way ANOVA was performed for all analysis using Bonferroni test (* p<0.05, ** p<0.01, *** p<0.001).

5.3.5 Identification of domains important for VP1-RdRp interaction

Based on the previous results, it was proposed that the mutations in loops 1 and 7 reduced the enhancement on the RdRp activity via a decreased VP1-RdRp interaction. The norovirus VP1 can self-assemble into virus-like particles (VLP) when expressed, indicating a strong VP1-VP1 interaction (Bertolotti-Ciarlet et al., 2002, Tresset et al., 2013b). Although the norovirus VP1 interacts with its cognate RdRp and modulates the RdRp activity, the interaction is relatively weak (Subba-Reddy et al., 2012). Therefore, a LUminescence-based Mammalian IntERactome (LUMIER) assay was introduced to measure the VP1-RdRp interaction and how it was affected by the VP1 mutations (Barrios-Rodiles et al., 2005). In LUMIER, renilla luciferase-fused "prey" and protein A-fused "bait" proteins are co-expressed and co-immunoprecipitated (co-IP) via protein A. The luciferase activity in the IP fraction indicate the strength of protein-protein interactions between the prey and the bait proteins. LUMIER is designed to measure dynamic protein-protein interactions and to convey semi-quantitative data. In the preliminary survey of all viral protein-protein interactions of GI, GII and GV noroviruses, VP1-RdRp was observed as weak interactions (A. de Rougemont, unpublished data). Instead of LUMIER intensity ratio (LIR), a robust z-score was used to account for sample variations and represent qualitative measurement of VP1-RdRp interaction (Birmingham et al., 2009).

For the purpose of high throughput screening, the WT and the mutant VP1 were amplified by PCR and sub-cloned into the Gateway entry clones by BP reactions, then the renilla luciferase (RL)- or the protein A-fused expression constructs were generated by LR reactions using entry clones. 293T cells were co-transfected with VP1 and a MNV RdRp constructs and the VP1-RdRp interaction was measured with VP1 being the prey or the bait protein. When VP1 was expressed as the prey protein (Figure 5.6A

prey), L7, L1,7 and L1,5,7 VP1 had significantly reduced VP1-RdRp interactions. When VP1 was used as bait protein, L1, L7, L1,7 and L1,5,7 had significantly reduced VP1-RdRp interactions (Figure 5.6A bait). The common presence of loop 7-containing VP1 with reduced VP1-RdRp indicates possibly loop 7 is most important for mediating VP1-RdRp interaction.

To validate the LUMIER results, RL-fused VP1 was co-expressed with GFP-fused RdRp. Immunoprecipitation of the RdRp using anti-GFP antibody showed that VP1 can be co-IP with RdRp (Figure 5.6B VP1/RL of IP). Quantification of 3 independent repeats by densitometry of the VP1 protein in the co-IP fraction showed that the L7, L1,7 and L1,5,7 VP1 significantly reduced the VP1-RdRp interaction (Figure 5.6C). While L1 VP1 had reduced VP1-RdRp interaction the results are not statistically significant. Except for L1,5,7 VP1 (non-viable), these mutants were previously shown to replicate slower *in vitro* (Figure 5.5). Together, the mutations in loops 1 and 7 reduce the VP1-RdRp interaction *in vitro*.

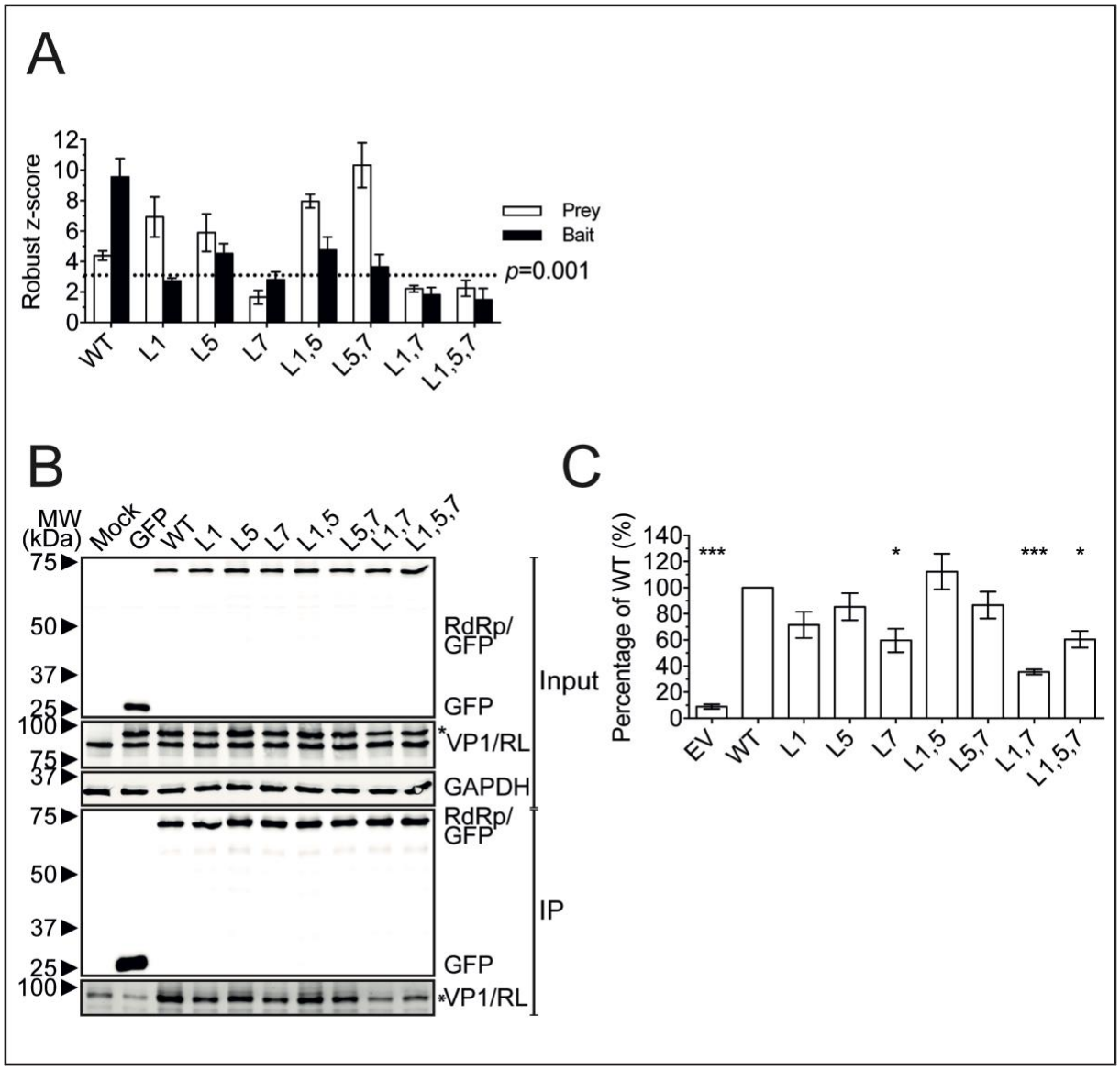

Figure 5.6 Characterisation of VP1-RdRp interaction. A) VP1-RdRp interaction measured by LUMIER. The WT and chimeric MNV VP1s were co-expressed with the MNV RdRp in 293T cells, the RL-fused prey proteins were co-immunoprecipitated with the protein A-fused bait proteins. Luciferase activity in the IP fraction was measured and robust z-score was used to represent the strength of interaction. B) The RL-fused VP1 (WT and chimeras) were co-expressed with GFP-fused MNV RdRp. Immunoprecipitation of GFP-RdRp pulled down RL-VP1 differentially. C) Densitometry of co-immunoprecipitated VP1 relative to WT, both normalised to input. The results showed mean±SEM of three independent experiments. One-way ANOVA was performed with Dunnett test (* p<0.05, ** p<0.01, *** p<0.001). LUMIER assay was performed by A. de Rougemont.

5.3.6 SD stimulates *de novo* initiation activity of RdRp

A previously published RNA synthesis assay was used to measure *de novo* initiation activity of MNV RdRp, Figure 1.8B and (Yunus et al., 2015, Lin et al., 2015). The purified MNV RdRp was incubated with MNV RNA proscript to synthesise the beginning of positive-sense, subgenomic RNA. The MNV RNA proscript (promoter + transcript) consists of the subgenomic promoter on the negative-sense genomic RNA, the antisense sequence of the first 8 nucleotides (nt) of MNV subgenomic RNA and 3 nonviral nucleotides (GCG) at the 5' termini to allow incorporation of [α-^{32}P]CTP. Through recognising the stem-loop of subgenomic promoter MNV RdRp initiate RNA synthesis *de novo* with defined product length (11nt). In addition to the *de novo* initiation product, a primer-extension product can be observed as incorporation of [α-^{32}P]CTP to the RNA template.

To test whether the MNV SD can enhance the *de novo* initiation activity of the MNV RdRp, MNV-1 shell domain (SD) was cloned into a pTriEx1.1 backbone, expressed in bacteria and purified to >95% purity (data not shown). In Figure 5.7A, without SD (SD = 0) MNV RdRp can generate RNA products through primer extension (PE) and *de novo* initiation (DN). With low SD ratios (0, 1 and 2), the addition of purified MNV SD (WT or mutants) had little impact on DN:PE ratios (normalised DN in Figure 5.7B). As more SD was added, more DN products as well as higher DN:PE ratio were observed. These results suggest that MNV SD is sufficient to enhance the *de novo* initiation activity of MNV RdRp. Addition of L1,7 SD increased normalised SD, yet the enhancement was significantly less compared to the effect of WT SD. This observation suggests that the loops 1 and 7 were involved in modulating *de novo* initiation activity of MNV RdRp, and the mutations in L1,7 likely account for the species specificity.

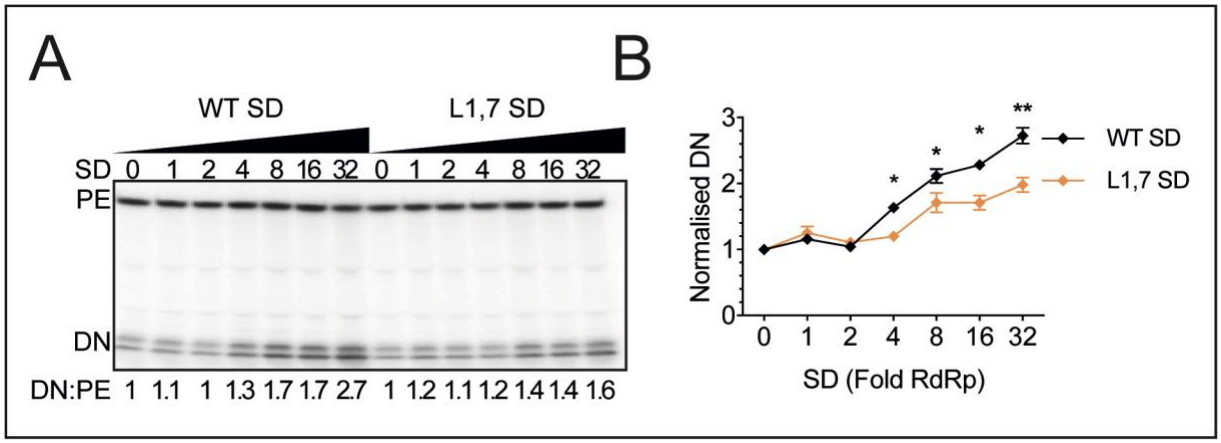

Figure 5.7 Stimulation of RdRp by SD. A) The MNV RdRp was incubated with the purified WT or L1,7 SD with different molar ratios to the MNV RdRp. After reaction, samples were separately by urea-polyacrylamide gel. The RNA synthesis products were visualised by phosphoimager and were quantified by ImageQuant software. B) Quantification results from two independent experiments. The *de novo* initiation products were normalised to primer extension products, then were represented as the fold of normalised DN product without SD (SD of 0). Statistical analysis was performed using Excel *t*-test (* $p<0.05$, ** $p<0.01$, *** $p<0.001$). RNA synthesis assay was performed by Xiaoyan Lin (Indiana University).

5.3.7 Recovery of chimeric MNV-3s

Our previous observations demonstrated that the SD is important for both viral capsid stability and regulating the RdRp activity (Subba-Reddy et al., 2012). The mutant L5 possesses less capsid stability, and it can be used to determine the impact of capsid stability on norovirus pathogenesis. Because VP1-RdRp interaction is conserved between HuNoV and MNV, it was used as a model system to study how norovirus pathogenesis would be impacted if the temporal regulation of replication was disturbed. Potentially, this can be exploited to generate an attenuated virus antigenically similar to the native virus.

Because the coding region of the MNV SD also overlaps that of the MNV VF1 (McFadden et al., 2011), the mutations in SD also affect VF1 protein sequences. In addition, it was shown that VF1 is not required for MNV replication *in vitro* and a VF1 knock-out mutant showed attenuated replication *in vivo* (McFadden et al., 2011). In order to study the impact of chimeric SD in norovirus pathogenesis, the homologous

mutations were generated in an MNV-3 VF1 knock-out backbone (MNV-3^{VF1-}). A previous *in vivo* characterisation showed that MNV-3^{VF1-} is replication-competent *in vitro*. The VF1 mutations remain stable *in vivo* but the MNV pathogenesis is attenuated. The following mutations were cloned into the MNV-3^{VF1-} backbone: L1, L5, L7 and L1,7, all of which are replication competent in MNV-1 (Figure 5.3). MNV-3^{VF1-} recovered with similar titre to MNV-3 WT, as did mutant MNV-3^{VF1-} L5 (Figure 5.8A). However, MNV-3^{VF1-} L1 showed defect in replication, whilst no observable CPE was seen in cells infected by mutants MNV-3^{VF1-} L7 or MNV-3^{VF1-} L1,7. To determine the infectivity of the loop 7 mutants, all the viruses were passaged once then titrated using a $TCID_{50}$ assay and also antigen staining (Figure 5.8B). $TCID_{50}$ by antigen was carried out the same as $TCID_{50}$ by CPE, only that after incubation immunofluorescent microscopy was used for detecting expression of NS3, one of the signatures of MNV infection. Similar differences in titre between CPE- and antigen-based $TCID_{50}$ in WT and MNV-3^{VF1-}, MNV-3^{VF1-} L1, MNV-3^{VF1-} L5, $TCID_{50}$ of mutants MNV-3^{VF1-} L7 and MNV-3^{VF1-} L1,7 were readily determined by NS3, indicating these mutants are infectious.

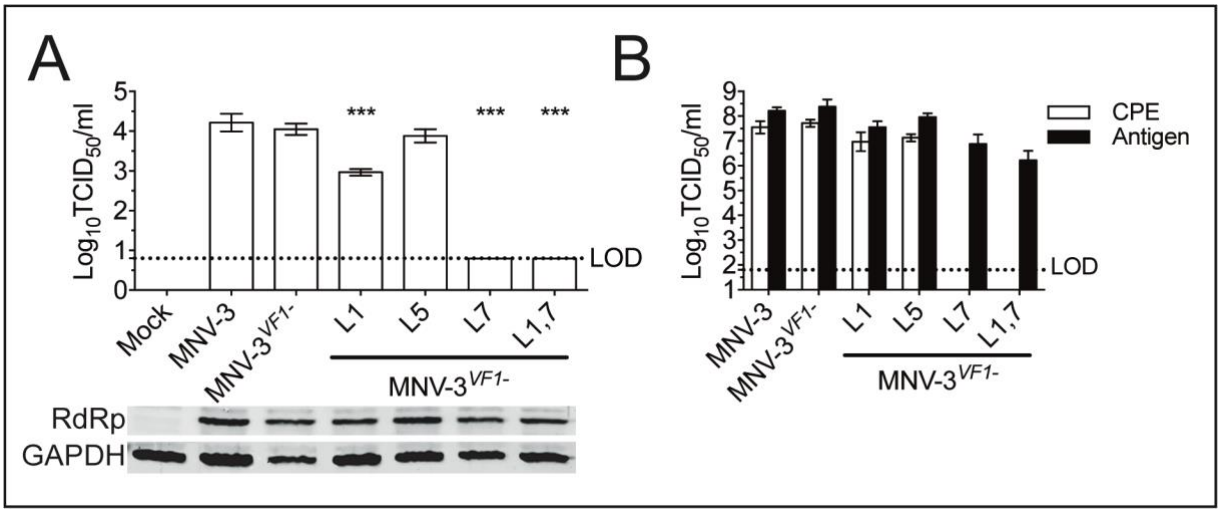

Figure 5.8 Recovery and titration of chimeric MNV-3s. A) DNA-based recovery of chimeric MNV-3s. Chimeric MNV-3s were recovered using previously published protocols and the virus yields were determined by $TCID_{50}$ (Chaudhry et al., 2007). Transfection efficiency was determined by measuring RdRp expression in total cell lysates. GAPDH was used as loading control. One-way ANOVA was performed using Dunnett test (* p<0.05, ** p<0.01, *** p<0.001). B) Titration of chimeric MNV-3s.

Chimeric MNV-3s from recovery were propagated in BV-2. The P1 virus was titrated using standard $TCID_{50}$ protocol (Hwang et al., 2014). The same virus stocks were titrated and stained for viral antigen NS3 and visualised by immunofluorescent microscopy. $TCID_{50}$ by antigen were calculated the same way as $TCID_{50}$ by CPE.

5.3.8 MNV-3^{VF1-} L1,7 is infectious but attenuated *in vitro*

Following titration, chimeric MNV-3s were characterised *in vitro* (Figure 5.9). To confirm that the mutant MNV-3^{VF1-} L1,7 is infectious, based on $TCID_{50}$ by antigen, Raw264.7 cells were infected at an MOI of 0.5 $TCID_{50}$ per cell for 12 hours. Infection markers (dsRNA and NS3) indicated the presence of infected cells in MNV-3^{VF1-} L1,7 (Figure 5.9A). Between different viruses, similar number of infected cells indicated that the MNV-3^{VF1-} L1,7 is capable of establishing infection.

The thermal inactivation and a multistep *in vitro* replication kinetics analysis were used to determine the virion stability and the replication capacity of chimeric MNV-3s, respectively. Heat inactivation reduced more viral RNA in the mutant MNV-3^{VF1-} L5 (Figure 5.9B), indicating the MNV-3^{VF1-} L5 is more susceptible to inactivation compared with the parental MNV-3^{VF1-}, despite that the magnitude of reduction is less than what was observed in MNV-1 L5 (Figure 5.4B). These results indicated that the same phenotype is observed in two MNVs.

In a multistep growth curve (Figure 5.9C), BV-2 cells were infected by the chimeric MNV-3s (MOI 0.01 $TCID_{50}$/cell) and the viral genomic RNA in infected cells was determined by RT-qPCR. Mutant MNV-3^{VF1-} L5 showed comparable replication kinetics as MNV-3^{VF1-}. While increased at 12hpi, vRNA of mutant MNV-3^{VF1-} L1,7 remained significantly less than that of MNV-3^{VF1-} throughout the course of infection. Together, the reduced thermal stability of the mutant MNV-3^{VF1-} L5 and the attenuated *in vitro* replication of the mutant MNV-3^{VF1-} L1,7 suggested that the phenotypes observed in chimeric MNV-1s are reproducible in MNV-3.

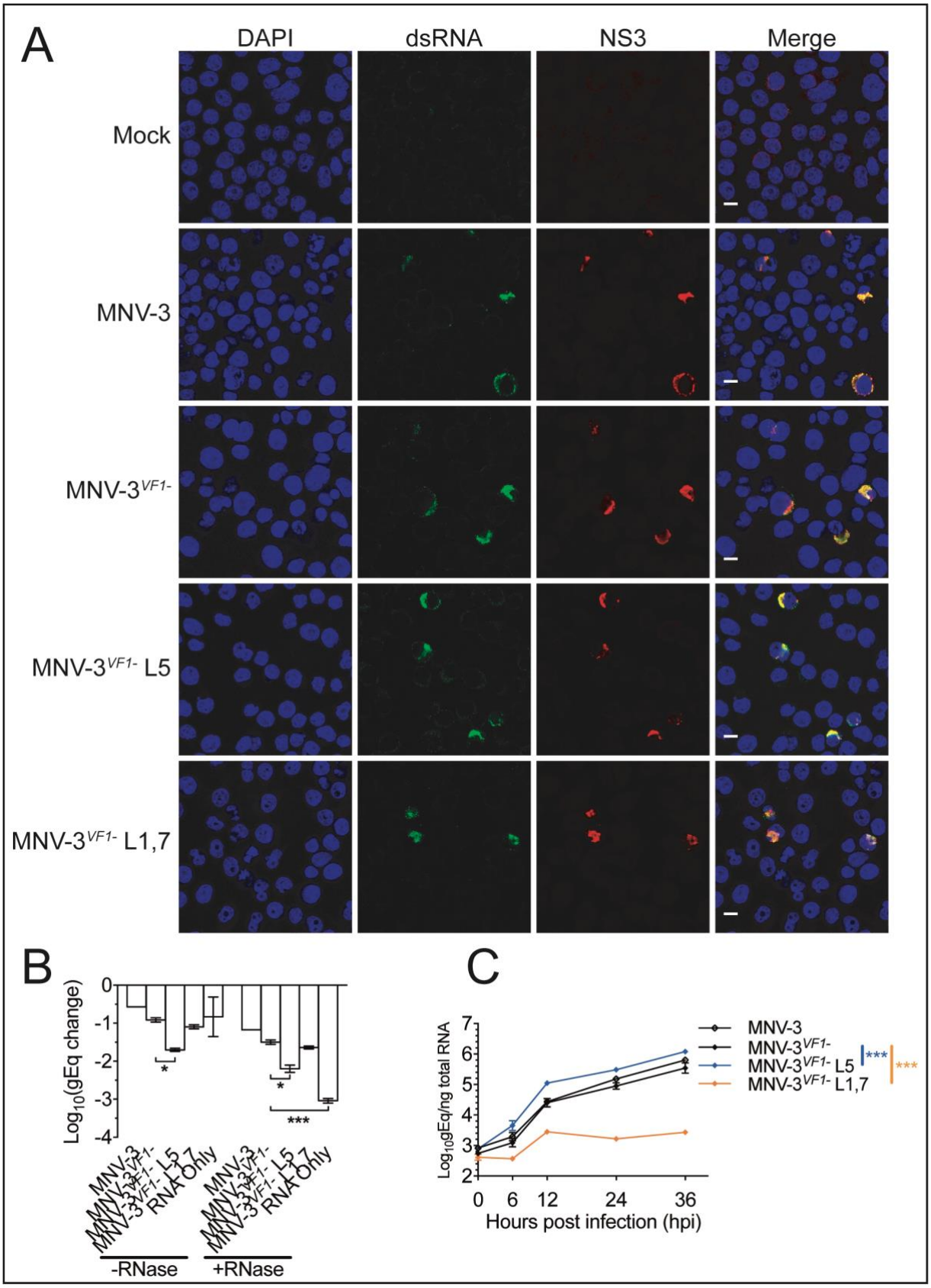

Figure 5.9 *In vitro* characterisation of chimeric MNV-3s. A) Validation of $TCID_{50}$ by antigen. Raw264.7 cells were infected by MNV-3s (MOI=0.5 $TCID_{50}$/cell) for 12 hours. The cells were fixed, permeabilised and stained with infection markers (dsRNA and NS3). DAPI was used to stain the nuclei. Infected Raw264.7 cells displayed co-localisation of dsRNA and NS3 staining at perinuclear foci. B) Thermal

stability of MNV-3s. Virus suspension was heated at 60 ℃ for 3 minutes, followed by incubation at 37 ℃ for 15 minutes, with or without RNase. Total RNA was then determined by RT-qPCR and compared with unprocessed virus stocks. One-way ANOVA was performed with Dunnett test (* p<0.05, ** p<0.01, *** p<0.001). C) *In vitro* replication kinetics of chimeric MNV-3s. BV-2 cells were infected with chimeric MNV-3s at MOI=0.01 TCID50 per cell and total cellular RNA was extracted at indicated time post infection. MNV vRNA in infected cells were determined by RT-qPCR. Two-way ANOVA was performed with Bonferroni test (* p<0.05, ** p<0.01, *** p<0.001).

5.3.9 VP1-RdRp interaction is important for MNV pathogenesis

In order to determine whether the chimeric MNV-3s were attenuated *in vivo*, 5-week old C57BL6/J mice were orally challenged with 10000 $TCID_{50}$ of MNV-3 WT, MNV-3^{VF1-}, MNV-3^{VF1-} L5 and MNV-3^{VF1-} L1,7. MNV-3 WT was replication competent, indicated by significantly higher faecal shedding of vRNA during both acute and persistent infections (Figure 5.10A). Compared with MNV-3 WT, both MNV-3^{VF1-} and MNV-3^{VF1-} L5 displayed reduced faecal shedding, suggesting both viruses are attenuated. At 8 weeks post primary challenge (56 dpi), vRNA was just detectable in faeces of mice infected with MNV-3^{VF1-} and MNV-3^{VF1-} L5. The faecal vRNA of mice infected with the mutant MNV-3^{VF1-} L5 was slightly less than that of MNV-3^{VF1-} during acute infection, but the difference was not statistically significant. For MNV-3^{VF1-} L1,7, faecal shedding was only observed on Day 1 post challenge, indicating MNV-3^{VF1-} L1,7 is replication deficient *in vivo*. In agreement with other previous studies (Perdue et al., 2007, Arias et al., 2012, Zhu et al., 2013), no clear impact on body weight changes upon MNV-3 infections was observed throughout the course of infection (Figure 5.10B). Induction of adaptive immune response was measured by serum IgG against MNV capsid proteins (Figure 5.10C). Over the course of 8 weeks significant production of MNV-specific serum IgG was observed in MNV-3-infected mice, which are more robust than in attenuated MNV-3^{VF1-}-infected mice. In the previous chapter (Figure 4.7A and

C), it was shown that in MNV-3 pathogenesis the induction of mucosal immunity correlated with virus replication, i.e. better virus replication induced quicker adaptive immune response. However, the correlation was not observed when comparing MNV-3^{VF1-} and MNV-3^{VF1-} L5. During the acute infection (before 7dpi) the faecal shedding of MNV-3^{VF1-} L5 remained less than that of MNV-3^{VF1-}, whist in MNV-3^{VF1-} L5 the serum IgG against MNV capsid remained slightly more than that of MNV-3^{VF1-}. This trend was observable until 8 weeks post infection. Although the mutant MNV-3^{VF1-} L1,7 is infectious *in vitro*, no significant increase of MNV-specific serum IgG was observed in the 8-week period.

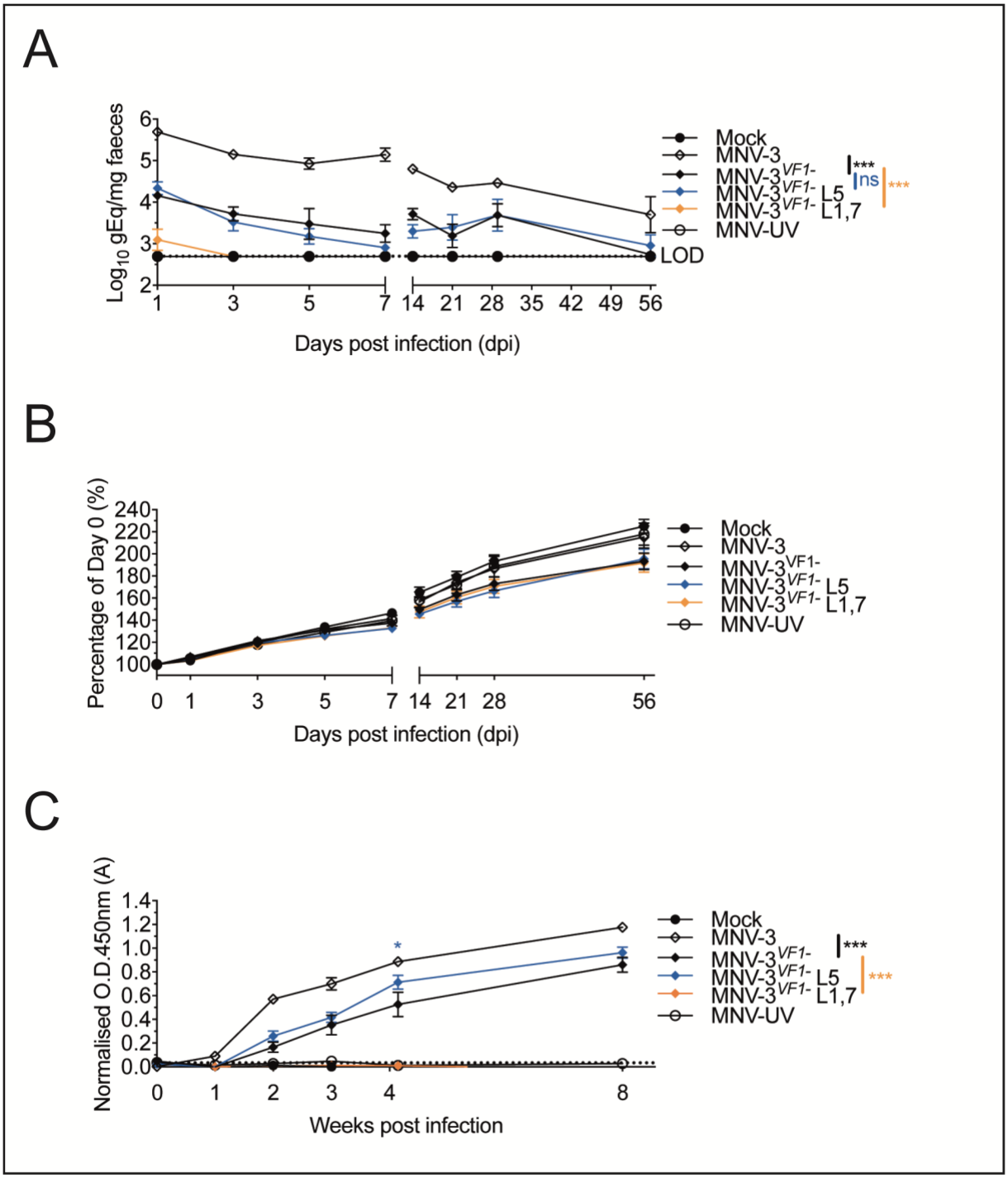

Figure 5.10 *In vivo* replication of chimeric MNV-3s. 5-week old C57BL6/J mice were mock infected or infected with MNV-3s, and A) faecal vRNA, B) body weight changes relative to pre-infection, and C) production of MNV-specific serum IgG were determined. Two-way ANOVA was performed with Bonferroni test (* p<0.05, ** p<0.01, *** p<0.001).

5.3.10 Infection of MNV provides partial protection against re-challenge

To determine if any protection against re-infection was generated upon the initial challenge of live attenuated or replication-deficient chimeric MNV-3s, these mice were re-challenged with a low dose (1000 $TCID_{50}$) of MNV-3 WT 8 weeks after primary challenge. This is sufficient to establish robust infection during primary challenge (Figure 4.6 and (Arias et al., 2012)). Prior to challenge, except for mice primarily infected with MNV-3, faecal shedding was barely detectable in other groups.

On 3 days post re-challenge (Figure 5.11A day 3), compared with the primary infection (mock-infected mice challenged with MNV-3), primary challenge with replication-competent MNV-3 and attenuated MNV-3^{VF1-} significantly reduced faecal shedding, indicating that a primary challenge with MNV reduces virus replication upon re-challenge with a homotypic (primary challenge with MNV-3) or a heterotypic virus (primary challenge with MNV-3^{VF1-}). Mice previously infected with MNV-3^{VF1-} L5 showed reduced faecal shedding on day 3 post infection compared with mock-infected mice, but the difference is not statistically significant. A primary infection with the MNV-3^{VF1-} L1,7 or the MNV-UV did not reduce faecal shedding upon re-infeciton, indicating that no protection is generated during primary challenge.

In all groups the re-challenge with MNV-3 established persistent infections (Figure 5.11A day 21). Only the faecal shedding of the MNV-3 group was statistically significantly less than mock, but there was no significant difference between different groups, indicating that although primary challenge with MNV-3 or MNV-3^{VF1-} significantly reduced faecal shedding during acute infection, the partial protection cannot prevent MNV-3 from establishing persistent infection.

The primary challenge with MNV-3, MNV-3^{VF1-} and MNV-3^{VF1-} L5 induced robust serum IgG against MNV prior to re-challenge (Figure 5.10C). One week post re-

challenge (Figure 5.11B week 1), the serum IgG of the MNV-3^{VF1-} group remained significantly lower than that of the MNV-3 group, whilst an addition a single amino acid mutation (MNV-3^{VF1-} L5) showed a comparable serum IgG to MNV-3. Upon 3 weeks post re-challenge, serum IgG of these three groups was indistinguishable. Together with Figure 5.11A, primary challenge of MNV-3^{VF1-} L5 partially reduced acute phase faecal shedding upon MNV-3 re-challenge, paralleled with comparable production of MNV-specific serum IgG, despite attenuated pathogenesis.

MNV-specific serum IgG of mock, MNV-3^{VF1-} L1,7 and MNV-UV groups were significantly lower than MNV-3 one week post re-challenge, suggesting no adaptive immunity activation upon primary challenge with MNV-3^{VF1-}L1,7 or MNV-UV. 3 weeks post re-challenge induced significant production of MNV-specific serum IgG in the same mice, indicating these mice were capable of responding to MNV infection, and that mutant MNV-3^{VF1-} L1,7 was likely replication defective *in vivo*, highlighting the importance of temporal regulation of norovirus genome replication by VP1-RdRp interaction and it subsequent impact on norovirus pathogenesis.

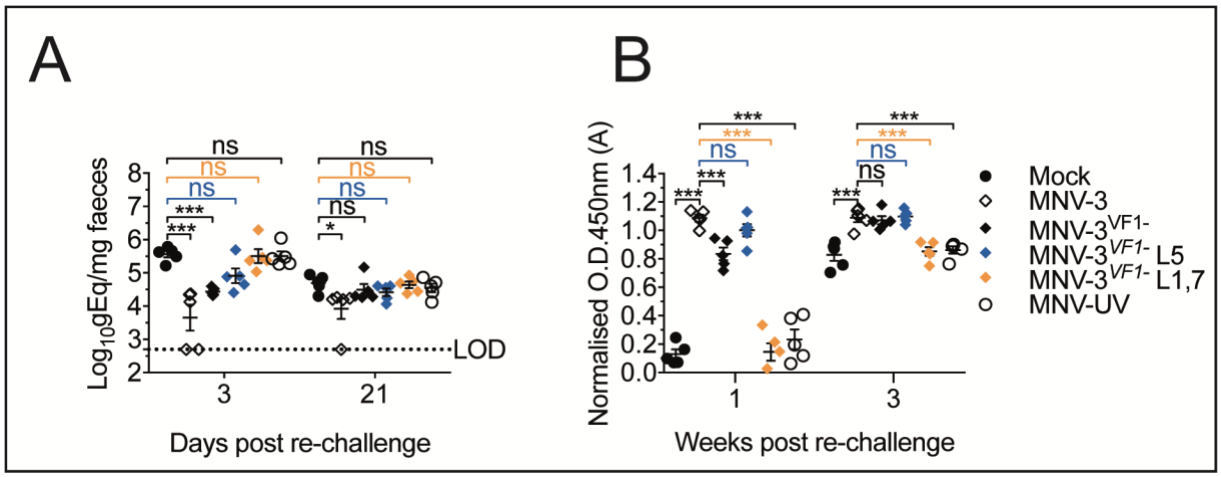

Figure 5.11 Partial protection by primary challenge with MNV. A) Faecal shedding during acute (day 3) and persistent (day 21) phases upon re-challenge. Mice initially mock infected or infected with MNV-3, MNV-3^{VF1-}, MNV-3^{VF1-} L5, MNV-3^{VF1-} L1,7 or MNV-UV were re-challenged with MNV-3. Faecal vRNA on day 3 and 21 post infection were determined by RT-qPCR. Two-way ANOVA was performed with Bonferroni test (* p<0.05, ** p<0.01, *** p<0.001). B) Induction of MNV-specific serum IgG upon MNV-3 re-challenge. On day 7 (week 1) and day 21 (week 3) post re-challenge as described in A), serum was

taken from mice and ELISA against MNV-3 VLP was used to determine MNV-specific serum IgG. Two-way ANOVA was performed with Bonferroni test (* $p<0.05$, ** $p<0.01$, *** $p<0.001$).

5.3.11 Recovery of infectious GII.4 HuNoV with homologous SD mutations

The importance of the VP1-RdRp interaction in regulating norovirus replication and pathogenesis inspired the exploration of attenuating HuNoV replication by mutating the corresponding domains in the HuNoV capsid shell domain. With the successful development of HuNoV cell culture system and our primary demonstration of recovering infectious HuNoV from a GII.4 full length cDNA clone ((Ettayebi et al., 2016) and Figure 3.7E), it was logical to determine if chimeric HuNoV carrying mutations important for species-specific recognition of VP1-RdRp interaction can be recovered. Although both loops 1 and 7 modulate the RdRp activity, the loop 7 contains more genogroup-specific residues than does loop 1 (Table 5.1) and results from both MNV-1 and MNV-3 showed that MNV replication was impacted by more significantly by the L7 mutations. Therefore, chimeric GII.4 HuNoV L7 (referred as HuNoV L7 thereafter) was generated by replacing according residues with those of MNV. DNA-based reverse genetics was then used to recover infectious HuNoV. Western blot analysis (Figure 5.12A) indicated the production of viral protein VPg and its precursors. As expression of viral proteins in DNA-mediated reverse genetics was mainly driven by FPV-T7, these results only indicate similar transfection efficiency between different cDNA clones. Also, a polymerase mutant F/S showed similar VPg expression as that of GII.4.

It was proposed that reverse genetics generated encapsidated HuNoV RNA, and infectious HuNoV should show more nuclease resistance than a non-infectious virus. Upon treatment with benzonase (Figure 5.12B), viral RNA was reduced. However, similar reduction was observed between infectious (GII.4) and non-infectious (F/S)

HuNoVs. These results indicate that in the current experiment set up, it is unclear whether the HuNoV L7 is infectious or not.

The recovered HuNoV was also used to infect differentiated duodenal organoids D196. In agreement with previous results (Figure 3.7), infection from recovered virus did not lead to obvious replication (Figure 5.12C). Due to the limiting availability, the slow replication cycle (doubling time 6-7 days) and complexity in culturing primary intestinal organoids, a subsequent passage of HuNoV L7 cannot be performed. Follow-up biochemical and *in vitro* characterisations are required to determine if the HuNoV L7 is infectious and whether HuNoV replication is impacted.

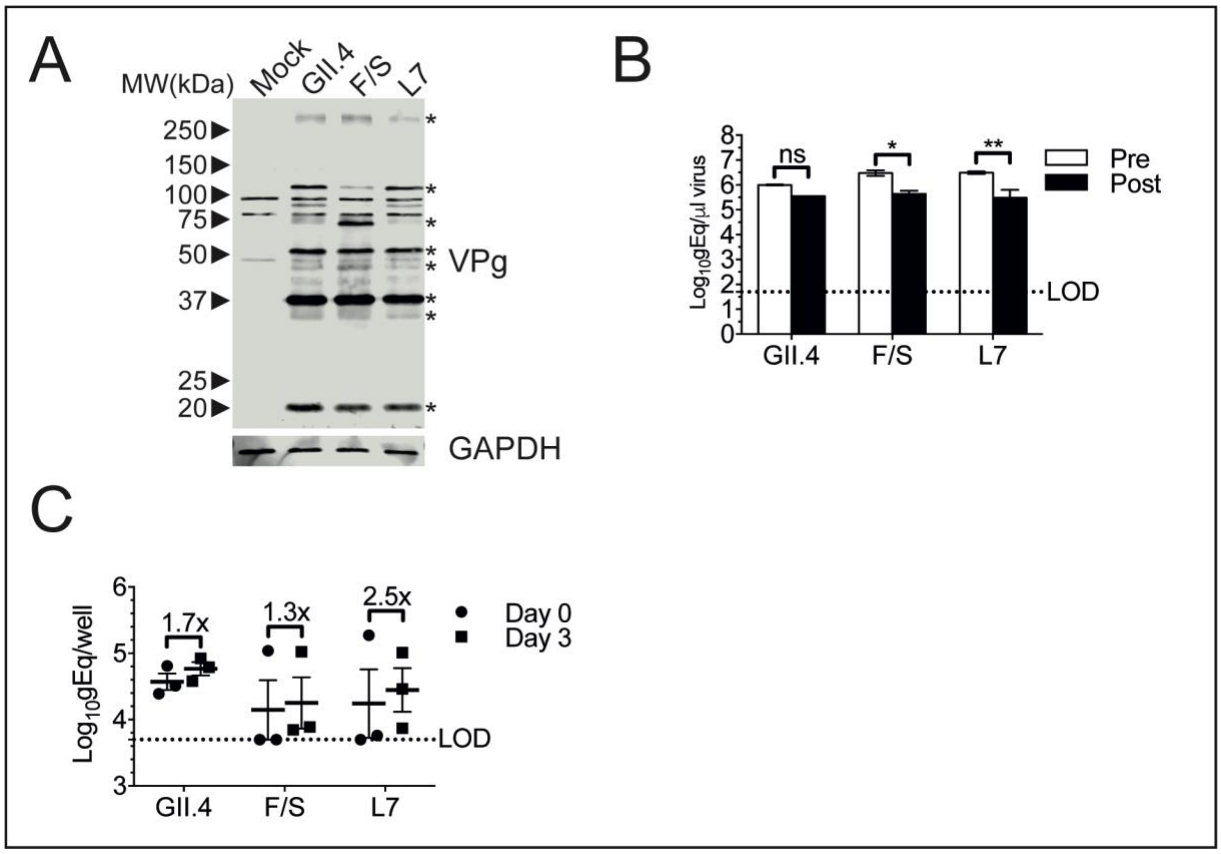

Figure 5.12 Recovery of chimeric GII.4 HuNoV. A) Recovery of GII.4 HuNoV by reverse genetics. BSR-T7 cells were infected with FPV-T7, followed by transfection of HuNoV cDNA clones of full length (GII.4), polymerase frameshift mutant (F/S), and mutant L7 (L7). Total cell lysates were harvested and production of viral protein VPg was assayed by western blot. * indicates mature or precursor forms of VPg. GAPDH was used as loading control. B) Nuclease treatment of HuNoV. Cell lysates containing HuNoV cDNA plasmids and potentially HuNoV were treated with recombinant bensonase at 37 ℃ for 2 hours and net HuNoV vRNA was determined by RT-qPCR. Two-way ANOVA was performed with Bonferroni test (* p<0.05, ** p<0.01, *** p<0.001). C) Primary infection of HuNoV in primary differentiated

duodenal organoids D196. Nuclease-digested GII.4, F/S and L7 were inoculated to differentiated organoids D196. Viral RNA of days 0 and 3 post infection were determined by RT-qPCR. Fold of increase was calculated by dividing total vRNA on day 3 over that on day 0. Mean fold of increase were represented above each sample.

5.4 Discussion

5.4.1 The multifunctional norovirus capsid shell domain

A previous characterisation of the norovirus VP1-RdRp interaction suggested that the specificity was conferred by the genogroup-specific residues in the VP1 shell domain. The limited sequence variations also means a loss-of-function approach can be applied to identify the residues important for this interaction. In this chapter, the functional importance of the norovirus SD in regulating norovirus replication was investigated under the context of biochemical characterisation and virus infection using MNV as the model system.

Different combinations of MNV SD flexible loop sequences were replaced by HuNoV sequences, and the importance of these domains was demonstrated by the observation that completely replacing the genogroup-specific residues abolishes MNV replication *in vitro* (Figure 5.3A). Subsequent characterisations identified a residue important for virus thermal stability in solution (Threonine 153) and domains important for VP1-RdRp interaction and regulation of genome replication (loops 1 and 7). The combination of mutations with different phenotypes resulted in additive effect in this end point assay. Mutants with single phenotype (L1, L5, L7 or L1,7) showed no defect in virus yield, but combinations of mutations in loop 5 and loops 1 or 7 generate attenuated viruses (L1,5 or L5,7), supporting the multiple roles of SD in norovirus life cycle.

5.4.2 Other domains important for VP1-RdRp interaction

Shell domains from both HuNoV and MNV bind their cognate RdRps and regulate genome replication by modulating RdRp activity (Subba-Reddy et al., 2012). Norovirus RdRp can initiate RNA synthesis by both VPg-primed and *de novo* initiation, it is possible that the binding of VP1 to RdRp promotes the conformation favouring *de novo* initiation.

Our study showed that the chimeric MNVs with mutated loops 1 and 7 reduce the enhancement of *de novo* activity of RdRp by reducing VP1-RdRp interaction (Figure 5.6 and 5.7). This is likely to occur through the non-optimal VP1-RdRp interactions. It also suggests that in addition to the genogroup-specific residues, there could be more residues or domains important for VP1-RdRp interaction. This is because with both loops 1 and 7 mutated to HuNoV sequences, the MNV VP1 can still bind the MNV RdRp (Figure 5.6B) and enhance RdRp activity (Figure 5.7). The retention of the VP1-RdRp interaction under this condition can be due to other highly conserved domains between the HuNoV- and MNV SD. For example, loop 3 is conserved between HuNoV and MNV (Figure 5.2 and Table 5.1) and is conserved among all noroviruses (data not shown), suggesting that this domain is evolutionarily conserved and can be crucial for norovirus replication. In a high-resolution functional profiling of the MNV genome, except for loop 7, loops 1, 3 and 5 cannot tolerate any insertions beyond P1 ((Thorne et al., 2012), supplementary). This result suggests that loops 1, 3 and 5 are all important for norovirus replication, whereas insertional tolerance of loop 7 may enable co-evolution of shell domain with RdRp without significant fitness cost.

5.4.3 Characterisation of chimeric MNV-3s

The impact on virus thermal stability and replication by SD mutations were observed in both acute (MNV-1) and persistent (MNV-3) chimeric MNVs. However, there are

variations between MNV-1 and MNV-3. For example, mutant L7 or L1,7 showed no defect in recovery in MNV-1 but failed to generate CPE in chimeric MNV-3^{VF1-}s (Figure 5.3A and 5.8A), indicating that the same mutations MNV-3 is more detrimental for virus replication in MNV-3. In addition, MNV-3^{VF1-} L5 showed less reduction in infectivity when heated than did MNV-1 L5 (Figure 5.4 and 5.9B), indicating that the mutant MNV-3^{VF1-} L5 is more resistant to heat inactivation. Such differences suggest that though MNV-1 and MNV-3 are genetically similar, the impact of homologous mutations can result in variable outcomes.

Although VF1 is nonessential for *in vitro* replication of MNV-1 and MNV-3, both MNV-1^{VF1-} and MNV-3^{VF1-} showed reduced virulence and pathology *in vivo* (McFadden et al., 2011). In this study, VF1 expression is retained in the chimeric MNV-1s, whilst chimeric MNV-3s were produced in the MNV-3^{VF1-}backbone to exclude the impact of VF1 mutation. VF1 shares the coding region with SD in MNV with a different reading frame, and it was not possible to introduce the studied SD mutations without changing the VF1 coding sequence. The current experimental set up cannot exclude the possibility that the mutated VF1 in chimeric MNV-1s contribute to the variations of the phenotypes, or the lack of VF1 expression affects the attenuation of chimeric MNV-3s. Despite this, MNV-3^{VF1-} was used as the backbone for generating chimeric MNV-3s, because this mutant virus is replication competent *in vitro*. MNV-3^{VF1-} causes persistent infection in immunocompetent mice, allowing us to test if the additional SD mutations result in additive effects, and whether the combination of mutations can result in clearance of persistent infection or can generate protective immune response against homotypic re-challenge.

In vivo characterisation showed no further attenuation in MNV-3^{VF1-} L5 compared to the already attenuated MNV-3^{VF1-}, indicating the marginal impact of the T153A mutation on virus replication or the induction of mucosal immunity against MNV

infection. The observation that mutant MNV-3^{VF1-} L5 still causes persistent infection in immunocompetent mice suggested that an acute strain MNV should be used in order to prevent persistence.

5.4.4 Host and viral correlates of norovirus persistence

MNV is an important model system to study host cell-virus interactions, as through different combinations of virus and mouse strain, outcome of infections can be lethal or asymptomatic, acute or persistent (Karst et al., 2003, Hsu et al., 2006, Smith et al., 2012). Using MNV as a model system, both host and viral correlates of persistence have been identified. For host correlates, the lack of type I interferon receptor in dendritic cells enables an acute MNV to persist systemically (Nice et al., 2016). The recent discovery of the role of type III interferon pathways in MNV pathogenesis suggests that IFN λ response in intestinal epithelial cells and gut microbiota are important for clearing persistent MNV infections (Baldridge et al., 2017, Baldridge et al., 2015, Nice et al., 2015). Viral correlates also contribute to persistence. For example, a residue in NS1-2 can affect viral tropism and is sufficient for an acute MNV to cause persistent infection (Nice et al., 2013). Compared to MNV-1 which causes acute infection, MNV-3 is less virulent but induces stronger mucosal immune response, and VP2 of MNV-3 antagonises antigen presentation of B cells, resulting in impaired control of acute infection (Zhu et al., 2013, Zhu et al., 2016).

From our study, primary challenge of MNV-3 WT induces high level of MNV-specific serum IgG in immunocompetent mice, paralleled with reduced faecal shedding in re-challenge study (Figure 5.10C and 5.11B). These results indicate that pre-existing mucosal immunity provides partial protection against norovirus infection, which agrees with previously published data (Liu et al., 2009). Despite this, persistent infections were established, indicating serum IgG is not a host correlate of persistence. Also,

attenuated MNV-3^{VF1-}can persistently infect immunocompetent mice, indicating that neither is MNV-3^{VF1-} a viral correlate of persistence.

5.4.5 Recovery of chimeric HuNoV

MNV-3^{VF1-} L1,7 is not only non-cytopathic *in vitro* but also replication defective *in vivo*, highlighting the crucial role of the temporal regulation of norovirus genome replication. The results of the MNV studies, along with the functional conservation of the norovirus VP1-RdRp interaction, led to the attempts to recover chimeric GII.4 HuNoV L7. Our initial characterisation showed successful production of viral protein VPg, while the infection of the primary intestinal organoids showed increases in viral RNA over time (Figure 5.12C). However, more evidence is needed to confirm the recovery of infectious HuNoV. Also, it remains to be determined whether the VP1-RdRp interaction is impacted by the L7 mutations in HuNoV, and whether L7 SD can reduce the enhancement on *de novo* initiation activity of a HuNoV RdRp. In the long term, it will be interesting to determine if HuNoV L7 is attenuated and whether this can be applied in norovirus vaccine design.

5.4.6 VP1-RdRp compatibility in norovirus evolution

The importance of VP1-RdRp interaction in regulating norovirus replication suggests that the VP1-RdRp compatibility may be important during recombination of human norovirus. A recent bioinformatic study investigated the evolution of VP1 and RdRp of GII.2 HuNoV (Mizukoshi et al., 2017), demonstrating that the evolution of norovirus VP1 and RdRp are similar. This supports the hypothesis that the norovirus VP1 and RdRp may co-evolve. The recombinations of norovirus genome usually occur at the ORF1/ORF2 junction through hybridisation at this highly conserved region (Bull et al., 2005). This may contribute to the emergence of new variants (Eden et al., 2013). The

functional compatibility requirement between the RdRp from ORF1 and the VP1 from ORF2 may therefore affect norovirus evolution by selecting only the variants with the compatible VP1 and RdRp pairs. It remains to determine whether the identified residues here show evidence of positive selection in HuNoV evolution.

Chapter 6

Summary and future perspectives

6.1 Cell culture systems for HuNoV

Viral gastroenteritis is a significant global cause of morbidity and mortality. Since the development of the rotavirus vaccine, norovirus has become the leading cause of gastroenteritis worldwide (Tam et al., 2012). In developed countries the main impact is an economic burden when outbreaks result in elevated healthcare costs and loss of productivity, with risks of severe outcomes in the young, the elderly and and the immunocompromised (Hall et al., 2013). In developing countries, where clean water supplies are limited, norovirus infection has a particularly higher risk of global mortality, though due to a lack of surveillance the morbidity rate in these countries is likely underestimated. The global impact of norovirus infections highlights the urgent need of antiviral interventions and vaccine development. The highly infectious nature of viral particles, fast onset of symptoms, prolonged faecal shedding in both symptomatic and asymptomatic infections, fast evolution by antigenic drift and recombination, and a lack of lasting immunity all contribute to the rapid and wide spread of the virus. In spite of this knowledge, details of some of the most basic aspects of norovirus life cycle are not known due to the inability to cultivate this important pathogen in cell culture. As such, the main goal of this project was to identify host and viral factors important for norovirus replication, and to provide information for rational attenuation of norovirus to permit better study of the virus in cell culture.

The first part of the thesis focused on the development of a cell culture system for HuNoV. To this aim HuNoV replication was examined in a range of cell lines (Table 6.1), and our observations, together with previous unsuccessful attempts to cultivate HuNoV, provide insight into factors that restrict HuNoV replication *in vitro*. The results showed

HuNoV likely binds to most of the cell lines tested, as HuNoV RNA can be readily detected after inoculation. The bound RNA remained associated with cells and does not decrease significantly over the course of infection, suggesting that the purified HuNoV stocks likely contain encapsidated HuNoV RNA that is resistant to environmental degradation. However, the lack of HuNOV replication in these cells indicate that HuNoV likely associate with the attachment factor rather than a receptor, as indeed we would expect to see reduction of surface bound RNA as the virus internalises during the entry process. In BJAB cells (Jones et al., 2015), we observed that HuNoV replication in BJABs is highly variable. Stable expression of FUT2 likely increases levels of H antigen on cell surface, and significantly increases entry of HuNoV pseudovirus particle into BJABs, suggesting that in this system insufficient cell surface expressed HBGA could be a limiting factor, supporting previous observations that enteric bacteria or HBGA enhances HuNoV replication in BJAB ((Jones et al., 2014) and unpublished data from L. Meredith). It will be interesting to determine if over expression of FUT2 can functionally replace HBGA or *E. cloacae* in B-cell culture of HuNoV. Also, there are ongoing efforts in the groups aiming to identify the proteinaceous receptor of HuNoV, as preliminary results and previous reports indicate viral entry is impaired by protease treatment of the target cells, including BJAB.

Type I IFNs are potent inhibitors of norovirus RNA replication, as shown in Norwalk virus RNA replicon systems, and in MNV infection (Chang and George, 2007, Changotra et al., 2009). Therefore, it was proposed that inhibiting innate immune response could promote low-level HuNoV replication. However, BVDV NPro expression had no positive effect on HuNoV replication in transduced cells, contrary to this hypothesis, replication of HuNoV in intestinal organoids can be enhanced by ruxolitinib, a JAK/STAT pathway inhibitor (M. Hosmillo, unpublished data), suggesting an antiviral role of JAK/STAT pathways in restricting HuNoV replication. Both type I and

type III IFN responses depend on JAK/STAT signalling pathways. Compared to type I IFN responses, type III IFN responses has been shown to be more important for mediating antiviral responses in epithelial cells (Pott et al., 2011, Hernandez et al., 2015). Therefore, the interactions between type III IFN responses and HuNoV replication should be further investigated using intestinal organoids as a model system, as these more closely represent physiological conditions compared with cell lines.

For the first time, this project demonstrated recovery of infectious HuNoV from a culture-based system. This was accomplished both by FPV-mediated DNA reverse genetics of HuNoV and from intestinal organoids in culture. Previously reported reverse genetic systems indirectly determined infectivity by detecting encapsidated viral RNA and observing viral particles (Asanaka et al., 2005, Katayama et al., 2014). HuNoV recovered using our reverse genetic system (RGS) showed virus replication in intestinal organoids, and importantly, progeny virus from primary infection could subsequently be propagated in culture, leading to more robust replication than observed in the published data (more than 2000 fold compared with 1.5 to 2.5 $\log_{10}$ increase, (Ettayebi et al., 2016)). While different viruses and cell types may contribute to the observed enhancement, the results show the potential of recovering replication-competent HuNoV from our reverse genetic system, and also provides the capacity to manipulate and recover genetically-defined HuNoV using standard molecular techniques. Cell culture-based recovery of HuNoV also prevents the introduction of potentially inhibitory contaminants from faecal samples, which may also contribute to the enhanced replication.

Despite the exciting findings in the initial experiments, the RGS-intestinal organoids can be improved in the following ways. A robust method is needed to consistently maintain and differentiate intestinal organoids. Early experiments showed the challenges of differentiating a sufficient enterocyte population from proliferating

organoids. Variations in some non-commercial components of the cell culture media also indicates the importance of developing a routine quality control protocol for differentiation. Studies have shown intestinal organoids can be directed to differentiate into enterocytes (van der Flier and Clevers, 2009), which can be applied to potentially produce more susceptible cells for infection. In addition, more direct evidence is needed to validate the reverse genetic system in both organoids and cell culture, including detection of viral proteins and negative-sense replication intermediates in the cells, and visualisation and characterisation of released of progeny particles by electron microscopy. A standardised titration assay is also needed to quantitatively determine the infectivity of HuNoV, such as a plaque- or focus-forming assay or a $TCID_{50}$ protocol. Current methods rely on detection of viral RNA and a RT-qPCR-based titration assay has been developed (Ettayebi et al., 2016). However, due to the complex nature of maintaining intestinal organoids traditional plate-based $TCID_{50}$ assays cannot be directly adopted. Possibly an infectious centre assay can be developed or adapted to quantify infectious HuNoV (Dutta and Myrup, 1983). However, all these issues, along with the limited availability of primary intestinal organoids highlights the need to identify cellular factors important for HuNoV replication to establish a robust, reproducible, immortalised cell culture system mimicking the expression of according factors in primary enterocytes.

Name	Epithelial/ Immune cells	Primary/ Immortalised cells	Lentiviral transduction (Y/N)	HuNoV replication (-/+/++/+++)
Caco-2	Epithelial	Immortalised	Y	-
LS174T	Epithelial	Immortalised	N	-
HIEC	Epithelial	Primary	Y	?
Tonsillar cells	Immune	Primary	N	+
KBM7	Immune	Immortalised	N	+
γ δ T cells	Immune	Primary	N	-/+
BJAB	Immune	Immortalised	Y	++
Intestinal organoids	Epithelial	Primary	N	+++

Table 6.1 Summary of screened cell lines and outcome of infection.

6.2 eIF4E phosphorylation and norovirus pathogenesis

The second part of this thesis was focused on characterising the role of eIF4E phosphorylation in norovirus translation control during infection. Using MNV as a model system, it has been demonstrated that norovirus facilitates translation initiation via a virus-specific, VPg-dependent mechanism (Daughenbaugh et al., 2003). This enables norovirus to effectively modulate the global translation landscape without impacting virus translation, as there is a substantially different requirements compared with cap-dependent translation (Chaudhry et al., 2006, Emmott et al., 2017). However, despite these differences, norovirus VPg interacts with cap-binding protein eIF4E, which is not essential for virus replication (Chaudhry et al., 2006). This, together with the observation that eIF4E phosphorylation is proviral *in vitro*, led to the hypothesis that

VPg-eIF4E interaction is a mechanism by which norovirus elicits translation control. eIF4E phosphorylation was previously proposed to be important for translation of a subset of mRNAs, including NF-κB inhibitor IκBα (Furic et al., 2010). Inhibition of eIF4E phosphorylation showed enhanced type I IFN response due to increased NF-κB activity, leading to restriction of several viruses (Herdy et al., 2012). We proposed that inhibiting eIF4E phosphorylation should negatively impact norovirus infection.

A mouse model containing eIF4E S209A mutation was developed to study the effect of eIF4E phosphorylation on MNV pathogenesis. Compared to wild type (WT), BMDMs with eIF4E S209A mutation (KI) showed more robust induction of *Ifnb* but not *Il6*, suggesting different regulation mechanisms of the two NF-κB target genes. MNV replication in BMDMs was not impacted by KI mutations, despite increased *Ifnb* induction and ISG production. A replication-competent MNV-3 showed no difference in replication between WT and KI mice. Interestingly, acute phase faecal shedding of attenuated MNV-3^{VF1-} was partially restored in KI mice. However, this phenotype is dose-dependent as a similar effect was not observed in a high-dose challenge model. There are several possible explanations of why our observations do not support the initial hypothesis. It is possible that the effect of eIF4E phosphorylation on MNV replication is specific to Raw264.7 cells. Compared to BMDM, Raw264.7 cells have higher expression of eIF4E and p-eIF4E, meaning inhibition of eIF4E phosphorylation may have a more significant impact on MNV replication in Raw264.7 cells than in BMDM, assuming that phosphorylation plays a direct role. As eIF4E phosphorylation has been implicated in controlling tumorigenesis and cancer progression (Furic et al., 2010), it is also possible that the effect of eIF4E phosphorylation in the context of immortalised cell lines is different from those in primary cell or mouse model, relating more to cell-cycle control and proliferation. However, this contradicts previous

observations (Royall et al., 2015, Herdy et al., 2012), so the proviral effect of eIF4E phosphorylation is unlikely to be cell line specific or virus specific. A more feasible explanation is that eIF4E phosphorylation has multiple functions in MNV replication. For example, the differences between *Ifnb* and *Il6* induction indicates that there are more factors involved than just eIF4E phosphorylation. Also, it remains to be determined whether type III IFN responses are regulated by eIF4E phosphorylation, and whether enhanced type I IFN responses have any feedback impacts on type III IFN-specific responses.

The observed differences between *in vitro* and *in vivo* models also highlights the influence of model systems in studying host-virus interactions. Although MNV pathogenesis is minimally impacted by the S209A mutation, possible mechanisms of translation control by other viruses can be studied using the established model system. Previous study has established a steady-state gene expression profile of KI MEF cells using microarrays, it may be interesting to characterise changes of gene expression during activation of viral translation. This demonstrates that the *in vivo* model systems will have a great utility in future studies.

6.3 A non-structural role of VP1 in norovirus replication

The third part of this thesis aimed to characterise VP1 shell domain (SD) in regulating norovirus replication. A previous study demonstrated that a genogroup-specific VP1-RdRp interaction modulates RdRp activity (Subba-Reddy et al., 2012). It was proposed that these genogroup-specific domains within the shell domain confer species restriction of this interaction and are important for norovirus replication.

Initially, domains important for VP1-RdRp interaction were identified by comparing the replication of chimeric MNVs with mutated genogroup-specific residues. The crucial role of these domains was demonstrated by the observation that a complete replacement abolished MNV replication. One mutant (L5) is replication competent but more susceptible to thermal inactivation. The point mutation in SD likely destabilised capsid, and thermal inactivation assays indicated that mutant L5 can be used together with WT MNV to evaluate the environmental stability of different MNVs. Mutations in another two domains (L1 and L7) resulted in both a reduced VP1-RdRp interaction and delayed virus replication kinetics. In an RNA synthesis assay, SD was sufficient to enhance the *de novo* initiation activity of RdRp, which is the first biochemical evidence of norovirus shell domain promoting a specific mode of initiation for RNA synthesis. MNV SD with HuNoV L1 and L7 showed less enhancement on RdRp activity, supporting the idea that the genogroup-specific residues in L1 and L7 confer species restriction of this interaction. In addition, MNV-3 carrying homologous mutations (MNV-3^{VF1-} L1,7) was replication defective *in vivo*, demonstrating the biological importance of this functionally-conserved interaction. Non-encapsidation activities of viral structural proteins have become an increasingly important subject (Ni and Cheng Kao, 2013) and these results demonstrate that norovirus capsid shell domain not only encapsidates viral RNA but also regulate RNA synthesis. Therefore, the VP1-RdRp interface can be potentially targeted for antiviral intervention or vaccine development.

In conjunction with the HuNoV reverse genetic system, we can now raise the possibility of characterising genetically-manipulated HuNoV *in vitro*. As a proof of concept, chimeric HuNoV with MNV L7 was also cloned and produced. There is evidence of encapsidated viral RNA produced. However, further characterisation is required to evaluate the potential of these mutations for rational attenuation of HuNoV.

Summary and future perspectives

Together, this thesis aimed to address one of the most challenging questions in the norovirus field and has demonstrated successful recovery of infectious HuNoV by reverse genetics. Using a stringent experiment set up to understand the role of eIF4E phosphorylation in norovirus pathogenesis highlights the importance of studying virus-host interactions in a physiologically-relevant context. The characterisation of a non-structural function of a viral structural protein probes the possibility of using surrogate systems to study functionally-conserved interactions for antiviral design and rational attenuation. Further investigations should focus on improving the organoids culture and reverse genetics system. Host and viral factors should also be characterised to better understand and control this clinically and economically important pathogen.

References

ABENTE, E. J., SOSNOVTSEV, S. V., SANDOVAL-JAIME, C., PARRA, G. I., BOK, K. & GREEN, K. Y. 2013. The feline calicivirus leader of the capsid protein is associated with cytopathic effect. *J Virol,* 87**,** 3003-17.

ALAM, I., LEE, J. H., CHO, K. J., HAN, K. R., YANG, J. M., CHUNG, M. S. & KIM, K. H. 2012. Crystal structures of murine norovirus-1 RNA-dependent RNA polymerase in complex with 2-thiouridine or ribavirin. *Virology,* 426**,** 143-51.

ALMANZA, H., CUBILLOS, C., ANGULO, I., MATEOS, F., CASTON, J. R., VAN DER POEL, W. H., VINJE, J., BARCENA, J. & MENA, I. 2008. Self-assembly of the recombinant capsid protein of a swine norovirus into virus-like particles and evaluation of monoclonal antibodies cross-reactive with a human strain from genogroup II. *J Clin Microbiol,* 46**,** 3971-9.

ALONSO, C., OVIEDO, J. M., MARTIN-ALONSO, J. M., DIAZ, E., BOGA, J. A. & PARRA, F. 1998. Programmed cell death in the pathogenesis of rabbit hemorrhagic disease. *Arch Virol,* 143**,** 321-32.

ANDREJEVA, J., CHILDS, K. S., YOUNG, D. F., CARLOS, T. S., STOCK, N., GOODBOURN, S. & RANDALL, R. E. 2004. The V proteins of paramyxoviruses bind the IFN-inducible RNA helicase, mda-5, and inhibit its activation of the IFN-beta promoter. *Proc Natl Acad Sci U S A,* 101**,** 17264-9.

ARIAS, A., BAILEY, D., CHAUDHRY, Y. & GOODFELLOW, I. 2012. Development of a reverse-genetics system for murine norovirus 3: long-term persistence occurs in the caecum and colon. *J Gen Virol,* 93**,** 1432-41.

ARIAS, A., THORNE, L. & GOODFELLOW, I. 2014. Favipiravir elicits antiviral mutagenesis during virus replication in vivo. *Elife,* 3**,** e03679.

ARTHUR, S. E. & GIBSON, K. E. 2015. Comparison of methods for evaluating the thermal stability of human enteric viruses. *Food Environ Virol,* 7**,** 14-26.

ASANAKA, M., ATMAR, R. L., RUVOLO, V., CRAWFORD, S. E., NEILL, F. H. & ESTES, M. K. 2005. Replication and packaging of Norwalk virus RNA in cultured mammalian cells. *Proc Natl Acad Sci U S A,* 102**,** 10327-32.

ATMAR, R. L., BERNSTEIN, D. I., HARRO, C. D., AL-IBRAHIM, M. S., CHEN, W. H., FERREIRA, J., ESTES, M. K., GRAHAM, D. Y., OPEKUN, A. R., RICHARDSON, C. & MENDELMAN, P. M. 2011. Norovirus vaccine against experimental human Norwalk Virus illness. *N Engl J Med,* 365**,** 2178-87.

ATMAR, R. L., OPEKUN, A. R., GILGER, M. A., ESTES, M. K., CRAWFORD, S. E., NEILL, F. H. & GRAHAM, D. Y. 2008. Norwalk virus shedding after experimental human infection. *Emerg Infect Dis,* 14**,** 1553-7.

ATMAR, R. L., OPEKUN, A. R., GILGER, M. A., ESTES, M. K., CRAWFORD, S. E., NEILL, F. H., RAMANI, S., HILL, H., FERREIRA, J. & GRAHAM, D. Y. 2014. Determination of the 50% human infectious dose for Norwalk virus. *J Infect Dis,* 209**,** 1016-22.

AVERY, R. K., LONZE, B. E., KRAUS, E. S., MARR, K. A. & MONTGOMERY, R. A. 2017. Severe chronic norovirus diarrheal disease in transplant recipients: Clinical features of an under-recognized syndrome. *Transpl Infect Dis,* 19.

BAILEY, D., KAISER, W. J., HOLLINSHEAD, M., MOFFAT, K., CHAUDHRY, Y., WILEMAN, T., SOSNOVTSEV, S. V. & GOODFELLOW, I. G. 2010a. Feline calicivirus p32, p39 and p30 proteins localize to the endoplasmic reticulum to initiate replication complex formation. *J Gen Virol,* 91**,** 739-49.

BAILEY, D., KARAKASILIOTIS, I., VASHIST, S., WAH CHUNG, L. M., REES, J., MCFADDEN, N., BENSON, A., YAROVINSKY, F., SIMMONDS, P. & GOODFELLOW, I. 2010b. Functional Analysis of RNA Structures Present at the 3′ Extremity of the Murine Norovirus Genome: the Variable Polypyrimidine Tract Plays a Role in Viral Virulence. *Journal of Virology,* 84**,**

10943-10943.
BAILEY, D., THACKRAY, L. B. & GOODFELLOW, I. G. 2008. A single amino acid substitution in the murine norovirus capsid protein is sufficient for attenuation in vivo. *J Virol,* 82**,** 7725-8.
BALDRIDGE, M. T., LEE, S., BROWN, J. J., MCALLISTER, N., URBANEK, K., DERMODY, T. S., NICE, T. J. & VIRGIN, H. W. 2017. Expression of Ifnlr1 on Intestinal Epithelial Cells Is Critical to the Antiviral Effects of Interferon Lambda against Norovirus and Reovirus. *J Virol,* 91.
BALDRIDGE, M. T., NICE, T. J., MCCUNE, B. T., YOKOYAMA, C. C., KAMBAL, A., WHEADON, M., DIAMOND, M. S., IVANOVA, Y., ARTYOMOV, M. & VIRGIN, H. W. 2015. Commensal microbes and interferon-lambda determine persistence of enteric murine norovirus infection. *Science,* 347**,** 266-9.
BALL, J. M., GRAHAM, D. Y., OPEKUN, A. R., GILGER, M. A., GUERRERO, R. A. & ESTES, M. K. 1999. Recombinant Norwalk virus-like particles given orally to volunteers: phase I study. *Gastroenterology,* 117**,** 40-8.
BALL, J. M., HARDY, M. E., ATMAR, R. L., CONNER, M. E. & ESTES, M. K. 1998. Oral immunization with recombinant Norwalk virus-like particles induces a systemic and mucosal immune response in mice. *J Virol,* 72**,** 1345-53.
BANK-WOLF, B. R., KONIG, M. & THIEL, H. J. 2010. Zoonotic aspects of infections with noroviruses and sapoviruses. *Vet Microbiol,* 140**,** 204-12.
BARIC, R. S., YOUNT, B., LINDESMITH, L., HARRINGTON, P. R., GREENE, S. R., TSENG, F. C., DAVIS, N., JOHNSTON, R. E., KLAPPER, D. G. & MOE, C. L. 2002. Expression and self-assembly of norwalk virus capsid protein from venezuelan equine encephalitis virus replicons. *J Virol,* 76**,** 3023-30.
BARRIOS-RODILES, M., BROWN, K. R., OZDAMAR, B., BOSE, R., LIU, Z., DONOVAN, R. S., SHINJO, F., LIU, Y., DEMBOWY, J., TAYLOR, I. W., LUGA, V., PRZULJ, N., ROBINSON, M., SUZUKI, H., HAYASHIZAKI, Y., JURISICA, I. & WRANA, J. L. 2005. High-throughput mapping of a dynamic signaling network in mammalian cells. *Science,* 307**,** 1621-5.
BARTOLINI, L., MARDARI, R., TOLDO, I., CALDERONE, M., BATTISTELLA, P. A., LAVERDA, A. M. & SARTORI, S. 2011. Norovirus gastroenteritis and seizures: an atypical case with neuroradiological abnormalities. *Neuropediatrics,* 42**,** 167-9.
BARTSCH, S. M., LOPMAN, B. A., HALL, A. J., PARASHAR, U. D. & LEE, B. Y. 2012. The potential economic value of a human norovirus vaccine for the United States. *Vaccine,* 30**,** 7097-104.
BARTSCH, S. M., LOPMAN, B. A., OZAWA, S., HALL, A. J. & LEE, B. Y. 2016. Global Economic Burden of Norovirus Gastroenteritis. *PLoS One,* 11**,** e0151219.
BEERENS, N., SELISKO, B., RICAGNO, S., IMBERT, I., VAN DER ZANDEN, L., SNIJDER, E. J. & CANARD, B. 2007. De novo initiation of RNA synthesis by the arterivirus RNA-dependent RNA polymerase. *J Virol,* 81**,** 8384-95.
BELLIOT, G., SOSNOVTSEV, S. V., CHANG, K. O., BABU, V., UCHE, U., ARNOLD, J. J., CAMERON, C. E. & GREEN, K. Y. 2005. Norovirus proteinase-polymerase and polymerase are both active forms of RNA-dependent RNA polymerase. *J Virol,* 79**,** 2393-403.
BELLIOT, G., SOSNOVTSEV, S. V., CHANG, K. O., MCPHIE, P. & GREEN, K. Y. 2008. Nucleotidylylation of the VPg protein of a human norovirus by its proteinase-polymerase precursor protein. *Virology,* 374**,** 33-49.
BELLIOT, G., SOSNOVTSEV, S. V., MITRA, T., HAMMER, C., GARFIELD, M. & GREEN, K. Y. 2003. In vitro proteolytic processing of the MD145 norovirus

ORF1 nonstructural polyprotein yields stable precursors and products similar to those detected in calicivirus-infected cells. *J Virol,* 77**,** 10957-74.
BELSHAM, G. J. 2009. Divergent picornavirus IRES elements. *Virus Res,* 139**,** 183-92.
BERNSTEIN, D. I., ATMAR, R. L., LYON, G. M., TREANOR, J. J., CHEN, W. H., JIANG, X., VINJE, J., GREGORICUS, N., FRENCK, R. W., JR., MOE, C. L., AL-IBRAHIM, M. S., BARRETT, J., FERREIRA, J., ESTES, M. K., GRAHAM, D. Y., GOODWIN, R., BORKOWSKI, A., CLEMENS, R. & MENDELMAN, P. M. 2015. Norovirus vaccine against experimental human GII.4 virus illness: a challenge study in healthy adults. *J Infect Dis,* 211**,** 870-8.
BERTOLOTTI-CIARLET, A., CRAWFORD, S. E., HUTSON, A. M. & ESTES, M. K. 2003. The 3' end of Norwalk virus mRNA contains determinants that regulate the expression and stability of the viral capsid protein VP1: a novel function for the VP2 protein. *J Virol,* 77**,** 11603-15.
BERTOLOTTI-CIARLET, A., WHITE, L. J., CHEN, R., PRASAD, B. V. & ESTES, M. K. 2002. Structural requirements for the assembly of Norwalk virus-like particles. *J Virol,* 76**,** 4044-55.
BIRMINGHAM, A., SELFORS, L. M., FORSTER, T., WROBEL, D., KENNEDY, C. J., SHANKS, E., SANTOYO-LOPEZ, J., DUNICAN, D. J., LONG, A., KELLEHER, D., SMITH, Q., BEIJERSBERGEN, R. L., GHAZAL, P. & SHAMU, C. E. 2009. Statistical methods for analysis of high-throughput RNA interference screens. *Nat Methods,* 6**,** 569-75.
BLAKENEY, S. J., CAHILL, A. & REILLY, P. A. 2003. Processing of Norwalk virus nonstructural proteins by a 3C-like cysteine proteinase. *Virology,* 308**,** 216-24.
BOHNKER, B. K. & THORNTON, S. 2003. Explosive outbreaks of gastroenteritis in the shipboard environment attributed to Norovirus. *Mil Med,* 168**,** iv.
BOK, K., CAVANAUGH, V. J., MATSON, D. O., GONZALEZ-MOLLEDA, L., CHANG, K. O., ZINTZ, C., SMITH, A. W., IVERSEN, P., GREEN, K. Y. & CAMPBELL, A. E. 2008. Inhibition of norovirus replication by morpholino oligomers targeting the 5'-end of the genome. *Virology,* 380**,** 328-37.
BOK, K., PARRA, G. I., MITRA, T., ABENTE, E., SHAVER, C. K., BOON, D., ENGLE, R., YU, C., KAPIKIAN, A. Z., SOSNOVTSEV, S. V., PURCELL, R. H. & GREEN, K. Y. 2011. Chimpanzees as an animal model for human norovirus infection and vaccine development. *Proc Natl Acad Sci U S A,* 108**,** 325-30.
BOK, K., PRIKHODKO, V. G., GREEN, K. Y. & SOSNOVTSEV, S. V. 2009. Apoptosis in murine norovirus-infected RAW264.7 cells is associated with downregulation of survivin. *J Virol,* 83**,** 3647-56.
BOL, J. F. 2008. Role of capsid proteins. *Methods Mol Biol,* 451**,** 21-31.
BOON, D., MAHAR, J. E., ABENTE, E. J., KIRKWOOD, C. D., PURCELL, R. H., KAPIKIAN, A. Z., GREEN, K. Y. & BOK, K. 2011. Comparative evolution of GII.3 and GII.4 norovirus over a 31-year period. *J Virol,* 85**,** 8656-66.
BRIDGER, J. C., HALL, G. A. & BROWN, J. F. 1984. Characterization of a calici-like virus (Newbury agent) found in association with astrovirus in bovine diarrhea. *Infect Immun,* 43**,** 133-8.
BROWN, J. R., GILMOUR, K. & BREUER, J. 2016. Norovirus Infections Occur in B-Cell-Deficient Patients. *Clin Infect Dis,* 62**,** 1136-8.
BUI, T., KOCHER, J., LI, Y., WEN, K., LI, G., LIU, F., YANG, X., LEROITH, T., TAN, M., XIA, M., ZHONG, W., JIANG, X. & YUAN, L. 2013. Median infectious dose of human norovirus GII.4 in gnotobiotic pigs is decreased by simvastatin treatment and increased by age. *J Gen Virol,* 94**,** 2005-16.
BULL, R. A., EDEN, J. S., RAWLINSON, W. D. & WHITE, P. A. 2010. Rapid

evolution of pandemic noroviruses of the GII.4 lineage. *PLoS Pathog,* 6**,** e1000831.
BULL, R. A., HANSMAN, G. S., CLANCY, L. E., TANAKA, M. M., RAWLINSON, W. D. & WHITE, P. A. 2005. Norovirus recombination in ORF1/ORF2 overlap. *Emerg Infect Dis,* 11**,** 1079-85.
BULL, R. A., HYDE, J., MACKENZIE, J. M., HANSMAN, G. S., OKA, T., TAKEDA, N. & WHITE, P. A. 2011. Comparison of the replication properties of murine and human calicivirus RNA-dependent RNA polymerases. *Virus Genes,* 42**,** 16-27.
BULL, R. A., TU, E. T., MCIVER, C. J., RAWLINSON, W. D. & WHITE, P. A. 2006. Emergence of a new norovirus genotype II.4 variant associated with global outbreaks of gastroenteritis. *J Clin Microbiol,* 44**,** 327-33.
BURROUGHS, J. N. & BROWN, F. 1978. Presence of a covalently linked protein on calicivirus RNA. *J Gen Virol,* 41**,** 443-6.
CADDY, S., BREIMAN, A., LE PENDU, J. & GOODFELLOW, I. 2014. Genogroup IV and VI canine noroviruses interact with histo-blood group antigens. *J Virol,* 88**,** 10377-91.
CADDY, S., EMMOTT, E., EL-ATTAR, L., MITCHELL, J., DE ROUGEMONT, A., BROWNLIE, J. & GOODFELLOW, I. 2013. Serological evidence for multiple strains of canine norovirus in the UK dog population. *PLoS One,* 8**,** e81596.
CADDY, S. L., DE ROUGEMONT, A., EMMOTT, E., EL-ATTAR, L., MITCHELL, J. A., HOLLINSHEAD, M., BELLIOT, G., BROWNLIE, J., LE PENDU, J. & GOODFELLOW, I. 2015. Evidence for human norovirus infection of dogs in the United kingdom. *J Clin Microbiol,* 53**,** 1873-83.
CAMERON, P. U. & STENT, G. 2001. Isolation of human tonsillar dendritic cells. *Methods Mol Med,* 64**,** 121-36.
CARLSSON, B., KINDBERG, E., BUESA, J., RYDELL, G. E., LIDON, M. F., MONTAVA, R., ABU MALLOUH, R., GRAHN, A., RODRIGUEZ-DIAZ, J., BELLIDO, J., ARNEDO, A., LARSON, G. & SVENSSON, L. 2009. The G428A nonsense mutation in FUT2 provides strong but not absolute protection against symptomatic GII.4 Norovirus infection. *PLoS One,* 4**,** e5593.
CHACHU, K. A., LOBUE, A. D., STRONG, D. W., BARIC, R. S. & VIRGIN, H. W. 2008a. Immune mechanisms responsible for vaccination against and clearance of mucosal and lymphatic norovirus infection. *PLoS Pathog,* 4**,** e1000236.
CHACHU, K. A., STRONG, D. W., LOBUE, A. D., WOBUS, C. E., BARIC, R. S. & VIRGIN, H. W. T. 2008b. Antibody is critical for the clearance of murine norovirus infection. *J Virol,* 82**,** 6610-7.
CHAKRAVARTY, S., HUTSON, A. M., ESTES, M. K. & PRASAD, B. V. 2005. Evolutionary trace residues in noroviruses: importance in receptor binding, antigenicity, virion assembly, and strain diversity. *J Virol,* 79**,** 554-68.
CHAN, M. C., LEE, N., HUNG, T. N., KWOK, K., CHEUNG, K., TIN, E. K., LAI, R. W., NELSON, E. A., LEUNG, T. F. & CHAN, P. K. 2015. Rapid emergence and predominance of a broadly recognizing and fast-evolving norovirus GII.17 variant in late 2014. *Nat Commun,* 6**,** 10061.
CHAN, M. C., WONG, Y. P., SUNG, J. J. & LEUNG, W. K. 2008. Histo-blood group antigens and susceptibility to infection with norovirus genogroup II genotype 4. *J Infect Dis,* 198**,** 940; author reply 942-3.
CHANG, K. O. 2009. Role of cholesterol pathways in norovirus replication. *J Virol,* 83**,** 8587-95.
CHANG, K. O. & GEORGE, D. W. 2007. Interferons and ribavirin effectively inhibit Norwalk virus replication in replicon-bearing cells. *J Virol,* 81**,** 12111-8.

CHANG, K. O., GEORGE, D. W., PATTON, J. B., GREEN, K. Y. & SOSNOVTSEV, S. V. 2008. Leader of the capsid protein in feline calicivirus promotes replication of Norwalk virus in cell culture. *J Virol,* 82**,** 9306-17.

CHANG, K. O., KIM, Y., GREEN, K. Y. & SAIF, L. J. 2002. Cell-culture propagation of porcine enteric calicivirus mediated by intestinal contents is dependent on the cyclic AMP signaling pathway. *Virology,* 304**,** 302-10.

CHANG, K. O., SOSNOVTSEV, S. V., BELLIOT, G., KIM, Y., SAIF, L. J. & GREEN, K. Y. 2004. Bile acids are essential for porcine enteric calicivirus replication in association with down-regulation of signal transducer and activator of transcription 1. *Proc Natl Acad Sci U S A,* 101**,** 8733-8.

CHANG, K. O., SOSNOVTSEV, S. V., BELLIOT, G., KING, A. D. & GREEN, K. Y. 2006. Stable expression of a Norwalk virus RNA replicon in a human hepatoma cell line. *Virology,* 353**,** 463-73.

CHANG, K. O., SOSNOVTSEV, S. V., BELLIOT, G., WANG, Q., SAIF, L. J. & GREEN, K. Y. 2005. Reverse genetics system for porcine enteric calicivirus, a prototype sapovirus in the Caliciviridae. *J Virol,* 79**,** 1409-16.

CHANGOTRA, H., JIA, Y., MOORE, T. N., LIU, G., KAHAN, S. M., SOSNOVTSEV, S. V. & KARST, S. M. 2009. Type I and type II interferons inhibit the translation of murine norovirus proteins. *J Virol,* 83**,** 5683-92.

CHAUDHRY, Y., NAYAK, A., BORDELEAU, M. E., TANAKA, J., PELLETIER, J., BELSHAM, G. J., ROBERTS, L. O. & GOODFELLOW, I. G. 2006. Caliciviruses differ in their functional requirements for eIF4F components. *J Biol Chem,* 281**,** 25315-25.

CHAUDHRY, Y., SKINNER, M. A. & GOODFELLOW, I. G. 2007. Recovery of genetically defined murine norovirus in tissue culture by using a fowlpox virus expressing T7 RNA polymerase. *J Gen Virol,* 88**,** 2091-100.

CHEESBROUGH, J. S., GREEN, J., GALLIMORE, C. I., WRIGHT, P. A. & BROWN, D. W. 2000. Widespread environmental contamination with Norwalk-like viruses (NLV) detected in a prolonged hotel outbreak of gastroenteritis. *Epidemiol Infect,* 125**,** 93-8.

CHEETHAM, S., SOUZA, M., MCGREGOR, R., MEULIA, T., WANG, Q. & SAIF, L. J. 2007. Binding patterns of human norovirus-like particles to buccal and intestinal tissues of gnotobiotic pigs in relation to A/H histo-blood group antigen expression. *J Virol,* 81**,** 3535-44.

CHEETHAM, S., SOUZA, M., MEULIA, T., GRIMES, S., HAN, M. G. & SAIF, L. J. 2006. Pathogenesis of a genogroup II human norovirus in gnotobiotic pigs. *J Virol,* 80**,** 10372-81.

CHEN, S. Y., TSAI, C. N., LAI, M. W., CHEN, C. Y., LIN, K. L., LIN, T. Y. & CHIU, C. H. 2009. Norovirus infection as a cause of diarrhea-associated benign infantile seizures. *Clin Infect Dis,* 48**,** 849-55.

CHHABRA, P., RANJAN, P., CROMEANS, T., SAMBHARA, S. & VINJE, J. 2017. Critical role of RIG-I and MDA5 in early and late stages of Tulane virus infection. *J Gen Virol,* 98**,** 1016-1026.

CHIBA, S., SAKUMA, Y., KOGASAKA, R., AKIHARA, M., HORINO, K., NAKAO, T. & FUKUI, S. 1979. An outbreak of gastroenteritis associated with calicivirus in an infant home. *J Med Virol,* 4**,** 249-54.

CHILDS, K., STOCK, N., ROSS, C., ANDREJEVA, J., HILTON, L., SKINNER, M., RANDALL, R. & GOODBOURN, S. 2007. mda-5, but not RIG-I, is a common target for paramyxovirus V proteins. *Virology,* 359**,** 190-200.

CHOI, J. M., HUTSON, A. M., ESTES, M. K. & PRASAD, B. V. 2008. Atomic resolution structural characterization of recognition of histo-blood group

antigens by Norwalk virus. *Proc Natl Acad Sci U S A,* 105**,** 9175-80.
CLAVARINO, G., CLAUDIO, N., COUDERC, T., DALET, A., JUDITH, D., CAMOSSETO, V., SCHMIDT, E. K., WENGER, T., LECUIT, M., GATTI, E. & PIERRE, P. 2012. Induction of GADD34 is necessary for dsRNA-dependent interferon-beta production and participates in the control of Chikungunya virus infection. *PLoS Pathog,* 8**,** e1002708.
COTTEN, M., PETROVA, V., PHAN, M. V., RABAA, M. A., WATSON, S. J., ONG, S. H., KELLAM, P. & BAKER, S. 2014. Deep sequencing of norovirus genomes defines evolutionary patterns in an urban tropical setting. *J Virol,* 88**,** 11056-69.
COTTON, B. T., HYDE, J. L., SARVESTANI, S. T., SOSNOVTSEV, S. V., GREEN, K. Y., WHITE, P. A. & MACKENZIE, J. M. 2017. The Norovirus NS3 Protein Is a Dynamic Lipid- and Microtubule-Associated Protein Involved in Viral RNA Replication. *J Virol,* 91.
COX, C., CAO, S. & LU, Y. 2009. Enhanced detection and study of murine norovirus-1 using a more efficient microglial cell line. *Virol J,* 6**,** 196.
CROCI, R., PEZZULLO, M., TARANTINO, D., MILANI, M., TSAY, S. C., SURESHBABU, R., TSAI, Y. J., MASTRANGELO, E., ROHAYEM, J., BOLOGNESI, M. & HWU, J. R. 2014a. Structural bases of norovirus RNA dependent RNA polymerase inhibition by novel suramin-related compounds. *PLoS One,* 9**,** e91765.
CROCI, R., TARANTINO, D., MILANI, M., PEZZULLO, M., ROHAYEM, J., BOLOGNESI, M. & MASTRANGELO, E. 2014b. PPNDS inhibits murine Norovirus RNA-dependent RNA-polymerase mimicking two RNA stacking bases. *FEBS Lett,* 588**,** 1720-5.
CROOKS, G. E., HON, G., CHANDONIA, J. M. & BRENNER, S. E. 2004. WebLogo: a sequence logo generator. *Genome Res,* 14**,** 1188-90.
DA SILVA, A. K., KAVANAGH, O. V., ESTES, M. K. & ELIMELECH, M. 2011. Adsorption and aggregation properties of norovirus GI and GII virus-like particles demonstrate differing responses to solution chemistry. *Environ Sci Technol,* 45**,** 520-6.
DAUGHENBAUGH, K. F., FRASER, C. S., HERSHEY, J. W. & HARDY, M. E. 2003. The genome-linked protein VPg of the Norwalk virus binds eIF3, suggesting its role in translation initiation complex recruitment. *EMBO J,* 22**,** 2852-9.
DAUGHENBAUGH, K. F., WOBUS, C. E. & HARDY, M. E. 2006. VPg of murine norovirus binds translation initiation factors in infected cells. *Virol J,* 3**,** 33.
DE GRAAF, M., VAN BEEK, J. & KOOPMANS, M. P. 2016. Human norovirus transmission and evolution in a changing world. *Nat Rev Microbiol,* 14**,** 421-33.
DEBBINK, K., LINDESMITH, L. C., DONALDSON, E. F., COSTANTINI, V., BELTRAMELLO, M., CORTI, D., SWANSTROM, J., LANZAVECCHIA, A., VINJE, J. & BARIC, R. S. 2013. Emergence of new pandemic GII.4 Sydney norovirus strain correlates with escape from herd immunity. *J Infect Dis,* 208**,** 1877-87.
DEBBINK, K., LINDESMITH, L. C., FERRIS, M. T., SWANSTROM, J., BELTRAMELLO, M., CORTI, D., LANZAVECCHIA, A. & BARIC, R. S. 2014. Within-host evolution results in antigenically distinct GII.4 noroviruses. *J Virol,* 88**,** 7244-55.
DELACOUR, H., DUBROUS, P. & KOECK, J. L. 2010. Noroviruses: a challenge for military forces. *J R Army Med Corps,* 156**,** 251-4.
DENG, L., MUHAXHIRI, Z., ESTES, M. K., PALZKILL, T., PRASAD, B. V. & SONG,

Y. 2013. Synthesis, Activity and Structure-Activity Relationship of Noroviral Protease Inhibitors. *Medchemcomm,* 4.

DESAI, R., HEMBREE, C. D., HANDEL, A., MATTHEWS, J. E., DICKEY, B. W., MCDONALD, S., HALL, A. J., PARASHAR, U. D., LEON, J. S. & LOPMAN, B. 2012. Severe outcomes are associated with genogroup 2 genotype 4 norovirus outbreaks: a systematic literature review. *Clin Infect Dis,* 55**,** 189-93.

DI MARTINO, B., DI PROFIO, F., MELEGARI, I., SARCHESE, V., MASSIRIO, I., PALERMO, G., ROMITO, G., LORUSSO, E., LANAVE, G., BODNAR, L., BUONAVOGLIA, C., MARSILIO, F., GREEN, K. Y. & MARTELLA, V. 2017. Seroprevalence for norovirus genogroup II, IV and VI in dogs. *Vet Microbiol,* 203**,** 68-72.

DOERFLINGER, S. Y., WEICHERT, S., KOROMYSLOVA, A., CHAN, M., SCHWERK, C., ADAM, R., JENNEWEIN, S., HANSMAN, G. S. & SCHROTEN, H. 2017. Human Norovirus Evolution in a Chronically Infected Host. *mSphere,* 2.

DOROBANTU, C. M., ALBULESCU, L., HARAK, C., FENG, Q., VAN KAMPEN, M., STRATING, J. R., GORBALENYA, A. E., LOHMANN, V., VAN DER SCHAAR, H. M. & VAN KUPPEVELD, F. J. 2015. Modulation of the Host Lipid Landscape to Promote RNA Virus Replication: The Picornavirus Encephalomyocarditis Virus Converges on the Pathway Used by Hepatitis C Virus. *PLoS Pathog,* 11**,** e1005185.

DUIZER, E., SCHWAB, K. J., NEILL, F. H., ATMAR, R. L., KOOPMANS, M. P. & ESTES, M. K. 2004. Laboratory efforts to cultivate noroviruses. *J Gen Virol,* 85**,** 79-87.

DUTTA, S. K. & MYRUP, A. C. 1983. Infectious center assay of intracellular virus and infective virus titer for equine mononuclear cells infected in vivo and in vitro with equine herpesviruses. *Can J Comp Med,* 47**,** 64-9.

ECHENIQUE, I. A., STOSOR, V., GALLON, L., KAUFMAN, D., QI, C. & ZEMBOWER, T. R. 2016. Prolonged norovirus infection after pancreas transplantation: a case report and review of chronic norovirus. *Transpl Infect Dis,* 18**,** 98-104.

EDEN, J. S., CHISHOLM, R. H., BULL, R. A., WHITE, P. A., HOLMES, E. C. & TANAKA, M. M. 2017. Persistent infections in immunocompromised hosts are rarely sources of new pathogen variants. *Virus Evol,* 3**,** vex018.

EDEN, J. S., HEWITT, J., LIM, K. L., BONI, M. F., MERIF, J., GREENING, G., RATCLIFF, R. M., HOLMES, E. C., TANAKA, M. M., RAWLINSON, W. D. & WHITE, P. A. 2014. The emergence and evolution of the novel epidemic norovirus GII.4 variant Sydney 2012. *Virology,* 450-451**,** 106-13.

EDEN, J. S., TANAKA, M. M., BONI, M. F., RAWLINSON, W. D. & WHITE, P. A. 2013. Recombination within the pandemic norovirus GII.4 lineage. *J Virol,* 87**,** 6270-82.

ELFTMAN, M. D., GONZALEZ-HERNANDEZ, M. B., KAMADA, N., PERKINS, C., HENDERSON, K. S., NUNEZ, G. & WOBUS, C. E. 2013. Multiple effects of dendritic cell depletion on murine norovirus infection. *J Gen Virol,* 94**,** 1761-8.

EMMOTT, E. & GOODFELLOW, I. 2014. Identification of protein interaction partners in mammalian cells using SILAC-immunoprecipitation quantitative proteomics. *J Vis Exp*.

EMMOTT, E., SORGELOOS, F., CADDY, S. L., VASHIST, S., SOSNOVTSEV, S., LLOYD, R., HEESOM, K., LOCKER, N. & GOODFELLOW, I. 2017. Norovirus-mediated modification of the translational landscape via virus and host-induced cleavage of translation initiation factors. *Mol Cell Proteomics*.

EMMOTT, E., SWEENEY, T. R. & GOODFELLOW, I. 2015. A Cell-based Fluorescence Resonance Energy Transfer (FRET) Sensor Reveals Inter- and Intragenogroup Variations in Norovirus Protease Activity and Polyprotein Cleavage. *J Biol Chem,* 290**,** 27841-53.
ENGELEN, M. A., GUNIA, S. & STYPMANN, J. 2011. Elimination of norovirus in a chronic carrier under immunosuppression after heart transplantation--effect of everolimus. *Transpl Int,* 24**,** e102-3.
ESCUDERO-ABARCA, B. I., RAWSTHORNE, H., GOULTER, R. M., SUH, S. H. & JAYKUS, L. A. 2014. Molecular methods used to estimate thermal inactivation of a prototype human norovirus: more heat resistant than previously believed? *Food Microbiol,* 41**,** 91-5.
ETTAYEBI, K., CRAWFORD, S. E., MURAKAMI, K., BROUGHMAN, J. R., KARANDIKAR, U., TENGE, V. R., NEILL, F. H., BLUTT, S. E., ZENG, X. L., QU, L., KOU, B., OPEKUN, A. R., BURRIN, D., GRAHAM, D. Y., RAMANI, S., ATMAR, R. L. & ESTES, M. K. 2016. Replication of human noroviruses in stem cell-derived human enteroids. *Science,* 353**,** 1387-1393.
ETTAYEBI, K. & HARDY, M. E. 2003. Norwalk virus nonstructural protein p48 forms a complex with the SNARE regulator VAP-A and prevents cell surface expression of vesicular stomatitis virus G protein. *J Virol,* 77**,** 11790-7.
FAN, Y. S., LIU, C., ZHU, H. J., DING, Y., ZENG, W. J., YIN, X. F., DING, S. S. & ZHANG, J. 2015. A PCR-based Rapid Neutralization Assay for GII.4 Norovirus Infection in HIEC6 Cell Culture. *Biomed Environ Sci,* 28**,** 219-21.
FARKAS, T., FEY, B., KELLER, G., MARTELLA, V. & EGYED, L. 2012. Molecular detection of murine noroviruses in laboratory and wild mice. *Vet Microbiol,* 160**,** 463-7.
FARKAS, T., SESTAK, K., WEI, C. & JIANG, X. 2008. Characterization of a rhesus monkey calicivirus representing a new genus of Caliciviridae. *J Virol,* 82**,** 5408-16.
FENG, K., DIVERS, E., MA, Y. & LI, J. 2011. Inactivation of a human norovirus surrogate, human norovirus virus-like particles, and vesicular stomatitis virus by gamma irradiation. *Appl Environ Microbiol,* 77**,** 3507-17.
FENG, X. & JIANG, X. 2007. Library screen for inhibitors targeting norovirus binding to histo-blood group antigen receptors. *Antimicrob Agents Chemother,* 51**,** 324-31.
FEOKTISTOVA, K., TUVSHINTOGS, E., DO, A. & FRASER, C. S. 2013. Human eIF4E promotes mRNA restructuring by stimulating eIF4A helicase activity. *Proc Natl Acad Sci U S A,* 110**,** 13339-44.
FERNANDEZ-VEGA, V., SOSNOVTSEV, S. V., BELLIOT, G., KING, A. D., MITRA, T., GORBALENYA, A. & GREEN, K. Y. 2004. Norwalk virus N-terminal nonstructural protein is associated with disassembly of the Golgi complex in transfected cells. *J Virol,* 78**,** 4827-37.
FLYNN, W. T. & SAIF, L. J. 1988. Serial propagation of porcine enteric calicivirus-like virus in primary porcine kidney cell cultures. *J Clin Microbiol,* 26**,** 206-12.
FLYNN, W. T., SAIF, L. J. & MOORHEAD, P. D. 1988. Pathogenesis of porcine enteric calicivirus-like virus in four-day-old gnotobiotic pigs. *Am J Vet Res,* 49**,** 819-25.
FORRESTER, N. L., TROUT, R. C. & GOULD, E. A. 2007. Benign circulation of rabbit haemorrhagic disease virus on Lambay Island, Eire. *Virology,* 358**,** 18-22.
FRANCK, K. T., LISBY, M., FONAGER, J., SCHULTZ, A. C., BOTTIGER, B., VILLIF, A., ABSALONSEN, H. & ETHELBERG, S. 2015. Sources of Calicivirus

contamination in foodborne outbreaks in Denmark, 2005-2011--the role of the asymptomatic food handler. *J Infect Dis,* 211**,** 563-70.
FU, L., NIU, B., ZHU, Z., WU, S. & LI, W. 2012. CD-HIT: accelerated for clustering the next-generation sequencing data. *Bioinformatics,* 28**,** 3150-2.
FUKUSHI, S., KOJIMA, S., TAKAI, R., HOSHINO, F. B., OKA, T., TAKEDA, N., KATAYAMA, K. & KAGEYAMA, T. 2004. Poly(A)- and primer-independent RNA polymerase of Norovirus. *J Virol,* 78**,** 3889-96.
FULLERTON, S. W., BLASCHKE, M., COUTARD, B., GEBHARDT, J., GORBALENYA, A., CANARD, B., TUCKER, P. A. & ROHAYEM, J. 2007. Structural and functional characterization of sapovirus RNA-dependent RNA polymerase. *J Virol,* 81**,** 1858-71.
FURIC, L., RONG, L., LARSSON, O., KOUMAKPAYI, I. H., YOSHIDA, K., BRUESCHKE, A., PETROULAKIS, E., ROBICHAUD, N., POLLAK, M., GABOURY, L. A., PANDOLFI, P. P., SAAD, F. & SONENBERG, N. 2010. eIF4E phosphorylation promotes tumorigenesis and is associated with prostate cancer progression. *Proc Natl Acad Sci U S A,* 107**,** 14134-9.
FURMAN, L. M., MAATY, W. S., PETERSEN, L. K., ETTAYEBI, K., HARDY, M. E. & BOTHNER, B. 2009. Cysteine protease activation and apoptosis in Murine norovirus infection. *Virol J,* 6**,** 139.
GALASITI KANKANAMALAGE, A. C., KIM, Y., RATHNAYAKE, A. D., ALLISTON, K. R., BUTLER, M. M., CARDINALE, S. C., BOWLIN, T. L., GROUTAS, W. C. & CHANG, K. O. 2017a. Design, Synthesis, and Evaluation of Novel Prodrugs of Transition State Inhibitors of Norovirus 3CL Protease. *J Med Chem*.
GALASITI KANKANAMALAGE, A. C., KIM, Y., RATHNAYAKE, A. D., DAMALANKA, V. C., WEERAWARNA, P. M., DOYLE, S. T., ALSOUDI, A. F., DISSANAYAKE, D. M., LUSHINGTON, G. H., MEHZABEEN, N., BATTAILE, K. P., LOVELL, S., CHANG, K. O. & GROUTAS, W. C. 2017b. Structure-based exploration and exploitation of the S4 subsite of norovirus 3CL protease in the design of potent and permeable inhibitors. *Eur J Med Chem,* 126**,** 502-516.
GALASITI KANKANAMALAGE, A. C., KIM, Y., WEERAWARNA, P. M., UY, R. A., DAMALANKA, V. C., MANDADAPU, S. R., ALLISTON, K. R., MEHZABEEN, N., BATTAILE, K. P., LOVELL, S., CHANG, K. O. & GROUTAS, W. C. 2015. Structure-guided design and optimization of dipeptidyl inhibitors of norovirus 3CL protease. Structure-activity relationships and biochemical, X-ray crystallographic, cell-based, and in vivo studies. *J Med Chem,* 58**,** 3144-55.
GALLIMORE, C. I., LEWIS, D., TAYLOR, C., CANT, A., GENNERY, A. & GRAY, J. J. 2004. Chronic excretion of a norovirus in a child with cartilage hair hypoplasia (CHH). *J Clin Virol,* 30**,** 196-204.
GANDHI, K. M., MANDRELL, R. E. & TIAN, P. 2010. Binding of virus-like particles of Norwalk virus to romaine lettuce veins. *Appl Environ Microbiol,* 76**,** 7997-8003.
GARY, G. W., ANDERSON, L. J., KESWICK, B. H., JOHNSON, P. C., DUPONT, H. L., STINE, S. E. & BARTLETT, A. V. 1987. Norwalk virus antigen and antibody response in an adult volunteer study. *J Clin Microbiol,* 25**,** 2001-3.
GEISSLER, K., PARRISH, C. R., SCHNEIDER, K. & TRUYEN, U. 1999. Feline calicivirus capsid protein expression and self-assembly in cultured feline cells. *Vet Microbiol,* 69**,** 63-6.
GERONDOPOULOS, A., JACKSON, T., MONAGHAN, P., DOYLE, N. & ROBERTS, L. O. 2010. Murine norovirus-1 cell entry is mediated through a non-clathrin-, non-caveolae-, dynamin- and cholesterol-dependent pathway. *J Gen Virol,* 91**,** 1428-38.

GITLIN, L., BENOIT, L., SONG, C., CELLA, M., GILFILLAN, S., HOLTZMAN, M. J. & COLONNA, M. 2010. Melanoma differentiation-associated gene 5 (MDA5) is involved in the innate immune response to Paramyxoviridae infection in vivo. *PLoS Pathog,* 6**,** e1000734.

GLASS, P. J., WHITE, L. J., BALL, J. M., LEPARC-GOFFART, I., HARDY, M. E. & ESTES, M. K. 2000. Norwalk virus open reading frame 3 encodes a minor structural protein. *J Virol,* 74**,** 6581-91.

GODOY, P., ALSEDA, M., BARTOLOME, R., CLAVERIA, D., MODOL, I., BACH, P., MIRADA, G. & DOMINGUEZ, A. 2016. Norovirus gastroenteritis outbreak transmitted by food and vomit in a high school. *Epidemiol Infect,* 144**,** 1951-8.

GONZALEZ-HERNANDEZ, M. B., LIU, T., PAYNE, H. C., STENCEL-BAERENWALD, J. E., IKIZLER, M., YAGITA, H., DERMODY, T. S., WILLIAMS, I. R. & WOBUS, C. E. 2014. Efficient norovirus and reovirus replication in the mouse intestine requires microfold (M) cells. *J Virol,* 88**,** 6934-43.

GOODFELLOW, I., CHAUDHRY, Y., GIOLDASI, I., GERONDOPOULOS, A., NATONI, A., LABRIE, L., LALIBERTE, J. F. & ROBERTS, L. 2005. Calicivirus translation initiation requires an interaction between VPg and eIF 4 E. *EMBO Rep,* 6**,** 968-72.

GRAY, J. J., CUNLIFFE, C., BALL, J., GRAHAM, D. Y., DESSELBERGER, U. & ESTES, M. K. 1994. Detection of immunoglobulin M (IgM), IgA, and IgG Norwalk virus-specific antibodies by indirect enzyme-linked immunosorbent assay with baculovirus-expressed Norwalk virus capsid antigen in adult volunteers challenged with Norwalk virus. *J Clin Microbiol,* 32**,** 3059-63.

GREEN, K. Y., ANDO, T., BALAYAN, M. S., BERKE, T., CLARKE, I. N., ESTES, M. K., MATSON, D. O., NAKATA, S., NEILL, J. D., STUDDERT, M. J. & THIEL, H. J. 2000. Taxonomy of the caliciviruses. *J Infect Dis,* 181 Suppl 2**,** S322-30.

GREEN, K. Y., KAPIKIAN, A. Z., VALDESUSO, J., SOSNOVTSEV, S., TREANOR, J. J. & LEW, J. F. 1997. Expression and self-assembly of recombinant capsid protein from the antigenically distinct Hawaii human calicivirus. *J Clin Microbiol,* 35**,** 1909-14.

GREEN, K. Y., MORY, A., FOGG, M. H., WEISBERG, A., BELLIOT, G., WAGNER, M., MITRA, T., EHRENFELD, E., CAMERON, C. E. & SOSNOVTSEV, S. V. 2002. Isolation of enzymatically active replication complexes from feline calicivirus-infected cells. *J Virol,* 76**,** 8582-95.

GUIX, S., ASANAKA, M., KATAYAMA, K., CRAWFORD, S. E., NEILL, F. H., ATMAR, R. L. & ESTES, M. K. 2007. Norwalk virus RNA is infectious in mammalian cells. *J Virol,* 81**,** 12238-48.

GUO, M., QIAN, Y., CHANG, K. O. & SAIF, L. J. 2001. Expression and self-assembly in baculovirus of porcine enteric calicivirus capsids into virus-like particles and their use in an enzyme-linked immunosorbent assay for antibody detection in swine. *J Clin Microbiol,* 39**,** 1487-93.

GUTIERREZ-ESCOLANO, A. L., BRITO, Z. U., DEL ANGEL, R. M. & JIANG, X. 2000. Interaction of cellular proteins with the 5' end of Norwalk virus genomic RNA. *J Virol,* 74**,** 8558-62.

GUTIERREZ-ESCOLANO, A. L., VAZQUEZ-OCHOA, M., ESCOBAR-HERRERA, J. & HERNANDEZ-ACOSTA, J. 2003. La, PTB, and PAB proteins bind to the 3(') untranslated region of Norwalk virus genomic RNA. *Biochem Biophys Res Commun,* 311**,** 759-66.

HADI, C. M., GOBA, A., KHAN, S. H., BANGURA, J., SANKOH, M., KOROMA, S., JUANA, B., BAH, A., COULIBALY, M. & BAUSCH, D. G. 2010. Ribavirin for

Lassa fever postexposure prophylaxis. *Emerg Infect Dis,* 16**,** 2009-11.
HAGA, K., FUJIMOTO, A., TAKAI-TODAKA, R., MIKI, M., DOAN, Y. H., MURAKAMI, K., YOKOYAMA, M., MURATA, K., NAKANISHI, A. & KATAYAMA, K. 2016. Functional receptor molecules CD300lf and CD300ld within the CD300 family enable murine noroviruses to infect cells. *Proc Natl Acad Sci U S A,* 113**,** E6248-E6255.
HALL, A. J., LOPMAN, B. A., PAYNE, D. C., PATEL, M. M., GASTANADUY, P. A., VINJE, J. & PARASHAR, U. D. 2013. Norovirus disease in the United States. *Emerg Infect Dis,* 19**,** 1198-205.
HAN, K. R., CHOI, Y., MIN, B. S., JEONG, H., CHEON, D., KIM, J., JEE, Y., SHIN, S. & YANG, J. M. 2010. Murine norovirus-1 3Dpol exhibits RNA-dependent RNA polymerase activity and nucleotidylylates on Tyr of the VPg. *J Gen Virol,* 91**,** 1713-22.
HAN, L., KITOVA, E. N., TAN, M., JIANG, X., PLUVINAGE, B., BORASTON, A. B. & KLASSEN, J. S. 2015. Affinities of human histo-blood group antigens for norovirus capsid protein complexes. *Glycobiology,* 25**,** 170-80.
HAN, M. G., WANG, Q., SMILEY, J. R., CHANG, K. O. & SAIF, L. J. 2005. Self-assembly of the recombinant capsid protein of a bovine norovirus (BoNV) into virus-like particles and evaluation of cross-reactivity of BoNV with human noroviruses. *J Clin Microbiol,* 43**,** 778-85.
HARRINGTON, P. R., LINDESMITH, L., YOUNT, B., MOE, C. L. & BARIC, R. S. 2002. Binding of Norwalk virus-like particles to ABH histo-blood group antigens is blocked by antisera from infected human volunteers or experimentally vaccinated mice. *J Virol,* 76**,** 12335-43.
HARRIS, J. P., EDMUNDS, W. J., PEBODY, R., BROWN, D. W. & LOPMAN, B. A. 2008. Deaths from norovirus among the elderly, England and Wales. *Emerg Infect Dis,* 14**,** 1546-52.
HARRIS, J. P., ITURRIZA-GOMARA, M. & O'BRIEN, S. J. 2017. Re-assessing the total burden of norovirus circulating in the United Kingdom population. *Vaccine,* 35**,** 853-855.
HASING, M. E., HAZES, B., LEE, B. E., PREIKSAITIS, J. K. & PANG, X. L. 2016. A next generation sequencing-based method to study the intra-host genetic diversity of norovirus in patients with acute and chronic infection. *BMC Genomics,* 17**,** 480.
HERBERT, T. P., BRIERLEY, I. & BROWN, T. D. 1996. Detection of the ORF3 polypeptide of feline calicivirus in infected cells and evidence for its expression from a single, functionally bicistronic, subgenomic mRNA. *J Gen Virol,* 77 (Pt 1)**,** 123-7.
HERBERT, T. P., BRIERLEY, I. & BROWN, T. D. 1997. Identification of a protein linked to the genomic and subgenomic mRNAs of feline calicivirus and its role in translation. *J Gen Virol,* 78 (Pt 5)**,** 1033-40.
HERBST-KRALOVETZ, M. M., RADTKE, A. L., LAY, M. K., HJELM, B. E., BOLICK, A. N., SARKER, S. S., ATMAR, R. L., KINGSLEY, D. H., ARNTZEN, C. J., ESTES, M. K. & NICKERSON, C. A. 2013. Lack of norovirus replication and histo-blood group antigen expression in 3-dimensional intestinal epithelial cells. *Emerg Infect Dis,* 19**,** 431-8.
HERDY, B., JARAMILLO, M., SVITKIN, Y. V., ROSENFELD, A. B., KOBAYASHI, M., WALSH, D., ALAIN, T., SEAN, P., ROBICHAUD, N., TOPISIROVIC, I., FURIC, L., DOWLING, R. J., SYLVESTRE, A., RONG, L., COLINA, R., COSTA-MATTIOLI, M., FRITZ, J. H., OLIVIER, M., BROWN, E., MOHR, I. & SONENBERG, N. 2012. Translational control of the activation of transcription

factor NF-kappaB and production of type I interferon by phosphorylation of the translation factor eIF4E. *Nat Immunol,* 13**,** 543-50.
HERNANDEZ, B. A., SANDOVAL-JAIME, C., SOSNOVTSEV, S. V., GREEN, K. Y. & GUTIERREZ-ESCOLANO, A. L. 2016. Nucleolin promotes in vitro translation of feline calicivirus genomic RNA. *Virology,* 489**,** 51-62.
HERNANDEZ, P. P., MAHLAKOIV, T., YANG, I., SCHWIERZECK, V., NGUYEN, N., GUENDEL, F., GRONKE, K., RYFFEL, B., HOELSCHER, C., DUMOUTIER, L., RENAULD, J. C., SUERBAUM, S., STAEHELI, P. & DIEFENBACH, A. 2015. Interferon-lambda and interleukin 22 act synergistically for the induction of interferon-stimulated genes and control of rotavirus infection. *Nat Immunol,* 16**,** 698-707.
HEROD, M. R., SALIM, O., SKILTON, R. J., PRINCE, C. A., WARD, V. K., LAMBDEN, P. R. & CLARKE, I. N. 2014. Expression of the murine norovirus (MNV) ORF1 polyprotein is sufficient to induce apoptosis in a virus-free cell model. *PLoS One,* 9**,** e90679.
HILTON, L., MOGANERADJ, K., ZHANG, G., CHEN, Y. H., RANDALL, R. E., MCCAULEY, J. W. & GOODBOURN, S. 2006. The NPro product of bovine viral diarrhea virus inhibits DNA binding by interferon regulatory factor 3 and targets it for proteasomal degradation. *J Virol,* 80**,** 11723-32.
HOA TRAN, T. N., TRAINOR, E., NAKAGOMI, T., CUNLIFFE, N. A. & NAKAGOMI, O. 2013. Molecular epidemiology of noroviruses associated with acute sporadic gastroenteritis in children: global distribution of genogroups, genotypes and GII.4 variants. *J Clin Virol,* 56**,** 185-93.
HOGBOM, M., JAGER, K., ROBEL, I., UNGE, T. & ROHAYEM, J. 2009. The active form of the norovirus RNA-dependent RNA polymerase is a homodimer with cooperative activity. *J Gen Virol,* 90**,** 281-91.
HOSMILLO, M., SORGELOOS, F., HIRAIDE, R., LU, J., GOODFELLOW, I. & CHO, K. O. 2015. Porcine sapovirus replication is restricted by the type I interferon response in cell culture. *J Gen Virol,* 96**,** 74-84.
HSU, C. C., RILEY, L. K. & LIVINGSTON, R. S. 2007. Molecular characterization of three novel murine noroviruses. *Virus Genes,* 34**,** 147-55.
HSU, C. C., RILEY, L. K., WILLS, H. M. & LIVINGSTON, R. S. 2006. Persistent infection with and serologic cross-reactivity of three novel murine noroviruses. *Comp Med,* 56**,** 247-51.
HU, M. H., LIN, K. L., WU, C. T., CHEN, S. Y. & HUANG, G. S. 2017. Clinical Characteristics and Risk Factors for Seizures Associated With Norovirus Gastroenteritis in Childhood. *J Child Neurol***,** 883073817707302.
HUANG, P., FARKAS, T., MARIONNEAU, S., ZHONG, W., RUVOEN-CLOUET, N., MORROW, A. L., ALTAYE, M., PICKERING, L. K., NEWBURG, D. S., LEPENDU, J. & JIANG, X. 2003. Noroviruses bind to human ABO, Lewis, and secretor histo-blood group antigens: identification of 4 distinct strain-specific patterns. *J Infect Dis,* 188**,** 19-31.
HUANG, Z., ELKIN, G., MALONEY, B. J., BEUHNER, N., ARNTZEN, C. J., THANAVALA, Y. & MASON, H. S. 2005. Virus-like particle expression and assembly in plants: hepatitis B and Norwalk viruses. *Vaccine,* 23**,** 1851-8.
HUDSON, J. B., SHARMA, M. & PETRIC, M. 2007. Inactivation of Norovirus by ozone gas in conditions relevant to healthcare. *J Hosp Infect,* 66**,** 40-5.
HUTSON, A. M., AIRAUD, F., LEPENDU, J., ESTES, M. K. & ATMAR, R. L. 2005. Norwalk virus infection associates with secretor status genotyped from sera. *J Med Virol,* 77**,** 116-20.
HUTSON, A. M., ATMAR, R. L. & ESTES, M. K. 2004. Norovirus disease: changing

epidemiology and host susceptibility factors. *Trends Microbiol,* 12**,** 279-87.
HUTSON, A. M., ATMAR, R. L., GRAHAM, D. Y. & ESTES, M. K. 2002. Norwalk virus infection and disease is associated with ABO histo-blood group type. *J Infect Dis,* 185**,** 1335-7.
HUTSON, A. M., ATMAR, R. L., MARCUS, D. M. & ESTES, M. K. 2003. Norwalk virus-like particle hemagglutination by binding to h histo-blood group antigens. *J Virol,* 77**,** 405-15.
HWANG, S., ALHATLANI, B., ARIAS, A., CADDY, S. L., CHRISTODOULOU, C., CUNHA, J. B., EMMOTT, E., GONZALEZ-HERNANDEZ, M., KOLAWOLE, A., LU, J., RIPPINGER, C., SORGELOOS, F., THORNE, L., VASHIST, S., GOODFELLOW, I. & WOBUS, C. E. 2014. Murine norovirus: propagation, quantification, and genetic manipulation. *Curr Protoc Microbiol,* 33**,** 15K 2 1-61.
HYDE, J. L., GILLESPIE, L. K. & MACKENZIE, J. M. 2012. Mouse norovirus 1 utilizes the cytoskeleton network to establish localization of the replication complex proximal to the microtubule organizing center. *J Virol,* 86**,** 4110-22.
HYDE, J. L. & MACKENZIE, J. M. 2010. Subcellular localization of the MNV-1 ORF1 proteins and their potential roles in the formation of the MNV-1 replication complex. *Virology,* 406**,** 138-48.
INTERNATIONAL COMMITTEE ON TAXONOMY OF VIRUSES., KING, A. M. Q. & INTERNATIONAL UNION OF MICROBIOLOGICAL SOCIETIES. VIROLOGY DIVISION. 2012. *Virus taxonomy : classification and nomenclature of viruses : ninth report of the International Committee on Taxonomy of Viruses,* Amsterdam, Elsevier/Academic Press.
IVASHKIV, L. B. & DONLIN, L. T. 2014. Regulation of type I interferon responses. *Nat Rev Immunol,* 14**,** 36-49.
JIANG, B., MCCLURE, H. M., FANKHAUSER, R. L., MONROE, S. S. & GLASS, R. I. 2004. Prevalence of rotavirus and norovirus antibodies in non-human primates. *J Med Primatol,* 33**,** 30-3.
JIANG, X., MATSON, D. O., RUIZ-PALACIOS, G. M., HU, J., TREANOR, J. & PICKERING, L. K. 1995. Expression, self-assembly, and antigenicity of a snow mountain agent-like calicivirus capsid protein. *J Clin Microbiol,* 33**,** 1452-5.
JIANG, X., WANG, M., GRAHAM, D. Y. & ESTES, M. K. 1992. Expression, self-assembly, and antigenicity of the Norwalk virus capsid protein. *J Virol,* 66**,** 6527-32.
JIN, Z., TUCKER, K., LIN, X., KAO, C. C., SHAW, K., TAN, H., SYMONS, J., BEHERA, I., RAJWANSHI, V. K., DYATKINA, N., WANG, G., BEIGELMAN, L. & DEVAL, J. 2015. Biochemical Evaluation of the Inhibition Properties of Favipiravir and 2'-C-Methyl-Cytidine Triphosphates against Human and Mouse Norovirus RNA Polymerases. *Antimicrob Agents Chemother,* 59**,** 7504-16.
JOHNSON, M., ZARETSKAYA, I., RAYTSELIS, Y., MEREZHUK, Y., MCGINNIS, S. & MADDEN, T. L. 2008. NCBI BLAST: a better web interface. *Nucleic Acids Res,* 36**,** W5-9.
JOHNSON, P. C., MATHEWSON, J. J., DUPONT, H. L. & GREENBERG, H. B. 1990. Multiple-challenge study of host susceptibility to Norwalk gastroenteritis in US adults. *J Infect Dis,* 161**,** 18-21.
JONES, M. K., GRAU, K. R., COSTANTINI, V., KOLAWOLE, A. O., DE GRAAF, M., FREIDEN, P., GRAVES, C. L., KOOPMANS, M., WALLET, S. M., TIBBETTS, S. A., SCHULTZ-CHERRY, S., WOBUS, C. E., VINJE, J. & KARST, S. M. 2015. Human norovirus culture in B cells. *Nat Protoc,* 10**,** 1939-47.

JONES, M. K., WATANABE, M., ZHU, S., GRAVES, C. L., KEYES, L. R., GRAU, K. R., GONZALEZ-HERNANDEZ, M. B., IOVINE, N. M., WOBUS, C. E., VINJE, J., TIBBETTS, S. A., WALLET, S. M. & KARST, S. M. 2014. Enteric bacteria promote human and mouse norovirus infection of B cells. *Science,* 346**,** 755-9.
JOUBERT, P. E., STAPLEFORD, K., GUIVEL-BENHASSINE, F., VIGNUZZI, M., SCHWARTZ, O. & ALBERT, M. L. 2015. Inhibition of mTORC1 Enhances the Translation of Chikungunya Proteins via the Activation of the MnK/eIF4E Pathway. *PLoS Pathog,* 11**,** e1005091.
JULIAN, T. R., BAUGHER, J. D., RIPPINGER, C. M., PINEKENSTEIN, R., KOLAWOLE, A. O., MEHOKE, T. S., WOBUS, C. E., FELDMAN, A. B., PINEDA, F. J. & SCHWAB, K. J. 2016. Murine norovirus (MNV-1) exposure in vitro to the purine nucleoside analog Ribavirin increases quasispecies diversity. *Virus Res,* 211**,** 165-73.
JUNG, K., WANG, Q., KIM, Y., SCHEUER, K., ZHANG, Z., SHEN, Q., CHANG, K. O. & SAIF, L. J. 2012. The effects of simvastatin or interferon-alpha on infectivity of human norovirus using a gnotobiotic pig model for the study of antivirals. *PLoS One,* 7**,** e41619.
JURGENS, P. T., ALLEN, L. A., AMBARDEKAR, A. V. & MCILVENNAN, C. K. 2017. Chronic Norovirus Infections in Cardiac Transplant Patients. *Prog Transplant,* 27**,** 69-72.
KAGEYAMA, T., KOJIMA, S., SHINOHARA, M., UCHIDA, K., FUKUSHI, S., HOSHINO, F. B., TAKEDA, N. & KATAYAMA, K. 2003. Broadly reactive and highly sensitive assay for Norwalk-like viruses based on real-time quantitative reverse transcription-PCR. *J Clin Microbiol,* 41**,** 1548-57.
KAHAN, S. M., LIU, G., REINHARD, M. K., HSU, C. C., LIVINGSTON, R. S. & KARST, S. M. 2011. Comparative murine norovirus studies reveal a lack of correlation between intestinal virus titers and enteric pathology. *Virology,* 421**,** 202-10.
KAHVEJIAN, A., SVITKIN, Y. V., SUKARIEH, R., M'BOUTCHOU, M. N. & SONENBERG, N. 2005. Mammalian poly(A)-binding protein is a eukaryotic translation initiation factor, which acts via multiple mechanisms. *Genes Dev,* 19**,** 104-13.
KAO, C. C., SINGH, P. & ECKER, D. J. 2001. De novo initiation of viral RNA-dependent RNA synthesis. *Virology,* 287**,** 251-60.
KAPIKIAN, A. Z., WYATT, R. G., DOLIN, R., THORNHILL, T. S., KALICA, A. R. & CHANOCK, R. M. 1972. Visualization by immune electron microscopy of a 27-nm particle associated with acute infectious nonbacterial gastroenteritis. *J Virol,* 10**,** 1075-81.
KARAKASILIOTIS, I., CHAUDHRY, Y., ROBERTS, L. O. & GOODFELLOW, I. G. 2006. Feline calicivirus replication: requirement for polypyrimidine tract-binding protein is temperature-dependent. *J Gen Virol,* 87**,** 3339-47.
KARAKASILIOTIS, I., VASHIST, S., BAILEY, D., ABENTE, E. J., GREEN, K. Y., ROBERTS, L. O., SOSNOVTSEV, S. V. & GOODFELLOW, I. G. 2010. Polypyrimidine tract binding protein functions as a negative regulator of feline calicivirus translation. *PLoS One,* 5**,** e9562.
KARANDIKAR, U. C., CRAWFORD, S. E., AJAMI, N. J., MURAKAMI, K., KOU, B., ETTAYEBI, K., PAPANICOLAOU, G. A., JONGWUTIWES, U., PERALES, M. A., SHIA, J., MERCER, D., FINEGOLD, M. J., VINJE, J., ATMAR, R. L. & ESTES, M. K. 2016. Detection of human norovirus in intestinal biopsies from immunocompromised transplant patients. *J Gen Virol,* 97**,** 2291-300.
KARST, S. M., WOBUS, C. E., LAY, M., DAVIDSON, J. & VIRGIN, H. W. T. 2003.

STAT1-dependent innate immunity to a Norwalk-like virus. *Science,* 299**,** 1575-8.

KATAYAMA, K., MURAKAMI, K., SHARP, T. M., GUIX, S., OKA, T., TAKAI-TODAKA, R., NAKANISHI, A., CRAWFORD, S. E., ATMAR, R. L. & ESTES, M. K. 2014. Plasmid-based human norovirus reverse genetics system produces reporter-tagged progeny virus containing infectious genomic RNA. *Proc Natl Acad Sci U S A,* 111**,** E4043-52.

KATPALLY, U., VOSS, N. R., CAVAZZA, T., TAUBE, S., RUBIN, J. R., YOUNG, V. L., STUCKEY, J., WARD, V. K., VIRGIN, H. W. T., WOBUS, C. E. & SMITH, T. J. 2010. High-resolution cryo-electron microscopy structures of murine norovirus 1 and rabbit hemorrhagic disease virus reveal marked flexibility in the receptor binding domains. *J Virol,* 84**,** 5836-41.

KIM, D. S., HOSMILLO, M., ALFAJARO, M. M., KIM, J. Y., PARK, J. G., SON, K. Y., RYU, E. H., SORGELOOS, F., KWON, H. J., PARK, S. J., LEE, W. S., CHO, D., KWON, J., CHOI, J. S., KANG, M. I., GOODFELLOW, I. & CHO, K. O. 2014. Both alpha2,3- and alpha2,6-linked sialic acids on O-linked glycoproteins act as functional receptors for porcine Sapovirus. *PLoS Pathog,* 10**,** e1004172.

KIM, Y., SHIVANNA, V., NARAYANAN, S., PRIOR, A. M., WEERASEKARA, S., HUA, D. H., KANKANAMALAGE, A. C., GROUTAS, W. C. & CHANG, K. O. 2015. Broad-spectrum inhibitors against 3C-like proteases of feline coronaviruses and feline caliciviruses. *J Virol,* 89**,** 4942-50.

KIRBY, A. E., STREBY, A. & MOE, C. L. 2016. Vomiting as a Symptom and Transmission Risk in Norovirus Illness: Evidence from Human Challenge Studies. *PLoS One,* 11**,** e0143759.

KITAJIMA, M., OKA, T., TAKAGI, H., TOHYA, Y., KATAYAMA, H., TAKEDA, N. & KATAYAMA, K. 2010. Development and application of a broadly reactive real-time reverse transcription-PCR assay for detection of murine noroviruses. *J Virol Methods,* 169**,** 269-73.

KITAJIMA, M., OKA, T., TOHYA, Y., KATAYAMA, H., TAKEDA, N. & KATAYAMA, K. 2009. Development of a broadly reactive nested reverse transcription-PCR assay to detect murine noroviruses, and investigation of the prevalence of murine noroviruses in laboratory mice in Japan. *Microbiol Immunol,* 53**,** 531-4.

KOCHER, J., BUI, T., GIRI-RACHMAN, E., WEN, K., LI, G., YANG, X., LIU, F., TAN, M., XIA, M., ZHONG, W., JIANG, X. & YUAN, L. 2014. Intranasal P particle vaccine provided partial cross-variant protection against human GII.4 norovirus diarrhea in gnotobiotic pigs. *J Virol,* 88**,** 9728-43.

KOJIMA, S., KAGEYAMA, T., FUKUSHI, S., HOSHINO, F. B., SHINOHARA, M., UCHIDA, K., NATORI, K., TAKEDA, N. & KATAYAMA, K. 2002. Genogroup-specific PCR primers for detection of Norwalk-like viruses. *J Virol Methods,* 100**,** 107-14.

KOOPMAN, J. S., ECKERT, E. A., GREENBERG, H. B., STROHM, B. C., ISAACSON, R. E. & MONTO, A. S. 1982. Norwalk virus enteric illness acquired by swimming exposure. *Am J Epidemiol,* 115**,** 173-7.

KORNEEVA, N. L., SONG, A., GRAM, H., EDENS, M. A. & RHOADS, R. E. 2016. Inhibition of Mitogen-activated Protein Kinase (MAPK)-interacting Kinase (MNK) Preferentially Affects Translation of mRNAs Containing Both a 5'-Terminal Cap and Hairpin. *J Biol Chem,* 291**,** 3455-67.

KREUTZ, L. C., SEAL, B. S. & MENGELING, W. L. 1994. Early interaction of feline calicivirus with cells in culture. *Arch Virol,* 136**,** 19-34.

KRONEMAN, A., VEGA, E., VENNEMA, H., VINJE, J., WHITE, P. A., HANSMAN,

G., GREEN, K., MARTELLA, V., KATAYAMA, K. & KOOPMANS, M. 2013. Proposal for a unified norovirus nomenclature and genotyping. *Arch Virol,* 158**,** 2059-68.
KUTNER, R. H., ZHANG, X. Y. & REISER, J. 2009. Production, concentration and titration of pseudotyped HIV-1-based lentiviral vectors. *Nat Protoc,* 4**,** 495-505.
KUUSI, M., NUORTI, J. P., MAUNULA, L., MINH TRAN, N. N., RATIA, M., KARLSSON, J. & VON BONSDORFF, C. H. 2002. A prolonged outbreak of Norwalk-like calicivirus (NLV) gastroenteritis in a rehabilitation centre due to environmental contamination. *Epidemiol Infect,* 129**,** 133-8.
L'HOMME, Y., SANSREGRET, R., PLANTE-FORTIER, E., LAMONTAGNE, A. M., OUARDANI, M., LACROIX, G. & SIMARD, C. 2009. Genomic characterization of swine caliciviruses representing a new genus of Caliciviridae. *Virus Genes,* 39**,** 66-75.
LAMBREGTS, M. M., ALLEMAN, M. A., RUYS, G. J. & GROENEVELD, P. H. 2010. [Chronic norovirus infection in an immunocompromised patient]. *Ned Tijdschr Geneeskd,* 154**,** A1067.
LAURENT, S., KUT, E., REMY-DELAUNAY, S. & RASSCHAERT, D. 2002. Folding of the rabbit hemorrhagic disease virus capsid protein and delineation of N-terminal domains dispensable for assembly. *Arch Virol,* 147**,** 1559-71.
LAURING, A. S., JONES, J. O. & ANDINO, R. 2010. Rationalizing the development of live attenuated virus vaccines. *Nat Biotechnol,* 28**,** 573-9.
LAY, M. K., ATMAR, R. L., GUIX, S., BHARADWAJ, U., HE, H., NEILL, F. H., SASTRY, K. J., YAO, Q. & ESTES, M. K. 2010. Norwalk virus does not replicate in human macrophages or dendritic cells derived from the peripheral blood of susceptible humans. *Virology,* 406**,** 1-11.
LAZEAR, H. M., LANCASTER, A., WILKINS, C., SUTHAR, M. S., HUANG, A., VICK, S. C., CLEPPER, L., THACKRAY, L., BRASSIL, M. M., VIRGIN, H. W., NIKOLICH-ZUGICH, J., MOSES, A. V., GALE, M., JR., FRUH, K. & DIAMOND, M. S. 2013. IRF-3, IRF-5, and IRF-7 coordinately regulate the type I IFN response in myeloid dendritic cells downstream of MAVS signaling. *PLoS Pathog,* 9**,** e1003118.
LE GUYADER, F., LOISY, F., ATMAR, R. L., HUTSON, A. M., ESTES, M. K., RUVOEN-CLOUET, N., POMMEPUY, M. & LE PENDU, J. 2006. Norwalk virus-specific binding to oyster digestive tissues. *Emerg Infect Dis,* 12**,** 931-6.
LE PENDU, J., RUVOEN-CLOUET, N., KINDBERG, E. & SVENSSON, L. 2006. Mendelian resistance to human norovirus infections. *Semin Immunol,* 18**,** 375-86.
LEE, B. E., PANG, X. L., ROBINSON, J. L., BIGAM, D., MONROE, S. S. & PREIKSAITIS, J. K. 2008. Chronic norovirus and adenovirus infection in a solid organ transplant recipient. *Pediatr Infect Dis J,* 27**,** 360-2.
LEE, J. H., ALAM, I., HAN, K. R., CHO, S., SHIN, S., KANG, S., YANG, J. M. & KIM, K. H. 2011. Crystal structures of murine norovirus-1 RNA-dependent RNA polymerase. *J Gen Virol,* 92**,** 1607-16.
LEE, S. H., STARKEY, P. M. & GORDON, S. 1985. Quantitative analysis of total macrophage content in adult mouse tissues. Immunochemical studies with monoclonal antibody F4/80. *J Exp Med,* 161**,** 475-89.
LEEN, E. N., KWOK, K. Y., BIRTLEY, J. R., SIMPSON, P. J., SUBBA-REDDY, C. V., CHAUDHRY, Y., SOSNOVTSEV, S. V., GREEN, K. Y., PRATER, S. N., TONG, M., YOUNG, J. C., CHUNG, L. M., MARCHANT, J., ROBERTS, L. O., KAO, C. C., MATTHEWS, S., GOODFELLOW, I. G. & CURRY, S. 2013. Structures of the compact helical core domains of feline calicivirus and murine

norovirus VPg proteins. *J Virol,* 87**,** 5318-30.
LEEN, E. N., SORGELOOS, F., CORREIA, S., CHAUDHRY, Y., CANNAC, F., PASTORE, C., XU, Y., GRAHAM, S. C., MATTHEWS, S. J., GOODFELLOW, I. G. & CURRY, S. 2016. A Conserved Interaction between a C-Terminal Motif in Norovirus VPg and the HEAT-1 Domain of eIF4G Is Essential for Translation Initiation. *PLoS Pathog,* 12**,** e1005379.
LEI, S., RYU, J., WEN, K., TWITCHELL, E., BUI, T., RAMESH, A., WEISS, M., LI, G., SAMUEL, H., CLARK-DEENER, S., JIANG, X., LEE, K. & YUAN, L. 2016a. Increased and prolonged human norovirus infection in RAG2/IL2RG deficient gnotobiotic pigs with severe combined immunodeficiency. *Sci Rep,* 6**,** 25222.
LEI, S., SAMUEL, H., TWITCHELL, E., BUI, T., RAMESH, A., WEN, K., WEISS, M., LI, G., YANG, X., JIANG, X. & YUAN, L. 2016b. Enterobacter cloacae inhibits human norovirus infectivity in gnotobiotic pigs. *Sci Rep,* 6**,** 25017.
LEMES, L. G., CORREA, T. S., FIACCADORI, F. S., CARDOSO, D., ARANTES ADE, M., SOUZA, K. M. & SOUZA, M. 2014. Prospective study on Norovirus infection among allogeneic stem cell transplant recipients: prolonged viral excretion and viral RNA in the blood. *J Clin Virol,* 61**,** 329-33.
LEONARD, S., VIEL, C., BEAUCHEMIN, C., DAIGNEAULT, N., FORTIN, M. G. & LALIBERTE, J. F. 2004. Interaction of VPg-Pro of turnip mosaic virus with the translation initiation factor 4E and the poly(A)-binding protein in planta. *J Gen Virol,* 85**,** 1055-63.
LEUNG, W. K., CHAN, P. K., LEE, N. L. & SUNG, J. J. 2010. Development of an in vitro cell culture model for human noroviruses and its clinical application. *Hong Kong Med J,* 16**,** 18-21.
LIBERMANN, T. A. & BALTIMORE, D. 1990. Activation of interleukin-6 gene expression through the NF-kappa B transcription factor. *Mol Cell Biol,* 10**,** 2327-34.
LIN, X., THORNE, L., JIN, Z., HAMMAD, L. A., LI, S., DEVAL, J., GOODFELLOW, I. G. & KAO, C. C. 2015. Subgenomic promoter recognition by the norovirus RNA-dependent RNA polymerases. *Nucleic Acids Res,* 43**,** 446-60.
LINDESMITH, L., MOE, C., LEPENDU, J., FRELINGER, J. A., TREANOR, J. & BARIC, R. S. 2005. Cellular and humoral immunity following Snow Mountain virus challenge. *J Virol,* 79**,** 2900-9.
LINDESMITH, L., MOE, C., MARIONNEAU, S., RUVOEN, N., JIANG, X., LINDBLAD, L., STEWART, P., LEPENDU, J. & BARIC, R. 2003. Human susceptibility and resistance to Norwalk virus infection. *Nat Med,* 9**,** 548-53.
LINDESMITH, L. C., FERRIS, M. T., MULLAN, C. W., FERREIRA, J., DEBBINK, K., SWANSTROM, J., RICHARDSON, C., GOODWIN, R. R., BAEHNER, F., MENDELMAN, P. M., BARGATZE, R. F. & BARIC, R. S. 2015. Broad blockade antibody responses in human volunteers after immunization with a multivalent norovirus VLP candidate vaccine: immunological analyses from a phase I clinical trial. *PLoS Med,* 12**,** e1001807.
LIU, B., CLARKE, I. N. & LAMBDEN, P. R. 1996. Polyprotein processing in Southampton virus: identification of 3C-like protease cleavage sites by in vitro mutagenesis. *J Virol,* 70**,** 2605-10.
LIU, B. L., CLARKE, I. N., CAUL, E. O. & LAMBDEN, P. R. 1995. Human enteric caliciviruses have a unique genome structure and are distinct from the Norwalk-like viruses. *Arch Virol,* 140**,** 1345-56.
LIU, B. L., VILJOEN, G. J., CLARKE, I. N. & LAMBDEN, P. R. 1999. Identification of further proteolytic cleavage sites in the Southampton calicivirus polyprotein by

expression of the viral protease in E. coli. *J Gen Virol,* 80 (Pt 2)**,** 291-6.
LIU, G., KAHAN, S. M., JIA, Y. & KARST, S. M. 2009. Primary high-dose murine norovirus 1 infection fails to protect from secondary challenge with homologous virus. *J Virol,* 83**,** 6963-8.
LIU, G., NI, Z., YUN, T., YU, B., CHEN, L., ZHAO, W., HUA, J. & CHEN, J. 2008. A DNA-launched reverse genetics system for rabbit hemorrhagic disease virus reveals that the VP2 protein is not essential for virus infectivity. *J Gen Virol,* 89**,** 3080-5.
LIU, G. Q., NI, Z., YUN, T., YU, B., ZHU, J. M., HUA, J. G. & CHEN, J. P. 2007. [Construction of rabbit hemorrhagic disease virus replicons and its replication in RK-13 cells]. *Bing Du Xue Bao,* 23**,** 481-4.
LIU, K. & NUSSENZWEIG, M. C. 2010. Origin and development of dendritic cells. *Immunol Rev,* 234**,** 45-54.
LIVAK, K. J. & SCHMITTGEN, T. D. 2001. Analysis of relative gene expression data using real-time quantitative PCR and the 2(-Delta Delta C(T)) Method. *Methods,* 25**,** 402-8.
LOBUE, A. D., LINDESMITH, L., YOUNT, B., HARRINGTON, P. R., THOMPSON, J. M., JOHNSTON, R. E., MOE, C. L. & BARIC, R. S. 2006. Multivalent norovirus vaccines induce strong mucosal and systemic blocking antibodies against multiple strains. *Vaccine,* 24**,** 5220-34.
LOCHRIDGE, V. P. & HARDY, M. E. 2003. Snow Mountain virus genome sequence and virus-like particle assembly. *Virus Genes,* 26**,** 71-82.
LOMMER, M. J. & VERSTRAETE, F. J. 2003. Concurrent oral shedding of feline calicivirus and feline herpesvirus 1 in cats with chronic gingivostomatitis. *Oral Microbiol Immunol,* 18**,** 131-4.
LOPEZ-MANRIQUEZ, E., VASHIST, S., URENA, L., GOODFELLOW, I., CHAVEZ, P., MORA-HEREDIA, J. E., CANCIO-LONCHES, C., GARRIDO, E. & GUTIERREZ-ESCOLANO, A. L. 2013. Norovirus genome circularization and efficient replication are facilitated by binding of PCBP2 and hnRNP A1. *J Virol,* 87**,** 11371-87.
LOPMAN, B., ARMSTRONG, B., ATCHISON, C. & GRAY, J. J. 2009. Host, weather and virological factors drive norovirus epidemiology: time-series analysis of laboratory surveillance data in England and Wales. *PLoS One,* 4**,** e6671.
LOPMAN, B., VENNEMA, H., KOHLI, E., POTHIER, P., SANCHEZ, A., NEGREDO, A., BUESA, J., SCHREIER, E., REACHER, M., BROWN, D., GRAY, J., ITURRIZA, M., GALLIMORE, C., BOTTIGER, B., HEDLUND, K. O., TORVEN, M., VON BONSDORFF, C. H., MAUNULA, L., POLJSAK-PRIJATELJ, M., ZIMSEK, J., REUTER, G., SZUCS, G., MELEGH, B., SVENNSON, L., VAN DUIJNHOVEN, Y. & KOOPMANS, M. 2004. Increase in viral gastroenteritis outbreaks in Europe and epidemic spread of new norovirus variant. *Lancet,* 363**,** 682-8.
LOU, F., HUANG, P., NEETOO, H., GURTLER, J. B., NIEMIRA, B. A., CHEN, H., JIANG, X. & LI, J. 2012. High-pressure inactivation of human norovirus virus-like particles provides evidence that the capsid of human norovirus is highly pressure resistant. *Appl Environ Microbiol,* 78**,** 5320-7.
LOU, F., YE, M., MA, Y., LI, X., DICAPRIO, E., CHEN, H., KRAKOWKA, S., HUGHES, J., KINGSLEY, D. & LI, J. 2015. A Gnotobiotic Pig Model for Determining Human Norovirus Inactivation by High-Pressure Processing. *Appl Environ Microbiol,* 81**,** 6679-87.
LU, J., FANG, L., ZHENG, H., LAO, J., YANG, F., SUN, L., XIAO, J., LIN, J., SONG, T., NI, T., RAGHWANI, J., KE, C., FARIA, N. R., BOWDEN, T. A., PYBUS, O.

G. & LI, H. 2016. The Evolution and Transmission of Epidemic GII.17 Noroviruses. *J Infect Dis,* 214**,** 556-64.

LUCERO, Y., VIDAL, R. & O'RYAN, G. M. 2017. Norovirus vaccines under development. *Vaccine*.

LUTTERMANN, C. & MEYERS, G. 2007. A bipartite sequence motif induces translation reinitiation in feline calicivirus RNA. *J Biol Chem,* 282**,** 7056-65.

MADELEY, C. R. & COSGROVE, B. P. 1976. Letter: Caliciviruses in man. *Lancet,* 1**,** 199-200.

MAKINO, A., SHIMOJIMA, M., MIYAZAWA, T., KATO, K., TOHYA, Y. & AKASHI, H. 2006. Junctional adhesion molecule 1 is a functional receptor for feline calicivirus. *J Virol,* 80**,** 4482-90.

MAKISON BOOTH, C. 2014. Vomiting Larry: a simulated vomiting system for assessing environmental contamination from projectile vomiting related to norovirus infection. *J Infect Prev,* 15**,** 176-180.

MALM, M., TAMMINEN, K., LAPPALAINEN, S., UUSI-KERTTULA, H., VESIKARI, T. & BLAZEVIC, V. 2015. Genotype considerations for virus-like particle-based bivalent norovirus vaccine composition. *Clin Vaccine Immunol,* 22**,** 656-63.

MALONEY, N. S., THACKRAY, L. B., GOEL, G., HWANG, S., DUAN, E., VACHHARAJANI, P., XAVIER, R. & VIRGIN, H. W. 2012. Essential cell-autonomous role for interferon (IFN) regulatory factor 1 in IFN-gamma-mediated inhibition of norovirus replication in macrophages. *J Virol,* 86**,** 12655-64.

MARCELIN, J. R., WILSON, J. W., RAZONABLE, R. R., MAYO CLINIC, H. O. & TRANSPLANT INFECTIOUS DISEASES, S. 2014. Oral ribavirin therapy for respiratory syncytial virus infections in moderately to severely immunocompromised patients. *Transpl Infect Dis,* 16**,** 242-50.

MARCOTRIGIANO, J., GINGRAS, A. C., SONENBERG, N. & BURLEY, S. K. 1999. Cap-dependent translation initiation in eukaryotes is regulated by a molecular mimic of eIF4G. *Mol Cell,* 3**,** 707-16.

MARIONNEAU, S., AIRAUD, F., BOVIN, N. V., LE PENDU, J. & RUVOEN-CLOUET, N. 2005. Influence of the combined ABO, FUT2, and FUT3 polymorphism on susceptibility to Norwalk virus attachment. *J Infect Dis,* 192**,** 1071-7.

MARIONNEAU, S., RUVOEN, N., LE MOULLAC-VAIDYE, B., CLEMENT, M., CAILLEAU-THOMAS, A., RUIZ-PALACOIS, G., HUANG, P., JIANG, X. & LE PENDU, J. 2002. Norwalk virus binds to histo-blood group antigens present on gastroduodenal epithelial cells of secretor individuals. *Gastroenterology,* 122**,** 1967-77.

MARTELLA, V., MEDICI, M. C., DE GRAZIA, S., TUMMOLO, F., CALDERARO, A., BONURA, F., SAPORITO, L., TERIO, V., CATELLA, C., LANAVE, G., BUONAVOGLIA, C. & GIAMMANCO, G. M. 2013. Evidence for recombination between pandemic GII.4 norovirus strains New Orleans 2009 and Sydney 2012. *J Clin Microbiol,* 51**,** 3855-7.

MASTRANGELO, E., PEZZULLO, M., TARANTINO, D., PETAZZI, R., GERMANI, F., KRAMER, D., ROBEL, I., ROHAYEM, J., BOLOGNESI, M. & MILANI, M. 2012. Structure-based inhibition of Norovirus RNA-dependent RNA polymerases. *J Mol Biol,* 419**,** 198-210.

MATSON, D. O., ZHONG, W. M., NAKATA, S., NUMATA, K., JIANG, X., PICKERING, L. K., CHIBA, S. & ESTES, M. K. 1995. Molecular characterization of a human calicivirus with sequence relationships closer to animal caliciviruses than other known human caliciviruses. *J Med Virol,* 45**,** 215-22.

MAUROY, A., GILLET, L., MATHIJS, E., VANDERPLASSCHEN, A. & THIRY, E. 2011. Alternative attachment factors and internalization pathways for GIII.2 bovine noroviruses. *J Gen Virol,* 92**,** 1398-409.
MCCARTNEY, S. A., THACKRAY, L. B., GITLIN, L., GILFILLAN, S., VIRGIN, H. W. & COLONNA, M. 2008. MDA-5 recognition of a murine norovirus. *PLoS Pathog,* 4**,** e1000108.
MCCORMICK, C. J., SALIM, O., LAMBDEN, P. R. & CLARKE, I. N. 2008. Translation termination reinitiation between open reading frame 1 (ORF1) and ORF2 enables capsid expression in a bovine norovirus without the need for production of viral subgenomic RNA. *J Virol,* 82**,** 8917-21.
MCCUNE, B. T., TANG, W., LU, J., EAGLESHAM, J. B., THORNE, L., MAYER, A. E., CONDIFF, E., NICE, T. J., GOODFELLOW, I., KREZEL, A. M. & VIRGIN, H. W. 2017. Noroviruses Co-opt the Function of Host Proteins VAPA and VAPB for Replication via a Phenylalanine-Phenylalanine-Acidic-Tract-Motif Mimic in Nonstructural Viral Protein NS1/2. *MBio,* 8.
MCFADDEN, N., ARIAS, A., DRY, I., BAILEY, D., WITTEVELDT, J., EVANS, D. J., GOODFELLOW, I. & SIMMONDS, P. 2013. Influence of genome-scale RNA structure disruption on the replication of murine norovirus--similar replication kinetics in cell culture but attenuation of viral fitness in vivo. *Nucleic Acids Res,* 41**,** 6316-31.
MCFADDEN, N., BAILEY, D., CARRARA, G., BENSON, A., CHAUDHRY, Y., SHORTLAND, A., HEENEY, J., YAROVINSKY, F., SIMMONDS, P., MACDONALD, A. & GOODFELLOW, I. 2011. Norovirus regulation of the innate immune response and apoptosis occurs via the product of the alternative open reading frame 4. *PLoS Pathog,* 7**,** e1002413.
MEDVEDEV, A., VISWANATHAN, P., MAY, J. & KORBA, B. 2017. Regulation of human norovirus VPg nucleotidylylation by ProPol and nucleoside triphosphate binding by its amino terminal sequence in vitro. *Virology,* 503**,** 37-45.
MESA, R. A. 2010. Ruxolitinib, a selective JAK1 and JAK2 inhibitor for the treatment of myeloproliferative neoplasms and psoriasis. *IDrugs,* 13**,** 394-403.
MEYERS, G. 2003. Translation of the minor capsid protein of a calicivirus is initiated by a novel termination-dependent reinitiation mechanism. *J Biol Chem,* 278**,** 34051-60.
MEYERS, G., WIRBLICH, C. & THIEL, H. J. 1991a. Genomic and subgenomic RNAs of rabbit hemorrhagic disease virus are both protein-linked and packaged into particles. *Virology,* 184**,** 677-86.
MEYERS, G., WIRBLICH, C. & THIEL, H. J. 1991b. Rabbit hemorrhagic disease virus--molecular cloning and nucleotide sequencing of a calicivirus genome. *Virology,* 184**,** 664-76.
MEYERS, G., WIRBLICH, C., THIEL, H. J. & THUMFART, J. O. 2000. Rabbit hemorrhagic disease virus: genome organization and polyprotein processing of a calicivirus studied after transient expression of cDNA constructs. *Virology,* 276**,** 349-63.
MIKALSEN, A. B., NILSEN, P., FROYSTAD-SAUGEN, M., LINDMO, K., ELIASSEN, T. M., RODE, M. & EVENSEN, O. 2014. Characterization of a novel calicivirus causing systemic infection in atlantic salmon (Salmo salar L.): proposal for a new genus of caliciviridae. *PLoS One,* 9**,** e107132.
MIURA, T., SANO, D., SUENAGA, A., YOSHIMURA, T., FUZAWA, M., NAKAGOMI, T., NAKAGOMI, O. & OKABE, S. 2013. Histo-blood group antigen-like substances of human enteric bacteria as specific adsorbents for human

noroviruses. *J Virol,* 87**,** 9441-51.
MIZUKOSHI, F., NAGASAWA, K., DOAN, Y. H., HAGA, K., YOSHIZUMI, S., UEKI, Y., SHINOHARA, M., ISHIKAWA, M., SAKON, N., SHIGEMOTO, N., OKAMOTO-NAKAGAWA, R., OCHI, A., MURAKAMI, K., RYO, A., SUZUKI, Y., KATAYAMA, K. & KIMURA, H. 2017. Molecular Evolution of the RNA-Dependent RNA Polymerase and Capsid Genes of Human Norovirus Genotype GII.2 in Japan during 2004-2015. *Front Microbiol,* 8**,** 705.
MORI, K., MOTOMURA, K., SOMURA, Y., KIMOTO, K., AKIBA, T. & SADAMASU, K. 2017. Comparison of genetic characteristics in the evolution of Norovirus GII.4 and GII.17. *J Med Virol,* 89**,** 1480-1484.
MUMPHREY, S. M., CHANGOTRA, H., MOORE, T. N., HEIMANN-NICHOLS, E. R., WOBUS, C. E., REILLY, M. J., MOGHADAMFALAHI, M., SHUKLA, D. & KARST, S. M. 2007. Murine norovirus 1 infection is associated with histopathological changes in immunocompetent hosts, but clinical disease is prevented by STAT1-dependent interferon responses. *J Virol,* 81**,** 3251-63.
MURAKAMI, K., KURIHARA, C., OKA, T., SHIMOIKE, T., FUJII, Y., TAKAI-TODAKA, R., PARK, Y., WAKITA, T., MATSUDA, T., HOKARI, R., MIURA, S. & KATAYAMA, K. 2013. Norovirus binding to intestinal epithelial cells is independent of histo-blood group antigens. *PLoS One,* 8**,** e66534.
NAGESHA, H. S., WANG, L. F., HYATT, A. D., MORRISSY, C. J., LENGHAUS, C. & WESTBURY, H. A. 1995. Self-assembly, antigenicity, and immunogenicity of the rabbit haemorrhagic disease virus (Czechoslovakian strain V-351) capsid protein expressed in baculovirus. *Arch Virol,* 140**,** 1095-1108.
NAGY, P. D. & POGANY, J. 2011. The dependence of viral RNA replication on co-opted host factors. *Nat Rev Microbiol,* 10**,** 137-49.
NAKAJIMA, H., WATANABE, T., MIYAZAKI, T., TAKEUCHI, M., HONDA, Y., SHIMADA, N., NAKANISHI, K., URITA, Y. & SUGIMOTO, M. 2012. Acute liver dysfunction in the course of norovirus gastroenteritis. *Case Rep Gastroenterol,* 6**,** 69-73.
NAKANISHI, K., TATSUMI, M., KINOSHITA-NUMATA, K., TSUGAWA, T., NAKATA, S. & TSUTSUMI, H. 2011. Full sequence analysis of the original Sapporo virus. *Microbiol Immunol,* 55**,** 657-60.
NALDINI, L., BLOMER, U., GALLAY, P., ORY, D., MULLIGAN, R., GAGE, F. H., VERMA, I. M. & TRONO, D. 1996. In vivo gene delivery and stable transduction of nondividing cells by a lentiviral vector. *Science,* 272**,** 263-7.
NAPTHINE, S., LEVER, R. A., POWELL, M. L., JACKSON, R. J., BROWN, T. D. & BRIERLEY, I. 2009. Expression of the VP2 protein of murine norovirus by a translation termination-reinitiation strategy. *PLoS One,* 4**,** e8390.
NEILL, J. D. 2002. The subgenomic RNA of feline calicivirus is packaged into viral particles during infection. *Virus Res,* 87**,** 89-93.
NEWMAN, K. L., MOE, C. L., KIRBY, A. E., FLANDERS, W. D., PARKOS, C. A. & LEON, J. S. 2016. Norovirus in symptomatic and asymptomatic individuals: cytokines and viral shedding. *Clin Exp Immunol,* 184**,** 347-57.
NG, K. K., CHERNEY, M. M., VAZQUEZ, A. L., MACHIN, A., ALONSO, J. M., PARRA, F. & JAMES, M. N. 2002. Crystal structures of active and inactive conformations of a caliciviral RNA-dependent RNA polymerase. *J Biol Chem,* 277**,** 1381-7.
NG, K. K., PENDAS-FRANCO, N., ROJO, J., BOGA, J. A., MACHIN, A., ALONSO, J. M. & PARRA, F. 2004. Crystal structure of norwalk virus polymerase reveals the carboxyl terminus in the active site cleft. *J Biol Chem,* 279**,** 16638-45.
NI, P. & CHENG KAO, C. 2013. Non-encapsidation activities of the capsid proteins of

positive-strand RNA viruses. *Virology,* 446**,** 123-32.
NICE, T. J., BALDRIDGE, M. T., MCCUNE, B. T., NORMAN, J. M., LAZEAR, H. M., ARTYOMOV, M., DIAMOND, M. S. & VIRGIN, H. W. 2015. Interferon-lambda cures persistent murine norovirus infection in the absence of adaptive immunity. *Science,* 347**,** 269-73.
NICE, T. J., OSBORNE, L. C., TOMOV, V. T., ARTIS, D., WHERRY, E. J. & VIRGIN, H. W. 2016. Type I Interferon Receptor Deficiency in Dendritic Cells Facilitates Systemic Murine Norovirus Persistence Despite Enhanced Adaptive Immunity. *PLoS Pathog,* 12**,** e1005684.
NICE, T. J., STRONG, D. W., MCCUNE, B. T., POHL, C. S. & VIRGIN, H. W. 2013. A single-amino-acid change in murine norovirus NS1/2 is sufficient for colonic tropism and persistence. *J Virol,* 87**,** 327-34.
NICOLLIER-JAMOT, B., PICO, V., POTHIER, P. & KOHLI, E. 2003. Molecular cloning, expression, self-assembly, antigenicity, and seroepidemiology of a genogroup II norovirus isolated in France. *J Clin Microbiol,* 41**,** 3901-4.
NIENDORF, S., KLEMM, U., MAS MARQUES, A., BOCK, C. T. & HOHNE, M. 2016. Infection with the Persistent Murine Norovirus Strain MNV-S99 Suppresses IFN-Beta Release and Activation of Stat1 In Vitro. *PLoS One,* 11**,** e0156898.
NILSSON, M., HEDLUND, K. O., THORHAGEN, M., LARSON, G., JOHANSEN, K., EKSPONG, A. & SVENSSON, L. 2003. Evolution of human calicivirus RNA in vivo: accumulation of mutations in the protruding P2 domain of the capsid leads to structural changes and possibly a new phenotype. *J Virol,* 77**,** 13117-24.
NORDGREN, J., KINDBERG, E., LINDGREN, P. E., MATUSSEK, A. & SVENSSON, L. 2010. Norovirus gastroenteritis outbreak with a secretor-independent susceptibility pattern, Sweden. *Emerg Infect Dis,* 16**,** 81-7.
NUMATA, K., HARDY, M. E., NAKATA, S., CHIBA, S. & ESTES, M. K. 1997. Molecular characterization of morphologically typical human calicivirus Sapporo. *Arch Virol,* 142**,** 1537-52.
OHLINGER, V. F., HAAS, B., MEYERS, G., WEILAND, F. & THIEL, H. J. 1990. Identification and characterization of the virus causing rabbit hemorrhagic disease. *J Virol,* 64**,** 3331-6.
OHSUGI, T., MATSUURA, K., KAWABE, S., NAKAMURA, N., KUMAR, J. M., WAKAMIYA, M., MORIKAWA, S. & URANO, T. 2013. Natural infection of murine norovirus in conventional and specific pathogen-free laboratory mice. *Front Microbiol,* 4**,** 12.
OKA, T., YAMAMOTO, M., MIYASHITA, K., OGAWA, S., KATAYAMA, K., WAKITA, T. & TAKEDA, N. 2009. Self-assembly of sapovirus recombinant virus-like particles from polyprotein in mammalian cells. *Microbiol Immunol,* 53**,** 49-52.
OKA, T., YAMAMOTO, M., YOKOYAMA, M., OGAWA, S., HANSMAN, G. S., KATAYAMA, K., MIYASHITA, K., TAKAGI, H., TOHYA, Y., SATO, H. & TAKEDA, N. 2007. Highly conserved configuration of catalytic amino acid residues among calicivirus-encoded proteases. *J Virol,* 81**,** 6798-806.
OKABAYASHI, T., YOKOTA, S., OHKOSHI, Y., OHUCHI, H., YOSHIDA, Y., KIKUCHI, M., YANO, K. & FUJII, N. 2008. Occurrence of norovirus infections unrelated to norovirus outbreaks in an asymptomatic food handler population. *J Clin Microbiol,* 46**,** 1985-8.
OKHUYSEN, P. C., JIANG, X., YE, L., JOHNSON, P. C. & ESTES, M. K. 1995. Viral shedding and fecal IgA response after Norwalk virus infection. *J Infect Dis,* 171**,** 566-9.
OLIVER, S. L., DASTJERDI, A. M., WONG, S., EL-ATTAR, L., GALLIMORE, C.,

BROWN, D. W., GREEN, J. & BRIDGER, J. C. 2003. Molecular characterization of bovine enteric caliciviruses: a distinct third genogroup of noroviruses (Norwalk-like viruses) unlikely to be of risk to humans. *J Virol,* 77**,** 2789-98.

OLSPERT, A., HOSMILLO, M., CHAUDHRY, Y., PEIL, L., TRUVE, E. & GOODFELLOW, I. 2016. Protein-RNA linkage and posttranslational modifications of feline calicivirus and murine norovirus VPg proteins. *PeerJ,* 4**,** e2134.

ORCHARD, R. C., WILEN, C. B., DOENCH, J. G., BALDRIDGE, M. T., MCCUNE, B. T., LEE, Y. C., LEE, S., PRUETT-MILLER, S. M., NELSON, C. A., FREMONT, D. H. & VIRGIN, H. W. 2016. Discovery of a proteinaceous cellular receptor for a norovirus. *Science,* 353**,** 933-6.

PAPAFRAGKOU, E., HEWITT, J., PARK, G. W., GREENING, G. & VINJE, J. 2014. Challenges of culturing human norovirus in three-dimensional organoid intestinal cell culture models. *PLoS One,* 8**,** e63485.

PARK, G. W., BOSTON, D. M., KASE, J. A., SAMPSON, M. N. & SOBSEY, M. D. 2007. Evaluation of liquid- and fog-based application of Sterilox hypochlorous acid solution for surface inactivation of human norovirus. *Appl Environ Microbiol,* 73**,** 4463-8.

PARRA, F. & PRIETO, M. 1990. Purification and characterization of a calicivirus as the causative agent of a lethal hemorrhagic disease in rabbits. *J Virol,* 64**,** 4013-5.

PARRINO, T. A., SCHREIBER, D. S., TRIER, J. S., KAPIKIAN, A. Z. & BLACKLOW, N. R. 1977. Clinical immunity in acute gastroenteritis caused by Norwalk agent. *N Engl J Med,* 297**,** 86-9.

PARWANI, A. V., FLYNN, W. T., GADFIELD, K. L. & SAIF, L. J. 1991. Serial propagation of porcine enteric calicivirus in a continuous cell line. Effect of medium supplementation with intestinal contents or enzymes. *Arch Virol,* 120**,** 115-22.

PATHAK, H. B., OH, H. S., GOODFELLOW, I. G., ARNOLD, J. J. & CAMERON, C. E. 2008. Picornavirus genome replication: roles of precursor proteins and rate-limiting steps in oriI-dependent VPg uridylylation. *J Biol Chem,* 283**,** 30677-88.

PERDUE, K. A., GREEN, K. Y., COPELAND, M., BARRON, E., MANDEL, M., FAUCETTE, L. J., WILLIAMS, E. M., SOSNOVTSEV, S. V., ELKINS, W. R. & WARD, J. M. 2007. Naturally occurring murine norovirus infection in a large research institution. *J Am Assoc Lab Anim Sci,* 46**,** 39-45.

PERRY, J. W., TAUBE, S. & WOBUS, C. E. 2009. Murine norovirus-1 entry into permissive macrophages and dendritic cells is pH-independent. *Virus Res,* 143**,** 125-9.

PERRY, J. W. & WOBUS, C. E. 2010. Endocytosis of murine norovirus 1 into murine macrophages is dependent on dynamin II and cholesterol. *J Virol,* 84**,** 6163-76.

PERVOLARAKI, K., STANIFER, M. L., MUNCHAU, S., RENN, L. A., ALBRECHT, D., KURZHALS, S., SENIS, E., GRIMM, D., SCHRODER-BRAUNSTEIN, J., RABIN, R. L. & BOULANT, S. 2017. Type I and Type III Interferons Display Different Dependency on Mitogen-Activated Protein Kinases to Mount an Antiviral State in the Human Gut. *Front Immunol,* 8**,** 459.

PETER, D., IGREJA, C., WEBER, R., WOHLBOLD, L., WEILER, C., EBERTSCH, L., WEICHENRIEDER, O. & IZAURRALDE, E. 2015. Molecular architecture of 4E-BP translational inhibitors bound to eIF4E. *Mol Cell,* 57**,** 1074-87.

PHILLIPS, G., TAM, C. C., RODRIGUES, L. C. & LOPMAN, B. 2010. Prevalence and

characteristics of asymptomatic norovirus infection in the community in England. *Epidemiol Infect,* 138**,** 1454-8.
POTT, J., MAHLAKOIV, T., MORDSTEIN, M., DUERR, C. U., MICHIELS, T., STOCKINGER, S., STAEHELI, P. & HORNEF, M. W. 2011. IFN-lambda determines the intestinal epithelial antiviral host defense. *Proc Natl Acad Sci U S A,* 108**,** 7944-9.
PRASAD, B. V., HARDY, M. E., DOKLAND, T., BELLA, J., ROSSMANN, M. G. & ESTES, M. K. 1999. X-ray crystallographic structure of the Norwalk virus capsid. *Science,* 286**,** 287-90.
PRASAD, B. V., ROTHNAGEL, R., JIANG, X. & ESTES, M. K. 1994. Three-dimensional structure of baculovirus-expressed Norwalk virus capsids. *J Virol,* 68**,** 5117-25.
QU, L., MURAKAMI, K., BROUGHMAN, J. R., LAY, M. K., GUIX, S., TENGE, V. R., ATMAR, R. L. & ESTES, M. K. 2016. Replication of Human Norovirus RNA in Mammalian Cells Reveals Lack of Interferon Response. *J Virol,* 90**,** 8906-23.
QU, L., VONGPUNSAWAD, S., ATMAR, R. L., PRASAD, B. V. & ESTES, M. K. 2014. Development of a Gaussia luciferase-based human norovirus protease reporter system: cell type-specific profile of Norwalk virus protease precursors and evaluation of inhibitors. *J Virol,* 88**,** 10312-26.
RAJAGOPALAN, S. & YOSHIKAWA, T. T. 2016. Norovirus Infections in Long-Term Care Facilities. *J Am Geriatr Soc,* 64**,** 1097-103.
RAMANI, S., ATMAR, R. L. & ESTES, M. K. 2014. Epidemiology of human noroviruses and updates on vaccine development. *Curr Opin Gastroenterol,* 30**,** 25-33.
RAMIREZ, K., WAHID, R., RICHARDSON, C., BARGATZE, R. F., EL-KAMARY, S. S., SZTEIN, M. B. & PASETTI, M. F. 2012. Intranasal vaccination with an adjuvanted Norwalk virus-like particle vaccine elicits antigen-specific B memory responses in human adult volunteers. *Clin Immunol,* 144**,** 98-108.
RANJITH-KUMAR, C. T., WEN, Y., BAXTER, N., BHARDWAJ, K. & CHENG KAO, C. 2011. A cell-based assay for RNA synthesis by the HCV polymerase reveals new insights on mechanism of polymerase inhibitors and modulation by NS5A. *PLoS One,* 6**,** e22575.
RAO, X., HUANG, X., ZHOU, Z. & LIN, X. 2013. An improvement of the 2^(-delta delta CT) method for quantitative real-time polymerase chain reaction data analysis. *Biostat Bioinforma Biomath,* 3**,** 71-85.
RAU, M., OHLMANN, T., MORLEY, S. J. & PAIN, V. M. 1996. A reevaluation of the cap-binding protein, eIF4E, as a rate-limiting factor for initiation of translation in reticulocyte lysate. *J Biol Chem,* 271**,** 8983-90.
ROBERTS, L. O., AL-MOLAWI, N., CARTER, M. J. & KASS, G. E. 2003. Apoptosis in cultured cells infected with feline calicivirus. *Ann N Y Acad Sci,* 1010**,** 587-90.
ROCHA-PEREIRA, J., JOCHMANS, D., DALLMEIER, K., LEYSSEN, P., CUNHA, R., COSTA, I., NASCIMENTO, M. S. & NEYTS, J. 2012a. Inhibition of norovirus replication by the nucleoside analogue 2'-C-methylcytidine. *Biochem Biophys Res Commun,* 427**,** 796-800.
ROCHA-PEREIRA, J., JOCHMANS, D., DALLMEIER, K., LEYSSEN, P., NASCIMENTO, M. S. & NEYTS, J. 2012b. Favipiravir (T-705) inhibits in vitro norovirus replication. *Biochem Biophys Res Commun,* 424**,** 777-80.
ROCHA-PEREIRA, J., JOCHMANS, D., DEBING, Y., VERBEKEN, E., NASCIMENTO, M. S. & NEYTS, J. 2013. The viral polymerase inhibitor 2'-C-methylcytidine inhibits Norwalk virus replication and protects against

norovirus-induced diarrhea and mortality in a mouse model. *J Virol,* 87**,** 11798-805.
ROCHA-PEREIRA, J., JOCHMANS, D. & NEYTS, J. 2015. Prophylactic treatment with the nucleoside analogue 2'-C-methylcytidine completely prevents transmission of norovirus. *J Antimicrob Chemother,* 70**,** 190-7.
ROCKX, B. H., BOGERS, W. M., HEENEY, J. L., VAN AMERONGEN, G. & KOOPMANS, M. P. 2005. Experimental norovirus infections in non-human primates. *J Med Virol,* 75**,** 313-20.
ROERINK, F., HASHIMOTO, M., TOHYA, Y. & MOCHIZUKI, M. 1999. Genetic analysis of a canine calicivirus: evidence for a new clade of animal caliciviruses. *Vet Microbiol,* 69**,** 69-72.
ROHAYEM, J., JAGER, K., ROBEL, I., SCHEFFLER, U., TEMME, A. & RUDOLPH, W. 2006a. Characterization of norovirus 3Dpol RNA-dependent RNA polymerase activity and initiation of RNA synthesis. *J Gen Virol,* 87**,** 2621-30.
ROHAYEM, J., MUNCH, J. & RETHWILM, A. 2005. Evidence of recombination in the norovirus capsid gene. *J Virol,* 79**,** 4977-90.
ROHAYEM, J., ROBEL, I., JAGER, K., SCHEFFLER, U. & RUDOLPH, W. 2006b. Protein-primed and de novo initiation of RNA synthesis by norovirus 3Dpol. *J Virol,* 80**,** 7060-9.
RONDY, M., KOOPMANS, M., ROTSAERT, C., VAN LOON, T., BELJAARS, B., VAN DIJK, G., SIEBENGA, J., SVRAKA, S., ROSSEN, J. W., TEUNIS, P., VAN PELT, W. & VERHOEF, L. 2011. Norovirus disease associated with excess mortality and use of statins: a retrospective cohort study of an outbreak following a pilgrimage to Lourdes. *Epidemiol Infect,* 139**,** 453-63.
ROTH, H., MAGG, V., UCH, F., MUTZ, P., KLEIN, P., HANEKE, K., LOHMANN, V., BARTENSCHLAGER, R., FACKLER, O. T., LOCKER, N., STOECKLIN, G. & RUGGIERI, A. 2017. Flavivirus Infection Uncouples Translation Suppression from Cellular Stress Responses. *MBio,* 8.
ROYALL, E., DOYLE, N., ABDUL-WAHAB, A., EMMOTT, E., MORLEY, S. J., GOODFELLOW, I., ROBERTS, L. O. & LOCKER, N. 2015. Murine norovirus 1 (MNV1) replication induces translational control of the host by regulating eIF4E activity during infection. *J Biol Chem,* 290**,** 4748-58.
RUVOEN-CLOUET, N., BELLIOT, G. & LE PENDU, J. 2013. Noroviruses and histo-blood groups: the impact of common host genetic polymorphisms on virus transmission and evolution. *Rev Med Virol,* 23**,** 355-66.
RUVOEN-CLOUET, N., GANIERE, J. P., ANDRE-FONTAINE, G., BLANCHARD, D. & LE PENDU, J. 2000. Binding of rabbit hemorrhagic disease virus to antigens of the ABH histo-blood group family. *J Virol,* 74**,** 11950-4.
RYDELL, G. E., NILSSON, J., RODRIGUEZ-DIAZ, J., RUVOEN-CLOUET, N., SVENSSON, L., LE PENDU, J. & LARSON, G. 2009. Human noroviruses recognize sialyl Lewis x neoglycoprotein. *Glycobiology,* 19**,** 309-20.
SAHOO, M. K., HOLUBAR, M., HUANG, C., MOHAMED-HADLEY, A., LIU, Y., WAGGONER, J. J., TROY, S. B., GARCIA-GARCIA, L., FERREYRA-REYES, L., MALDONADO, Y. & PINSKY, B. A. 2017. Detection of Emerging Vaccine-Related Polioviruses by Deep Sequencing. *J Clin Microbiol,* 55**,** 2162-2171.
SAIF, M. A., BONNEY, D. K., BIGGER, B., FORSYTHE, L., WILLIAMS, N., PAGE, J., BABIKER, Z. O., GUIVER, M., TURNER, A. J., HUGHES, S. & WYNN, R. F. 2011. Chronic norovirus infection in pediatric hematopoietic stem cell transplant recipients: a cause of prolonged intestinal failure requiring intensive nutritional support. *Pediatr Transplant,* 15**,** 505-9.
SAN GABRIEL, M. C., TOHYA, Y., SUGIMURA, T., SHIMIZU, T., ISHIGURO, S. &

MOCHIZUKI, M. 1997. Identification of canine calicivirus capsid protein and its immunoreactivity in western blotting. *J Vet Med Sci,* 59**,** 97-101.
SANDMANN, F. G., JIT, M., ROBOTHAM, J. V. & DEENY, S. R. 2017. Burden, duration and costs of hospital bed closures due to acute gastroenteritis in England per winter, 2010/11-2015/16. *J Hosp Infect*.
SANDOVAL-JAIME, C. & GUTIERREZ-ESCOLANO, A. L. 2009. Cellular proteins mediate 5'-3' end contacts of Norwalk virus genomic RNA. *Virology,* 387**,** 322-30.
SATO, T., STANGE, D. E., FERRANTE, M., VRIES, R. G., VAN ES, J. H., VAN DEN BRINK, S., VAN HOUDT, W. J., PRONK, A., VAN GORP, J., SIERSEMA, P. D. & CLEVERS, H. 2011. Long-term expansion of epithelial organoids from human colon, adenoma, adenocarcinoma, and Barrett's epithelium. *Gastroenterology,* 141**,** 1762-72.
SAXENA, K., BLUTT, S. E., ETTAYEBI, K., ZENG, X. L., BROUGHMAN, J. R., CRAWFORD, S. E., KARANDIKAR, U. C., SASTRI, N. P., CONNER, M. E., OPEKUN, A. R., GRAHAM, D. Y., QURESHI, W., SHERMAN, V., FOULKE-ABEL, J., IN, J., KOVBASNJUK, O., ZACHOS, N. C., DONOWITZ, M. & ESTES, M. K. 2015. Human Intestinal Enteroids: a New Model To Study Human Rotavirus Infection, Host Restriction, and Pathophysiology. *J Virol,* 90**,** 43-56.
SCHAFFER, F. L., EHRESMANN, D. W., FRETZ, M. K. & SOERGEL, M. I. 1980. A protein, VPg, covalently linked to 36S calicivirus RNA. *J Gen Virol,* 47**,** 215-20.
SCHEFFLER, U., RUDOLPH, W., GEBHARDT, J. & ROHAYEM, J. 2007. Differential cleavage of the norovirus polyprotein precursor by two active forms of the viral protease. *J Gen Virol,* 88**,** 2013-8.
SCHLISSEL, M. 2013. Immunology: B-cell development in the gut. *Nature,* 501**,** 42-3.
SCHORN, R., HOHNE, M., MEERBACH, A., BOSSART, W., WUTHRICH, R. P., SCHREIER, E., MULLER, N. J. & FEHR, T. 2010. Chronic norovirus infection after kidney transplantation: molecular evidence for immune-driven viral evolution. *Clin Infect Dis,* 51**,** 307-14.
SCHWARTZ, S., VERGOULIDOU, M., SCHREIER, E., LODDENKEMPER, C., REINWALD, M., SCHMIDT-HIEBER, M., FLEGEL, W. A., THIEL, E. & SCHNEIDER, T. 2011. Norovirus gastroenteritis causes severe and lethal complications after chemotherapy and hematopoietic stem cell transplantation. *Blood,* 117**,** 5850-6.
SESTAK, K., FEELY, S., FEY, B., DUFOUR, J., HARGITT, E., ALVAREZ, X., PAHAR, B., GREGORICUS, N., VINJE, J. & FARKAS, T. 2012. Experimental inoculation of juvenile rhesus macaques with primate enteric caliciviruses. *PLoS One,* 7**,** e37973.
SETH, R. B., SUN, L., EA, C. K. & CHEN, Z. J. 2005. Identification and characterization of MAVS, a mitochondrial antiviral signaling protein that activates NF-kappaB and IRF 3. *Cell,* 122**,** 669-82.
SHARP, T. M., CRAWFORD, S. E., AJAMI, N. J., NEILL, F. H., ATMAR, R. L., KATAYAMA, K., UTAMA, B. & ESTES, M. K. 2012. Secretory pathway antagonism by calicivirus homologues of Norwalk virus nonstructural protein p22 is restricted to noroviruses. *Virol J,* 9**,** 181.
SHARP, T. M., GUIX, S., KATAYAMA, K., CRAWFORD, S. E. & ESTES, M. K. 2010. Inhibition of cellular protein secretion by norwalk virus nonstructural protein p22 requires a mimic of an endoplasmic reticulum export signal. *PLoS One,* 5**,** e13130.
SHIVANNA, V., KIM, Y. & CHANG, K. O. 2014. The crucial role of bile acids in the

entry of porcine enteric calicivirus. *Virology,* 456-457**,** 268-78.
SHVEYGERT, M., KAISER, C., BRADRICK, S. S. & GROMEIER, M. 2010. Regulation of eukaryotic initiation factor 4E (eIF4E) phosphorylation by mitogen-activated protein kinase occurs through modulation of Mnk1-eIF4G interaction. *Mol Cell Biol,* 30**,** 5160-7.
SIBILIA, M., BONIOTTI, M. B., ANGOSCINI, P., CAPUCCI, L. & ROSSI, C. 1995. Two independent pathways of expression lead to self-assembly of the rabbit hemorrhagic disease virus capsid protein. *J Virol,* 69**,** 5812-5.
SIEBENGA, J. J., BEERSMA, M. F., VENNEMA, H., VAN BIEZEN, P., HARTWIG, N. J. & KOOPMANS, M. 2008. High prevalence of prolonged norovirus shedding and illness among hospitalized patients: a model for in vivo molecular evolution. *J Infect Dis,* 198**,** 994-1001.
SIEBENGA, J. J., VENNEMA, H., ZHENG, D. P., VINJE, J., LEE, B. E., PANG, X. L., HO, E. C., LIM, W., CHOUDEKAR, A., BROOR, S., HALPERIN, T., RASOOL, N. B., HEWITT, J., GREENING, G. E., JIN, M., DUAN, Z. J., LUCERO, Y., O'RYAN, M., HOEHNE, M., SCHREIER, E., RATCLIFF, R. M., WHITE, P. A., IRITANI, N., REUTER, G. & KOOPMANS, M. 2009. Norovirus illness is a global problem: emergence and spread of norovirus GII.4 variants, 2001-2007. *J Infect Dis,* 200**,** 802-12.
SIEVERS, F., WILM, A., DINEEN, D., GIBSON, T. J., KARPLUS, K., LI, W., LOPEZ, R., MCWILLIAM, H., REMMERT, M., SODING, J., THOMPSON, J. D. & HIGGINS, D. G. 2011. Fast, scalable generation of high-quality protein multiple sequence alignments using Clustal Omega. *Mol Syst Biol,* 7**,** 539.
SIMMONDS, P., KARAKASILIOTIS, I., BAILEY, D., CHAUDHRY, Y., EVANS, D. J. & GOODFELLOW, I. G. 2008. Bioinformatic and functional analysis of RNA secondary structure elements among different genera of human and animal caliciviruses. *Nucleic Acids Res,* 36**,** 2530-46.
SMILEY, J. R., CHANG, K. O., HAYES, J., VINJE, J. & SAIF, L. J. 2002. Characterization of an enteropathogenic bovine calicivirus representing a potentially new calicivirus genus. *J Virol,* 76**,** 10089-98.
SMITH, A. W., SKILLING, D. E. & BENIRSCHKE, K. 1985. Calicivirus isolation from three species of primates: an incidental finding. *Am J Vet Res,* 46**,** 2197-9.
SMITH, D. B., MCFADDEN, N., BLUNDELL, R. J., MEREDITH, A. & SIMMONDS, P. 2012. Diversity of murine norovirus in wild-rodent populations: species-specific associations suggest an ancient divergence. *J Gen Virol,* 93**,** 259-66.
SMYTHIES, L. E., SELLERS, M., CLEMENTS, R. H., MOSTELLER-BARNUM, M., MENG, G., BENJAMIN, W. H., ORENSTEIN, J. M. & SMITH, P. D. 2005. Human intestinal macrophages display profound inflammatory anergy despite avid phagocytic and bacteriocidal activity. *J Clin Invest,* 115**,** 66-75.
SON, Y. H., JEONG, Y. T., LEE, K. A., CHOI, K. H., KIM, S. M., RHIM, B. Y. & KIM, K. 2008. Roles of MAPK and NF-kappaB in interleukin-6 induction by lipopolysaccharide in vascular smooth muscle cells. *J Cardiovasc Pharmacol,* 51**,** 71-7.
SOSNOVTSEV, S. & GREEN, K. Y. 1995. RNA transcripts derived from a cloned full-length copy of the feline calicivirus genome do not require VpG for infectivity. *Virology,* 210**,** 383-90.
SOSNOVTSEV, S. V., BELLIOT, G., CHANG, K. O., ONWUDIWE, O. & GREEN, K. Y. 2005. Feline calicivirus VP2 is essential for the production of infectious virions. *J Virol,* 79**,** 4012-24.
SOSNOVTSEV, S. V., BELLIOT, G., CHANG, K. O., PRIKHODKO, V. G., THACKRAY, L. B., WOBUS, C. E., KARST, S. M., VIRGIN, H. W. & GREEN,

K. Y. 2006. Cleavage map and proteolytic processing of the murine norovirus nonstructural polyprotein in infected cells. *J Virol,* 80**,** 7816-31.
SOSNOVTSEV, S. V., GARFIELD, M. & GREEN, K. Y. 2002. Processing map and essential cleavage sites of the nonstructural polyprotein encoded by ORF1 of the feline calicivirus genome. *J Virol,* 76**,** 7060-72.
SOSNOVTSEV, S. V. & GREEN, K. Y. 2000. Identification and genomic mapping of the ORF3 and VPg proteins in feline calicivirus virions. *Virology,* 277**,** 193-203.
SOUZA, A. C., VASQUES, R. M., INOUE-NAGATA, A. K., LACORTE, C., MALDANER, F. R., NORONHA, E. F. & NAGATA, T. 2013. Expression and assembly of Norwalk virus-like particles in plants using a viral RNA silencing suppressor gene. *Appl Microbiol Biotechnol,* 97**,** 9021-7.
SOUZA, M., AZEVEDO, M. S., JUNG, K., CHEETHAM, S. & SAIF, L. J. 2008. Pathogenesis and immune responses in gnotobiotic calves after infection with the genogroup II.4-HS66 strain of human norovirus. *J Virol,* 82**,** 1777-86.
SOUZA, M., CHEETHAM, S. M., AZEVEDO, M. S., COSTANTINI, V. & SAIF, L. J. 2007a. Cytokine and antibody responses in gnotobiotic pigs after infection with human norovirus genogroup II.4 (HS66 strain). *J Virol,* 81**,** 9183-92.
SOUZA, M., COSTANTINI, V., AZEVEDO, M. S. & SAIF, L. J. 2007b. A human norovirus-like particle vaccine adjuvanted with ISCOM or mLT induces cytokine and antibody responses and protection to the homologous GII.4 human norovirus in a gnotobiotic pig disease model. *Vaccine,* 25**,** 8448-59.
STAPPENBECK, T. S. & VIRGIN, H. W. 2016. Accounting for reciprocal host-microbiome interactions in experimental science. *Nature,* 534**,** 191-9.
STENT, G., REECE, J. C., BAYLIS, D. C., IVINSON, K., PAUKOVICS, G., THOMSON, M. & CAMERON, P. U. 2002. Heterogeneity of freshly isolated human tonsil dendritic cells demonstrated by intracellular markers, phagocytosis, and membrane dye transfer. *Cytometry,* 48**,** 167-76.
STRAUB, T. M., BARTHOLOMEW, R. A., VALDEZ, C. O., VALENTINE, N. B., DOHNALKOVA, A., OZANICH, R. M., BRUCKNER-LEA, C. J. & CALL, D. R. 2011. Human norovirus infection of caco-2 cells grown as a three-dimensional tissue structure. *J Water Health,* 9**,** 225-40.
STRAUB, T. M., HONER ZU BENTRUP, K., OROSZ-COGHLAN, P., DOHNALKOVA, A., MAYER, B. K., BARTHOLOMEW, R. A., VALDEZ, C. O., BRUCKNER-LEA, C. J., GERBA, C. P., ABBASZADEGAN, M. & NICKERSON, C. A. 2007. In vitro cell culture infectivity assay for human noroviruses. *Emerg Infect Dis,* 13**,** 396-403.
STUART, A. D. & BROWN, T. D. 2006. Entry of feline calicivirus is dependent on clathrin-mediated endocytosis and acidification in endosomes. *J Virol,* 80**,** 7500-9.
STUART, A. D. & BROWN, T. D. 2007. Alpha2,6-linked sialic acid acts as a receptor for Feline calicivirus. *J Gen Virol,* 88**,** 177-86.
STUART, R. L., TAN, K., MAHAR, J. E., KIRKWOOD, C. D., ANDREW RAMSDEN, C., ANDRIANOPOULOS, N., JOLLEY, D., BAWDEN, K., DOHERTY, R., KOTSANAS, D., BRADFORD, J. & BUTTERY, J. P. 2010. An outbreak of necrotizing enterocolitis associated with norovirus genotype GII.3. *Pediatr Infect Dis J,* 29**,** 644-7.
SUBBA-REDDY, C. V., GOODFELLOW, I. & KAO, C. C. 2011. VPg-primed RNA synthesis of norovirus RNA-dependent RNA polymerases by using a novel cell-based assay. *J Virol,* 85**,** 13027-37.
SUBBA-REDDY, C. V., YUNUS, M. A., GOODFELLOW, I. G. & KAO, C. C. 2012. Norovirus RNA synthesis is modulated by an interaction between the viral

RNA-dependent RNA polymerase and the major capsid protein, VP1. *J Virol,* 86**,** 10138-49.

SUBEKTI, D. S., TJANIADI, P., LESMANA, M., MCARDLE, J., ISKANDRIATI, D., BUDIARSA, I. N., WALUJO, P., SUPARTO, I. H., WINOTO, I., CAMPBELL, J. R., PORTER, K. R., SAJUTHI, D., ANSARI, A. A. & OYOFO, B. A. 2002. Experimental infection of Macaca nemestrina with a Toronto Norwalk-like virus of epidemic viral gastroenteritis. *J Med Virol,* 66**,** 400-6.

SUGIEDA, M., NAGAOKA, H., KAKISHIMA, Y., OHSHITA, T., NAKAMURA, S. & NAKAJIMA, S. 1998. Detection of Norwalk-like virus genes in the caecum contents of pigs. *Arch Virol,* 143**,** 1215-21.

SUGIEDA, M. & NAKAJIMA, S. 2002. Viruses detected in the caecum contents of healthy pigs representing a new genetic cluster in genogroup II of the genus "Norwalk-like viruses". *Virus Res,* 87**,** 165-72.

SUKHRIE, F. H., TEUNIS, P., VENNEMA, H., COPRA, C., THIJS BEERSMA, M. F., BOGERMAN, J. & KOOPMANS, M. 2012. Nosocomial transmission of norovirus is mainly caused by symptomatic cases. *Clin Infect Dis,* 54**,** 931-7.

SUMMA, M., VON BONSDORFF, C. H. & MAUNULA, L. 2012. Pet dogs--a transmission route for human noroviruses? *J Clin Virol,* 53**,** 244-7.

SUMMERS, K. L., HOCK, B. D., MCKENZIE, J. L. & HART, D. N. 2001. Phenotypic characterization of five dendritic cell subsets in human tonsils. *Am J Pathol,* 159**,** 285-95.

TACKET, C. O., SZTEIN, M. B., LOSONSKY, G. A., WASSERMAN, S. S. & ESTES, M. K. 2003. Humoral, mucosal, and cellular immune responses to oral Norwalk virus-like particles in volunteers. *Clin Immunol,* 108**,** 241-7.

TAKANASHI, S., SAIF, L. J., HUGHES, J. H., MEULIA, T., JUNG, K., SCHEUER, K. A. & WANG, Q. 2014. Failure of propagation of human norovirus in intestinal epithelial cells with microvilli grown in three-dimensional cultures. *Arch Virol,* 159**,** 257-66.

TAKESHITA, S., KAJI, K. & KUDO, A. 2000. Identification and characterization of the new osteoclast progenitor with macrophage phenotypes being able to differentiate into mature osteoclasts. *Journal of Bone and Mineral Research,* 15**,** 1477-1488.

TAM, C. C. & O'BRIEN, S. J. 2016. Economic Cost of Campylobacter, Norovirus and Rotavirus Disease in the United Kingdom. *PLoS One,* 11**,** e0138526.

TAM, C. C., RODRIGUES, L. C., VIVIANI, L., DODDS, J. P., EVANS, M. R., HUNTER, P. R., GRAY, J. J., LETLEY, L. H., RAIT, G., TOMPKINS, D. S., O'BRIEN, S. J. & COMMITTEE, I. I. D. S. E. 2012. Longitudinal study of infectious intestinal disease in the UK (IID2 study): incidence in the community and presenting to general practice. *Gut,* 61**,** 69-77.

TAMURA, M., NATORI, K., KOBAYASHI, M., MIYAMURA, T. & TAKEDA, N. 2000. Interaction of recombinant norwalk virus particles with the 105-kilodalton cellular binding protein, a candidate receptor molecule for virus attachment. *J Virol,* 74**,** 11589-97.

TAMURA, M., NATORI, K., KOBAYASHI, M., MIYAMURA, T. & TAKEDA, N. 2004. Genogroup II noroviruses efficiently bind to heparan sulfate proteoglycan associated with the cellular membrane. *J Virol,* 78**,** 3817-26.

TAN, M., HEGDE, R. S. & JIANG, X. 2004. The P domain of norovirus capsid protein forms dimer and binds to histo-blood group antigen receptors. *J Virol,* 78**,** 6233-42.

TAN, M. & JIANG, X. 2005a. Norovirus and its histo-blood group antigen receptors: an answer to a historical puzzle. *Trends Microbiol,* 13**,** 285-93.

TAN, M. & JIANG, X. 2005b. The p domain of norovirus capsid protein forms a subviral particle that binds to histo-blood group antigen receptors. *J Virol,* 79**,** 14017-30.
TAN, M. & JIANG, X. 2008. Association of histo-blood group antigens with susceptibility to norovirus infection may be strain-specific rather than genogroup dependent. *J Infect Dis,* 198**,** 940-1; author reply 942-3.
TAN, M. & JIANG, X. 2011. Norovirus-host interaction: multi-selections by human histo-blood group antigens. *Trends Microbiol,* 19**,** 382-8.
TAN, M. & JIANG, X. 2014. Histo-blood group antigens: a common niche for norovirus and rotavirus. *Expert Rev Mol Med,* 16**,** e5.
TAN, M., XIA, M., CAO, S., HUANG, P., FARKAS, T., MELLER, J., HEGDE, R. S., LI, X., RAO, Z. & JIANG, X. 2008. Elucidation of strain-specific interaction of a GII-4 norovirus with HBGA receptors by site-directed mutagenesis study. *Virology,* 379**,** 324-34.
TAUBE, S., KOLAWOLE, A. O., HOHNE, M., WILKINSON, J. E., HANDLEY, S. A., PERRY, J. W., THACKRAY, L. B., AKKINA, R. & WOBUS, C. E. 2013. A mouse model for human norovirus. *MBio,* 4.
TAUBE, S., KURTH, A. & SCHREIER, E. 2005. Generation of recombinant norovirus-like particles (VLP) in the human endothelial kidney cell line 293T. *Arch Virol,* 150**,** 1425-31.
TAUBE, S., PERRY, J. W., MCGREEVY, E., YETMING, K., PERKINS, C., HENDERSON, K. & WOBUS, C. E. 2012. Murine noroviruses bind glycolipid and glycoprotein attachment receptors in a strain-dependent manner. *J Virol,* 86**,** 5584-93.
TAUBE, S., PERRY, J. W., YETMING, K., PATEL, S. P., AUBLE, H., SHU, L., NAWAR, H. F., LEE, C. H., CONNELL, T. D., SHAYMAN, J. A. & WOBUS, C. E. 2009. Ganglioside-linked terminal sialic acid moieties on murine macrophages function as attachment receptors for murine noroviruses. *J Virol,* 83**,** 4092-101.
TE, H. S., RANDALL, G. & JENSEN, D. M. 2007. Mechanism of action of ribavirin in the treatment of chronic hepatitis C. *Gastroenterol Hepatol (N Y),* 3**,** 218-25.
TEUNIS, P. F., SUKHRIE, F. H., VENNEMA, H., BOGERMAN, J., BEERSMA, M. F. & KOOPMANS, M. P. 2015. Shedding of norovirus in symptomatic and asymptomatic infections. *Epidemiol Infect,* 143**,** 1710-7.
THACKRAY, L. B., DUAN, E., LAZEAR, H. M., KAMBAL, A., SCHREIBER, R. D., DIAMOND, M. S. & VIRGIN, H. W. 2012. Critical role for interferon regulatory factor 3 (IRF-3) and IRF-7 in type I interferon-mediated control of murine norovirus replication. *J Virol,* 86**,** 13515-23.
THACKRAY, L. B., WOBUS, C. E., CHACHU, K. A., LIU, B., ALEGRE, E. R., HENDERSON, K. S., KELLEY, S. T. & VIRGIN, H. W. T. 2007. Murine noroviruses comprising a single genogroup exhibit biological diversity despite limited sequence divergence. *J Virol,* 81**,** 10460-73.
THORNE, L., BAILEY, D. & GOODFELLOW, I. 2012. High-resolution functional profiling of the norovirus genome. *J Virol,* 86**,** 11441-56.
THORNE, L. G. & GOODFELLOW, I. G. 2014. Norovirus gene expression and replication. *J Gen Virol,* 95**,** 278-91.
THORNHILL, T. S., KALICA, A. R., WYATT, R. G., KAPIKIAN, A. Z. & CHANOCK, R. M. 1975. Pattern of shedding of the Norwalk particle in stools during experimentally induced gastroenteritis in volunteers as determined by immune electron microscopy. *J Infect Dis,* 132**,** 28-34.
THORVEN, M., GRAHN, A., HEDLUND, K. O., JOHANSSON, H., WAHLFRID, C.,

LARSON, G. & SVENSSON, L. 2005. A homozygous nonsense mutation (428G-->A) in the human secretor (FUT2) gene provides resistance to symptomatic norovirus (GGII) infections. *J Virol,* 79**,** 15351-5.

TIAN, P., BRANDL, M. & MANDRELL, R. 2005. Porcine gastric mucin binds to recombinant norovirus particles and competitively inhibits their binding to histo-blood group antigens and Caco-2 cells. *Lett Appl Microbiol,* 41**,** 315-20.

TIAN, P., ENGELBREKTSON, A. L., JIANG, X., ZHONG, W. & MANDRELL, R. E. 2007. Norovirus recognizes histo-blood group antigens on gastrointestinal cells of clams, mussels, and oysters: a possible mechanism of bioaccumulation. *J Food Prot,* 70**,** 2140-7.

TIEW, K. C., HE, G., ARAVAPALLI, S., MANDADAPU, S. R., GUNNAM, M. R., ALLISTON, K. R., LUSHINGTON, G. H., KIM, Y., CHANG, K. O. & GROUTAS, W. C. 2011. Design, synthesis, and evaluation of inhibitors of Norwalk virus 3C protease. *Bioorg Med Chem Lett,* 21**,** 5315-9.

TOMOV, V. T., OSBORNE, L. C., DOLFI, D. V., SONNENBERG, G. F., MONTICELLI, L. A., MANSFIELD, K., VIRGIN, H. W., ARTIS, D. & WHERRY, E. J. 2013. Persistent enteric murine norovirus infection is associated with functionally suboptimal virus-specific CD8 T cell responses. *J Virol,* 87**,** 7015-31.

TRESSET, G., DECOUCHE, V., BRYCHE, J. F., CHARPILIENNE, A., LE COEUR, C., BARBIER, C., SQUIRES, G., ZEGHAL, M., PONCET, D. & BRESSANELLI, S. 2013a. Unusual self-assembly properties of Norovirus Newbury2 virus-like particles. *Arch Biochem Biophys,* 537**,** 144-52.

TRESSET, G., LE COEUR, C., BRYCHE, J. F., TATOU, M., ZEGHAL, M., CHARPILIENNE, A., PONCET, D., CONSTANTIN, D. & BRESSANELLI, S. 2013b. Norovirus capsid proteins self-assemble through biphasic kinetics via long-lived stave-like intermediates. *J Am Chem Soc,* 135**,** 15373-81.

TROEGER, H., LODDENKEMPER, C., SCHNEIDER, T., SCHREIER, E., EPPLE, H. J., ZEITZ, M., FROMM, M. & SCHULZKE, J. D. 2009. Structural and functional changes of the duodenum in human norovirus infection. *Gut,* 58**,** 1070-7.

TROUPLIN, V., BOUCHERIT, N., GORVEL, L., CONTI, F., MOTTOLA, G. & GHIGO, E. 2013. Bone marrow-derived macrophage production. *J Vis Exp***,** e50966.

TSE, H., CHAN, W. M., LAM, C. S., LAU, S. K., WOO, P. C. & YUEN, K. Y. 2012. Complete genome sequences of novel rat noroviruses in Hong Kong. *J Virol,* 86**,** 12435-6.

TU, E. T., BULL, R. A., GREENING, G. E., HEWITT, J., LYON, M. J., MARSHALL, J. A., MCIVER, C. J., RAWLINSON, W. D. & WHITE, P. A. 2008. Epidemics of gastroenteritis during 2006 were associated with the spread of norovirus GII.4 variants 2006a and 2006b. *Clin Infect Dis,* 46**,** 413-20.

TURCIOS-RUIZ, R. M., AXELROD, P., ST JOHN, K., BULLITT, E., DONAHUE, J., ROBINSON, N. & FRISS, H. E. 2008. Outbreak of necrotizing enterocolitis caused by norovirus in a neonatal intensive care unit. *J Pediatr,* 153**,** 339-44.

UEDA, H., TAJIRI, H., KIMURA, S., ETANI, Y., HOSOI, G., MARUYAMA, T., NOMA, H., KUSUMOTO, Y., TAKANO, T., BABA, Y. & NAGAI, T. 2015. Clinical characteristics of seizures associated with viral gastroenteritis in children. *Epilepsy Res,* 109**,** 146-54.

UEDA, T., WATANABE-FUKUNAGA, R., FUKUYAMA, H., NAGATA, S. & FUKUNAGA, R. 2004. Mnk2 and Mnk1 are essential for constitutive and inducible phosphorylation of eukaryotic initiation factor 4E but not for cell growth or development. *Mol Cell Biol,* 24**,** 6539-49.

URBANUCCI, A., MYRMEL, M., BERG, I., VON BONSDORFF, C. H. & MAUNULA, L. 2009. Potential internalisation of caliciviruses in lettuce. *Int J Food Microbiol,* 135**,** 175-8.
VAN BEEK, J., AMBERT-BALAY, K., BOTTELDOORN, N., EDEN, J. S., FONAGER, J., HEWITT, J., IRITANI, N., KRONEMAN, A., VENNEMA, H., VINJE, J., WHITE, P. A., KOOPMANS, M. & NORONET 2013. Indications for worldwide increased norovirus activity associated with emergence of a new variant of genotype II.4, late 2012. *Euro Surveill,* 18**,** 8-9.
VAN BEEK, J., VAN DER EIJK, A. A., FRAAIJ, P. L., CALISKAN, K., CRANSBERG, K., DALINGHAUS, M., HOEK, R. A., METSELAAR, H. J., ROODNAT, J., VENNEMA, H. & KOOPMANS, M. P. 2017. Chronic norovirus infection among solid organ recipients in a tertiary care hospital, the Netherlands, 2006-2014. *Clin Microbiol Infect,* 23**,** 265 e9-265 e13.
VAN DE WETERING, M., SANCHO, E., VERWEIJ, C., DE LAU, W., OVING, I., HURLSTONE, A., VAN DER HORN, K., BATLLE, E., COUDREUSE, D., HARAMIS, A. P., TJON-PON-FONG, M., MOERER, P., VAN DEN BORN, M., SOETE, G., PALS, S., EILERS, M., MEDEMA, R. & CLEVERS, H. 2002. The beta-catenin/TCF-4 complex imposes a crypt progenitor phenotype on colorectal cancer cells. *Cell,* 111**,** 241-50.
VAN DER FLIER, L. G. & CLEVERS, H. 2009. Stem cells, self-renewal, and differentiation in the intestinal epithelium. *Annu Rev Physiol,* 71**,** 241-60.
VASHIST, S., BAILEY, D., PUTICS, A. & GOODFELLOW, I. 2009. Model systems for the study of human norovirus Biology. *Future Virol,* 4**,** 353-367.
VASHIST, S., URENA, L., CHAUDHRY, Y. & GOODFELLOW, I. 2012a. Identification of RNA-protein interaction networks involved in the norovirus life cycle. *J Virol,* 86**,** 11977-90.
VASHIST, S., URENA, L., GONZALEZ-HERNANDEZ, M. B., CHOI, J., DE ROUGEMONT, A., ROCHA-PEREIRA, J., NEYTS, J., HWANG, S., WOBUS, C. E. & GOODFELLOW, I. 2015. Molecular chaperone Hsp90 is a therapeutic target for noroviruses. *J Virol,* 89**,** 6352-63.
VASHIST, S., URENA, L. & GOODFELLOW, I. 2012b. Development of a strand specific real-time RT-qPCR assay for the detection and quantitation of murine norovirus RNA. *J Virol Methods,* 184**,** 69-76.
VAZQUEZ, A. L., ALONSO, J. M. & PARRA, F. 2000. Mutation analysis of the GDD sequence motif of a calicivirus RNA-dependent RNA polymerase. *J Virol,* 74**,** 3888-91.
VERHOEF, L., HEWITT, J., BARCLAY, L., AHMED, S. M., LAKE, R., HALL, A. J., LOPMAN, B., KRONEMAN, A., VENNEMA, H., VINJE, J. & KOOPMANS, M. 2015. Norovirus genotype profiles associated with foodborne transmission, 1999-2012. *Emerg Infect Dis,* 21**,** 592-9.
VILDEVALL, M., GRAHN, A., OLIVER, S. L., BRIDGER, J. C., CHARPILIENNE, A., PONCET, D., LARSON, G. & SVENSSON, L. 2010. Human antibody responses to bovine (Newbury-2) norovirus (GIII.2) and association to histo-blood group antigens. *J Med Virol,* 82**,** 1241-6.
VINJE, J. 2015. Advances in laboratory methods for detection and typing of norovirus. *J Clin Microbiol,* 53**,** 373-81.
VIPOND, I. B., BARKER, J., BLOOMFIELD, S. F. & CAUL, E. O. 2002. Molecular epidemiology for detecting Norwalk-like viruses in clinical cases and associated environment contamination. *J Hosp Infect,* 50**,** 237-8.
VIVANCOS, R., KEENAN, A., SOPWITH, W., SMITH, K., QUIGLEY, C., MUTTON, K., DARDAMISSIS, E., NICHOLS, G., HARRIS, J., GALLIMORE, C.,

VERHOEF, L., SYED, Q. & REID, J. 2010. Norovirus outbreak in a cruise ship sailing around the British Isles: investigation and multi-agency management of an international outbreak. *J Infect,* 60**,** 478-85.
VONGPUNSAWAD, S., VENKATARAM PRASAD, B. V. & ESTES, M. K. 2013. Norwalk Virus Minor Capsid Protein VP2 Associates within the VP1 Shell Domain. *J Virol,* 87**,** 4818-25.
WAKITA, T. 2009. Isolation of JFH-1 strain and development of an HCV infection system. *Methods Mol Biol,* 510**,** 305-27.
WALSH, D. & MOHR, I. 2004. Phosphorylation of eIF4E by Mnk-1 enhances HSV-1 translation and replication in quiescent cells. *Genes Dev,* 18**,** 660-72.
WALSH, D., PEREZ, C., NOTARY, J. & MOHR, I. 2005. Regulation of the translation initiation factor eIF4F by multiple mechanisms in human cytomegalovirus-infected cells. *J Virol,* 79**,** 8057-64.
WANG, X., XU, F., LIU, J., GAO, B., LIU, Y., ZHAI, Y., MA, J., ZHANG, K., BAKER, T. S., SCHULTEN, K., ZHENG, D., PANG, H. & SUN, F. 2013. Atomic model of rabbit hemorrhagic disease virus by cryo-electron microscopy and crystallography. *PLoS Pathog,* 9**,** e1003132.
WARD, V. K., MCCORMICK, C. J., CLARKE, I. N., SALIM, O., WOBUS, C. E., THACKRAY, L. B., VIRGIN, H. W. T. & LAMBDEN, P. R. 2007. Recovery of infectious murine norovirus using pol II-driven expression of full-length cDNA. *Proc Natl Acad Sci U S A,* 104**,** 11050-5.
WATERS, A., COUGHLAN, S. & HALL, W. W. 2007. Characterisation of a novel recombination event in the norovirus polymerase gene. *Virology,* 363**,** 11-4.
WEERAWARNA, P. M., KIM, Y., GALASITI KANKANAMALAGE, A. C., DAMALANKA, V. C., LUSHINGTON, G. H., ALLISTON, K. R., MEHZABEEN, N., BATTAILE, K. P., LOVELL, S., CHANG, K. O. & GROUTAS, W. C. 2016. Structure-based design and synthesis of triazole-based macrocyclic inhibitors of norovirus protease: Structural, biochemical, spectroscopic, and antiviral studies. *Eur J Med Chem,* 119**,** 300-18.
WEI, C., FARKAS, T., SESTAK, K. & JIANG, X. 2008. Recovery of infectious virus by transfection of in vitro-generated RNA from tulane calicivirus cDNA. *J Virol,* 82**,** 11429-36.
WESTHOFF, T. H., VERGOULIDOU, M., LODDENKEMPER, C., SCHWARTZ, S., HOFMANN, J., SCHNEIDER, T., ZIDEK, W. & VAN DER GIET, M. 2009. Chronic norovirus infection in renal transplant recipients. *Nephrol Dial Transplant,* 24**,** 1051-3.
WHITE, L. J., BALL, J. M., HARDY, M. E., TANAKA, T. N., KITAMOTO, N. & ESTES, M. K. 1996. Attachment and entry of recombinant Norwalk virus capsids to cultured human and animal cell lines. *J Virol,* 70**,** 6589-97.
WHITE, P. A. 2014. Evolution of norovirus. *Clin Microbiol Infect,* 20**,** 741-5.
WOBUS, C. E., KARST, S. M., THACKRAY, L. B., CHANG, K. O., SOSNOVTSEV, S. V., BELLIOT, G., KRUG, A., MACKENZIE, J. M., GREEN, K. Y. & VIRGIN, H. W. 2004. Replication of Norovirus in cell culture reveals a tropism for dendritic cells and macrophages. *PLoS Biol,* 2**,** e432.
WOLF, S., REETZ, J., HOFFMANN, K., GRUNDEL, A., SCHWARZ, B. A., HANEL, I. & OTTO, P. H. 2012. Discovery and genetic characterization of novel caliciviruses in German and Dutch poultry. *Arch Virol,* 157**,** 1499-507.
WOLF, S., REETZ, J. & OTTO, P. 2011. Genetic characterization of a novel calicivirus from a chicken. *Arch Virol,* 156**,** 1143-50.
WOODE, G. N. & BRIDGER, J. C. 1978. Isolation of small viruses resembling astroviruses and caliciviruses from acute enteritis of calves. *J Med Microbiol,*

11, 441-52.
WOODWARD, J., GKRANIA-KLOTSAS, E. & KUMARARATNE, D. 2017. Chronic norovirus infection and common variable immunodeficiency. *Clin Exp Immunol,* 188, 363-370.
WU, H. M., FORNEK, M., SCHWAB, K. J., CHAPIN, A. R., GIBSON, K., SCHWAB, E., SPENCER, C. & HENNING, K. 2005. A norovirus outbreak at a long-term-care facility: the role of environmental surface contamination. *Infect Control Hosp Epidemiol,* 26, 802-10.
WYATT, R. G., GREENBERG, H. B., DALGARD, D. W., ALLEN, W. P., SLY, D. L., THORNHILL, T. S., CHANOCK, R. M. & KAPIKIAN, A. Z. 1978. Experimental infection of chimpanzees with the Norwalk agent of epidemic viral gastroenteritis. *J Med Virol,* 2, 89-96.
XI, J. N., GRAHAM, D. Y., WANG, K. N. & ESTES, M. K. 1990. Norwalk virus genome cloning and characterization. *Science,* 250, 1580-3.
YAN, W. W., CUI, Z. Z. & WANG, Y. K. 2005. [Study on the self-assembly ability of expressed capsid protein of rabbit haemorrhagic disease virus that fused with foreign epitope at the N-terminus]. *Wei Sheng Wu Xue Bao,* 45, 62-5.
YU, G., ZHANG, D., GUO, F., TAN, M., JIANG, X. & JIANG, W. 2013. Cryo-EM structure of a novel calicivirus, Tulane virus. *PLoS One,* 8, e59817.
YUMIKETA, Y., NARITA, T., INOUE, Y., SATO, G., KAMITANI, W., OKA, T., KATAYAMA, K., SAKAGUCHI, T. & TOHYA, Y. 2016. Nonstructural protein p39 of feline calicivirus suppresses host innate immune response by preventing IRF-3 activation. *Vet Microbiol,* 185, 62-7.
YUNUS, M. A., CHUNG, L. M., CHAUDHRY, Y., BAILEY, D. & GOODFELLOW, I. 2010. Development of an optimized RNA-based murine norovirus reverse genetics system. *J Virol Methods,* 169, 112-8.
YUNUS, M. A., LIN, X., BAILEY, D., KARAKASILIOTIS, I., CHAUDHRY, Y., VASHIST, S., ZHANG, G., THORNE, L., KAO, C. C. & GOODFELLOW, I. 2015. The murine norovirus core subgenomic RNA promoter consists of a stable stem-loop that can direct accurate initiation of RNA synthesis. *J Virol,* 89, 1218-29.
ZABOROWSKA, I. & WALSH, D. 2009. PI3K signaling regulates rapamycin-insensitive translation initiation complex formation in vaccinia virus-infected cells. *J Virol,* 83, 3988-92.
ZAKHOUR, M., MAALOUF, H., DI BARTOLO, I., HAUGARREAU, L., LE GUYADER, F. S., RUVOEN-CLOUET, N., LE SAUX, J. C., RUGGERI, F. M., POMMEPUY, M. & LE PENDU, J. 2010. Bovine norovirus: carbohydrate ligand, environmental contamination, and potential cross-species transmission via oysters. *Appl Environ Microbiol,* 76, 6404-11.
ZAKIKHANY, K., ALLEN, D. J., BROWN, D. & ITURRIZA-GOMARA, M. 2012. Molecular evolution of GII-4 Norovirus strains. *PLoS One,* 7, e41625.
ZAMYATKIN, D. F., PARRA, F., ALONSO, J. M., HARKI, D. A., PETERSON, B. R., GROCHULSKI, P. & NG, K. K. 2008. Structural insights into mechanisms of catalysis and inhibition in Norwalk virus polymerase. *J Biol Chem,* 283, 7705-12.
ZAMYATKIN, D. F., PARRA, F., MACHIN, A., GROCHULSKI, P. & NG, K. K. 2009. Binding of 2'-amino-2'-deoxycytidine-5'-triphosphate to norovirus polymerase induces rearrangement of the active site. *J Mol Biol,* 390, 10-6.
ZEITLER, C. E., ESTES, M. K. & VENKATARAM PRASAD, B. V. 2006. X-ray crystallographic structure of the Norwalk virus protease at 1.5-A resolution. *J Virol,* 80, 5050-8.

References

ZHANG, X. F., HUANG, Q., LONG, Y., JIANG, X., ZHANG, T., TAN, M., ZHANG, Q. L., HUANG, Z. Y., LI, Y. H., DING, Y. Q., HU, G. F., TANG, S. & DAI, Y. C. 2015. An outbreak caused by GII.17 norovirus with a wide spectrum of HBGA-associated susceptibility. *Sci Rep,* 5**,** 17687.

ZHU, S., JONES, M. K., HICKMAN, D., HAN, S., REEVES, W. & KARST, S. M. 2016. Norovirus antagonism of B-cell antigen presentation results in impaired control of acute infection. *Mucosal Immunol,* 9**,** 1559-1570.

ZHU, S., REGEV, D., WATANABE, M., HICKMAN, D., MOUSSATCHE, N., JESUS, D. M., KAHAN, S. M., NAPTHINE, S., BRIERLEY, I., HUNTER, R. N., 3RD, DEVABHAKTUNI, D., JONES, M. K. & KARST, S. M. 2013. Identification of immune and viral correlates of norovirus protective immunity through comparative study of intra-cluster norovirus strains. *PLoS Pathog,* 9**,** e1003592.

ZHU, S., WATANABE, M., KIRKPATRICK, E., MURRAY, A. B., SOK, R. & KARST, S. M. 2015. Regulation of Norovirus Virulence by the VP1 Protruding Domain Correlates with B Cell Infection Efficiency. *J Virol,* 90**,** 2858-67.

ZUBEREK, J., JEMIELITY, J., JABLONOWSKA, A., STEPINSKI, J., DADLEZ, M., STOLARSKI, R. & DARZYNKIEWICZ, E. 2004. Influence of electric charge variation at residues 209 and 159 on the interaction of eIF4E with the mRNA 5' terminus. *Biochemistry,* 43**,** 5370-9.

ZUBEREK, J., WYSLOUCH-CIESZYNSKA, A., NIEDZWIECKA, A., DADLEZ, M., STEPINSKI, J., AUGUSTYNIAK, W., GINGRAS, A. C., ZHANG, Z., BURLEY, S. K., SONENBERG, N., STOLARSKI, R. & DARZYNKIEWICZ, E. 2003. Phosphorylation of eIF4E attenuates its interaction with mRNA 5' cap analogs by electrostatic repulsion: intein-mediated protein ligation strategy to obtain phosphorylated protein. *RNA,* 9**,** 52-61.

ZUFFEREY, R., NAGY, D., MANDEL, R. J., NALDINI, L. & TRONO, D. 1997. Multiply attenuated lentiviral vector achieves efficient gene delivery in vivo. *Nat Biotechnol,* 15**,** 871-5.

Appendices

Antibodies

Antigen name	Species	Polyclonal/monoclonal	Manufacturer
MNV RdRp	rabbit	polyclonal	I. Goodfellow
MNV/NV NS3	rabbit	polyclonal	I. Goodfellow
LDV VPg	rabbit	polyclonal	I. Goodfellow
GFP N-terminal	rabbit	polyclonal	Sigma-Aldrich
IRF-3	rabbit	polyclonal	Santa Cruz
STAT1	rabbit	polyclonal	Abcam
MUC1	rabbit	polyclonal	Abcam
viperin	rabbit	polyclonal	Abcam
phospho-eIF4E	rabbit	monoclonal	Cell Signalling
eIF4E	mouse	polyclonal	Santa Cruz
actin1 (C-2)	mouse	monoclonal	Santa Cruz

Primers and probes

Primer name	Sequence	Experiment
IGUC2756	cactggatcctaaccGGttgagtgcaatggc	GII.6 F/S cloning
IGUC2757	cgacgccatcttcattcacac	
IGUC3469	tacacgccactccgcacaaacagcccgggtgatgagtcttttgtgttcacagtctcttgtcg	GII.4 L7 cloning
IGUC3470	cacaaaagactcatcacccgggctgtttgtgcggagtggcgtgtacagcattgctatc	
G1SKF	CTGCCCGAATTYGTAAATGA	GI Genotyping
G1SKR	CCAACCCARCCATTRTACA	
G2SKF	CNTGGGAGGGCGATCGCAA	GII Genotyping
G2SKR	CCRCCNGCATRHCCRTTRTACAT	
IGUC1383	AAAACGTACGGCCACCATGCTGGTCGTTCAGATGCCTTTC	FUT2 cloning
IGUC1384	AAAATCTAGATTAGTGCTTGAGTAAGGGGGACAGG	
COG1F	CGYTGGATGCGNTTYCATGA	GI qPCR
COG1R	CTTAGACGCCATCATCATTYAC	
RING1(b)-TP	FAM-AGATCGCGGTCTCCTGTCCA-TAMRA	
COG2F	CARGARBCNATGTTYAGRTGGATGAG	GII qPCR
COG2R	TCGACGCCATCTTCATTCACA	
RING2-TP	FAM-TGGGAGGGCGATCGCAATCT-TAMRA	
IGUC0963	ATGCCCTTGCGTCCATAACA	h*MUC2* qPCR
IGUC0964	ATGCCCTTGCGTCCATAACA	
IGUC0784	TTCTACAATGAGCTGCGTGTG	hACTB qPCR
IGUC0785	GGGGTGTTGAAGGTCTCAAA	
LGR5	Primer pair purchased from PrimerDesign	*LGR5* qPCR
ALPI	Primer pair purchased from PrimerDesign	*ALPI* qPCR
IGIC1076	GTTTTCCATCTCGCCTCGAAACGCACCAGGTGAAATACTGTTTGATTTGG	MNV-1 L1 cloning
IGIC1077	CCAAATCAAACAGTATTTCACCTGGTGCGTTTCGAGGCGAGATGGAAAAC	
IGIC1078	CCACATGTCATGTGTGATGTGCGCCAACTGGAGCCCATTCAACTCCC	MNV-1 L5 cloning
IGIC1079	GGGAGTTGAATGGGCTCCAGTTGGCGCACATCACACATGACATGTGG	
IGIC1080	GCATGCTGTACACGCCACTCCGCGCCAACAACGCCGGTGAGGATGTGTTTACGGTCTCTGGCCGCCTTCTTTCTAAGCCG	

IGIC1081	CGGCTTAGAAAGAAGGCGGCCAGAGACCGTAAACACATCC TCACCGGCGTTGTTGGCGCGGAGTGGCGTGTACAGCATGC	MNV-1 L7 cloning
IGUC1979	GTTTTCCATTTCACCCCGAAACGCACCAGGTGAAATACTG TTTGATTTGG	MNV-3 L1 cloning
IGUC1980	CCAAATCAAACAGTATTTCACCTGGTGCGTTTCGGGGTGA AATGGAAAAC	
IGUC2014	GTCATGTGTGATGTGCGCCAACTGGAGCCCATTCAACTTC CC	MNV-3 L5 cloning
IGUC2015	GGGAAGTTGAATGGGCTCCAGTTGGCGCACATCACACATG AC	
IGUC1981	GCATGTTGTACACGCCACTCCGCGCCAACAACGCCGGTGA GGATGTGTTTACGGTCTCTGGCCGCCTTCTTTCTAAGCCG	MNV-3 L7 cloning
IGUC1982	CGGCTTAGAAAGAAGGCGGCCAGAGACCGTAAACACATCC TCACCGGCGTTGTTGGCGCGGAGTGGCGTGTACAACATGC	
IGUC1889	ACTTCGTCTCACATGAGGATGAGCGACGGCGCAGCGCCAA AAGCC	MNV-1 SD cloning
IGUC1890	CACCCTCGAGTCTCTCTATGGGGGGAGTTAGG	
IGUC1891	CACCCTCGAGCTATCTCTCTATGGGGGGAGTTAGG	
IGUC2993	GCAATGCAAGTCGAAATGTG	4E KI genotyping
IGUC2994	TTTGAAATTGGTTTGTAAAGTTGG	
IGUC0339	ATGAACAACAGGTGGATCCTCC	m*Ifnb* qPCR
IGUC0340	AGGAGCTCCTGACATTTCCGAA	
IGUC1904	GAAGTTCCTCTCTGCAAGAGACTTCCATC	m*Il6* qPCR
IGUC1905	CAACTCTTTTCTCATTTCCACGATTTCCC	
IGUC1898	GGTTCAAGGACTATGGGGAGTATTTGGAC	m*Viperin* qPCR
IGUC1899	GAAATCTTTCTGCTTCCCTCAGGGCATC	
IGUC1902	GGTAACGATTTCCTGGTGTCCG	m*Isg15* qPCR
IGUC1903	GCTCAGCCAGAACTGGTCTTCG	
IGUC0945	CATGGCCTTCCGTGTTCCTA	m*Gapdh* qPCR
IGUC0946	GCGGCACGTCAGATCCA	
MNV-S	CCGCAGGAACGCTCAGCAG	MNV qPCR
MNV-AS	GGYTGAATGGGGACGGCCTG	
MNV-TP	FAM-ATGAGTGATGGCGCA-TAMRA	

Selected publications

Virus Evolution, 2016, 2(1): vew016

doi: 10.1093/ve/vew016
Rapid Communication

Rapid outbreak sequencing of Ebola virus in Sierra Leone identifies transmission chains linked to sporadic cases

Armando Arias,[1,#,†] Simon J. Watson,[2,#] Danny Asogun,[3,4,#] Ekaete Alice Tobin,[3,4,#] Jia Lu,[1,#] My V. T. Phan,[2,#] Umaru Jah,[5] Raoul Emeric Guetiya Wadoum,[5] Luke Meredith,[1] Lucy Thorne,[1] Sarah Caddy,[1] Alimamy Tarawalie,[5] Pinky Langat,[2] Gytis Dudas,[6] Nuno R. Faria,[7] Simon Dellicour,[7] Abdul Kamara,[8] Brima Kargbo,[8] Brima Osaio Kamara,[8] Sahr Gevao,[8] Daniel Cooper,[9] Matthew Newport,[9] Peter Horby,[10] Jake Dunning,[10] Foday Sahr,[11] Tim Brooks,[12] Andrew J.H. Simpson,[12] Elisabetta Groppelli,[12] Guoying Liu,[13] Nisha Mulakken,[13] Kate Rhodes,[13] James Akpablie,[14] Zabulon Yoti,[14] Margaret Lamunu,[14] Esther Vitto,[14] Patrick Otim,[14] Collins Owilli,[14] Isaac Boateng,[14] Lawrence Okoror,[15] Emmanuel Omomoh,[3,4] Jennifer Oyakhilome,[3,4] Racheal Omiunu,[3,4] Ighodalo Yemisis,[3,4] Donatus Adomeh,[3,4] Solomon Ehikhiametalor,[3,4] Patience Akhilomen,[3,4] Chris Aire,[3,4] Andreas Kurth,[4,16] Nicola Cook,[4,17] Jan Baumann,[4,18] Martin Gabriel,[4,18] Roman Wölfel,[4,19] Antonino Di Caro,[4,20,‡] Miles W. Carroll,[4,17] Stephan Günther,[4,18] John Redd,[21] Dhamari Naidoo,[14] Oliver G. Pybus,[7,§] Andrew Rambaut,[6,22,23,**] Paul Kellam,[2,24,*,††] Ian Goodfellow,[1,5,*] and Matthew Cotten[2,*]

[1]Division of Virology, Department of Pathology, University of Cambridge, Cambridge, United Kingdom, [2]Wellcome Trust Sanger Institute, Hinxton, United Kingdom, [3]Irrua Specialist Teaching Hospital, Institute of Lassa Fever Research and Control, Irrua, Nigeria, [4]The European Mobile Laboratory Consortium, Bernhard Nocht Institute for Tropical Medicine, Hamburg, Germany, [5]University of Makeni, Makeni, Sierra Leone, [6]Institute of Evolutionary Biology, Ashworth Laboratories, Edinburgh, United Kingdom, [7]Department of Zoology, University of Oxford, Oxford, UK, [8]Sierra Leone Ministry of Health, Freetown, Sierra Leone, [9]International Medical Corps, Los Angeles, CA, USA, [10]Department of Medicine, Epidemic Diseases Research Group Oxford (ERGO), Centre for Tropical Medicine and Global Health Nuffield, University of Oxford, Oxford,

United Kingdom, [11]Republic of Sierra Leone Armed Forces, Freetown, Sierra Leone, [12]Rare and Imported Pathogens Laboratory, Public Health England, United Kingdom, [13]Thermo Fisher Scientific, South San Francisco, CA, USA, [14]WHO Ebola Response Team, Geneva, Switzerland, [15]Federal University, Oye-Ekit, Nigeria, [16]Robert Koch Institute, Berlin, Germany, [17]Public Health England, Porton Down, United Kingdom, [18]Bernhard Nocht Institute for Tropical Medicine, Hamburg, Germany, [19]Bundeswehr Institute of Microbiology, Munich, Germany, [20]National Institute for Infectious Diseases "L. Spallanzani", Rome, Italy, [21]Sierra Leone and Division of Global Health Protection, CDC Country Office, Georgia Center for Global Health Centers for Disease Control and Prevention, Atlanta, GA, USA, [22]Fogarty International Center, NIH, Bethesda, MD, USA, [23]Infection and Evolution, Centre for Immunology, Ashworth Laboratories, Edinburgh, United Kingdom and [24]Division of Infection and Immunity, University College London, London, United Kingdom

[#]These authors are joint first authors.
* Corresponding authors. E-mail: pk5@sanger.ac.uk (P.K.), ig299@cam.ac.uk (I.G.), or mc13@sanger.ac.uk (M.C.)
[†]http://orcid.org/0000-0002-4138-4608
[‡]http://orcid.org/0000-0001-6027-3009
[§]http://orcid.org/0000-0002-8797-2667
[**]http://orcid.org/0000-0003-4337-3707
[††]http://orcid.org/0000-0003-3166-4734

Abstract

To end the largest known outbreak of Ebola virus disease (EVD) in West Africa and to prevent new transmissions, rapid epidemiological tracing of cases and contacts was required. The ability to quickly identify unknown sources and chains of transmission is key to ending the EVD epidemic and of even greater importance in the context of recent reports of Ebola virus (EBOV) persistence in survivors. Phylogenetic analysis of complete EBOV genomes can provide important information on the source of any new infection. A local deep sequencing facility was established at the Mateneh Ebola Treatment Centre in central Sierra Leone. The facility included all wetlab and computational resources to rapidly process EBOV diagnostic samples into full genome sequences. We produced 554 EBOV genomes from EVD cases across Sierra Leone. These genomes provided a detailed description of EBOV evolution and facilitated phylogenetic tracking of new EVD cases. Importantly, we show that linked genomic and epidemiological data can not only support contact tracing but also identify unconventional transmission chains involving body fluids, including semen. Rapid EBOV genome sequencing, when linked to epidemiological information and a comprehensive database of virus sequences across the outbreak, provided a powerful tool for public health epidemic control efforts.

Key words: Ebola virus; evolution; transmission; outbreak sequencing.

1. Introduction

Starting in December 2013, West Africa experienced the largest known outbreak of Ebola virus disease (EVD). Sierra Leone was the most widely affected country, with 14,124 cases and 3,956 confirmed deaths as of 21 February 2016 (WHO 2016). In the absence of large-scale vaccination and effective antiviral drugs, controlling the epidemic and maintaining the zero transmission status have relied on rapid patient identification and isolation, contact tracing and quarantine, as well as the implementation of safe burial practices (Kucharski et al. 2015; Nouvellet et al. 2015; Fang et al. 2016).

By January 2015, the decline in new cases in the three most-affected countries (Sierra Leone, Guinea, and Liberia) suggested that epidemiological containment efforts were succeeding, particularly in Liberia which was initially declared free of EVD by the WHO on 9 May 2015 (WHO 2015). However, the recurrence of EVD in Liberia (WHO 2015) and Sierra Leone (WHO 2016) indicated that sources of new infections remained; even after all recognized chains of transmission had been extinguished. Worryingly, evidence is accumulating that EVD survivors may harbor and transmit EBOV for several months after recovery (Deen et al. 2015; Christie et al. 2015; Mate et al. 2015; Blackley et al. 2016; Sow et al. 2016; Uyeki et al. 2016) raising the possibility that transmission through exposure to bodily fluids and/or sexual transmission can occur at times beyond the standard quarantine periods.

To facilitate the use of phylogenetics for tracing virus transmission, a local EBOV sequencing facility was established in a tent at the Ebola Treatment Centre in Makeni, Sierra Leone. The facility provided local capacity for rapid real-time sequencing of EBOV genomes directly from clinical samples and contributed important information on the transmission pathways of EBOV.

2. Methods

2.1. Samples

Samples were collected from patients being cared for in Ebola isolation and treatment centers in Makeni (Bombali district),

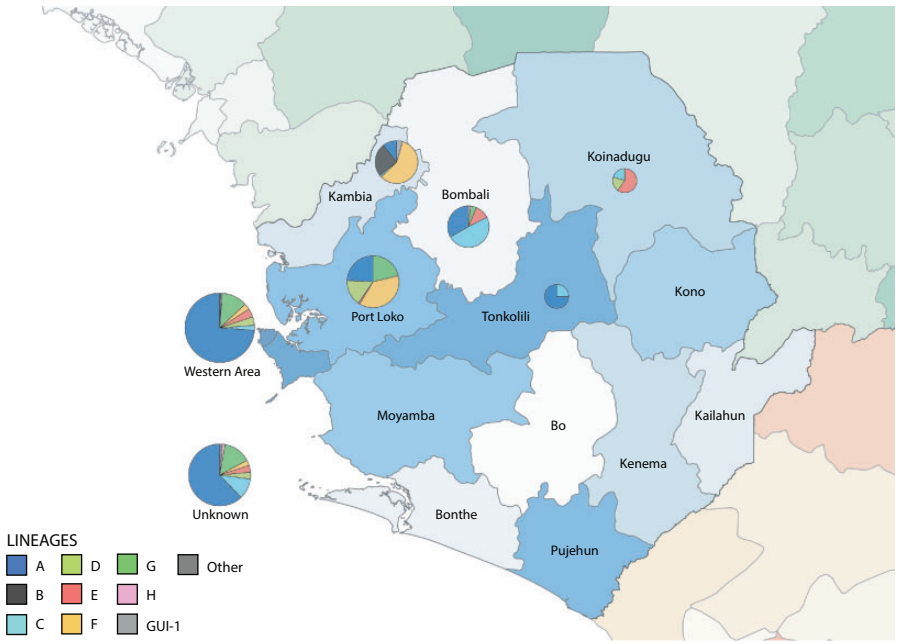

Figure 1. Lineages circulating in sampled regions. Districts of Sierra Leone (blue), Guinea (green), and Liberia (orange) are indicated. Pie charts are drawn over districts from which samples of this study were collected, with size relative to the number of samples, and segment area indicating the proportion of lineages (as defined in Figure 2) observed at that location. The number of genomes from each location was the following: Bombali: 63, Kambia: 67, Koinadugu: 5, Port Loko: 98, Tonkolili: 4, Western Area: 182, Unknown location: 135.

Port Loko (Port Loko district), Kambia district, Kerrytown (Western Urban district), and Koinadugu district (see Fig. 1, sample details are summarized in Supplementary Table 1). The study was conducted in compliance with principles expressed in the Declaration of Helsinki, and ethical approvals for the use of residual diagnostic samples for sequencing were obtained from the Sierra Leone Ethics and Scientific Review Committee and the Ministry of Health of Sierra Leone. The Sierra Leone Ethics and Scientific Review Committee approved the use of diagnostic leftover samples collected by EMLab and corresponding patient data for this study.

2.2. Logistics

Equipment and reagents for the establishment of the sequencing facility were initially shipped to the University of Cambridge, Cambridge, UK, for testing and repacking prior to transport to Makeni, Sierra Leone. These materials included reagents for sequencing, unassembled benches, PCR cabinets, centrifuges, general molecular biology reagents, N_2 canisters (required for Ion Torrent sequencing), and the equipment required to perform the sequencing workflow, namely an Ion Chef liquid handling robot and an Ion Torrent PGM sequencer. The Ion Torrent PGM sequencer and Chef were unpacked, installed and tested in Cambridge by the users with the aid of a Thermo Fisher Scientific engineer. Calibration sequencing runs were performed to ensure the required reagents and equipment functioned correctly, prior to repacking and transfer to East Midlands Airport for transport to Makeni via UK Department for International Development-funded humanitarian aid flights. The equipment arrived in Makeni on 15 April 2015 and was installed in a lined, air-conditioned tent in the Mateneh Ebola treatment centre (ETC) in Makeni, Bombali district, adjacent to the Public Health England (PHE) operated diagnostic facility. The sequencing facility was operational from 16 April 2015 and the first data files were transferred to the UK on 20 April 2015.

2.3. Sample preparation and sequencing

Total nucleic acid extracts were prepared from plasma obtained from collected blood samples or buccal swabs using either the Qiagen EZ-1 automated nucleic acid purification platform or the QIAamp manual RNA extraction procedure. Samples were tested for the presence of EBOV RNA using as previously described (Trombley et al. 2010) and were considered positive if Ct values were <40. Nucleic acid extracts from EBOV PCR-positive samples were then subjected to reverse transcription/PCR amplification using the Thermo Fisher Scientific Ion Ampliseq workflow according to the protocol manufacturer with EBOV specific reagents and the Ion Torrent sequencing platform. Following nucleic acid isolation, all subsequent procedures were performed within physically separated PCR cabinets dedicated for either reagent preparation or sample manipulations, with a 30 min UV treatment cycle between uses. Briefly, 5–7 μl of nucleic acid extract were reverse transcribed using the VILO reverse transcriptase kit (Life Technologies) in a total volume of 10 μl. Following reverse transcription, PCR amplification of the EBOV cDNA was performed with two multiplex PCR reactions: pool 1 containing 73 EBOV-specific primer pairs and five human housekeeping gene controls and pool 2 containing 72 EBOV-specific primer pairs and the same five human housekeeping gene controls. The amplicon sizes range from 80 to 237 bp (see Supplementary Table 2 for primer sequences and mapping positions). Following PCR amplification, primer sequences were removed from the amplicons and barcoded adapters ligated according to the protocol of the manufacturer. Amplicon purification and size selection were performed with the AMPure DNA purification system, followed by library quantification by qPCR using the Ion Library Quantitation Kit. Libraries were normalized

to 85 pM, combined in pools of 10–24 samples per pool and template libraries were prepared using the Ion PGM Hi-Q Sequencing Kit on an Ion Chef Instrument (Thermo Fisher Scientific). Libraries were subsequently sequenced on the Ion PGM System using Ion Torrent Hi-Q sequencing reagents (500 cycles).

2.4. Data handling and genomes assembly

Short read sets were processed to remove short and low quality reads, terminal primers were removed and the reads were sorted to retain reads with length >125 nt and median Phred score > 30 using QUASR (Watson et al. 2013). Chimeric reads were resolved using a Python script and the final reads were processed by *de novo* assembly using SPAdes 3.5.0 (Bankevich et al. 2012). EBOV contigs were further assembled into complete genomes (if not already complete) using Sequencher v5.3 (Gene Codes Corporation, USA). Conflicts were resolved by direct counting of the motif in the short read data set. Further details of the genome assembly process are included in the Supplementary material.

2.5. Phylogenetic methods

All available EBOV Makona genomes were downloaded from the NCBI Ebolavirus Resource (NCBI 2016). These 1019 genomes were combined with the 554 new genomes generated here, and aligned manually using the AliView alignment editor (Larsson 2014). A maximum-likelihood phylogenetic tree was inferred from this alignment using RAxML version 7.8.6 (Stamatakis 2014) under a general time reversible (GTR) substitution model, with among-site heterogeneity modelled using a 4-category discrete approximation of a gamma distribution, as previously described (Gire et al. 2014; Ladner et al. 2015). Robustness of the tree topology was assessed by bootstrap analysis of 1,000 pseudo-replicates, with support values for the topology calculated using the SumTrees program version 4.0.0 of the DendroPy package version 4.0.0 (Sukumaran and Holder 2010). The tree was rooted on the Gueckedou-C05 genome (GenBank accession no. KJ660348) and visualised using FigTree version 1.4.2 (http://tree.bio.ed.ac.uk/software/figtree/).

From this tree, the well-supported clades were identified, including the previously determined SL3 introduction into Sierra Leone. Viruses derived from the SL3 introduction that were isolated in Sierra Leone were extracted from the alignment. These did not include those that were derived from a re-importation of the virus from another country (e.g. Lineage B, which was derived from a reintroduction from Guinea). A molecular clock phylogenetic tree was inferred from these 1058 genomes using a Bayesian Markov chain Monte Carlo (MCMC) approach implemented in BEAST version 1.8.2 (Drummond et al. 2012). The alignment was partitioned into a concatenated coding region, containing the protein-coding sequences of the *NP*, *vp35*, *vp40*, *GP1*, *GP2*, *vp30*, *vp24*, and L genes, and a non-coding inter-genic region. The coding region was modeled under an SRD06 substitution model (Shapiro et al. 2006) to allow for partitioning of codon positions 1 + 2 and 3, while the inter-genic region was modeled under an HKY + Γ4 substitution model (Hasegawa et al. 1985), as previously applied for molecular dating of EBOV (Gire et al. 2014). The data were run under an uncorrelated log-normal relaxed molecular clock (Drummond et al. 2006), and a non-parametric Bayesian Skygrid coalescent model (Gill et al. 2013). Ten independent chains were run for a combined total of at least 30 million states, then combined after burn-in. Burn-in values were determined for each chain separately after checking for convergence using Tracer version 1.6 (http://tree.bio.ed.ac.uk/software/tracer/). The posterior tree sets were combined using LogCombiner version 1.8.2, then summarised as a maximum clade credibility tree using TreeAnnotator version 1.8.2. This tree was visualised using FigTree version 1.4.2.

3. Results and discussion

We produced 554 contemporary EBOV genome sequences from 855 EVD samples (64% success rate) collected in Sierra Leone between December 2014 and September 2015. PCR-positive EBOV samples were provided by EBOV diagnostic field laboratories (PHE Makeni, PHE Port Loko, PHE Kerrytown, EML Hastings, EML Kambia), collected primarily from the northern and western districts of Sierra Leone (Fig. 1, Supplementary Table 1), reflecting EVD case locations during this period (WHO 2016). Genomes were successfully obtained from blood, buccal swabs, semen and breast milk with successful genome yield dependent on EBOV reads of greater than 10,000 (Supplementary Fig. 1). The sequenced genomes represent 4.5% of the EVD cases reported for Sierra Leone, and 23.8% of all 2015 Sierra Leone cases (see Supplementary Fig. 2) and provide a detailed description of EBOV evolution during 2015. From these data we identified sources of infection for some of the final EVD cases in Sierra Leone and indicate potential routes of sexual and breast milk transmissions.

This was an unconventional use of new sequencing technology under harsh conditions (high temperature, dust, high humidity, unreliable power supplies, complicated reagent transport, in a tent). Accordingly, special care was taken to ensure that the sequencing process was reproducible and consistent with EBOV sequencing results obtained by other groups. Furthermore, we provided quantitative data on the level of residual primer content from the amplicon sequencing method and the potential level of sample cross contamination under the sequencing conditions used (see Supplementary material).

Evolutionary analysis of the complete set of EBOV Makona genomes revealed that at least nine viral lineages were circulating in Sierra Leone (Fig. 2). Eight of these lineages (A–H) were derived from the SL3 variant that emerged in Sierra Leone in June 2014 (Park et al. 2015) and became the most prevalent lineage (Tong et al. 2015). The remaining viruses were derived from a separate introduction into Sierra Leone of the GUI-1 lineage from Guinea (Simon-Loriere et al. 2015). By June 2015, reported EVD cases were from infections by only three viral lineages A, E, and F (Supplementary Fig. 3). The majority of these cases arose from two separate outbreaks: one with lineage F viruses that occurred primarily in the Port Loko and Kambia districts (80 genomes), and the other from lineage A viruses that were identified primarily in the Magazine Wharf area of Freetown in the Western Urban district (39 genomes). Both these outbreaks persisted for over a month, with the phylogenetic analyses revealing movement of the virus to surrounding districts. This virus movement was observed across the entire Sierra Leone outbreak, with viruses from all lineages except B and C found in more than one district (Supplementary Fig. 3).

The Ebola Outbreak Sequencing Support (EOSS) was established in July 2015 as a coordinated effort from the Sierra Leone Ministry of Health, WHO, CDC and the local sequencing facility to rapidly sequence all new Sierra Leone EVD cases and rapidly place them in phylogenetic context. EOSS processed 21 samples from July-September 2015 (median 4 days, range 1–12 days, Supplementary Fig. 4) and provided an additional level of information to field workers tracing the source of the infection. Three examples of the use of these sequence data follow.

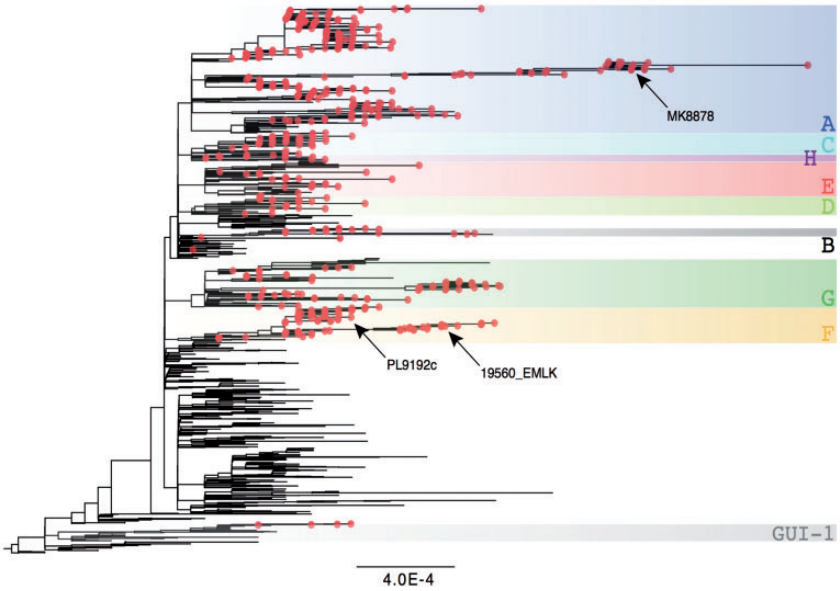

Figure 2. Maximum-likelihood tree showing the phylogenetic context of the viruses sequenced in this study. The 554 genomes generated here are shown as red circles, while the nine comprising lineages are highlighted with colored boxes and labeled A–H for those derived from the SL3 lineage, or GUI-1 for viruses derived from the divergent Guinean lineage. The tree was rooted on Gueckedou-C05 (GenBank accession no. KJ660348), with the scale bar indicating genetic distance in units of substitutions/site. Specific genomes in the three transmission vignettes (see Fig. 3), MK8878, 19560_EMLK, and PL9192c are highlighted.

An EVD cluster occurred in late June 2015 in Mamusa, Port Loko District. Case *B*, who was in the late stages of pregnancy, had been exposed to EVD in another village (Kom Brakai) and was under quarantine there. She fled quarantine and traveled to the house of her aunt (case *A*) in Mamusa (Fig. 3a). Case *B* went into labour, and died on 15 June during the birth of case *C*. Cases *B* and *C* were subsequently found to be EBOV positive. Consequently, all household contacts present at *C*'s birth were placed in quarantine, including cases *A*, *C* (*B*'s newborn daughter who died on 25 June), *D* (*B*'s sister), *E* (*A*'s 13-month old daughter), and *F* (*A*'s sister). Cases *A*, *E*, and *F* were released from quarantine on 7 July after completing their observation period without apparent illness other than red conjunctivae noted in *A* on 29 June, although no EBOV diagnostics were performed before release. Cases *E* and *F* subsequently developed symptoms of EVD on 10 July, 3 d after completing quarantine (see timeline, Fig. 3a), prompting evaluation of *A*, who remained asymptomatic. Although a blood sample from *A* was EBOV-negative on 17 July, two samples of her breast milk were EBOV-positive on 13 and 17 July (Fig. 3a). The full EBOV genome obtained from *A*'s breast milk (PL9192) was found to phylogenetically cluster with genomes from *E* (PL9150Rb) and *F* (PL9199Rb) (Fig. 3b). This cluster is strongly supported and is distinct from genomes from the earlier cases *B*, *C*, and *D*. We hypothesized three possible routes by which E was infected:

Route 1: *A*, *E*, and *F* were infected while attending *C*'s birth by direct contact with *B* or *C*.

Route 2: *A* was infected while attending C's birth. *A* transmitted the virus to *E*, through breastfeeding or direct contact; the virus was subsequently transmitted onward to *F* during quarantine due to close proximity of *F* with *A* or *E*.

Route 3: *A*, *E*, and *F* were infected by exposure to *C* or *D* during the quarantine.

If Route 1 or 3 were correct, the viruses isolated from *A*, *E*, and *F* would be more closely related to and cluster with viruses isolated from cases *B*, *C*, and *D*.

However, the viral genome isolated from *B* and the two genomes from *D* bear distinct nucleotide changes (12,485 T->C and 8,182 A->G), that were not in the genomes of viruses obtained from cases *A*, *E*, and *F*, with no evidence of mixed infections at these genome sites (results not show), suggesting a separate transmission chain. Based on these data, we therefore, concluded that transmission scenarios Routes 1 and 3 were less likely.

Although *A*'s viral genome contains a unique mutation (A8358G) not shared by any other virus, analysis of *A*'s viral reads shows that this was a polymorphic position with 65% of the reads having the G, and 35% containing the *A*. Therefore, as cases *A*, *E*, and *F* have evidence for identical viruses, and they all share a unique mutation (C1115A), they are likely to either all share a common direct ancestor (likely *B*, *C*, or *D* given the timings and locations) or one case gave rise to the others (e.g. case *A* was infected by *B*/*C*/*D* and transmitted to *E* and *F*) and the data best support Route 2.

It is important to note that given the practical difficulties of obtaining multiple samples from EVD patients and that the primary priority of field workers at that time was to contain the epidemic, further sampling of community members and additional body compartments and fluids was not performed, which could have provided clarification of the transmission route. The two EBOV-positive breast milk samples from *A*, and the fact that *E* was actively breastfed by *A* during the quarantine period, support the possibility of breast milk transmission. However, *A* and *E* also had close contact other than breastfeeding, and the lack of an earlier blood sample from *A* does not allow us to prove that transmission occurred via breast milk. Similar complexities of drawing conclusions about EBOV breast milk transmission have been reported (Moreau et al. 2015; Nordenstedt et al. 2016).

In a second cluster, on 24 July 2015, EVD case *G* was identified in a village in Tonkolili district which had been EVD-free for the previous 130 d. However, at that time, there were only three locations in Sierra Leone with on-going EBOV transmission (Magazine Wharf in Freetown, Kambia and Port Loko) in addition to cases in Guinea. Case *G* reported travel from

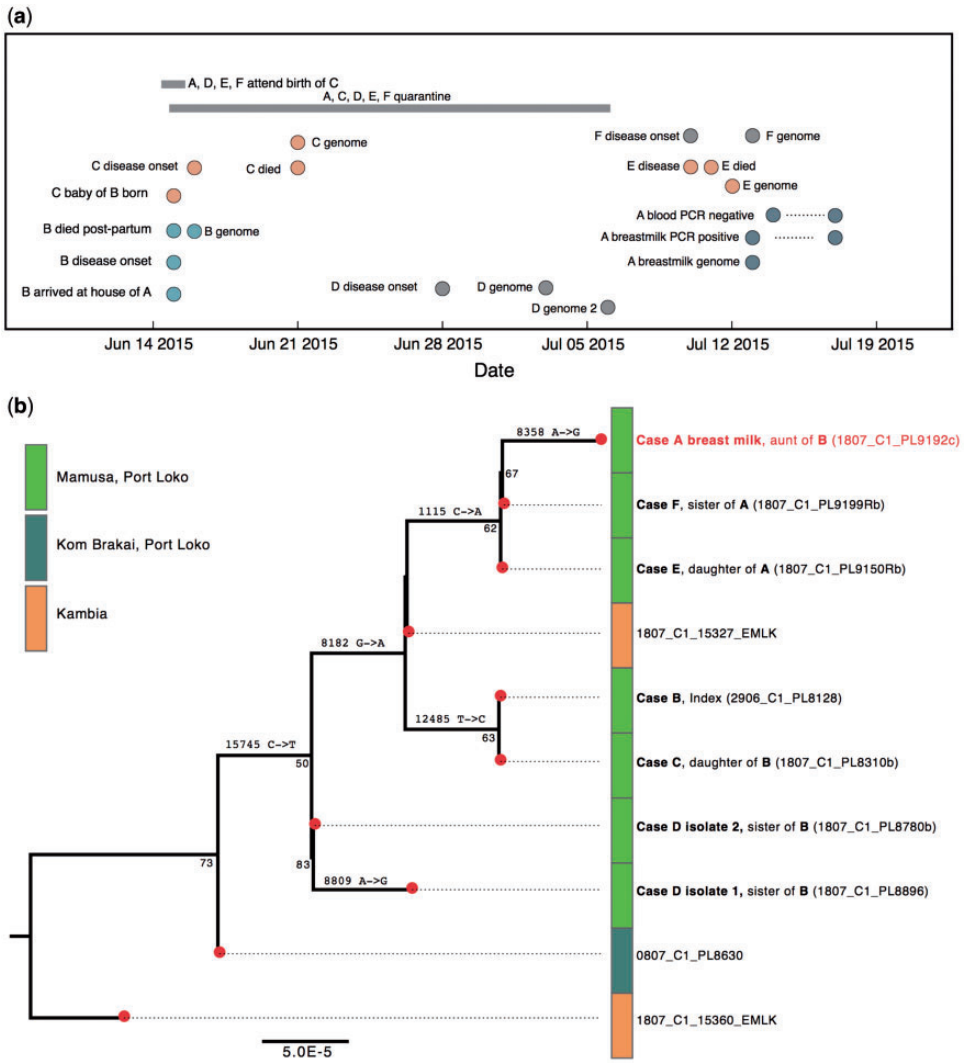

Figure 3. (a) Mamusa Cluster timeline. Key events in the Mamusa cluster examined in (b) are summarized. (b) Maximum-likelihood tree of the Mamusa cluster showing the phylogenetic relationship between each case's virus genome. The genome from the case *A* breast milk sample (PL9192, labeled in red, GenBank accession no. KU296401) is highlighted in red. Additional cases in the cluster include the earlier case *B* (most probable index case of the cluster, GenBank accession no. KU296340); case *C* (the 6 day-old newborn daughter of *B*, GenBank accession no. KU296618), and *D* (sister of *B*, includes two viruses sampled 3 d apart, GenBank accession nos. KU296404 and KU296342). Contacts of *A* include cases *E* (13 month-old daughter of *A*, GenBank accession no. KU296522) and *F* (sister of *A*, GenBank accession no. KU296371). Bootstrap support values greater than 50% are given below the respective node. The bar colors on the right indicate the place of sampling of each virus (legend is shown on the left). All mutations within the case cluster are given above the relevant branch as the position in the original alignment followed by the nucleotide change. The scale bar indicates the genetic distance in units of substitutions/site.

Freetown to Tonkolili on 16 July 2015, providing a hypothesis for EBOV appearance in Tonkolili. Phylogenetic analysis confirmed this hypothesis; the virus genome from *G* (MK8878) clustered with recent infections from Magazine Wharf and *not* with viruses from the other locations with active transmission at the time (Fig. 4 and Supplementary Fig. 3). Furthermore, genomes from two subsequent EVD cases from Tonkolili, *H* (MK10128; *G*'s brother), and *J* (MK10173; *G*'s aunt), both *G*'s caregivers, were closely related to the *G* genome expanding the transmission chain (Fig. 4). The combined data link case *G* to known infections in Magazine Wharf and exclude the possibility that this Tonkolili cluster was a re-emergence of EBOV from previous Tonkolili cases or from an unknown transmission chain.

There is accumulating evidence of EBOV sexual transmission (Deen et al. 2015; Christie et al. 2015; Mate et al. 2015; Blackley et al. 2016; Sow et al. 2016; Uyeki et al. 2016). On 29 August 2015 in the Kambia district, a post-mortem swab from case *K* tested positive for EBOV, some 50 d following the last confirmed case in this district. The viral genome from case *K* (020380_EMLK) clustered with a genome from case *L* from a blood sample collected on 7 July 2015 (19560R_EMLK, Fig. 5a). Case *L* was an EVD survivor, who was released from quarantine on 18 July 2015 and subsequently had sexual contact with *K* during August 2015. *L* provided a semen sample on 7 September 2015 from which an EBOV genome was obtained (19560_EMLK). The viral genome obtained from *L*'s semen was identical to the virus genome in *L*'s initial blood sample, collected 2 months earlier during acute EVD (Fig. 5a). The clustering of genomes from case *L* with those from *K*, and from several secondary contacts of *K* (cases *N*, *O*, *P*, and *Q*) indicates transmission among these cases in Kambia (Fig. 5a). In addition, the absence of nucleotide changes between the virus genomes of the two *L* samples suggests that the virus was maintained in a low replicating state within *L*. Consistent with this pattern, reduced

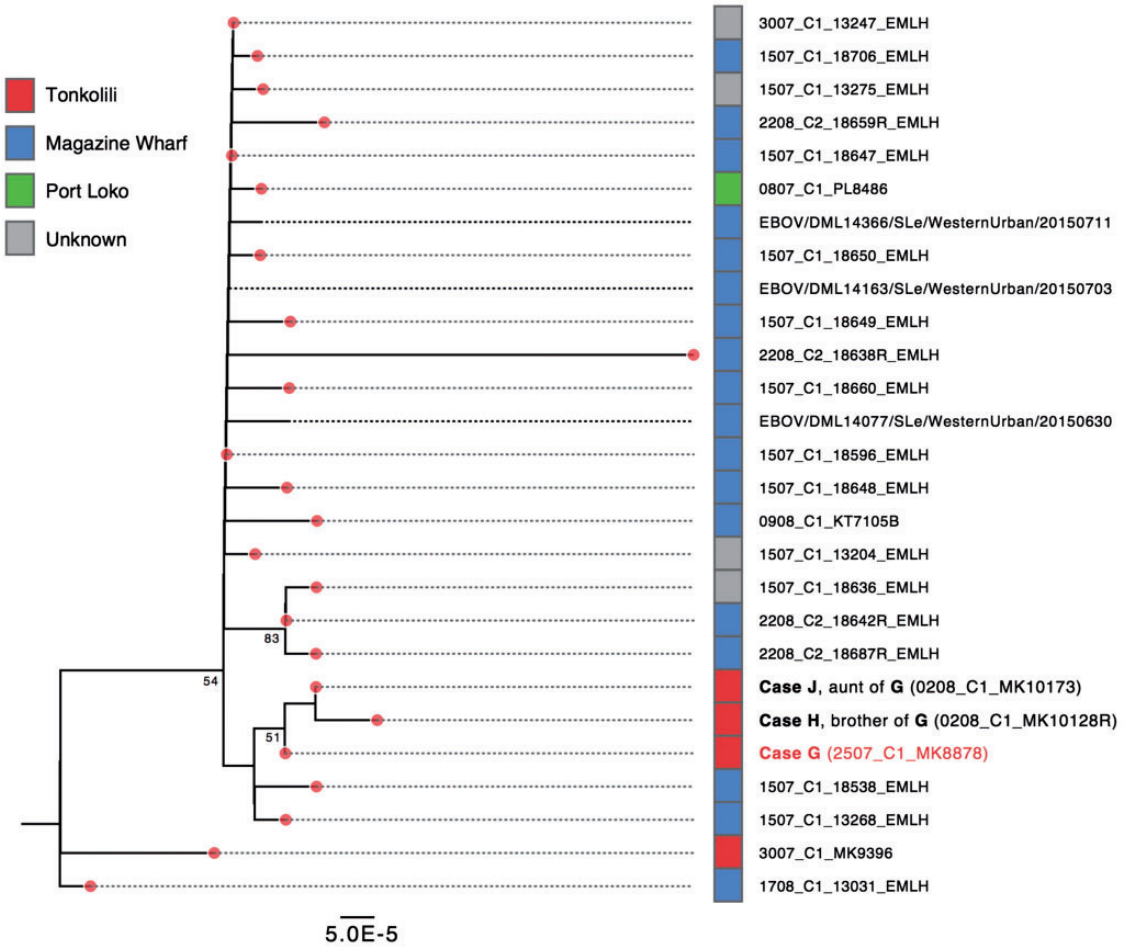

Figure 4. Maximum-likelihood tree showing that the Tonkolili case derived from the Magazine Wharf lineage. The Tonkolili index case *G* (MK8878, labeled in red, GenBank accession no. KU296684) was derived from a clade of viruses circulating predominantly in Magazine Wharf, and clusters with the two secondary Tonkolili secondary cases *H* (*G*'s brother, GenBank accession no. KU296502) and *J* (*G*'s aunt, GenBank accession no. KU296313). See legend of Fig. 3(a) for additional figure details.

virus evolutionary rate after virus re-emergence was also recently reported (Blackley et al. 2016). Furthermore, at three positions in the virus genome (3,993, 8,494 and 13,518), minority variants were present in the *K* and *M* read sets that show a transition between the majority nucleotide in *L* and the majority nucleotide in the viruses later in the putative transmission chain (Fig. 5b). Thus mixed nucleotide variants at three positions in *L*'s semen virus genome were consistent with *L* as the direct source of virus for *K* and *M*.

An alternate transmission route might be contact of *K* with unknown EVD cases in the community. However, such a hypothesis would require that the virus in this unidentified contact was as close, or more closely related to the viruses sequenced from the known cases, which had only three nucleotide differences between L and K. Alternately, transmission from *L* to *K* could have occurred via non-sexual contact or with other body fluids; however, given that *L*'s blood was negative but *L*'s semen was genome positive, between these two possibilities semen is the more likely source of *K*'s infection. There was no report of sexual contact between L and M, so tentatively M might have been infected from L's bodily fluid or while taking care of K. However, the phylogenetic analysis strongly supports viral transmission between these cases (Fig. 5a), with sexual transmission from *L* to *K* as the most likely component in the transmission chain.

The local sequencing described here was rapid enough to be epidemiologically useful; however, a comprehensive genome database across the outbreak was essential to identify sources of new infections. During the course of this project, the sequence data that were generated contributed more than a third of the 1500 EBOV Makona genomes now available and represent 23.8% of the 2015 Sierra Leone cases (see Supplementary Fig. 2). These data were made available to all groups involved in outbreak sequencing (Goodfellow et al. 2015a,b; Neher and Bedford 2015) and yielded a sufficiently comprehensive set of viral genomes to identify transmission chains in other countries and across borders (Gardy et al. 2015).

In future epidemics, rapid and local sequencing of pathogens at the onset and the end of the outbreak can support outbreak investigation and control, but sequencing and data sharing during peak transmission should also be maintained to provide the genetic context for contact tracing and control of new cases. With the increasing global risk of viral zoonosis, the success of this project provides a strong incentive to establish and maintain local sequencing facilities throughout the world.

Acknowledgments

The authors would like to thank the Public Health England diagnostic teams deployed to staff the laboratories in

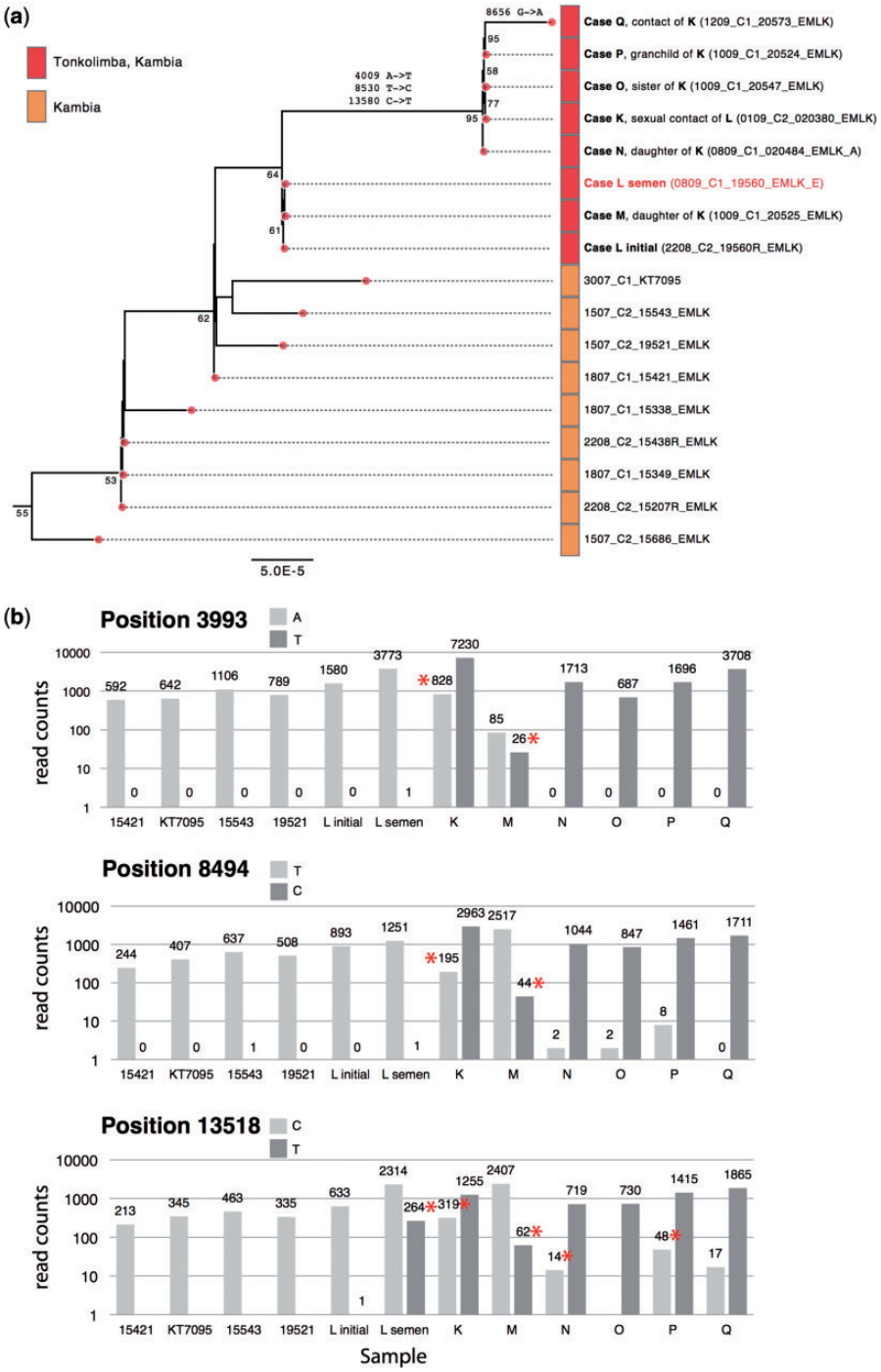

Figure 5. (a) Maximum-likelihood tree showing the Kambia cluster with possible sexual transmission and full genome from a semen sample. The virus from case *L*'s initial acute sample (19560R_EMLK, GenBank accession no. KU296580) is the most probable index case of the Kambian cluster. After a 21-d period of quarantine, case *L* was discharged on 18 July 2015. A sample from case *L*'s semen (19560_EMLK, labeled in red, GenBank accession no. KU296821) was collected on 7 September 2015. The virus genome isolated from the deceased case *K* (020380_EMLK, GenBank accession no. KU296775) is genetically identical to case *L*, which also clusters closely with case *M* (*K*'s 23-year-old daughter, 20525_EMLK, GenBank accession no. KU296487). For each cluster case, minority variants for three key positions can be found in (b). Symptom onset of case *M* (3 September 2015) was 15 d later than onset of case *K* (26 August 2015). Case *K* is genetically identical to three known contacts of *K*: case *N* (020484_EMLK, older daughter of *K*, GenBank accession no. KU296462), case *O* (20547_EMLK, sister of *K*, GenBank accession no. KU296455), case *P* (20524_EMLK, grandchild of K, GenBank accession no. KU296424). Case *Q* (20573_EMLK, GenBank accession no. KU296654), also from the same village, is the most recent sampled case from this cluster. The lineage is related to earlier viruses from lineage F (19521_EMLK, 15543_EMLK, KT7095, and 15421_EMLK, see Fig. 2). See legend of Fig. 3(b) for additional figure details. (b) Minor variants in the Kambia lineage. In genomes from the Kambia cluster (a) three genome positions (3993, 8494, and 13518) showed changes across the entire lineage leading from 19521 through to all genomes in the family cluster. The presence of each of the two variant nucleotides was counted in the raw read set for each sample to gain additional information about possible transmission patterns. Positions with minor variants at >1% frequency are marked with a red asterisk. Positions 3994, 8496, and 13520 showed mixed nucleotides in samples from cases *K* and *M*, similar to the case *L* semen sample (but not in the case *L* initial sample). Later cases in the lineage (*N*–*Q*) showed predominately one of the variants at each of the three positions, although position 13520 showed some persistence of the minor variant C. These data further support the phylogenetic conclusions based on the consensus genome sequence with the *L* semen sample containing minor variants at the three positions that increase in frequency in samples from cases *K* and *M* and become the dominant nucleotide in cases *N*–*Q*.

Kerrytown, Port Loko and Makeni for their dedicated contribution to the processing and identification of EBOV positive samples. The UK Department for International Development funded the PHE diagnostic laboratories and provided logistic support. The authors would also like to thank Deb Walsh (University of Cambridge), members of the Goodfellow laboratory at the Division of Virology, University of Cambridge, and Cathy Styles, Florence Pethick, Andrew Gaze, and Andrew Felton (Thermo Fisher Scientific) for their support. We thank Nick Loman for sharing MinION sequence data. Funding for this work includes Wellcome Trust Grants 098051 to P.K., 097997/Z/11/A and 097997/Z/11/Z to I.G. and 106491/Z/14/Z to P.H., EU [FP7/2007-2013] Grant Agreement no. 278433-PREDEMICS to A.R., and a Wellcome Trust Strategic Award (VIZIONS; 093724). This publication presents independent research supported by the Health Innovation Challenge Fund T5-344 (ICONIC), a parallel funding partnership between the Department of Health and Wellcome Trust and the COMPARE project Funded by the European Union's Horizon 2020 research and innovation programme under Grant agreement no. 643476. The work of EMLab was supported by the European Commission, Directorate-General for International Cooperation and Development (Contract IFS/2011/272-372 "EMLab"). The views expressed in this publication are those of the author(s) and not necessarily those of the Department of Health or Wellcome Trust and do not necessarily represent the official position of the US Centers for Disease Control and Prevention.

Author information

The 554 new EBOV genomes are deposited in GenBank (accession nos. KU296293–KU296846) and the short read data can be accessed under the study Accession no. SRP068607.

Conflict of interest: None declared.

Supplementary data

Supplementary data are available at *Virus Evolution* online.

References

Bankevich, A., et al. (2012) 'SPAdes: A New Genome Assembly Algorithm and Its Applications to Single-Cell Sequencing', *Journal of Computational Biology*, 19/5: 455–77

Blackley, D. J., et al. (2016) 'Reduced Evolutionary Rate in Reemerged Ebola Virus Transmission Chains', *Science Advances*, 2/4: e1600378. DOI: 10.1126/sciadv.1600378.

Christie, A., et al. (2015) 'Possible Sexual Transmission of Ebola Virus – Liberia, 2015', *MMWR Morbidity and Mortality Weekly Report*, 64/17: 479–81

Deen, G. F., et al. (2015) 'Ebola RNA Persistence in Semen of Ebola Virus Disease Survivors – Preliminary Report', *New England Journal of Medicine*. DOI: 10.1056/NEJMoa1511410.

Drummond, A. J., et al. (2006) 'Relaxed Phylogenetics and Dating with Confidence', *PLoS Biology*, 4/5: e88

——, et al. (2012) 'Bayesian Phylogenetics with BEAUti and the BEAST 1.7', *Molecular Biology and Evolution*, 29/8: 1969–73

Fang, L. Q., et al. (2016) 'Transmission Dynamics of Ebola Virus Disease and Intervention Effectiveness in Sierra Leone', *Proceedings of the National Academy of Sciences of the United States of America*, 113/16: 4488–93

Gardy, J., Loman, N. J., and Rambaut, A. (2015) 'Real-Time Digital Pathogen Surveillance – The Time is Now', *Genome Biology*, 16: 155

Gill, M. S., et al. (2013) 'Improving Bayesian Population Dynamics Inference: A Coalescent-Based Model for Multiple Loci', *Molecular Biology and Evolution*, 30/3: 713–24

Gire, S. K., et al. (2014) 'Genomic Surveillance Elucidates Ebola Virus Origin and Transmission During the 2014 Outbreak', *Science*, 345/6202: 1369–72

Goodfellow, I., et al. (2015a) Recent Evolution Patterns of Ebola Virus from December 2014–June 2015 Obtained by Direct Sequencing in Sierra Leone. http://virological.org/t/recent-evolution-patterns-of-ebola-virus-obtained-by-direct-sequencing-in-sierra-leone/150

——, et al. (2015b) Recent Evolution Patterns of Ebola Virus Inferred from Patient Samples Collected from February–May 2015 with Direct Deep Sequencing in Sierra Leone. http://virological.org/t/direct-deep-sequencing-in-sierra-leone-yields-73-new-ebov-genomes-from-february-may-2015/134.

Hasegawa, M., Kishino, H., and Yano, T. (1985) 'Dating of the Human–Ape Splitting by a Molecular Clock of Mitochondrial DNA', *Journal of Molecular Evolution*, 22/2: 160–74

Kucharski, A. J., et al. (2015) 'Measuring the Impact of Ebola Control Measures in Sierra Leone', *Proceedings of the National Academy of Sciences of the United States of America*, 112/46: 14366–71

Larsson, A. (2014) 'AliView: A Fast and Lightweight Alignment Viewer and Editor for Large Datasets', *Bioinformatics*, 30/22: 3276–8

Ladner, J. T., et al. (2015) 'Evolution and Spread of Ebola Virus in Liberia, 2014–2015', *Cell Host Microbe*, 18/6: 659–69

Mate, S. E., et al. (2015) 'Molecular Evidence of Sexual Transmission of Ebola Virus', *New England Journal of Medicine*, 373: 2448–2454

Moreau, M., et al. (2015) 'Lactating Mothers Infected with Ebola Virus: EBOV RT-PCR of Blood Only May be Insufficient', *Euro Surveillance*, 20/3:pii=21017. DOI: http://dx.doi.org/10.2807/1560-7917.ES2015.20.3.21017

NCBI Ebolavirus Resource. (2016) http://www.ncbi.nlm.nih.gov/genome/viruses/variation/ebola

Nordenstedt, H., et al. (2016) 'Ebola Virus in Breast Milk in an Ebola Virus-Positive Mother with Twin Babies, Guinea, 2015', *Emerging Infectious Diseases*, 22/4: 759–60

Neher, R. and Bedford, T. (2015) Real-Time Analysis of Ebola Virus Evolution. http://ebolanextfluorg/

Nouvellet, P., et al. (2015) 'The Role of Rapid Diagnostics in Managing Ebola Epidemics', *Nature*, 528/7580: S109–16

Park, D. J., et al. (2015) 'Ebola Virus Epidemiology, Transmission, and Evolution During Seven Months in Sierra Leone', *Cell*, 161/7: 1516–26

Shapiro, B., Rambaut, A., and Drummond, A. J. (2006) 'Choosing Appropriate Substitution Models for the Phylogenetic Analysis of Protein-Coding Sequences', *Molecular Biology and Evolution*, 23/1: 7–9

Simon-Loriere, E., et al. (2015) 'Distinct Lineages of Ebola Virus in Guinea During the 2014 West African Epidemic', *Nature*, 524/763: 102–4

Stamatakis, A. (2014) 'RAxML Version 8: A Tool for Phylogenetic Analysis and Post-Analysis of Large Phylogenies', *Bioinformatics*, 30/9: 1312–3

Sukumaran, J. and Holder, M. T. (2010) 'DendroPy: A Python Library for Phylogenetic Computing', *Bioinformatics*, 26/12: 1569–71

Sow, M. S., et al. (2016) 'New Evidence of Long-Lasting Persistence of Ebola Virus Genetic Material in Semen of Survivors'. *Journal of Infectious Diseases*. DOI: 10.1093/infdis/jiw078.

Uyeki, T. M., et al. (2016) 'Ebola Virus Persistence in Semen of Male Survivors', *Clinical Infectious Diseases: An Official Publication of the Infectious Diseases Society of America*, 62/12: 1552–1555

Tong, Y. G., et al. (2015) 'Genetic Diversity and Evolutionary Dynamics of Ebola Virus in Sierra Leone', *Nature*, 524/7563: 93–6

Trombley, A. R., et al. (2010) 'Comprehensive Panel of Real-Time TaqMan Polymerase Chain Reaction Assays for Detection and Absolute Quantification of filoviruses, Arenaviruses, and New World Hantaviruses', *The American Journal of Tropical Medicine and Hygiene*, 82/5: 954–60

Watson, S. J., et al. (2013) 'Viral Population Analysis and Minority-Variant Detection Using Short Read Next-Generation Sequencing', *Philosophical Transactions of the Royal Society B: Biological Sciences*, 368/1614: 20120205

WHO. Ebola Situation Report – 17 February 2016. http://apps.who.int/ebola/ebola-situation-reports

—— New Ebola case in Sierra Leone. (2016) WHO continues to stress risk of more flare-ups. http://www.who.int/mediacentre/news/statements/2016/new-ebola-case/en

—— Recurrence of Ebola transmission in Liberia. (2015) http://www.who.int/mediacentre/news/ebola/03-july-2015-liberia/en

——. The Ebola outbreak in Liberia is over. (2015) http://www.who.int/mediacentre/news/statements/2015/liberia-ends-ebola/en

ARTICLE

doi:10.1038/nature22040

Virus genomes reveal factors that spread and sustained the Ebola epidemic

A list of authors and their affiliations appears at the end of the paper

The 2013–2016 West African epidemic caused by the Ebola virus was of unprecedented magnitude, duration and impact. Here we reconstruct the dispersal, proliferation and decline of Ebola virus throughout the region by analysing 1,610 Ebola virus genomes, which represent over 5% of the known cases. We test the association of geography, climate and demography with viral movement among administrative regions, inferring a classic 'gravity' model, with intense dispersal between larger and closer populations. Despite attenuation of international dispersal after border closures, cross-border transmission had already sown the seeds for an international epidemic, rendering these measures ineffective at curbing the epidemic. We address why the epidemic did not spread into neighbouring countries, showing that these countries were susceptible to substantial outbreaks but at lower risk of introductions. Finally, we reveal that this large epidemic was a heterogeneous and spatially dissociated collection of transmission clusters of varying size, duration and connectivity. These insights will help to inform interventions in future epidemics.

At least 28,646 cases and 11,323 deaths[1] have been attributed to the Makona variant of Ebola virus (EBOV)[2] in the two and a half years it circulated in West Africa. The epidemic is thought to have begun in December 2013 in Guinea, but was not detected and reported until March 2014 (ref. 3). Initial efforts to control the outbreak in Guinea were considered to be succeeding[4], but in early 2014 the virus crossed international borders into the neighbouring countries Liberia (where the first cases were diagnosed in late March) and Sierra Leone (first documented case in late February[5,6], first diagnosed cases in May[7]). EBOV genomes sequenced from three patients in Guinea early in the epidemic[3] demonstrated that the progenitor of the Makona variant originated in Middle Africa and arrived in West Africa within the last 15 years[7,8]. Rapid sequencing from the first reported cases in Sierra Leone confirmed that EBOV had crossed the border from Guinea and that these cases were not the result of an independent zoonotic introduction[7]. Subsequent studies have analysed the genetic makeup of the Makona variant, focusing on Guinea[9,10,13], Sierra Leone[14,15] or Liberia[16,17], and have identified local viral lineages and transmission patterns within each country.

Although virus sequencing data have covered considerable fractions of the epidemic in each affected country, individual studies focused on either limited geographical areas or time periods, so that the regional level patterns and drivers of the epidemic across its entire duration have remained uncertain. Using 1,610 genome sequences collected throughout the epidemic, representing over 5% of recorded Ebola virus disease (EVD) cases (Extended Data Fig. 1), we reconstruct a detailed phylogenetic history of the movement of EBOV within and between the three most affected countries. Using a recently developed phylogeographic approach that integrates covariates of spatial spread[18], we test which features of each region (administrative, economic, climatic, infrastructural or demographic factors) were important in shaping the spatial dynamics of EVD. We also examine the effectiveness of international border closures on controlling virus dissemination. Finally, we investigate why regions that immediately border the most affected countries did not develop protracted outbreaks similar to those that ravaged Sierra Leone, Guinea and Liberia.

Origin, ignition and trajectory of the epidemic

Molecular clock dating indicates that the most recent common ancestor of the epidemic existed between December 2013 and February 2014 (mean, 22 Jan 2014; 95% credible interval (CI), 16 Dec 2013–20 Feb 2014) and phylogeographic estimation assigns this ancestor to the Guéckédou prefecture, Nzérékoré region, Guinea, with high credibility (Fig. 1). In addition, we find that initial EBOV lineages that were derived from this common ancestor circulated among the Guéckédou prefecture and its neighbouring prefectures of Macenta and Kissidougou until late February 2014 (Fig. 1). These results support the epidemiological evidence that the West African epidemic began in late 2013 in Guéckédou prefecture[3].

The first EBOV introduction from Guinea into another country that resulted in sustained transmission is estimated to have occurred in early April 2014 (Fig. 1), when the virus spread to the Kailahun district of Sierra Leone[5,6]. This lineage was first detected in Kailahun at the end of May 2014, from where it spread across the region (Figs 1, 2 and Extended Data Fig. 2). From Kailahun, EBOV spread very rapidly in May 2014 into several counties of Liberia (Lofa, Montserrado and Margibi)[17] and Guinea (Conakry, back into Guéckédou)[9,13]. The virus continued to spread westwards through Sierra Leone, and by July 2014 EBOV was present in the capital city, Freetown.

By mid-September 2014, Liberia was reporting more than 500 new EVD cases per week, mostly driven by a large outbreak in Montserrado county, which encompasses the capital city, Monrovia. Sierra Leone reported more than 700 new cases per week by mid-November, with large outbreaks in Port Loko, Western Urban (Freetown) and Western Rural districts (Freetown suburbs). December 2014 brought the first signs that efforts to control the epidemic in Sierra Leone were effective, as EVD incidence began to drop. By March 2015, the epidemic was largely under control in Liberia and eastern Guinea, although sustained transmission continued in the border area of western Guinea and western Sierra Leone. By the following month, prevalence had declined such that only a handful of lineages persisted[10,14] (Fig. 2).

The last EBOV genome obtained from a conventionally acquired infection was collected and sequenced in October 2015 in Forécariah prefecture (Guinea)[10]. After this, only sporadic cases of EVD were detected: in Montserrado (Liberia) in November 2015, Tonkolili (Sierra Leone) in January and February 2016, and Nzérékoré (Guinea) in March 2016. All these sporadic cases probably resulted from transmission from EVD survivors with established, persistent infections[11,12,14].

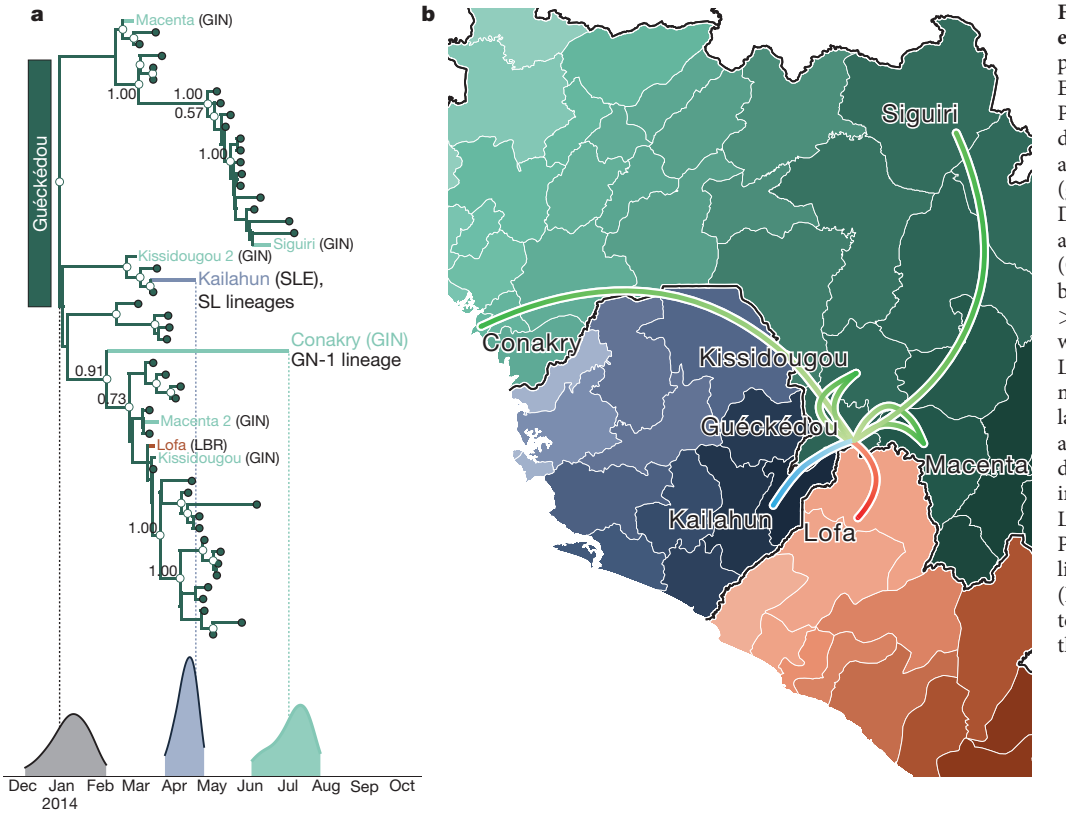

Figure 1 | Summary of early epidemic events. a, Temporal phylogeny of earliest sampled EBOV lineages in Guéckédou Prefecture, Guinea. 95% posterior densities of most recent common ancestor estimates for all lineages (grey) and lineages into Kailahun District, Sierra Leone (SLE; blue) and to Conakry Prefecture, Guinea (GIN; green) are shown at the bottom. Posterior probabilities >0.5 are shown for lineages with >5 descendent sequences. LBR, Liberia. **b**, Dispersal events marked by coloured lineages and labelled by name on the phylogeny are projected on a map with directionality indicated by colour intensity (from light to dark). Lineages that migrated to Conakry Prefecture (labelled as GN-1 lineage) and Kailahun District (labelled as SL lineages) have led to the vast majority of EVD cases throughout the region.

Factors associated with EBOV dispersal

To determine the factors that influenced the spread of EBOV among administrative regions at the district (Sierra Leone), prefecture (Guinea) and county (Liberia) levels, we used a phylogeographic generalized linear model (GLM)[18]. Of the 25 factors assessed (see Extended Data Table 1 for a full list and description), 5 were included in the model with categorical support (Table 1). In summary, EBOV tends to disperse between geographically close regions (great circle distance, Bayes factor (BF) support for inclusion: BF > 50). Half of all virus dispersals occurred between locations less than 72 km apart and only 5% involved movement over 232 km (Fig. 3a). Both origin and destination population sizes are very strongly (BF > 50) positively correlated with viral dissemination, with a stronger effect for origin population size. The positive effect of population sizes combined with the inverse effect of the geographic distance implies that the spread of the epidemic followed a classic gravity-model dynamic. Gravity models, widely used in economic and geographic studies and a natural choice for modelling infectious disease transmission[19–21], describe the movement of people between locations as a function of their population sizes and the distance that separates them. Here we use viral genomes to provide empirical evidence that such a process drove viral dissemination during the EVD epidemic.

In addition to geographical distance, we found a significant propensity for virus dispersal to occur within each country, relative to international dispersal (nat./int. effect, BF > 50), suggesting that country borders acted to curb the geographic spread of EBOV. When international dispersals do take place, they are more intense between administrative regions that are adjacent at an international border (IntBoSh, BF > 50).

We tested whether sharing of any of 17 vernacular languages explains virus spread, as common languages might reflect cultural links, including between non-contiguous or international regions, but we found no evidence that such linguistic links were correlated with EBOV spread. A variety of other possible predictors of EBOV transmission, such as aspects of urbanization (economic output, population density, travelling times to large settlements) as well as climatic effects, were not significantly associated with virus dispersal. However, these factors may have contributed to the size and longevity of transmission chains after introduction to a region (see below).

Finally, to investigate the potential of 'real-time' viral genome sequencing, we considered the degree to which the findings could have been obtained at the height of the epidemic, had sequences been available shortly after the samples were taken (see Methods for details). For the factors associated with EBOV dispersal, the results were highly comparable to those for the full dataset whereby the same five factors were strongly supported and these had similar effect sizes (Extended Data Fig. 3).

Factors associated with local EBOV proliferation

The analysis above identified predominantly geographical and administrative factors that predict the degree of importation risk, that is, the likelihood that a viral lineage initiates at least one infection in a new region. However, the epidemiological consequences of each introduction—the size and duration of resulting transmission chains—may be affected by different factors. Therefore, we investigated which demographic, economic and climatic factors might predict cumulative case counts[1] for each region (Bayesian GLM; see Methods) and found that these were associated with factors related to urbanization (Table 2): primarily population sizes (PopSize, BF = 29.6) and a significant inverse association with travel times to the nearest settlement with more than 50,000 inhabitants (TT50K, BF = 32.4). These results confirm the common perception that, in contrast to previous EVD outbreaks, widespread transmission within urban regions in West Africa was a major contributing factor to the scale of the epidemic of the Makona variant.

As the epidemic in West Africa progressed, there were fears that increased rainfall and humidity might prolong the environmental persistence of EBOV particles, increasing the likelihood of transmission[22]. Although we found no evidence of an association between EBOV dispersal and any aspects of local climate, we find that regions with less

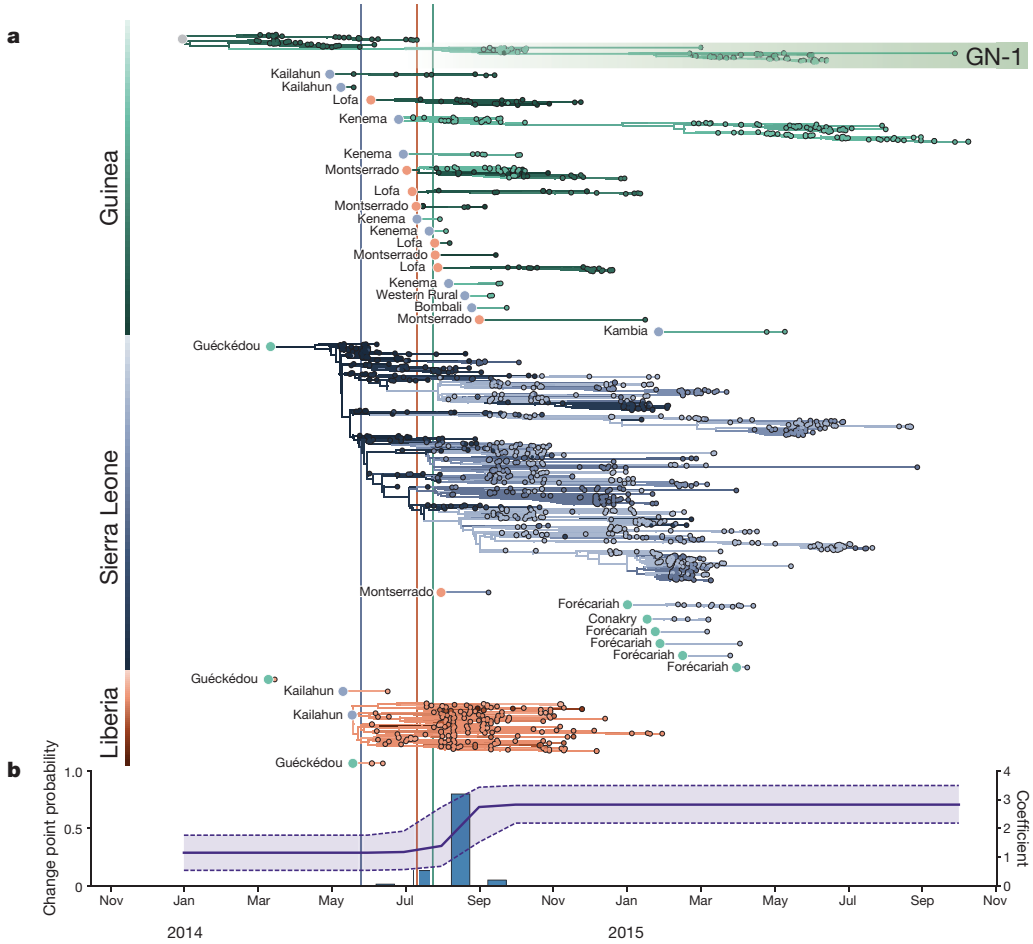

Figure 2 | Transmission chains arising from independent international movements. **a**, EBOV lineages by country (Guinea, green; Sierra Leone, blue; Liberia, red), tracked until the sampling date of their last known descendants. Circles at the roots of each subtree denote the country of origin for the introduced lineage. **b**, Estimates of the change point probability (left *y* axis) and log coefficient (mean and credible interval; right *y* axis) for the nat./int. factor. Vertical lines represent dates that border closures were announced by the respective countries.

seasonal variation in temperature, and with more rainfall, tended to have larger EVD outbreaks (TempSS, BF > 50 and Precip, BF = 4.4, respectively).

The impact of international travel restrictions

Porous borders between Liberia, Sierra Leone and Guinea may have allowed the unimpeded EBOV spread during the 2013–2016 epidemic[23–25]. Our results indicate that international borders were associated with a decreased rate of transmission events compared to national borders (Extended Data Fig. 4), but that frequent international cross-border transmission events still occurred. These events were concentrated in the Guéckédou prefecture (Guinea), Kailahun district (Sierra Leone) and Lofa county (Liberia) during the early stages of the epidemic (Extended Data Fig. 5a), and between the Forécariah prefecture (Guinea) and Kambia district (Sierra Leone) at the later stage (Extended Data Fig. 5b). These later EBOV movements hindered efforts to interrupt the final chains of transmission in late 2015, with EBOV from these chains moving back and forth across this border[10,14,26]. Sierra Leone announced border closures on 11 June 2014, followed by Liberia on 27 July 2014, and Guinea on 9 August 2014, but little information is available about what these border closures actually entailed. Although we show that the relative contribution of international spread to overall viral migration was lower after country borders were closed (mean nat./int. coefficient increasing from 1.15 to 2.83 between August and September 2014; 80.0% posterior support; (Fig. 2b)), it is difficult to ascertain whether the border closures themselves were responsible for the apparent reduction in cross-border transmissions, as opposed to concomitant control efforts or public information campaigns. However, even if border closures reduced international traffic, particularly over longer distances and between larger population centres, by the time that Sierra Leone and Liberia had closed their borders, the epidemic had become firmly established in both countries.

Table 1 | Summary of phylogenetic generalized linear model results

Predictor*	Description	Coefficient†	95% CI‡	Inclusion§	BF‖
Nat./int.	National dispersal relative to international	3.07	2.36, 3.77	1.0	>50
Distances	Great circle distances between the locations' population centroids¶	−0.77	−0.91, −0.63	1.0	>50
OrPop	Population size at the location of origin	1.36	0.86, 1.84	1.0	>50
DestPop	Population size at the destination location	0.74	0.43, 1.06	1.0	>50
IntBoSh	Two locations share an international border	3.39	2.42, 4.33	1.0	>50
OrTempSS	Index of temperature seasonality at origin	−0.47	−0.88, −0.11	0.1	3.79

*Predictors included in the model with Bayes factor >3.
†Mean coefficient.
‡95% highest posterior density credible interval (CI).
§Probability that the predictor was included in the model.
‖BF, Bayes factor.
¶Population centroids indicate the centre of a location weighted by population.

Why did the epidemic not spread further?

A few EBOV exportations were documented from Guinea by road transport into Mali and Senegal[27,28] and by air from Liberia to Nigeria and the USA[29,30]. However, apart from these limited exceptions, the West African Ebola virus epidemic did not spread into the neighbouring regions of Côte d'Ivoire, Guinea-Bissau, Mali and Senegal. By extending our GLM (the supported predictors and their estimated coefficients) to include these regions we were able to address whether

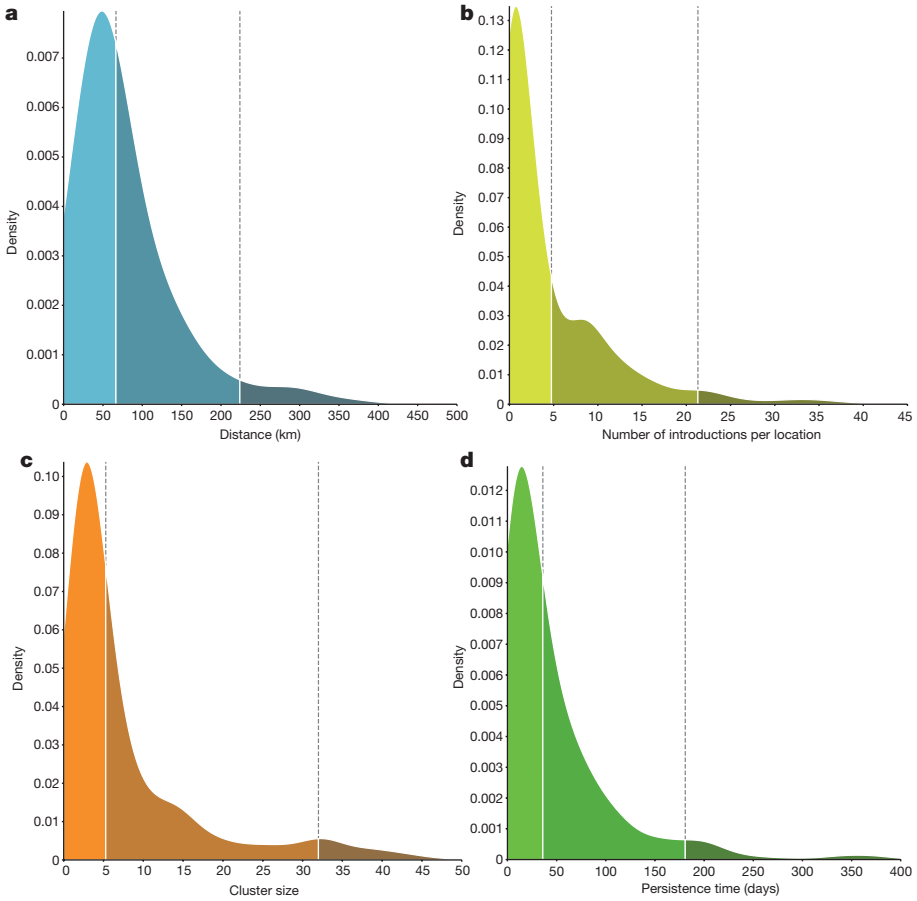

Figure 3 | The metapopulation structure of the epidemic. a, Kernel density estimate of distances associated with inferred EBOV dispersal events: 50% occur over distances <72 km and <5% occur over distances >232 km. **b**, Kernel density estimate of the number of independent EBOV introductions into each administrative region: 50% have fewer than 4.8 and <5% greater than 21.3. **c**, Kernel density estimate of the mean size of sampled cases resulting from each introduction with at least 2 sampled cases: 50% <5.3 cases, 95% <32 cases. **d**, Kernel density estimate of the persistence of clusters in days (from time of introduction to time of the last sampled case): 50% <36 days, 95% <181 days. **a**–**d**, 50% and 95% are indicated by the dashed lines.

these regions were spared EVD cases through good fortune, or because they were associated with an inherently lower risk of EBOV spread and transmission. We estimated the degree to which these, apparently EVD-free, regions had the potential to be exposed to viral introductions from affected regions (see Methods).

Overall, the contiguous regions in unaffected neighbouring countries were all predicted to have low numbers of EBOV introductions (Fig. 4a and Extended Data Fig. 6a) based on the phylogeographic history of the sampled cases. They were not, however, predicted to have particularly low levels of transmission if an outbreak had started (Fig. 4b and Extended Data Fig. 6b). Therefore, it is likely that some of these regions were at risk of becoming part of the EVD epidemic, but that their geographical distance from areas of active transmission and the attenuating effect of international borders prevented this from occurring. The Kati cercle in Mali and Tonkpi region in Côte d'Ivoire are to some extent exceptions to this general result, as these were more susceptible to EBOV introductions under the gravity model because of their large populations (1 million and 950,000, respectively) (Fig. 4a), and are predicted to have experienced many cases had EVD become established (Fig. 4b).

Table 2 | Summary of generalized linear model results with case counts as the response variable

Predictor*	Description	Coefficient†	95% CI‡	Inclusion§	BF‖
TempSS	Temperature seasonality	−1.1	−1.6, −0.5	0.83	>50
TT50K	Time to travel to a population centre of 50,000 people	−0.9	−1.4, −0.4	0.62	32.4
PopSize	Population size	0.9	0.3, 1.6	0.60	29.6
Precip	Precipitation	0.8	0.2, 1.3	0.18	4.4
TT100K	Time to travel to a population centre of 0.1 million people	−0.8	−1.7, −0.1	0.16	3.8

*Predictors included in the model with Bayes factor >3.
†Mean coefficient.
‡95% highest posterior density credible interval (CI).
§Probability that the predictor was included in the model.
‖BF, Bayes factor.

Metapopulation structure and dynamics of the epidemic

After the initial establishment of transmission in Sierra Leone and Liberia, Guinea experienced repeated reintroductions of viral lineages from disparate transmission chains from both countries (Fig. 2). Our analysis reveals that there were at least 21 (95% CI, 16–25) reintroductions into Guinea from April 2014 to February 2015. An early epidemic lineage was established around the Guinean capital, Conakry, and persisted for the duration of the epidemic (GN-1 in Figs 1, 2). However, the continual reintroduction of EBOV into Guinea without a clear peak in transmission suggests that the virus may have been failing to maintain transmission elsewhere. There were also numerous introductions into Sierra Leone over a similar time period (median, 9; 95% CI, 6–12), but the resulting transmission chains constituted a very small proportion of the country's EVD cases, with the bulk of transmission resulting from one early introduction (Fig. 2a).

In all three countries, repeated introductions into administrative regions seems to have been a large factor in the longevity of the EVD epidemic (Extended Data Fig. 7). As such, regional case numbers were generally the result of multiple overlapping introduction events followed by within-region spread and occasional onward transmission to other regions. This suggests a metapopulation model in which the persistence of the epidemic was driven by introduction into novel contact networks rather than by mass-action transmission, such as susceptible-infectious-removed dynamics[31,32]. We found that, on average, EBOV migrates between administrative regions at a rate of

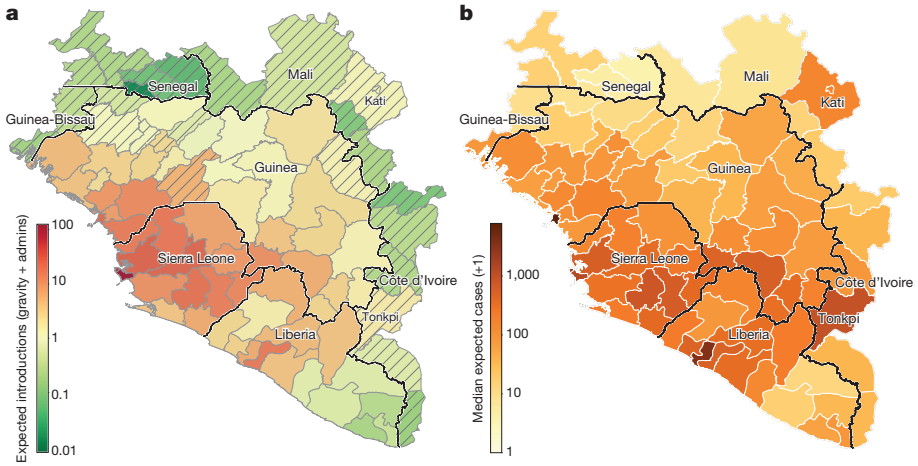

Figure 4 | Predicted destinations and consequences of viral dispersal. a, Predicted number of EBOV imports into each of the 63 regions in Guinea, Sierra Leone and Liberia (including 7 without recorded cases in Guinea) and the surrounding 18 regions of the neighbouring countries of Guinea-Bissau, Senegal, Mali and Côte d'Ivoire. The expected number of EBOV exports from locations in the phylogeographic tree and imports to any location were calculated on the basis of the phylogeographic GLM model estimates and associated predictors that were extended to apparently EVD-free locations (see Supplementary Methods). **b**, Predicted EVD cluster sizes from the Bayesian GLM fitted to case data.

0.85 events per lineage per year (95% CI, 0.72–0.97). Assuming a serial interval of 15.3 days[33], this rate translates to a 3.6% chance (95% CI, 3.0–4.1%) that over the course of a single infection, the transmission chain moved between regions. Given the key role that virus dispersal played in sustaining the epidemic, the detection and isolation of these relatively low proportions of mobile cases may have a disproportionate effect on the control of an EVD epidemic.

From our spatial phylogenetic model we conclude that many regions experienced numerous independent EBOV introductions (Fig. 3b). However, these introductions gave rise to clusters of cases that were generally small (a mean cluster size of 4.3 and only 5% larger than 17 in our sample; Fig. 3c) and of limited duration (a mean persistence time of 41.3 days with only 5% greater than 181 days; Fig. 3d). Here, we define a cluster as a group of sequenced cases in a region that derive from a single introduction event and define persistence as the time between the introduction event and the last sampled case in the cluster. These definitions are conservative regarding sampling intensity, as we expect additional samples would have split clusters apart rather than join them. Furthermore, introductions that were not detected will be disproportionately smaller, and so the cluster size estimate will be biased upwards. Segregating these observations by country (Extended Data Fig. 8 (left)) shows that districts of Sierra Leone had more introductions and that Guinea generally had smaller clusters, but that persistence was similar between the three countries. A comparison between introductions that occurred before October 2014 and those that occurred after this date shows that the number of introductions per location was comparable, whereas those that occurred early generally resulted in larger and more persistent clusters (Extended Data Fig. 8 (right)).

Therefore, with 5.8% sampling, we arrive at a conservative estimate of approximately 75 regional cases per introduction event. Although larger population centres, in particular capital cities, generally experienced more introductions (Extended Data Fig. 9a), the cluster sizes are less strongly associated with population size (Extended Data Fig. 9b), further highlighting the role of virus movement into urban areas as major factor for the high caseloads in large population centres. Frequent cluster extinction, despite a small fraction of individuals being infected, suggests that individual outbreaks were constrained by the degree of connectedness among contact networks. Thus, it appears that the West African EVD epidemic was sustained by frequent introductions that resulted in numerous small local clusters of cases, some of which went on to further seed clusters in other locations.

Viral genomics as a tool for outbreak response

The 2013–2016 EVD epidemic in West Africa has unfortunately become a costly lesson in addressing an infectious disease outbreak in the absence of preparedness of both the exposed population and the international community. Our work demonstrates the value of pathogen genome sequencing in a public healthcare emergency and the value of timely pre-publication data sharing to identify the origins of imported disease case clusters, to track pathogen transmission as the epidemic progresses, and to follow up on individual cases as the epidemic subsides.

It is inevitable that as sequencing costs decrease, accuracy increases and sequencing instruments become more portable, real-time viral surveillance and molecular epidemiology will be routinely deployed on the front lines of infectious disease outbreaks[10,14,16,34–36]. Although we have shown here that the broad pattern of EBOV spatial movement was discernible from virus genomes derived from samples collected up until October 2014 only, there was a notable hiatus in sequencing at this time[35] and the genomes in the present dataset from that time were sequenced retrospectively from archived material. The West African EVD epidemic has demonstrated that a steady sequencing pace[34–36], local sequencing capacity[10,14,16] and rapid dissemination of data[7] are key requirements in generating actionable sequence data from an infectious disease outbreak. However, as viral genome sequencing is scaled up and approaches the timescale of viral evolution, the analysis techniques will increasingly represent the bottleneck for timely communication of information for an outbreak response.

The analysis of the comprehensive EBOV genome set that was collected during the 2013–2016 EVD epidemic, including the findings presented here and in other studies[7,9,13–17,37,38], provides a framework for predicting the behaviour of future disease outbreaks caused by EBOV, other filoviruses and perhaps other human pathogens. However, many questions remain about the biology of EBOV. As sustained human-to-human transmission waned, West Africa experienced several instances of recrudescent transmission, often in regions that had not seen cases for many months as a result of persistent sub-clinical infections[11,12,39]. Although, in hindsight, such sequelae were not entirely unexpected[40], the magnitude of the 2013–2016 epidemic has put the region at ongoing risk of sporadic EVD re-emergence. Similarly, the nature of the reservoir of EBOV, and its geographic distribution, remain as fundamental gaps in our knowledge. Resolving these questions is critical to predicting the risk of zoonotic transmission and therefore of future EVD outbreaks.

Online Content Methods, along with any additional Extended Data display items and Source Data, are available in the online version of the paper; references unique to these sections appear only in the online paper.

Received 31 August 2016; accepted 2 March 2017.
Published online 12 April 2017.

1. World Health Organization. *Ebola Situation Report—10 June 2016* http://apps.who.int/iris/bitstream/10665/208883/1/ebolasitrep_10Jun2016_eng.pdf (2016).
2. Kuhn, J. H. *et al.* Nomenclature- and database-compatible names for the two Ebola virus variants that emerged in Guinea and the Democratic Republic of the Congo in 2014. *Viruses* **6,** 4760–4799 (2014).

3. Baize, S. *et al.* Emergence of Zaire Ebola virus disease in Guinea. *N. Engl. J. Med.* **371,** 1418–1425 (2014).
4. World Health Organization Regional Office for Africa. *Ebola Virus Disease, West Africa (situation as of 25 April 2014)* http://www.afro.who.int/en/clusters-a-programmes/dpc/epidemic-a-pandemic-alert-and-response/4121-ebola-virus-disease-west-africa-25-april-2014.html (2014).
5. Goba, A. *et al.* An outbreak of Ebola virus disease in the Lassa fever zone. *J. Infect. Dis.* **214,** S110–S121 (2016).
6. Sack, K., Fink, S., Belluck, P., Nossiter, A. & Berehulak, D. *How Ebola roared back* http://nyti.ms/1wwG5VX (2014).
7. Gire, S. K. *et al.* Genomic surveillance elucidates Ebola virus origin and transmission during the 2014 outbreak. *Science* **345,** 1369–1372 (2014).
8. Dudas, G. & Rambaut, A. Phylogenetic analysis of Guinea 2014 EBOV Ebolavirus outbreak. *PLoS Curr.* **6,** http://dx.doi.org/10.1371/currents.outbreaks.84eefe5ce43ec9dc0bf0670f7b8b417d (2014).
9. Carroll, M. W. *et al.* Temporal and spatial analysis of the 2014–2015 Ebola virus outbreak in West Africa. *Nature* **524,** 97–101 (2015).
10. Quick, J. *et al.* Real-time, portable genome sequencing for Ebola surveillance. *Nature* **530,** 228–232 (2016).
11. Blackley, D. J. *et al.* Reduced evolutionary rate in reemerged Ebola virus transmission chains. *Sci. Adv.* **2,** e1600378 (2016).
12. Mate, S. E. *et al.* Molecular evidence of sexual transmission of Ebola virus. *N. Engl. J. Med.* **373,** 2448–2454 (2015).
13. Simon-Loriere, E. *et al.* Distinct lineages of Ebola virus in Guinea during the 2014 West African epidemic. *Nature* **524,** 102–104 (2015).
14. Arias, A. *et al.* Rapid outbreak sequencing of Ebola virus in Sierra Leone identifies transmission chains linked to sporadic cases. *Virus Evol.* **2,** vew016 (2016).
15. Park, D. J. *et al.* Ebola virus epidemiology, transmission, and evolution during seven months in Sierra Leone. *Cell* **161,** 1516–1526 (2015).
16. Kugelman, J. R. *et al.* Monitoring of Ebola virus Makona evolution through establishment of advanced genomic capability in Liberia. *Emerg. Infect. Dis.* **21,** 1135–1143 (2015).
17. Ladner, J. T. *et al.* Evolution and spread of Ebola virus in Liberia, 2014–2015. *Cell Host Microbe* **18,** 659–669 (2015).
18. Lemey, P. *et al.* Unifying viral genetics and human transportation data to predict the global transmission dynamics of human influenza H3N2. *PLoS Pathog.* **10,** e1003932 (2014).
19. Viboud, C. *et al.* Synchrony, waves, and spatial hierarchies in the spread of influenza. *Science* **312,** 447–451 (2006).
20. Truscott, J. & Ferguson, N. M. Evaluating the adequacy of gravity models as a description of human mobility for epidemic modelling. *PLOS Comput. Biol.* **8,** e1002699 (2012).
21. Yang, W. *et al.* Transmission network of the 2014–2015 Ebola epidemic in Sierra Leone. *J. R. Soc. Interface* **12,** 20150536 (2015).
22. Fischer, R. *et al.* Ebola virus stability on surfaces and in fluids in simulated outbreak environments. *Emerg. Infect. Dis.* **21,** 1243–1246 (2015).
23. Bausch, D. G. & Schwarz, L. Outbreak of Ebola virus disease in Guinea: where ecology meets economy. *PLoS Negl. Trop. Dis.* **8,** e3056 (2014).
24. Chan, M. Ebola virus disease in West Africa—no early end to the outbreak. *N. Engl. J. Med.* **371,** 1183–1185 (2014).
25. Wesolowski, A. *et al.* Commentary: containing the Ebola outbreak—the potential and challenge of mobile network data. *PLoS Curr.* **6,** http://dx.doi.org/10.1371/currents.outbreaks.0177e7fcf52217b8b634376e2f3efc5e (2014).
26. Goodfellow, I., Reusken, C. & Koopmans, M. Laboratory support during and after the Ebola virus endgame: towards a sustained laboratory infrastructure. *Euro Surveill.* **20,** 21074 (2015).
27. World Health Organization. *Ebola Response Roadmap Situation Report Update—12 November 2014* http://apps.who.int/iris/bitstream/10665/141468/1/roadmapsitrep_12Nov2014_eng.pdf (2014).
28. Folarin, O. A. *et al.* Ebola virus epidemiology and evolution in Nigeria. *J. Infect. Dis.* **214,** S102–S109 (2016).
29. Abdoulaye, B. *et al.* Experience on the management of the first imported Ebola virus disease case in Senegal. *Pan Afr. Med. J.* **22,** 6 (2015).
30. Whitmer, S. L. M. *et al.* Preliminary evaluation of the effect of investigational Ebola virus disease treatments on viral genome sequences. *J. Infect. Dis.* **214,** S333–S341 (2016).
31. Xia, Y., Bjørnstad, O. N. & Grenfell, B. T. Measles metapopulation dynamics: a gravity model for epidemiological coupling and dynamics. *Am. Nat.* **164,** 267–281 (2004).
32. Ferrari, M. J. *et al.* The dynamics of measles in sub-Saharan Africa. *Nature* **451,** 679–684 (2008).
33. WHO Ebola Response Team. Ebola virus disease in West Africa — the first 9 months of the epidemic and forward projections. *N. Engl. J. Med.* **371,** 1481–1495 (2014).
34. Gardy, J., Loman, N. J. & Rambaut, A. Real-time digital pathogen surveillance — the time is now. *Genome Biol.* **16,** 155 (2015).
35. Yozwiak, N. L., Schaffner, S. F. & Sabeti, P. C. Data sharing: make outbreak research open access. *Nature* **518,** 477–479 (2015).
36. Woolhouse, M. E. J., Rambaut, A. & Kellam, P. Lessons from Ebola: improving infectious disease surveillance to inform outbreak management. *Sci. Transl. Med.* **7,** 307rv5 (2015).
37. Stadler, T., Kühnert, D., Rasmussen, D. A. & du Plessis, L. Insights into the early epidemic spread of Ebola in Sierra Leone provided by viral sequence data. *PLoS Curr.* **6,** http://dx.doi.org/10.1371/currents.outbreaks.02bc6d927ecee7bbd33532ec8ba6a25f (2014).
38. Tong, Y.-G. *et al.* Genetic diversity and evolutionary dynamics of Ebola virus in Sierra Leone. *Nature* **524,** 93–96 (2015).
39. Diallo, B. *et al.* Resurgence of Ebola virus disease in Guinea linked to a survivor with virus persistence in seminal fluid for more than 500 days. *Clin. Infect. Dis.* **63,** 1353–1356 (2016).
40. Rowe, A. K. *et al.* Clinical, virologic, and immunologic follow-up of convalescent Ebola hemorrhagic fever patients and their household contacts, Kikwit, Democratic Republic of the Congo. *J. Infect. Dis.* **179,** S28–S35 (1999).

Supplementary Information is available in the online version of the paper.

Acknowledgements The authors acknowledge support from: European Union Seventh Framework 278433-PREDEMICS (P.L., A.R.) and ERC 260864 (P.L., A.R., M.A.S.) European Union Horizon 2020 643476-COMPARE (M.P.G.K., A.R.), 634650-VIROGENESIS (P.L., M.P.G.K.), 666100-EVIDENT and European Commission IFS/2011/272-372, EMLab (S.G.), National Institutes of Health R01 AI107034, R01 AI117011 and R01 HG006139 and National Science Foundation IIS 1251151 and DMS 1264153 (M.A.S.), NIH AI081982, AI082119, AI082805 AI088843, AI104216, AI104621, AI115754, HSN272200900049C, HHSN272201400048C (R.F.G.), NIH R35 GM119774-01 (T.B.) National Health & Medical Research Council (Australia) (E.C.H.). The Research Foundation - Flanders G0D5117N (G.B., P.L.), Work in Liberia was funded by the Defense Threat Reduction Agency, the Global Emerging Infections System and the Targeted Acquisition of Reference Materials Augmenting Capabilities (TARMAC) Initiative agencies from the US Department of Defense (G.Pa.), Bill and Melinda Gates Foundation OPP1106427, 1032350, OPP1134076, Wellcome Trust 106866/Z/15/Z, Clinton Health Access Initiative (A.J.T.), National Institute for Health Research Health Protection Research Unit in Emerging and Zoonotic Infections (J.A.H.), Key Research and Development Program from the Ministry of Science and Technology of China 2016YFC1200800 (D.L.), National Natural Science Foundation of China 81590760 and 81321063 (G.F.G.), Mahan Post-doctoral fellowship Fred Hutchinson Cancer Research Center (G.D.), National Institute of Allergy and Infectious Disease U19AI110818, 5R01AI114855-03, United States Agency for International Development OAA-G-15-00001 and the Bill and Melinda Gates Foundation OPP1123407 (P.C.S.), NIH 1U01HG007480-01 and the World Bank ACE019 (C.T.H.), PEW Biomedical Scholarship, NIH UL1TR001114, and NIAID contract HHSN272201400048C (K.G.A.). J.H.K., an employee of Tunnell Government Services, Inc., is a subcontractor under Battelle Memorial Institute's prime contract with the NIAID (contract HHSN272200700016I). Colour-blind-friendly colour palettes were designed by C. Brewer, Pennsylvania State University (http://colorbrewer2.org). Matplotlib (http://matplotlib.org) was used extensively throughout this article for data visualisation. We acknowledge support from NVIDIA Corporation with the donation of parallel computing resources used for this research. Finally, we recognize the contributions made by our colleagues who died from Ebola virus disease whilst fighting the epidemic.

Author Contributions G.D., L.M.C., T.B., C.F., M.A.S., P.L. and A.R. designed the study. G.D., L.M.C., T.B., A.J.T., G.B., P.L. and A.R. performed the analysis. G.D., T.B., M.A.S, P.L. and A.R. wrote the manuscript. L.M.C., A.J.T., G.B., N.R.F., J.T.L., M.C., S.F.S., K.G.A., M.W.C., R.F.G., I.G., E.C.H., P.K., M.P.G.K., J.H.K., S.T.N., G.Pa., O.G.P., P.C.S. and U.S. edited the manuscript. The other authors were critical for the coordination, collection, processing of virus samples or the sequencing and bioinformatics of virus genomes. All authors read and approved the contents of the manuscript.

Author Information Reprints and permissions information is available at www.nature.com/reprints. The authors declare no competing financial interests. Readers are welcome to comment on the online version of the paper. Publisher's note: Springer Nature remains neutral with regard to jurisdictional claims in published maps and institutional affiliations. Correspondence and requests for materials should be addressed to A.R. (a.rambaut@ed.ac.uk), G.D. (gdudas@fredhutch.org) or P.L. (philippe.lemey@kuleuven.be).

Reviewer Information *Nature* thanks R. Biek, C. Viboud, M. Worobey and the other anonymous reviewer(s) for their contribution to the peer review of this work.

Gytis Dudas[1,2], Luiz Max Carvalho[1], Trevor Bedford[2], Andrew J. Tatem[3,4], Guy Baele[5], Nuno R. Faria[6], Daniel J. Park[7], Jason T. Ladner[8], Armando Arias[9,10], Danny Asogun[11,12], Filip Bielejec[5], Sarah L. Caddy[9], Matthew Cotten[13,14], Jonathan D'Ambrozio[8], Simon Dellicour[5], Antonino Di Caro[12,15], Joseph W. Diclaro II[16], Sophie Duraffour[12,17], Michael J. Elmore[18], Lawrence S. Fakoli III[19], Ousmane Faye[20], Merle L. Gilbert[8], Sahr M. Gevao[21], Stephen Gire[7,22], Adrianne Gladden-Young[7], Andreas Gnirke[7], Augustine Goba[23,24], Donald S. Grant[23,24], Bart L. Haagmans[14], Julian A. Hiscox[25,26], Umaru Jah[27], Jeffrey R. Kugelman[8], Di Liu[28], Jia Lu[9], Christine M. Malboeuf[7], Suzanne Mate[8], David A. Matthews[29], Christian B. Matranga[7], Luke W. Meredith[9,27], James Qu[7], Joshua Quick[30], Suzan D. Pas[14], My V. T. Phan[13,14], Georgios Pollakis[25], Chantal B. Reusken[14], Mariano Sanchez-Lockhart[8,31], Stephen F. Schaffner[7], John S. Schieffelin[32], Rachel S. Sealfon[7,33,34], Etienne Simon-Loriere[35,36], Saskia L. Smits[14], Kilian Stoecker[12,37], Lucy Thorne[9], Ekaete Alice Tobin[11,12], Mohamed A. Vandi[23,24], Simon J. Watson[13], Kendra West[7], Shannon Whitmer[38], Michael R. Wiley[8,31], Sarah M. Winnicki[7,32], Shirlee Wohl[7,22], Roman Wölfel[12,37],

Nathan L. Yozwiak[7,22], Kristian G. Andersen[39,40], Sylvia O. Blyden[41], Fatorma Bolay[19], Miles W. Carroll[12,18,26,42], Bernice Dahn[43], Boubacar Diallo[44], Pierre Formenty[45], Christophe Fraser[46], George F. Gao[28,47], Robert F. Garry[48], Ian Goodfellow[9,27], Stephan Günther[12,17], Christian T. Happi[49,50], Edward C. Holmes[51], Brima Kargbo[24], Sakoba Keïta[52], Paul Kellam[13,53], Marion P. G. Koopmans[14], Jens H. Kuhn[54], Nicholas J. Loman[30], N'Faly Magassouba[55], Dhamari Naidoo[45], Stuart T. Nichol[38], Tolbert Nyenswah[43], Gustavo Palacios[8], Oliver G. Pybus[6], Pardis C. Sabeti[7,22], Amadou Sall[20], Ute Ströher[38], Isatta Wurie[21], Marc A. Suchard[56,57,58], Philippe Lemey[5] & Andrew Rambaut[1,59,60]

[1]Institute of Evolutionary Biology, University of Edinburgh, King's Buildings, Edinburgh EH9 3FL, UK. [2]Vaccine and Infectious Disease Division, Fred Hutchinson Cancer Research Center, Seattle, Washington 98109, USA. [3]WorldPop, Department of Geography and Environment, University of Southampton, Highfield, Southampton SO17 1BJ, UK. [4]Flowminder Foundation, Stockholm, Sweden. [5]Department of Microbiology and Immunology, Rega Institute, KU Leuven – University of Leuven, 3000 Leuven, Belgium. [6]Department of Zoology, University of Oxford, South Parks Road, Oxford OX1 3PS, UK. [7]Broad Institute of Harvard and MIT, Cambridge, Massachusetts 02142, USA. [8]Center for Genome Sciences, US Army Medical Research Institute of Infectious Diseases, Fort Detrick, Frederick, Maryland 21702, USA. [9]Department of Pathology, University of Cambridge, Addenbrooke's Hospital, Cambridge CB2 2QQ, UK. [10]National Veterinary Institute, Technical University of Denmark, Bülowsvej 27, 1870, Frederiksberg C, Denmark. [11]Institute of Lassa Fever Research and Control, Irrua Specialist Teaching Hospital, Irrua, Nigeria. [12]The European Mobile Laboratory Consortium, 20359 Hamburg, Germany. [13]Virus Genomics, Wellcome Trust Sanger Institute, Hinxton, Cambridge CB10 1SA, UK. [14]Department of Viroscience, Erasmus University Medical Centre, PO Box 2040, 300 CA Rotterdam, the Netherlands. [15]National Institute for Infectious Diseases 'L. Spallanzani'—IRCCS, Via Portuense 292, 00149 Rome, Italy. [16]Naval Medical Research Unit 3, 3A Imtidad Ramses Street, Cairo 11517, Egypt. [17]Bernhard Nocht Institute for Tropical Medicine, 20359 Hamburg, Germany. [18]National Infections Service, Public Health England, Porton Down, Salisbury, Wilts SP4 0JG, UK. [19]Liberian Institute for Biomedical Research, Charlesville, Liberia. [20]Institut Pasteur de Dakar, Arbovirus and Viral Hemorrhagic Fever Unit, 36 Avenue Pasteur, BP 220, Dakar, Sénégal. [21]University of Sierra Leone, Freetown, Sierra Leone. [22]Center for Systems Biology, Department of Organismic and Evolutionary Biology, Harvard University, Cambridge, Massachusetts 02138, USA. [23]Viral Hemorrhagic Fever Program, Kenema Government Hospital, 1 Combema Road, Kenema, Sierra Leone. [24]Ministry of Health and Sanitation, 4th Floor Youyi Building, Freetown, Sierra Leone. [25]Institute of Infection and Global Health, University of Liverpool, Liverpool L69 2BE, UK. [26]NIHR Health Protection Research Unit in Emerging and Zoonotic Infections, University of Liverpool, Liverpool L69 3GL, UK. [27]University of Makeni, Makeni, Sierra Leone. [28]Institute of Microbiology, Chinese Academy of Sciences, Beijing 100101, China. [29]University of Bristol, Bristol BS8 1TD, UK. [30]Institute of Microbiology and Infection, University of Birmingham, Birmingham B15 2TT, UK. [31]University of Nebraska Medical Center, Omaha, Nebraska 68198, USA. [32]Department of Pediatrics, Section of Infectious Diseases, New Orleans, Louisiana 70112, USA. [33]Center for Computational Biology, Flatiron Institute, New York, New York 10010, USA. [34]Lewis-Sigler Institute for Integrative Genomics, Princeton University, Princeton, New Jersey 08544, USA. [35]Institut Pasteur, Functional Genetics of Infectious Diseases Unit, 28 rue du Docteur Roux, 75724 Paris Cedex 15, France. [36]Génétique Fonctionelle des Maladies Infectieuses, CNRS URA3012, Paris 75015, France. [37]Bundeswehr Institute of Microbiology, Neuherbergstrasse 11, 80937 Munich, Germany. [38]Viral Special Pathogens Branch, Centers for Disease Control and Prevention, 1600 Clifton Road NE, Atlanta, Georgia 30333, USA. [39]The Scripps Research Institute, Department of Immunology and Microbial Science, La Jolla, California 92037, USA. [40]Scripps Translational Science Institute, La Jolla, California 92037, USA. [41]Ministry of Social Welfare, Gender and Children's Affairs, New Englandville, Freetown, Sierra Leone. [42]University of Southampton, South General Hospital, Southampton SO16 6YD, UK. [43]Minstry of Health Liberia, Monrovia, Liberia. [44]World Health Organization, Conakry, Guinea. [45]World Health Organization, Geneva, Switzerland. [46]Oxford Big Data Institute, Li Ka Shing Centre for Health Information and Discovery, Nuffield Department of Medicine, University of Oxford, Oxford OX3 7FZ, UK. [47]Chinese Center for Disease Control and Prevention (China CDC), Beijing 102206, China. [48]Department of Microbiology and Immunology, New Orleans, Louisiana 70112, USA. [49]Department of Biological Sciences, Redeemer's University, Ede, Osun State, Nigeria. [50]African Center of Excellence for Genomics of Infectious Diseases (ACEGID), Redeemer's University, Ede, Osun State, Nigeria. [51]Marie Bashir Institute for Infectious Diseases and Biosecurity, Charles Perkins Centre, School of Life and Environmental Sciences and Sydney Medical School, the University of Sydney, Sydney, New South Wales 2006, Australia. [52]Ministry of Health Guinea, Conakry, Guinea. [53]Division of Infectious Diseases, Faculty of Medicine, Imperial College London, London W2 1PG, UK. [54]Integrated Research Facility at Fort Detrick, National Institute of Allergy and Infectious Diseases, National Institutes of Health, B-8200 Research Plaza, Fort Detrick, Frederick, Maryland 21702, USA. [55]Université Gamal Abdel Nasser de Conakry, Laboratoire des Fièvres Hémorragiques en Guinée, Conakry, Guinea. [56]Department of Biostatistics, UCLA Fielding School of Public Health, University of California, Los Angeles, California 90095, USA. [57]Department of Biomathematics David Geffen School of Medicine at UCLA, University of California, Los Angeles, California 90095, USA. [58]Department of Human Genetics, David Geffen School of Medicine at UCLA, University of California, Los Angeles, California 90095, USA. [59]Centre for Immunology, Infection and Evolution, University of Edinburgh, King's Buildings, Edinburgh, EH9 3FL, UK. [60]Fogarty International Center, National Institutes of Health, Bethesda, Maryland 20892, USA.

METHODS

Sequence data. We compiled a dataset of 1,610 publicly available full EBOV genomes sampled between 17 March 2014 and 24 October 2015 (see https://github/ebov/space-time/data/ for the full list and metadata). The number of sequences and the proportion of cases sequenced varies between countries; our dataset contains 209 sequences from Liberia (3.8% of known and suspected cases), 982 from Sierra Leone (8.0%) and 368 from Guinea (9.2%) (Supplementary Table 1). Most ($n = 1{,}100$) genomes are of high quality, with ambiguous sites and gaps comprising less than 1% of the total alignment length, followed by sequences with between 1% and 2% of sites that comprised ambiguous bases or gaps ($n = 266$), 98 sequences with 2–5%, 120 sequences with 5–10% and 26 sequences with more than 10% of sites that are ambiguous or are gaps. Sequences known to be associated with sexual transmission or latent infections were excluded, as these viruses often exhibit anomalous molecular clock signals[11,12]. Sequences were aligned using MAFFT[41] and edited manually. The alignment was partitioned into coding regions and non-coding intergenic regions with a final alignment length of 18,992 nucleotides (available from https://github/ebov/space-time/data/).

Masking putative ADAR-edited sites. As noticed in previous studies[15,38], some EBOV isolates contain clusters of T-to-C mutations within relatively short stretches of the genome. Interferon-inducible adenosine deaminases acting on RNA (ADAR) are known to induce adenosine to inosine hypermutations in double-stranded RNA[43]. ADARs have been suggested to act on RNAs from numerous groups of viruses[42]. When negative-sense single-stranded RNA virus genomes are edited by ADARs, A-to-G hypermutations seem to preferentially occur on the negative strand, which results in U/T-to-C mutations on the positive strand[44–46]. Multiple T-to-C mutations are introduced simultaneously by ADAR-mediated RNA editing which would interfere with molecular clock estimates and, by extension, the tree topology. We therefore designated that four or more T-to-C mutations within 300 nucleotides of each other as a putative hypermutation tract, whenever there is evidence that all T-to-C mutations within such stretches were introduced at the same time, that is, every T-to-C mutation in a stretch occurred on a single branch. We detected a total of 15 hypermutation patterns with up to 13 T-to-C mutations within 35 to 145 nucleotides. Of these patterns, 11 are unique to a single genome and 4 are shared across multiple isolates, suggesting that occasionally viruses that survive hypermutation are transmitted[47]. Putative tracts of T-to-C hypermutation almost exclusively occur within non-coding intergenic regions, where their effects on viral fitness are presumably minimal. In each case, we mask out these sites as ambiguous nucleotides, but leave the first T-to-C mutation unmasked to provide phylogenetic information on the relatedness of these sequences.

Phylogenetic inference. Molecular evolution was modelled according to a HKY+Γ_4 substitution model (refs 48, 49) independently across four partitions (codon positions 1, 2, 3 and non-coding intergenic regions). Site-specific rates were scaled by relative rates in the four partitions. Evolutionary rates were allowed to vary across the tree according to a relaxed molecular clock that draws branch-specific rates from a log-normal distribution[50]. A non-parametric coalescent 'Skygrid' model was used to act as a prior density on trees[51]. The overall evolutionary rate was given an uninformative continuous-time Markov chain (CTMC) reference prior[52], while the rate multipliers for each partition were given an uninformative uniform prior over their bounds. All other priors used to infer the phylogenetic tree were left at their default values. BEAST XML files are available from https://github/ebov/space-time/data/. We ran an additional analysis with a subset of data (787 sequences collected up to November 2014—the peak of case numbers in Sierra Leone) to test the robustness of inference if they had been performed mid-epidemic.

Geographic history reconstruction. The level of administrative regions within each country was chosen so that population sizes between regions are comparable. For each country the appropriate administrative regions were: prefecture for Guinea (administrative subdivision level 2), county for Liberia (level 1) and district for Sierra Leone (level 2). We refer to them as regions (63 in total, but only 56 are recorded to have had EVD cases) and each sequence, where available, was assigned the region where the patient was recorded to have been infected as a discrete trait. When the region within a country was unknown ($n = 223$), we inferred the sequence location as a latent variable with equal prior probability over all available regions within that country. Most of the sequences with unknown regional origins were from Sierra Leone ($n = 151$), followed by Liberia ($n = 69$) and Guinea ($n = 3$). In the absence of any geographic information ($n = 2$) we inferred both the country and the region of a sequence.

We used an asymmetric CTMC[53,55] matrix to infer instantaneous transitions between regions. For 56 regions with recorded EVD cases, a total of 3,080 independent transition rates would be challenging to infer from one realization of the process, even when reduced to a sparse migration matrix using stochastic search variable selection[53].

Therefore, to infer the spatial phylogenetic diffusion history between the $K = 56$ locations, we adopt a sparse GLM formulation of CTMC diffusion[18]. This model parameterizes the instantaneous movement rate Λ_{ij} from location i to location j as a log-linear function of P potential predictors $\boldsymbol{X}_{ij} = (x_{ij1}, \ldots, x_{ijP})'$ with unknown coefficients $\boldsymbol{\beta} = (\beta_1, \ldots, \beta_P)'$ and diagonal matrix δ with entries $(\delta_1, \ldots, \delta_p)$. These latter unknown indicators $\delta_p \in \{0,1\}$ determine the inclusion in or exclusion from the model of a single predictor. We generalize this formulation here to include two-way random effects that allow for location origin- and destination-specific variability. Our two-way random effects GLM becomes

$$\log(\Lambda_{ij}) = \boldsymbol{X}'_{ij}\boldsymbol{\delta}\boldsymbol{\beta} + \varepsilon_i + \varepsilon_j \quad (1)$$

where ε_k is distributed as normal$(0, \sigma^2)$ for $k = 1, ..., K$, and σ^2 is distributed as inverse-$\Gamma(0.001, 0.001)$, and where $\varepsilon = (\varepsilon_1, \ldots, \varepsilon_K)$ are the location-specific effects. These random effects account for unexplained variability in the diffusion process that may otherwise lead to spurious inclusion of predictors.

We follow ref. 18 by specifying that *a priori* all β_p are independent and normally distributed with mean 0 and a relatively large variance of 4 and by assigning independent Bernoulli prior probability distributions on δ_p.

Let q be the inclusion probability and w be the probability of no predictors being included. Then, using the distribution function of a binomial random variable $q = 1 - w^{1/P}$, where P is the number of predictors, as before. We use a small success probability on each predictor's inclusion that reflects a 50% prior probability (w) on no predictors being included.

In our main analysis, we consider 25 individual predictors that can be classified as geographic, administrative, demographic, cultural and climatic covariates of spatial spread (Extended Data Table 1). Where measures are region-specific (rather than pairwise region measures), we specify both an origin and destination predictor. We also tested for sampling bias by including an additional origin and destination predictor based on the residuals for the regression of sample size against case count (Extended Data Fig. 1b), but these predictors did not receive any support (data not shown).

To draw posterior inference, we follow ref. 18 by integrating $\boldsymbol{\beta}$ and $\boldsymbol{\delta}$, and further employ a random-walk Metropolis transition kernel on ε and sample σ^2 directly from its full conditional distribution using Gibbs sampling.

To obtain a joint posterior estimate from this joint genetic and phylogeographic model, an MCMC chain was run in BEAST 1.8.4 (ref. 54) for 100 million states, sampling every 10,000 states. The first 1,000 samples in each chain were removed as burnin, and the remaining 9,000 samples used to estimate a maximum clade credibility tree and to estimate posterior densities for individual parameters. A second independent run of 100 million states was performed to check convergence of the first.

To consider the feasibility of 'real-time' inference from virus genome data from the height of the EVD epidemic we took only those sequences derived from samples taken up until the end of October 2014 ($n = 787$). We undertook the same joint phylogenetic and spatial GLM analysis as for the full dataset including the same set of 25 predictors. We ran this analysis for 200 million states, sampling every 20,000 states and removing the first 10% of samples.

To obtain realizations of the phylogenetic CTMC process, including both transitions (Markov jumps) between states and waiting times (Markov rewards) within states, we used posterior inference of the complete Markov jump history through time[18,56]. In addition to transitions 'within' the phylogeny, we also estimate the expected number of transitions 'from' origin location i in the phylogeographic tree to arbitrary 'destination' location j as follows:

$$\zeta_{ij} = \tau_i \mu \Lambda_{ij} \pi_i / c \quad (2)$$

where τ_i is the waiting time (or Markov reward) in 'origin' state i throughout the phylogeny, μ is the overall rate scalar of the location transition process, π_i is the equilibrium frequency of 'origin' state i, and c is the normalizing constant applied to the CTMC rate matrices in BEAST. To obtain the expected number of transitions to a particular destination location from any phylogeographic location (integrating over all possible locations across the phylogeny), we sum over all 56 origin locations included in the analysis. We note that the destination location can also be a location that was not included in the analysis because we only need to consider destination j in the instantaneous movement rates Λ_{ij}; since the log of these rates are parameterized as a log-linear function of the predictors, we can obtain these rates through the coefficient estimates from the analysis and the predictors extended to include these additional locations. Specifically, we use this to predict introductions in regions in Guinea, for which no cases were reported ($n = 7$) and for regions in neighbouring countries along the borders with Guinea or Liberia that remained disease free ($n = 18$). To obtain such estimates under different predictors or predictor combinations, we perform a specific analysis under the GLM

model including only the relevant predictors or predictor combinations without the two-way random effects. For computational expedience, we performed these analyses, as well as the time-inhomogeneous analyses below, by conditioning on a set of 1,000 trees from the posterior distribution of the main phylogenetic analysis[18]. We summarize mean posterior estimates for the transition expectations based on the samples obtained by our MCMC analysis; we also note that the value of c is sample-specific.

Time-dependent spatial diffusion. To consider time-inhomogeneity in the spatial diffusion process, we start by borrowing epoch modelling concepts from ref. 57. The epoch GLM parameterizes the instantaneous movement rate Λ_{ijt} from state i to state j within epoch t as a log-linear function of P epoch-specific predictors $\boldsymbol{X}_{ijt} = (x_{ijt1}, \ldots, x_{ijtP})'$ with constant-through-time, unknown coefficients β. We generalize this model to incorporate a time-varying contribution of the predictors through time-varying coefficients $\beta(t)$ using a series of change-point processes. Specifically, the time-varying epoch GLM models

$$\begin{aligned} \log \Lambda_{ijt} &= \boldsymbol{X}'_{ijt}\beta(t) \\ \beta(t) &= (\boldsymbol{I} - \phi(t))\beta_B + (\phi(t))\beta_A \end{aligned} \tag{3}$$

where $\boldsymbol{\beta}_B = (\beta_{B1}, \ldots, \beta_{BP})'$ are the unknown coefficients before the change-points, $\beta_A = (\beta_{A1}, \ldots, \beta_{AP})'$ are the unknown coefficients after the change-points, diagonal matrix $\varphi(t)$ has entries $(1_{t>t1}(t), \ldots, 1_{t>tP}(t))$, $1_{(\cdot)}(t)$ is the indicator function and $\boldsymbol{T} = (t_1, \ldots, t_P)$ are the unknown change-point times. In this general form, the contribution of predictor p before its change-point time t_p is β_{Bp} and its contribution after is β_{Ap} for $P = 1, \ldots, P$. Fixing t_p to be less than the time of the first epoch or greater than the time of the last epoch results in a time-invariant coefficient for that predictor.

Similar to the constant-through-time GLM, we specify *a priori* that all β_{Bp} and β_{Ap} are independent and normally distributed with mean 0 and a relatively large variance of 4. Under the prior, each t_p is equally probable to lie before any epoch.

We used random-walk Metropolis transition kernels on $\boldsymbol{\beta}_B$, $\boldsymbol{\beta}_A$ and T.

In a first epoch GLM analysis, we keep the five predictors that are convincingly supported by the time-homogeneous analysis included in the model and estimate an independent change-point t_p for their associated effect sizes: distance, nat./int. effect, shared international border and origin and destination population size change-points. To quantify the evidence in favour of each change-point, we calculate Bayes factor support on the basis of the prior and posterior odds that t_p is less than the time of the first epoch or greater than the time of the last epoch. Because we find only very strong support for a change-point in the nat./int. effect, we subsequently estimate the effect sizes before and after its associated change-point, keeping the remaining four predictors homogeneous through time.

Within-location generalized linear models. EVD case numbers are reported by the WHO for every country division (region) at the appropriate administrative level, split by epidemiological week. For every region and for each epidemiological week four numbers are reported: new cases in the patient and situation report databases as well as whether the new cases are confirmed or probable. At the height of the epidemic many cases went unconfirmed, even though they were likely to have been genuine EVD. As such, we treat probable EVD cases in WHO reports as confirmed and combine them with laboratory-confirmed EVD case numbers. Following this we take the higher combined case number of situation report and patient databases. The latest situation report in our data goes up to the epidemiological week spanning 8 to 14 February 2016, with all case numbers being downloaded on 22 February 2016. There are apparent discrepancies between cumulative case numbers reported for each country over the entire epidemic and case numbers reported per administrative division over time, such that our estimate for the final size of the epidemic, based on case numbers over time reported by the WHO, is on the order of 22,000 confirmed and suspected cases of EVD compared to the official estimate of around 28,000 cases across the entire epidemic. This likely arose because case numbers are easier to track at the country level, but become more difficult to narrow down to administrative subdivision level, especially over time (only 86% of the genome sequences had a known location of infection).

We studied the association between disease case counts using generalized linear models in a very similar fashion to the framework presented above. A list of the location-level predictors we used for these analyses can be found in Extended Data Table 1. We also employed stochastic search variable selection as described above, in order to compute Bayes factors (BFs) for each predictor. In keeping with the genetic GLM analyses, we also set the prior inclusion probabilities such that there was a 50% probability of no predictors being included.

$$\begin{aligned} Y_i &\sim \text{negative}-\text{binomial}(p_i, r) \\ p_i &= \frac{r}{(r+\lambda_i)} \\ \log(\lambda_i) &= \alpha + \beta_1\delta_1 x_{i1} + \ldots + \beta_P\delta_P x_{iP} \end{aligned}$$

where r is the over-dispersion parameter, δ_i are the indicators as before. Prior distributions on model parameters for these analyses were the same as those used for the genetic analyses whenever possible. We then use this model to predict how many cases the locations which reported zero EVD cases would have gathered, that is, the potential size of the epidemic in each location.

Computational details. To fit the models described above we took advantage of the routines already built in BEAST (https://github.com/beast-dev/beast-mcmc) but in a non-phylogenetic setting. Once again, posterior distributions for the parameters were explored using MCMC. We ran each chain for 50 million iterations and discarded at least 10% of the samples as burn-in. Convergence was checked by visual inspection of the chains and checking that all parameters had effective sample sizes greater than 200. We ran multiple chains to ensure that results were consistent. To make predictions, we used 50,000 Monte Carlo samples from the posterior distribution of coefficients and the overdispersion parameter (r) to simulate case counts for all locations with zero recorded EVD cases.

Data availability. All collated data, genetic sequence alignments, phylogenetic trees, analysis scripts and analysis output are available at https://github.com/ebov/space-time and http://dx.doi.org/10.7488/ds/1711. Individual virus genetic sequences are published in earlier works and are available from NCBI GenBank (see https://github.com/ebov/space-time for a list of accession numbers and references).

41. Katoh, K., Misawa, K., Kuma, K. & Miyata, T. MAFFT: a novel method for rapid multiple sequence alignment based on fast Fourier transform. *Nucleic Acids Res.* **30,** 3059–3066 (2002).
42. Gélinas, J.-F., Clerzius, G., Shaw, E. & Gatignol, A. Enhancement of replication of RNA viruses by ADAR1 via RNA editing and inhibition of RNA-activated protein kinase. *J. Virol.* **85,** 8460–8466 (2011).
43. Bass, B. L. & Weintraub, H. An unwinding activity that covalently modifies its double-stranded RNA substrate. *Cell* **55,** 1089–1098 (1988).
44. Cattaneo, R. *et al.* Biased hypermutation and other genetic changes in defective measles viruses in human brain infections. *Cell* **55,** 255–265 (1988).
45. Rueda, P., García-Barreno, B. & Melero, J. A. Loss of conserved cysteine residues in the attachment (G) glycoprotein of two human respiratory syncytial virus escape mutants that contain multiple A–G substitutions (hypermutations). *Virology* **198,** 653–662 (1994).
46. Carpenter, J. A., Keegan, L. P., Wilfert, L., O'Connell, M. A. & Jiggins, F. M. Evidence for ADAR-induced hypermutation of the Drosophila sigma virus (Rhabdoviridae). *BMC Genet.* **10,** 75 (2009).
47. Smits, S. L. *et al.* Genotypic anomaly in Ebola virus strains circulating in Magazine Wharf area, Freetown, Sierra Leone, 2015. *Euro Surveill.* **20,** 30035 (2015).
48. Hasegawa, M., Kishino, H. & Yano, T. Dating of the human–ape splitting by a molecular clock of mitochondrial DNA. *J. Mol. Evol.* **22,** 160–174 (1985).
49. Yang, Z. Maximum likelihood phylogenetic estimation from DNA sequences with variable rates over sites: approximate methods. *J. Mol. Evol.* **39,** 306–314 (1994).
50. Drummond, A. J., Ho, S. Y. W., Phillips, M. J. & Rambaut, A. Relaxed phylogenetics and dating with confidence. *PLoS Biol.* **4,** e88 (2006).
51. Gill, M. S. *et al.* Improving Bayesian population dynamics inference: a coalescent-based model for multiple loci. *Mol. Biol. Evol.* **30,** 713–724 (2013).
52. Ferreira, M. A. R. & Suchard, M. A. Bayesian analysis of elapsed times in continuous-time Markov chains. *Can. J. Stat.* **36,** 355–368 (2008).
53. Lemey, P., Suchard, M. & Rambaut, A. Reconstructing the initial global spread of a human influenza pandemic: a Bayesian spatial-temporal model for the global spread of H1N1pdm. *PLoS Curr.* **1,** RRN1031 (2009).
54. Drummond, A. J., Suchard, M. A., Xie, D. & Rambaut, A. Bayesian phylogenetics with BEAUti and the BEAST 1.7. *Mol. Biol. Evol.* **29,** 1969–1973 (2012).
55. Edwards, C. J. *et al.* Ancient hybridization and an Irish origin for the modern polar bear matriline. *Curr. Biol.* **21,** 1251–1258 (2011).
56. Minin, V. N. & Suchard, M. A. Fast, accurate and simulation-free stochastic mapping. *Phil. Trans. R. Soc. B* **363,** 3985–3995 (2008).
57. Bielejec, F., Lemey, P., Baele, G., Rambaut, A. & Suchard, M. A. Inferring heterogeneous evolutionary processes through time: from sequence substitution to phylogeography. *Syst. Biol.* **63,** 493–504 (2014).

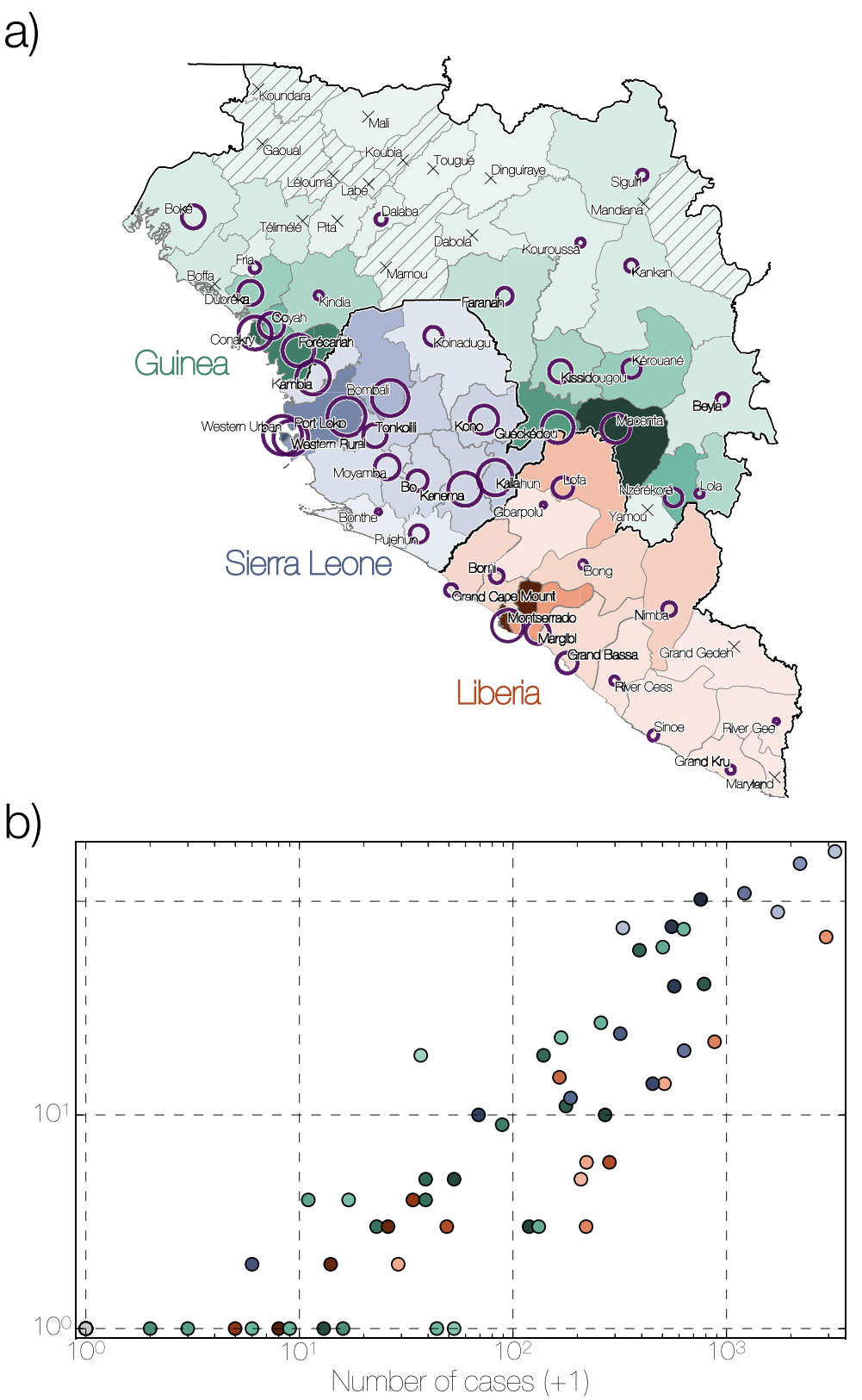

Extended Data Figure 1 | Distribution and correlation of EVD cases and EBOV sequences. a, Administrative regions within Guinea (green), Sierra Leone (blue) and Liberia (red); shading is proportional to the cumulative number of known and suspected EVD cases in each region. Darkest shades represent 784 cases for Guinea (Macenta prefecture); 3,219 cases for Sierra Leone (Western Area urban district); and 2,925 cases for Liberia (Montserrado county); hatching indicate regions without reported EVD cases. Circle diameters are proportional to the number of EBOV genomes available from that region over the entire EVD epidemic with the largest circle representing 152 sequences. Crosses mark regions for which no sequences are available. Circles and crosses are positioned at population centroids within each region. **b**, A plot of number of EBOV genomes sampled against the known and suspected cumulative EVD case numbers. Regions in Guinea are denoted in green, Sierra Leone in blue and Liberia in red. Spearman correlation coefficient: 0.93.

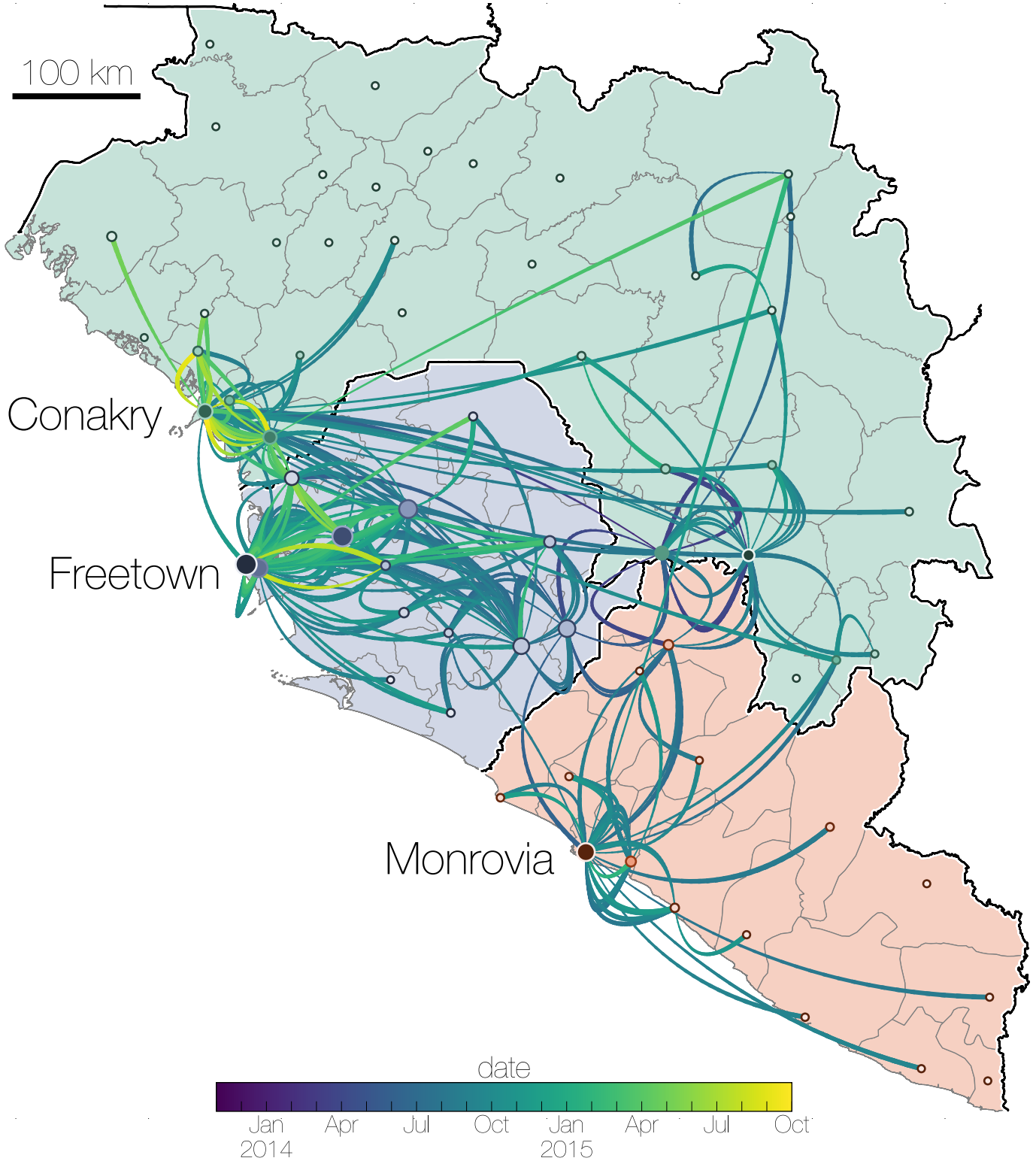

Extended Data Figure 2 | Dispersal of virus lineages over time. Virus dispersal between administrative regions estimated using the GLM phylogeography model (see Methods). The arcs are between population centroids of each region, show directionality from the thin end to the thick end and are coloured in a scale denoting time from December 2013 in blue to October 2015 in yellow. Countries are coloured with Liberia in red, Guinea in green and Sierra Leone in blue.

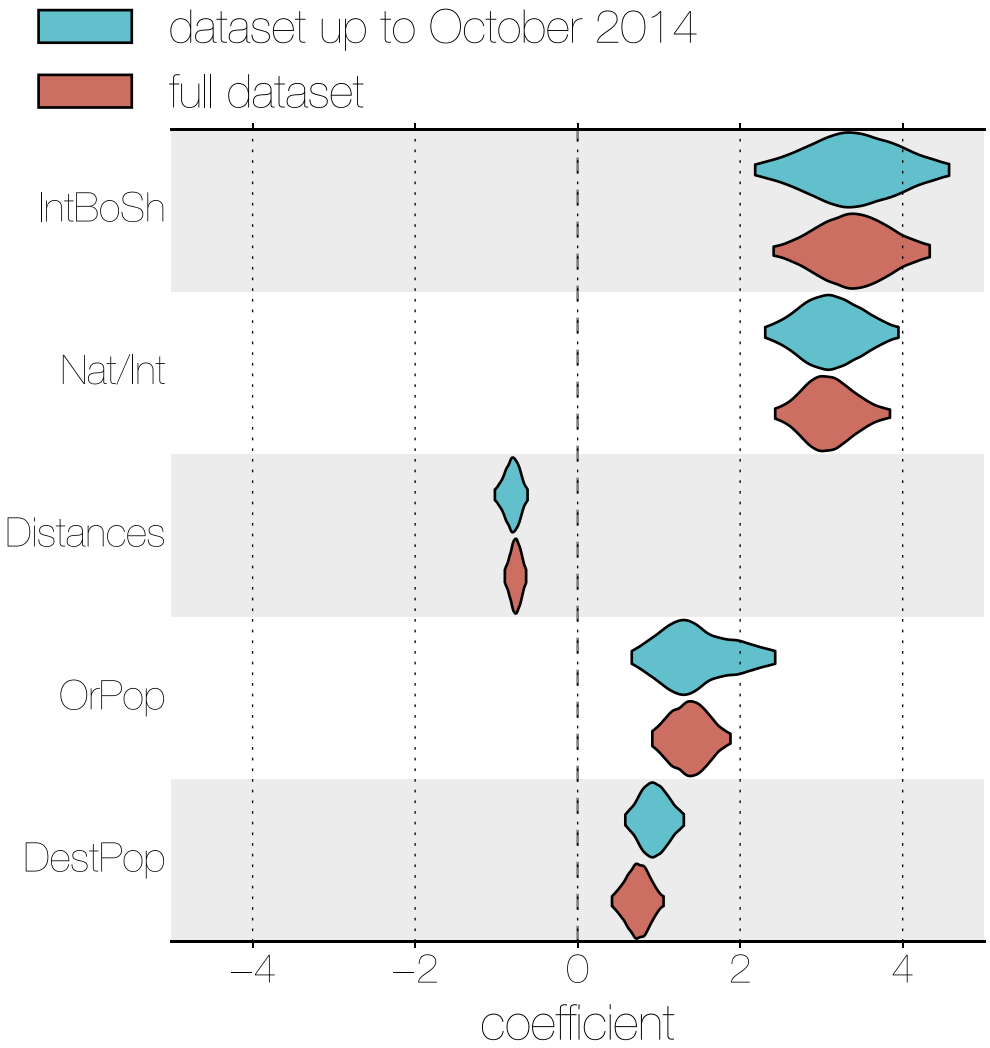

Extended Data Figure 3 | Inference of GLM predictors in a 'real-time' context. For the dataset constructed from EBOV genome sequences derived from samples taken up until October 2014 (blue), the same 5 spatial EBOV movement predictors were given categorical support (inclusion probabilities = 1.0) as for the full dataset (red). Likewise, the coefficients for these predictors are consistent in their sign and magnitude.

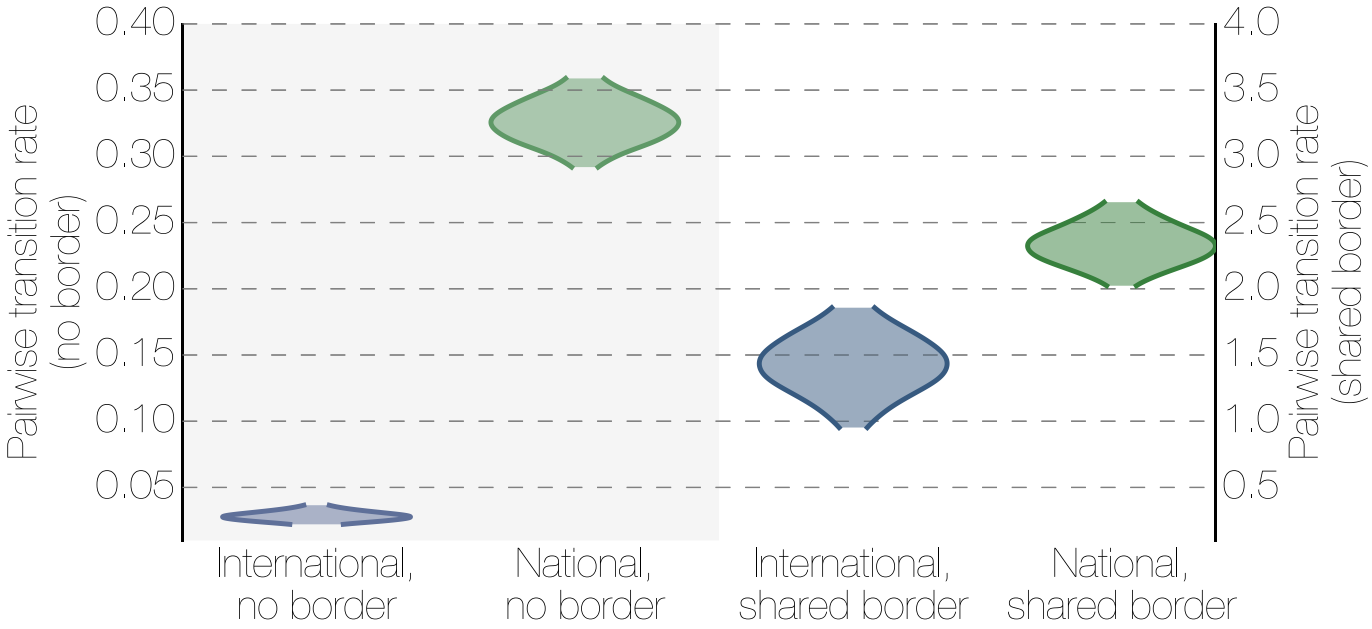

Extended Data Figure 4 | The effect of borders on EBOV migration rates between regions. Posterior densities for the migration rates between locations that share a geographical border and those that do not share borders for international migrations and national migrations. Where two regions share a border (right *y* axis), national migrations are only marginally more frequent than international migrations showing that both types of borders are porous to short local movement. Where the two regions are not adjacent (left *y* axis), international migrations are much rarer than national migrations.

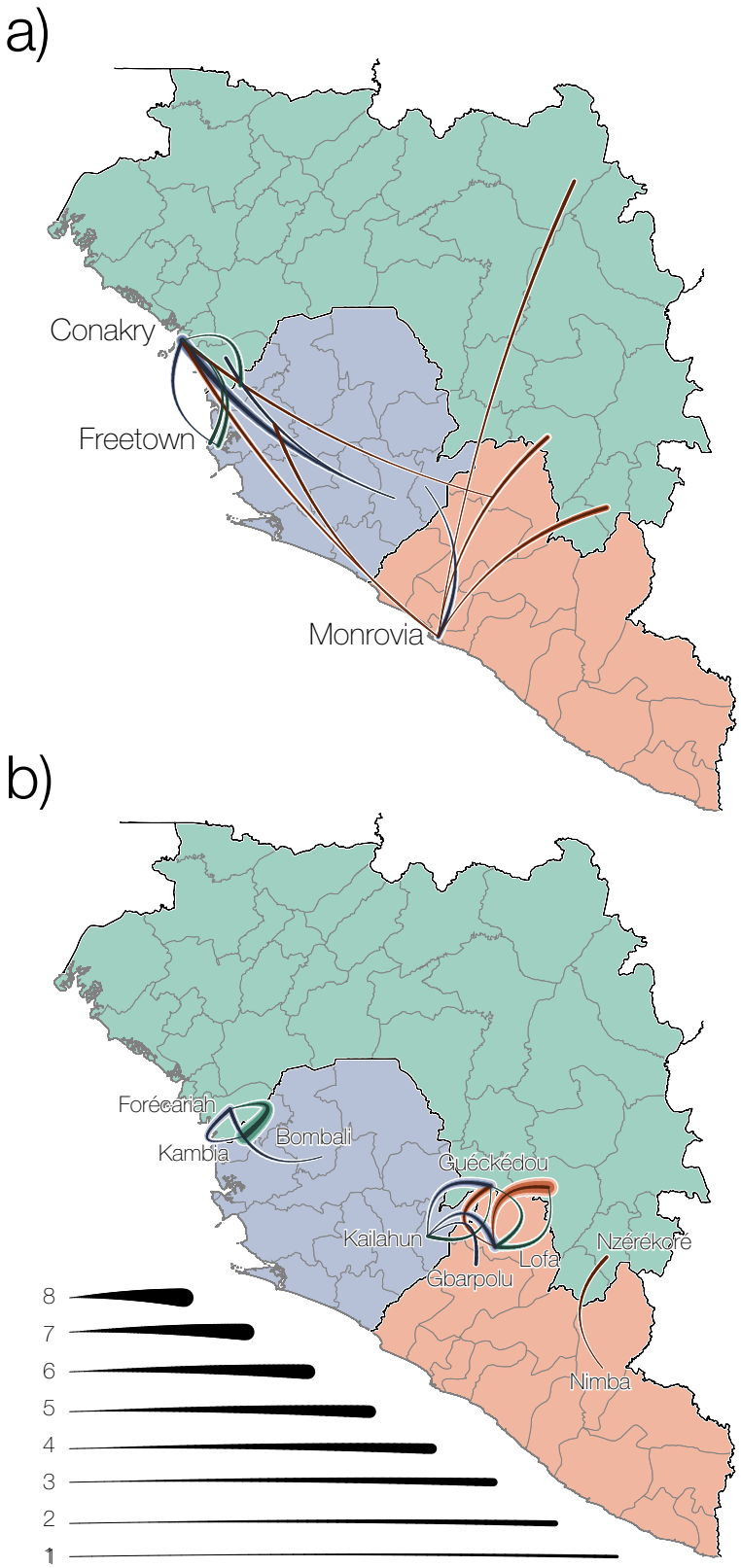

Extended Data Figure 5 | Summarized international migration history of the epidemic. a, **b**, All viral movement events between countries (Guinea, green; Sierra Leone, blue; Liberia, red) are shown split by whether they are between regions that are geographically distant (**a**) or regions that share the international border (**b**). Curved lines indicate median (intermediate colour intensity), and 95% highest posterior density intervals (lightest and darkest colour intensities) for the number of migrations that are inferred to have taken place between countries.

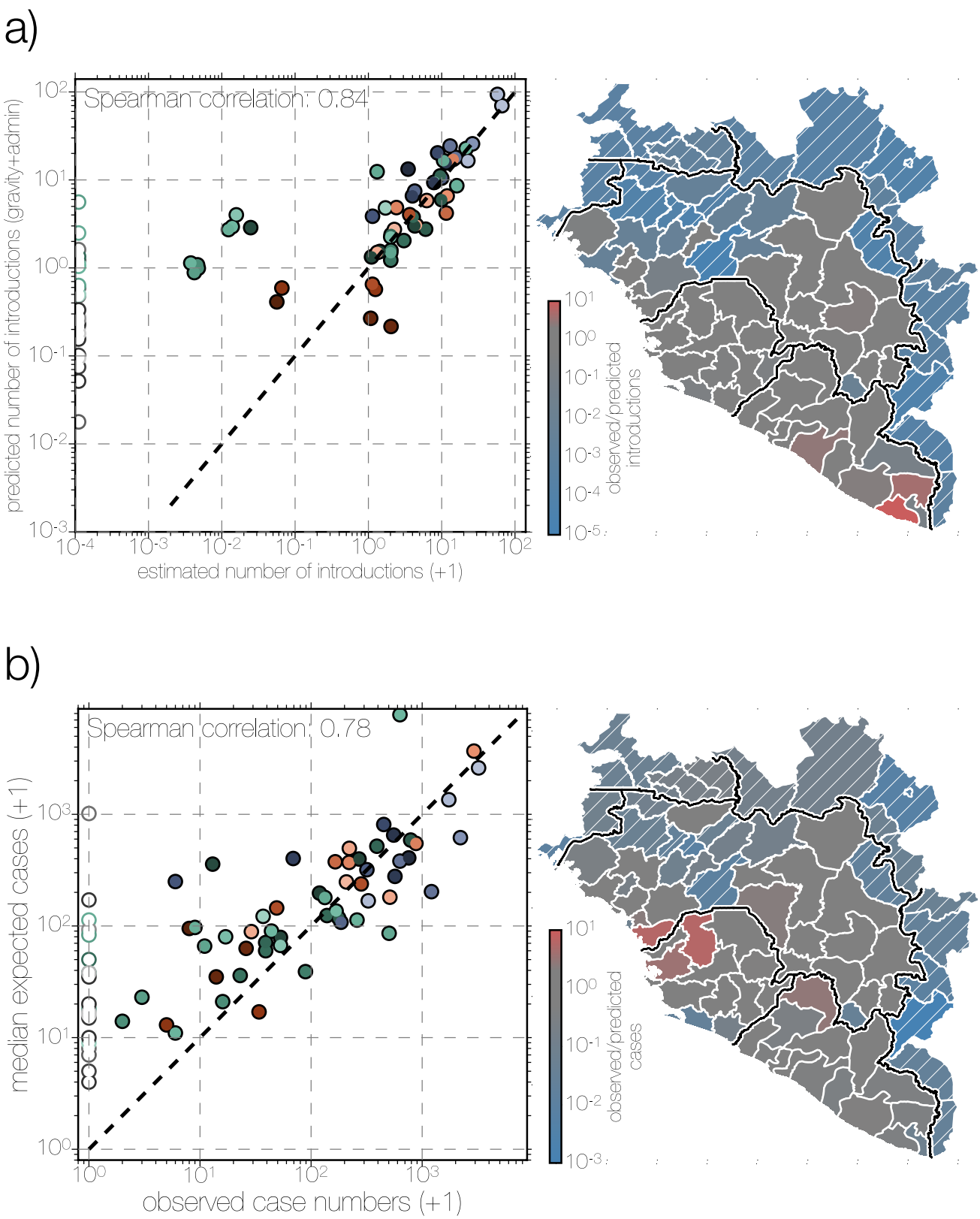

Extended Data Figure 6 | Comparison of predicted and observed numbers of introductions and case numbers. a, **b**, Left, scatter plots show inferred introduction numbers (**a**) or observed case numbers (**b**), coloured by region as in Extended Data Fig. 1. Administrative regions that did not report any cases are indicated with empty circles on the scatter plot. Right, administrative regions on the map are coloured by the residuals (as observed/predicted) of the scatter plot. Regions are coloured grey where $0.5 <$ observed/predicted < 2.0 and transition into red or blue colours for overestimation or underestimation, respectively.

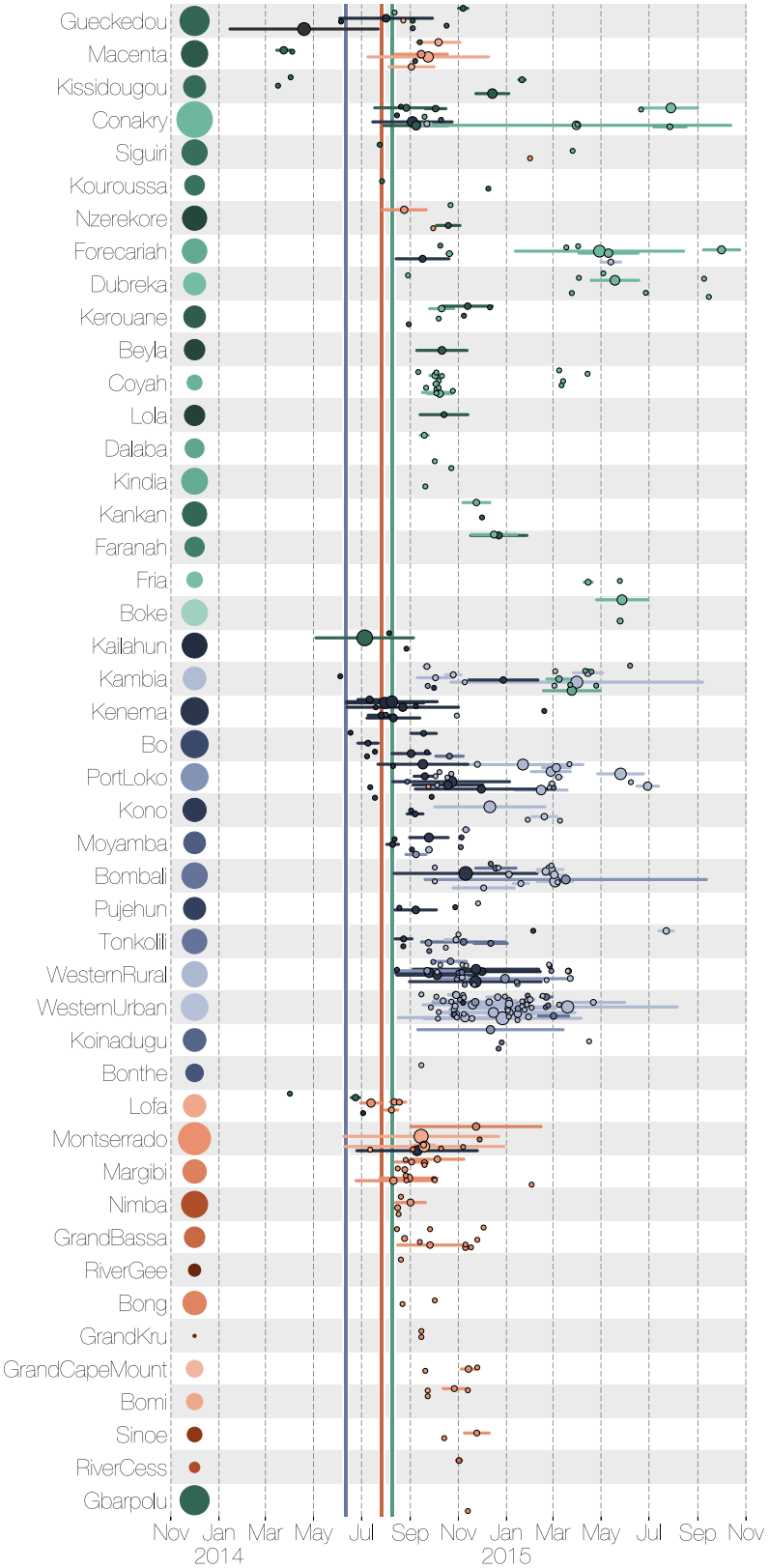

Extended Data Figure 7 | Region-specific introductions, cluster sizes and persistence. Each row summarizes independent introductions and the sizes (as numbers of sequences) of resulting outbreak clusters. Clusters are coloured by their inferred region of origin (colours are the same as in Extended Data Fig. 1). The horizontal lines represent the persistence of each cluster from the time of introduction to the last sampled case (individual tips have persistence 0). The areas of the circles in the middle of the lines are proportional to the number of sequenced cases in the cluster. The areas of the circles next to the labels on the left represent the population sizes of each administrative region. Vertical lines within each cell indicate the dates of declared border closures by each of the three countries: 11 June 2014 in Sierra Leone (blue), 27 July 2014 in Liberia (red) and 09 August 2014 in Guinea (green).

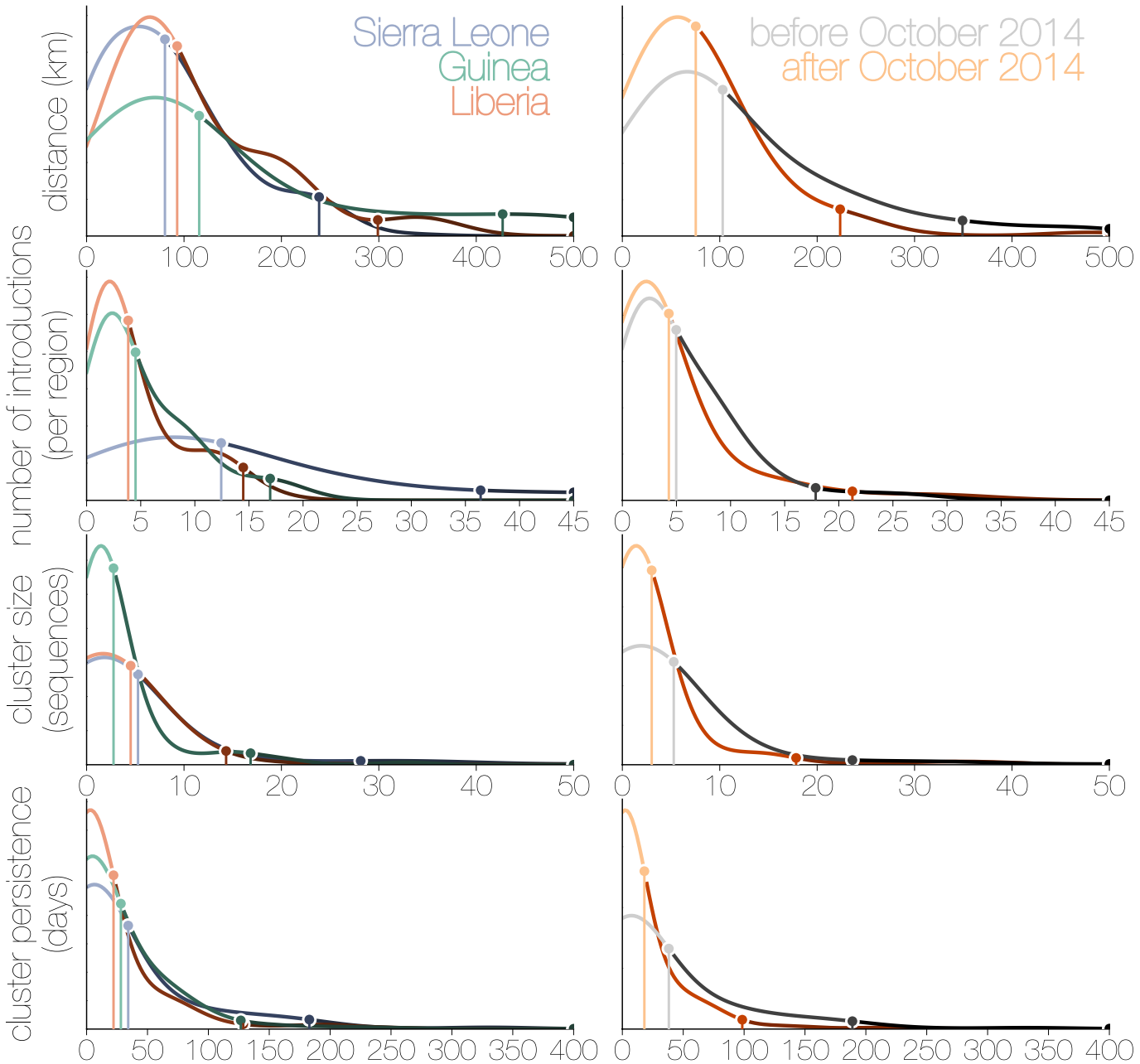

Extended Data Figure 8 | Kernel density estimates for inferred epidemiological statistics. From top to bottom, distance travelled (distance between population centroids, in kilometres); number of introductions that each location experienced; cluster size (number of sequences collected in a location as a result of a single introduction); cluster persistence (days from the common ancestor of a cluster to its last descendent, single tips have persistence of 0. Left, analysis for Sierra Leone (blue), Liberia (red) and Guinea (green). Right, analysis for before October 2014 (grey) and after October 2014 (orange). Points with vertical lines connected to the *x* axis indicate the 50% and 95% quantiles of the parameter density estimates. Within Sierra Leone, Liberia and Guinea, 50% of all migrations occurred over distances of around 100 km and persisted for around 25 days. Exceptions were for Sierra Leone, which experienced more introductions per location (around 12) than Guinea and Liberia (around 4); and Guinea, where migrations tended to occur over larger distances owing to the size of the country and whose cluster sizes following introductions tended to be lower (3 sequences versus Liberia and Sierra Leone, which had 5 sequences each). Between the first (grey) and second (orange) years of the epidemic there were considerable reductions in cluster persistence, cluster sizes and distances travelled by viruses, whereas dispersal intensity remained largely the same.

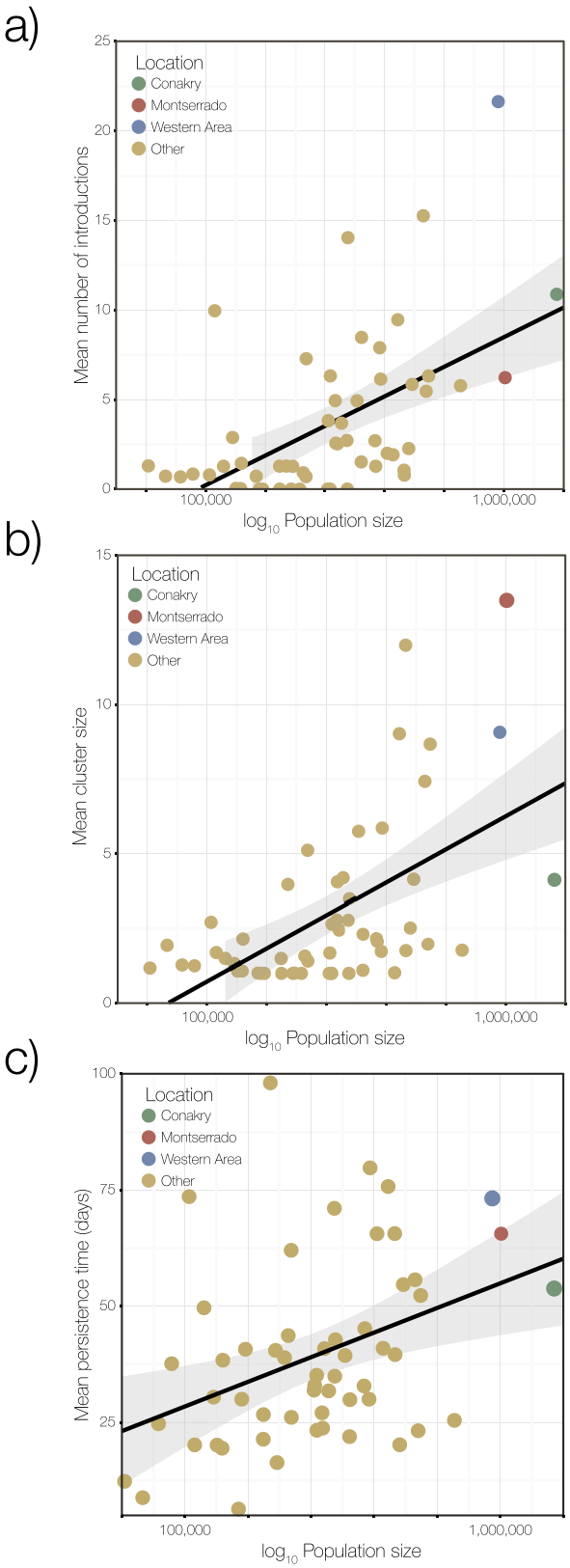

Extended Data Figure 9 | Relationship between cluster size, introductions or persistence and population size. a, The mean number of introductions into each location against (log) population sizes. The Western Area (in Sierra Leone) received the most introductions, whereas Conakry and Montserrado were closer to the average. The association between population size and the number of introductions was not very strong ($R^2 = 0.28$, Pearson correlation = 0.54, Spearman correlation = 0.57). **b**, The mean cluster size for each location plotted against (log) population sizes. The association is weaker than for **a** ($R^2 = 0.11$, Pearson correlation = 0.35, Spearman correlation = 0.57). **c**, The mean persistence times (per cluster, in days) against population sizes. A similarly weak association is observed as in **b** ($R^2 = 0.12$, Pearson correlation = 0.37, Spearman correlation = 0.36). All computations were based on a sample of 10,000 trees from the posterior distribution.

Extended Data Table 1 | Predictors included in the time-homogenous GLM

Predictor type	Abbreviation	Predictor description
Geographic	Distances	Great circle distances between the locations' population centroids, log-transformed, standardized
Administrative	Nat/Int	Two locations are in the same country verses in different countries
Administrative	Nat/Int	The relative preference of transitioning between locations in the same country over transitioning between locations in two different countries
Administrative	IntBoSh	The relative preference of transitioning between location pairs that are in different countries and share a border
Administrative	NatBoSh	The relative preference of transitioning between location pairs that are in the same country and share a border
Administrative	LibGinAsym	Between Liberia-Guinea asymmetry
Administrative	LibSLeAsym	Between Liberia-Sierra Leone asymmetry
Administrative	GinSLeAsym	Between Guinea-Sierra Leone asymmetry
Demographic	OrPop	Origin population size, log-transformed, standardized
Demographic	DestPop	Destination population size, log-transformed, standardized
Demographic	OrPopDens	Origin population density, log-transformed, standardized
Demographic	DestPopDens	Destination population density, log-transformed, standardized
Demographic	OrTT100k	Estimated mean travel time in minutes to reach the nearest major settlement of at least 100,000 people at origin, log-transformed, standardized
Demographic	DestTT100k	estimated mean travel time in minutes to reach the nearest major settlement of at least 100,000 people at destination, log-transformed, standardized
Demographic	OrGrEcon	Origin Gridded economic output, log-transformed, standardized
Demographic	DestGrEcon	Destination Gridded economic output, log-transformed, standardized
Cultural	IntLangShared	The relative preference of transitioning between location pairs that are in different countries and share at least one of 17 vernacular languages
Cultural	NatLangShared	The relative preference of transitioning between location pairs that are in the same country and share at least one of 17 vernacular languages
Climatic	OrTemp	Temperature annual mean at origin, log-transformed, standardized
Climatic	DestTemp	Temperature annual mean at destination, log-transformed, standardized
Climatic	OrTempSS	Index of temperature seasonality at origin, log-transformed, standardized
Climatic	DestTempSS	Index of temperature seasonality at destination, log-transformed, standardized
Climatic	OrPrecip	Precipitation annual mean at origin, log-transformed, standardized
Climatic	DestPrecip	Precipitation annual mean at destination, log-transformed, standardized
Climatic	OrPrecipSS	Index of precipitation seasonality at origin, log-transformed, standardized
Climatic	DestPrecipSS	Index of precipitation seasonality at destination, log-transformed, standardized

AMERICAN SOCIETY FOR MICROBIOLOGY | mBio®

RESEARCH ARTICLE

Noroviruses Co-opt the Function of Host Proteins VAPA and VAPB for Replication via a Phenylalanine–Phenylalanine-Acidic-Tract-Motif Mimic in Nonstructural Viral Protein NS1/2

Broc T. McCune,[a] Wei Tang,[b] Jia Lu,[c] James B. Eaglesham,[c] Lucy Thorne,[c] Anne E. Mayer,[a] Emily Condiff,[a] Timothy J. Nice,[a]* Ian Goodfellow,[c] Andrzej M. Krezel,[b] Herbert W. Virgin[a]

Department of Pathology and Immunology, Washington University School of Medicine, St. Louis, Missouri, USA[a]; Department of Biochemistry and Molecular Biophysics, Washington University School of Medicine, St. Louis, Missouri, USA[b]; Department of Pathology, Division of Virology, University of Cambridge, Cambridge, United Kingdom[c]

ABSTRACT The *Norovirus* genus contains important human pathogens, but the role of host pathways in norovirus replication is largely unknown. Murine noroviruses provide the opportunity to study norovirus replication in cell culture and in small animals. The human norovirus nonstructural protein NS1/2 interacts with the host protein VAMP-associated protein A (VAPA), but the significance of the NS1/2-VAPA interaction is unexplored. Here we report decreased murine norovirus replication in VAPA- and VAPB-deficient cells. We characterized the role of VAPA in detail. VAPA was required for the efficiency of a step(s) in the viral replication cycle after entry of viral RNA into the cytoplasm but before the synthesis of viral minus-sense RNA. The interaction of VAPA with viral NS1/2 proteins is conserved between murine and human noroviruses. Murine norovirus NS1/2 directly bound the major sperm protein (MSP) domain of VAPA through its NS1 domain. Mutations within NS1 that disrupted interaction with VAPA inhibited viral replication. Structural analysis revealed that the viral NS1 domain contains a mimic of the phenylalanine–phenylalanine-acidic-tract (FFAT) motif that enables host proteins to bind to the VAPA MSP domain. The NS1/2-FFAT mimic region interacted with the VAPA-MSP domain in a manner similar to that seen with bona fide host FFAT motifs. Amino acids in the FFAT mimic region of the NS1 domain that are important for viral replication are highly conserved across murine norovirus strains. Thus, VAPA interaction with a norovirus protein that functionally mimics host FFAT motifs is important for murine norovirus replication.

IMPORTANCE Human noroviruses are a leading cause of gastroenteritis worldwide, but host factors involved in norovirus replication are incompletely understood. Murine noroviruses have been studied to define mechanisms of norovirus replication. Here we defined the importance of the interaction between the hitherto poorly studied NS1/2 norovirus protein and the VAPA host protein. The NS1/2-VAPA interaction is conserved between murine and human noroviruses and was important for early steps in murine norovirus replication. Using structure-function analysis, we found that NS1/2 contains a short sequence that molecularly mimics the FFAT motif that is found in multiple host proteins that bind VAPA. This represents to our knowledge the first example of functionally important mimicry of a host FFAT motif by a microbial protein.

KEYWORDS noroviruses, plus-strand RNA virus, protein structure-function, reverse genetic analysis, viral replication, virus-host interactions

Received 29 April 2017 **Accepted** 4 May 2017 **Published** 11 July 2017

Citation McCune BT, Tang W, Lu J, Eaglesham JB, Thorne L, Mayer AE, Condiff E, Nice TJ, Goodfellow I, Krezel AM, Virgin HW. 2017. Noroviruses co-opt the function of host proteins VAPA and VAPB for replication via a phenylalanine–phenylalanine-acidic-tract-motif mimic in nonstructural viral protein NS1/2. mBio 8:e00668-17. https://doi.org/10.1128/mBio.00668-17.

Editor Terence S. Dermody, University of Pittsburgh School of Medicine

Address correspondence to Herbert W. Virgin, virgin@wustl.edu.

* Present address: Department of Molecular Microbiology and Immunology, Oregon Health and Science University, Portland, Oregon, USA.

This article is a direct contribution from a Fellow of the American Academy of Microbiology. External solicited reviewers: Ralph Baric, University of North Carolina at Chapel Hill; Daniele Fabris, The RNA Institute, State University of New York at Albany.

Noroviruses (NoVs) are nonenveloped positive-sense single-stranded RNA viruses that primarily infect the gastrointestinal tract. They are a leading cause of gastroenteritis worldwide (1–3). Noroviruses are divided into genogroups GI to GVI. Among those genogroups, GI, GII, and GIV viruses cause human disease and GV encompasses more recently discovered rodent NoVs, including murine norovirus (MNoV) (4). As MNoVs replicate robustly in mice and cells and can be studied via mutagenesis of infectious molecular clones, they serve as a powerful model for molecular studies of norovirus replication, tropism, and pathogenesis (5, 6).

The norovirus genome encodes nine known proteins: seven nonstructural (NS) proteins derived by proteolysis of the open reading frame (ORF) 1 polyprotein (7) and two structural proteins, VP1 and VP2, derived from ORFs 2 and 3, respectively (6). MNoV encodes virulence protein VF1 from ORF 4, which overlaps ORF 2 and has not been found in human noroviruses (8). The N-terminal protein in the norovirus polyprotein, NS1/2, comprises three domains: NS1, NS2, and a putative transmembrane domain (9). The MNoV NS1 domain in isolation has a structured region preceded by an unstructured domain (9, 10). A single aspartic acid-to-glutamic acid difference within NS1 confers an altered conformation within the NS1 structured domain (10) and is associated with enteric tropism and the capacity of MNoV to persistently infect and be shed from the mouse intestine (11). Ectopically expressed NS1/2 from GI human norovirus ($NS1/2^{GI}$) disrupts the Golgi apparatus and vesicular trafficking (12, 13) and is reported to interact with the host protein VAMP-associated protein A (VAPA) (12). The role of VAPA interactions with NS1/2 during viral replication has not been defined.

VAPA is a type II endoplasmic reticulum (ER)-resident protein that is conserved in eukaryotes (14). VAPB is structurally related to VAPA (15). VAPA comprises a major sperm protein (MSP) domain, a coiled-coil domain (CCD), and a transmembrane domain. Initially found to bind to proteins within the SNARE superfamily of vesicle trafficking proteins (16–18), VAPA also binds a variety of client interacting proteins (14). Importantly, through its cytosolic MSP domain, VAPA interacts with client proteins primarily involved in lipid trafficking (14, 19–23). These client proteins interact with the VAPA-MSP domain via a phenylalanine–phenylalanine-acidic-tract (FFAT) linear motif (22, 24–27).

VAPA performs important functions during infection as both microbes and antimicrobial host molecules target VAPA and its client proteins. VAPA and VAPB enhance the replication of hepatitis C virus (28, 29), rhinoviruses (30), tombusvirus (31, 32), and the intracellular bacteria *Chlamydia trachomatis* (33, 34). Some of these microbes encode molecules that interact with VAPA and VAPB and/or their client proteins, including hepatitis C virus proteins NS5a and NS5b (28, 29), tombusvirus p33 (31, 32), and *C. trachomatis* IncD (33, 34). Several observations support the idea that VAPA and VAPA client proteins assist in organization of membranous structures critical for virus replication (35, 36), possibly by manipulating the lipid composition of these membranes (30–32). Furthermore, VAPA binds to proteins regulated by interferon, interferon-induced transmembrane protein 3 (37), and viperin (38, 39), suggesting that VAPA may be involved in antiviral responses.

Here we found that VAPA enhances MNoV replication and defined the molecular basis of NS1/2-VAPA interactions. Disruption of VAPA in permissive cells delayed MNoV replication due to effects occurring after viral entry but prior to synthesis of viral minus-sense RNA. VAPB was also important for MNoV replication and bound MNoV NS1/2. The interaction between NS1/2 and VAPA was conserved between human norovirus and MNoV NS1/2 proteins. The NS1 domain of MNoV NS1/2 interacted with the MSP domain of VAPA. This interaction occurred independently of other cellular or viral proteins and mapped to a short region in the NS1 domain sharing features of the FFAT motif found in host proteins that also interact with the VAPA MSP domain. NS1 engaged VAPA MSP domain residues crucial for interaction with FFAT motifs found in VAPA client proteins. Mutagenesis of conserved amino acids in NS1 to abrogate VAPA interaction impaired recovery of infectious MNoV after transfection of permissive cells with plasmids encoding the viral genome. These data indicate that NS1/2-VAPA binding

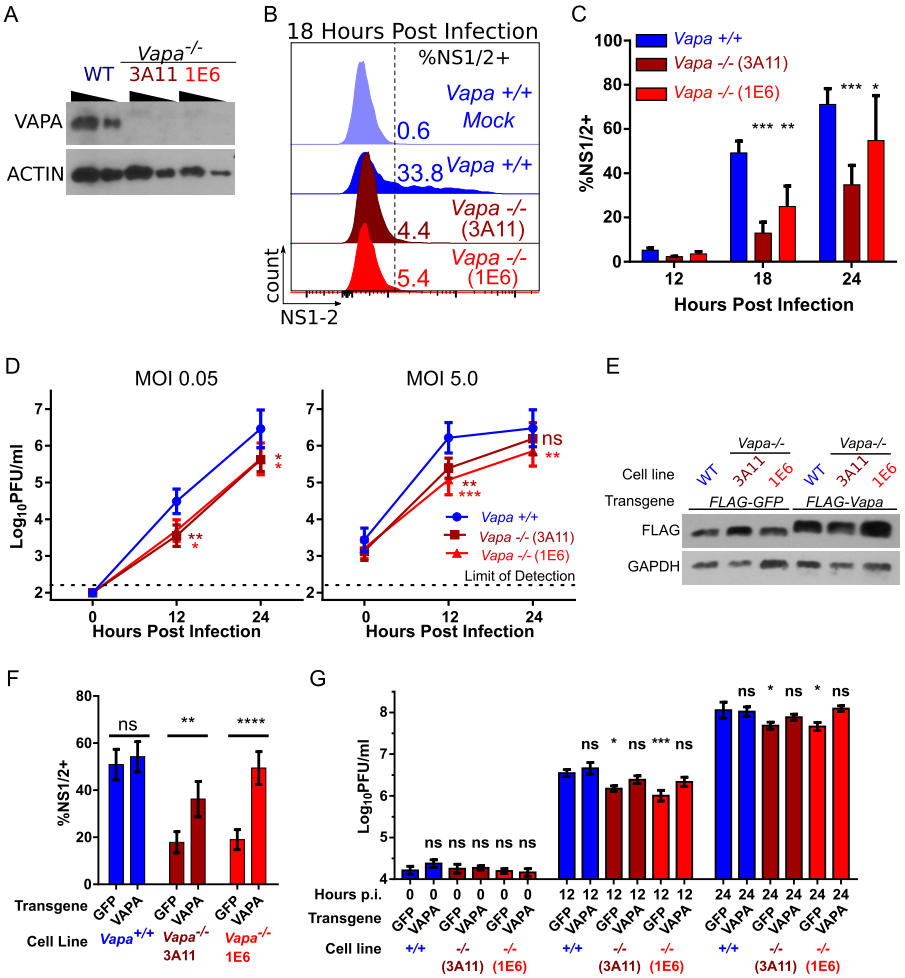

FIG 1 Murine norovirus replication in *Vapa*$^{-/-}$ cells is diminished. (A) VAPA Western blot of *Vapa*$^{-/-}$ cell lines. (B) Representative infection frequency of MNoV-CW3 in *Vapa*$^{-/-}$ cells, measured by FACS analysis of intracellular NS1/2 (18 h postinfection; MOI of 5.0). (C) Same as panel B. Data represent results of combined experiments (repeated-measure two-way ANOVA, Dunnett posttest; $n = 3$). (D) MNoV strain CW3 growth in *Vapa*$^{-/-}$ and *Vapa*$^{+/+}$ cell lines (MOI, 0.05 [left] or 5.0 [right] PFU/cell). Data represent results of repeated-measure one-way ANOVA and the Dunnett posttest ($n = 6$). (E) Western blot of *Vapa*$^{+/+}$ or *Vapa*$^{-/-}$ cell lines lentivirally transduced with *FLAG-GFP* or *FLAG-Vapa*. (F) Infection frequency in *Vapa*- or *GFP*-transduced cells determined as described for panel B (two-way ANOVA, Sidak posttest; $n = 9$). (G) CW3 growth in *Vapa*- or *GFP*-transduced cells. Data represent results of repeated-measure two-way ANOVA and the Dunnett posttest ($n = 5$). For G the asterisks refer to a comparison to the time-matched +/+ GFP control.

is critical for efficient MNoV replication and that this occurs through viral mimicry of the host FFAT motif by amino acids in the NS1 domain of the nonstructural NS1/2 protein.

RESULTS

Murine norovirus replication is diminished in VAPA-deficient cells. To test the hypothesis that MNoV replication involves VAPA, we genetically engineered RAW 264.7 cells deficient in VAPA expression (here *Vapa*$^{-/-}$) using clustered regularly interspaced short palindromic repeats (CRISPR)-Cas9. In two single-cell cloned *Vapa*$^{-/-}$ cell lines, 3A11 and 1E6, frameshifts in the first 37 nucleotides (see Fig. S1A in the supplemental material) of coding sequence resulted in loss of VAPA protein expression (Fig. 1A). *Vapa*$^{-/-}$ cells infected with MNoV strain CW3 had 2.2-fold-fewer (1E6) or 4.0-fold-fewer (3A11) NS1/2-positive cells by flow cytometry at 18 h postinfection (hpi) than wild-type (WT) cells (Fig. 1B and C). We observed lower levels of replication of MNoV strains CW3 and CR6 in both *Vapa*$^{-/-}$ cell lines (Fig. 1D; Fig. S1B). Reconstituting VAPA production in *Vapa*$^{-/-}$ cells via lentivirus transduction (Fig. 1E) increased the percentage of cells

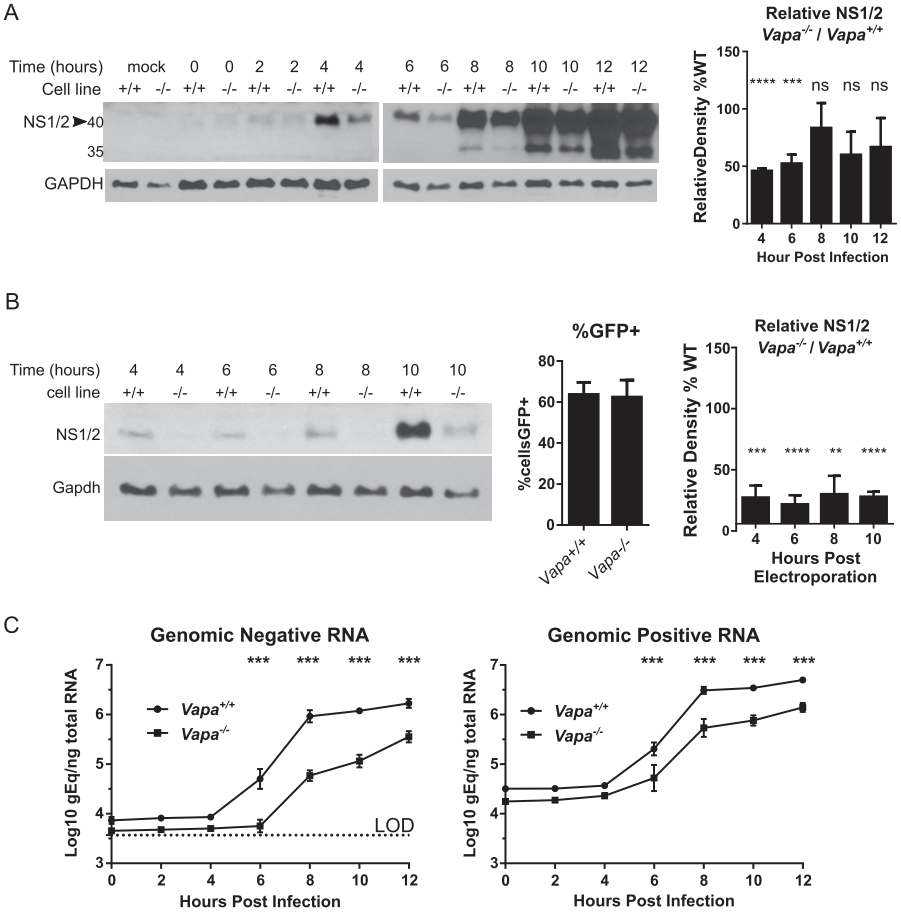

FIG 2 Murine norovirus replication in RAW 264.7-*Vapa*$^{-/-}$ cells is impaired early in the viral life cycle. (A) Western blot of NS1/2 in *Vapa*$^{+/+}$ and *Vapa*$^{-/-}$ (3A11) cell lines (MOI of 5). (Right panel) Combined densitometry data from multiple experiments performed on film exposures for each time point within the linear range of assay (n = 2 to 4) (unpaired t test, means compared to H_o = 100). (B) NS1/2 Western blot after electroporation of viral RNA (vRNA) into *Vapa*$^{+/+}$ and *Vapa*$^{-/-}$ 3A11 cells (representative, n = 3 to 5). (Middle panel) *Vapa*$^{+/+}$ and *Vapa*$^{-/-}$ cells were transfected equivalently with pMAX-GFP. (Right panel) Combined densitometry data determined as described for panel A (n = 3 to 5). (C) Viral-strand-specific quantitative PCR for negative strand (left) and positive strand (right) over time in infected *Vapa*$^{+/+}$ and *Vapa*$^{-/-}$ 3A11 cells (MOI of 5; n = 3; two-way ANOVA).

expressing NS1/2 at 18 h postinfection by 2.7-fold (3A11) or 4.1-fold (1E6) compared to transduction with green fluorescent protein (GFP) (Fig. 1F). Expression of VAPA, but not GFP, rescued viral replication in *Vapa*$^{-/-}$ cells (Fig. 1G). Because VAPA deficiency incompletely blocked MNoV replication, we considered the possibility that VAPB might compensate for VAPA function. We found that VAPB was also important for MNoV replication (Fig. S1C). We were unable to efficiently isolate cell lines containing out-of-frame mutations in both VAPA and VAPB to directly test the possibility that these two proteins might compensate for each other (not shown). Furthermore, we were unable to test the role of VAPA in mice as mutation of *Vapa* led to embryonic lethality (Fig. S1D to F). We conclude that MNoV infectivity was enhanced by VAPA expression and chose to examine the mechanism responsible in more detail for VAPA.

VAPA is important for an early postentry step in norovirus replication. To investigate the role of VAPA in MNoV replication, we analyzed nonstructural protein expression by assessing NS1/2 protein levels in infected cells by Western blotting. Infected *Vapa*$^{-/-}$ cells expressed lower levels of NS1/2 protein at 4 and 6 hpi (Fig. 2A), with the difference diminishing later in infection. This supports the notion of a role for VAPA in early events of MNoV replication. Because VAPA is associated with efficient entry of an enveloped virus (37) as well as with the function of endosomes (19, 37, 40),

through which MNoV likely passes to establish infection (41–43), we tested whether impaired viral entry in *Vapa*$^{-/-}$ cells accounted for decreased NS1/2 production and viral replication. We reasoned that transfection of viral RNA would bypass any effect of VAPA on viral entry and uncoating. After electroporating purified viral RNA into cells, we continued to detect decreased NS1/2 levels in *Vapa*$^{-/-}$ cells (Fig. 2B), despite observing no difference in transfectability as measured by plasmid-driven GFP expression (Fig. 2B, middle panel). These data indicate that VAPA plays a role in viral protein expression downstream of viral entry.

After the viral RNA accesses the cytoplasm, NS1/2 protein can be produced either by translation of virion-derived plus-sense viral RNA or by transcription of plus-sense viral RNA from newly synthesized minus-sense RNA. Using strand-specific reverse transcription-quantitative PCR (RT-PCR) (44), we observed delayed accumulation of both negative-sense and positive-sense MNoV RNA in the *Vapa*$^{-/-}$ 3A11 (Fig. 2C) and 1E6 (Fig. S2) cell lines, indicating that production of NS1/2 is impaired prior to synthesis of new viral minus-sense RNA. Collectively, these observations support the notion of a role for VAPA downstream of viral RNA delivery into the cytosol but upstream of minus-sense viral RNA synthesis.

NS1/2 interaction with VAPA is conserved among norovirus strains. Prior work showed that VAPA interacts with GI human norovirus NS1/2 protein (NS1/2^{GI}) (12). To test if VAPA interaction with NS1/2 is conserved across genogroups and species boundaries, we engineered MNoV to express a FLAG tag in NS1/2 (nucleotide 383) and also studied a previously described virus with a FLAG tag in NS4 (nucleotide 2600) (Fig. S3A) (45). We selected NS4 for this experiment as it is known to bind NS1/2 (45). Both MNoV-NS1/2^{FLAG} and MNoV-NS4^{FLAG} replicated similarly to wild-type virus (Fig. S3B). FLAG-tagged viral proteins of appropriate molecular mass were expressed during infection (Fig. 3A, top left). As expected, virus-derived FLAG-NS1/2 and FLAG-NS4 localized with NS7, a marker for the viral replication complex (Fig. S3C) (46). Having validated the use of FLAG-tagged viruses to study replication, we infected the BV2 microglial cell line with MNoV-NS1/2^{FLAG} and MNoV-NS4^{FLAG}. Both FLAG-NS1/2 and FLAG-NS4 coprecipitated with VAPA but not NS7 or GAPDH (glyceraldehyde-3-phosphate dehydrogenase) (Fig. 3A, bottom). Thus, NS1/2, either independently or together with NS4, interacts with VAPA (45).

To test for direct NS1/2-VAPA interaction independently of the presence of other viral proteins, we assessed NS1/2 interaction with VAPA by mammalian 2-hybrid (M2H) analysis. In this assay, interaction between a "bait" protein and a "prey" protein generates a luciferase signal. As previously reported (12, 23, 47), we detected VAPA interaction with itself, the host protein oxysterol-binding protein 1 (OSBP), and human norovirus NS1/2^{GI}, validating use of M2H analysis as an approach to assess VAPA interactions (Fig. 3B). NS1/2^{MNoV} from either MNoV strain CW3 or MNoV strain CR6 interacted with VAPA (Fig. 3B). Of interest, NS1/2 also interacted with VAPB (Fig. 3B).

NS1/2 interacts with FFAT-binding residues in VAPA MSP domain. Many VAPA protein-protein interactions occur between the VAPA MSP domain and host cell proteins containing FFAT motifs. Structure-function analyses of FFAT-VAPA interactions support a model in which FFAT motifs from VAPA client proteins rest within a groove present on the surface of the VAPA-MSP domain (24–26). Within this groove, VAPA residues K50, K52, K94, M96, and K125 are critical for interaction with FFAT motifs. To test if these residues also engage NS1/2, we introduced the following mutations into VAPA: K50E/K52E, K94A/M96A, and K125E/R127E (Fig. 4A). Each of these mutation pairs decreased VAPA interaction with NS1/2 (Fig. 4A) as measured by M2H analysis. To test if NS1/2 interacts with sets of positively charged residues elsewhere in VAPA, we mutated additional sites in VAPA selected to have the sequence (H/R/K)X(H/R/K). Mutations K161E/H163E, H195E/R197E, and R202E/R204E had no effect on the NS1/2-VAPA interaction (Fig. 4A). We conclude that the NS1/2 interaction specifically required positively charged residues within the VAPA MSP domain.

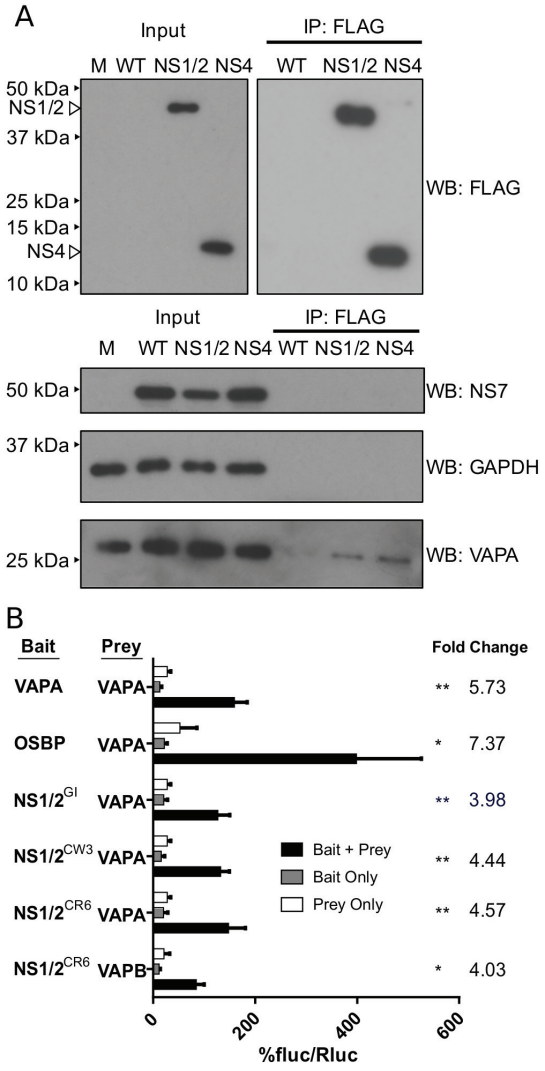

FIG 3 NS1/2 interactions with VAPA are conserved between norovirus strains and occur during infection. (A) BV2 cells were infected with NS1/2-FLAG or NS4-FLAG MNV for 8 h (MOI of 10 $TCID_{50}$/cell). FLAG pulldown was performed on lysates, and immunoblotting was performed with the specified antibodies. M, molecular marker. (B) M2H interaction of $NS1/2^{GI}$, $NS1/2^{MNoV}$ (CR6 and CW3), OSBP, and VAPA with VAPA or VAPB (bottom) (one-way ANOVA, Dunnett posttest; fold change data are shown on the right; $n = 3$). fluc, firefly luciferase; Rluc, *Renilla* luciferase.

In work presented below, we found that the NS1 domain of NS1/2 is required for NS1/2-VAPA interactions. To map the physical interactions between NS1 and the VAPA-MSP domain, we used nuclear magnetic resonance (NMR) to analyze the chemical shift perturbations of the ^{15}N-labeled VAPA-MSP domain (M8–M132 of VAPA) titrated with increasing amounts of unlabeled NS1 (S28–R114 of NS1/2). This analysis revealed interactions between NS1/2 and four groups of residues on VAPA (Fig. 4B; K52–T54, C60–N64, K92–V97, and D123–L126). These groups of residues all mapped to the FFAT binding groove on a positively charged surface of the MSP domain. Furthermore, the VAPA residues that bind NS1/2 coincide with the FFAT-motif interaction surface on the MSP domain (24, 25). Using the same experimental approach, we did not observe any interactions of NS1 with the isolated coiled-coil domain (P133–S226 of VAPA; data not shown).

We independently verified the role of the VAPA residues identified above in NS1/2-VAPA interactions using M2H analysis (Fig. 4A). To this end, we replaced selected amino acids in the VAPA MSP domain with either glutamate or alanine and tested for the

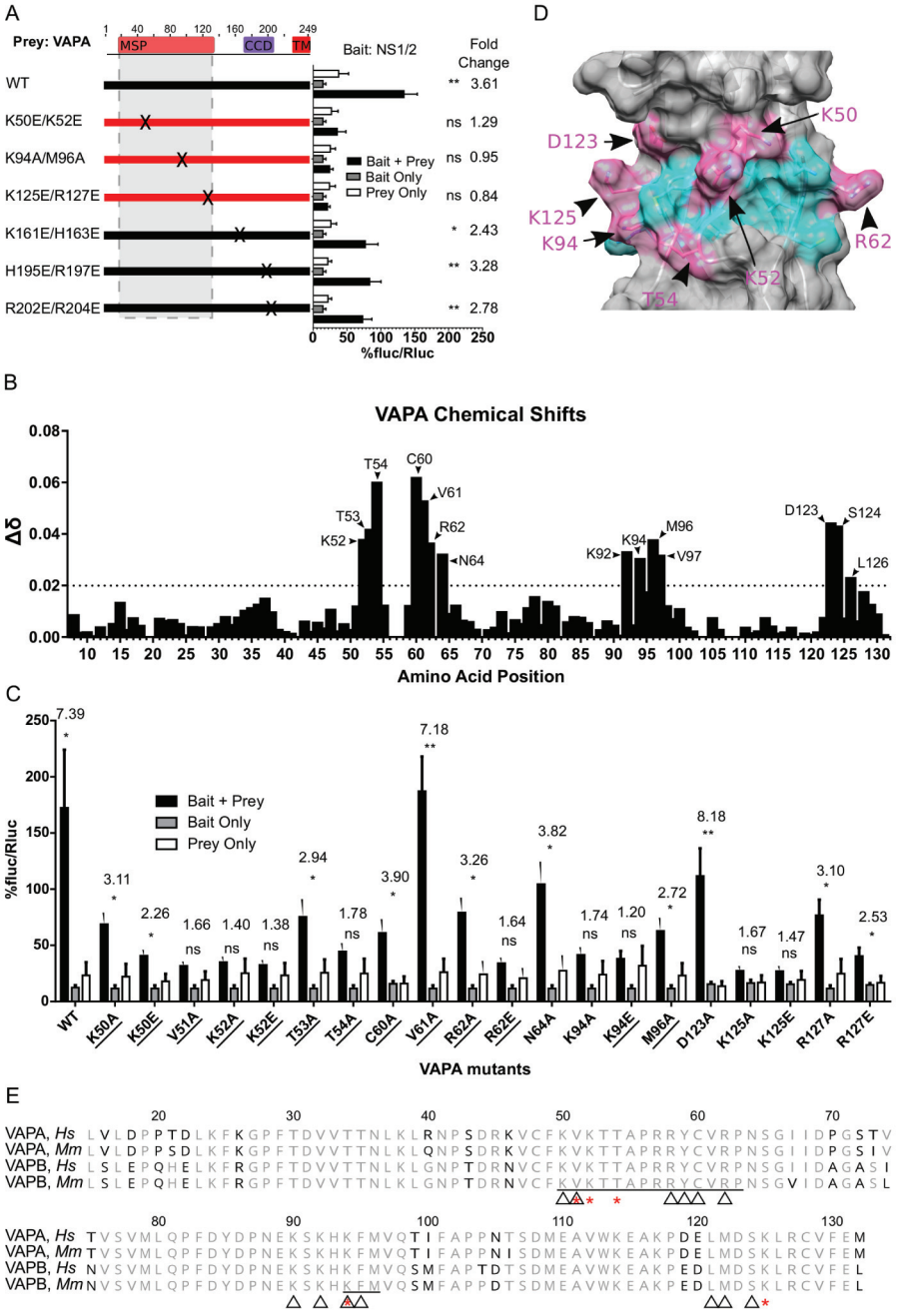

FIG 4 NS1/2 binds FFAT-interacting residues in MSP domain of VAPA. (A) M2H interaction of NS1/2^{MNoV} with VAPA mutants. (B) Chemical shift perturbations of amide resonances upon unlabeled-NS1^{CW3} titration into ^{15}N-labeled VAPA MSP. The horizontal broken line represents the threshold. (C) M2H analysis of additional single-residue mutant VAPA. Designations of residues interacting with FFAT are underlined (one-way ANOVA, Dunnett posttest; fold change data are shown at the top; $n = 3$). (D) Murine VAPA MSP domain (PDB 2CRI). Pink highlighting indicates residues that disrupted the NS1/2-VAPA interaction in M2H analysis when mutated; mutations in cyan residues did not disrupt interaction. (E) Multiple alignment of VAPA and VAPB MSP domains from human (*Hs*) and mouse (*Mm*). Residues indicated with a black character differ from consensus data. Red asterisks mark residues necessary for interaction in M2H analysis, and triangles mark residues that shifted in NMR during NS1/2 titration.

interaction of these mutant molecules with NS1/2. No interaction was detected with glutamate or alanine substitutions at positions V51, K52, T54, K94, and K125 (Fig. 4C and D). No interaction occurred after mutation of R62 to glutamate, but an interaction was present with alanine at this site (Fig. 4C). At positions K50, T53, V61, N64, M96, and R127, however, we observed interaction after replacing those residues with either glutamate or

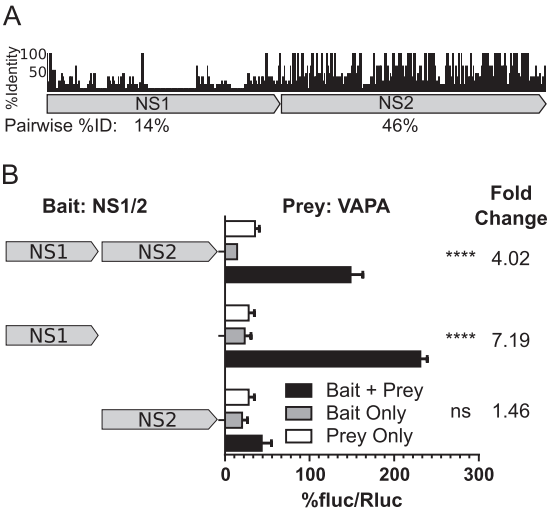

FIG 5 A poorly conserved NS1 domain within NS1/2^{MNoV} interacts with VAPA. (A) Alignment of NS1/2 from representative strains from each norovirus genogroup. %ID, percent identity. (B) M2H analysis of full-length or domain truncations of NS1/2^{MNoV} (CR6) with VAPA (one-way ANOVA and Dunnett posttest; fold change data are shown at the top; $n = 3$).

alanine (Fig. 4C and D). Notably, the residues within the VAPA-MSP domain that are necessary for interaction with NS1 are conserved in VAPB (Fig. 4E).

Residues 47 to 54 of murine norovirus NS1 are necessary for interaction with VAPA. While the NS2 domain is well conserved within the *norovirus* genus, NS1 is not (Fig. 5A). Accordingly, we predicted that the conserved NS2 domain contributed to the NS1/2 interaction with VAPA. Surprisingly, the MNoV NS1 domain containing residues 1 to 131 was sufficient to interact with VAPA whereas the NS2 domain did not interact (Fig. 5B). To define the specific NS1 residues interacting with VAPA-MSP, we analyzed the chemical shift perturbations of the NMR spectra of ^{15}N-labeled NS1 (S28–R114 of NS1/2) with increasing amounts of unlabeled VAPA (M8–S226 of VAPA). The largest perturbations in NS1 from both the CR6 and CW3 strains of MNoV were observed for a core of interacting residues centered on Y47–Q53 (YMTPPEQ) (Fig. 6A and Fig. S4A). A longer sequence, encompassing residues I45 to A61, showed consistent but smaller perturbations (Fig. 6A and Fig. S4A). There are no observable amides in prolines; hence, no data were available for P50, P51, and P57.

To test the importance of this core of interacting residues, we carried out experiments with three mutant forms of NS1, namely, NS1-CR6^{M48G}, CW3^{T49G}, and CW3^{E52K}. The heteronuclear single-quantum coherence (HSQC) spectra obtained for the mutants were similar, indicating that these mutations did not destabilize tertiary structures (data not shown). NS1-CW3^{T49G} and CW3^{E52K} mutations decreased binding to VAPA to undetectable levels, while NS1-CR6^{M48G} interacted with VAPA (Fig. 6A and Fig. S4B). Within the NS1 domain, the VAPA interacting residues are predominantly within the segment K26–P57, which shows a highly dynamic conformation in isolated NS1 (10). The last few interacting residues of the core residues of NS1 that interact with VAPA are in the structured domain of NS1 (G58–R114) (10).

Murine norovirus NS1 contains a mimic of host FFAT domains. The FFAT motif is responsible for interactions of host proteins with the MSP domain of VAPA. We identified residues 40 to 54 as the domain of NS1 which interacts with the MSP domain of VAPA. Thus, we compared this region of NS1 with FFAT motifs. Generally, FFAT motifs contain a core bulky aromatic residue flanked by acidic residues (22, 27). Correspondingly, residues 40 to 54 of NS1/2 contain a bulky aromatic (Y47) flanked by acidic residues E40, E42, D43, E44, E52, and E54 (Fig. 6B). Interestingly, this sequence is conserved across MNoV strains (Fig. 6B and Fig. S4C), though positions 45, 46, and 48 are variable. The strong conservation of certain amino acids in this region suggested that this motif has functional importance.

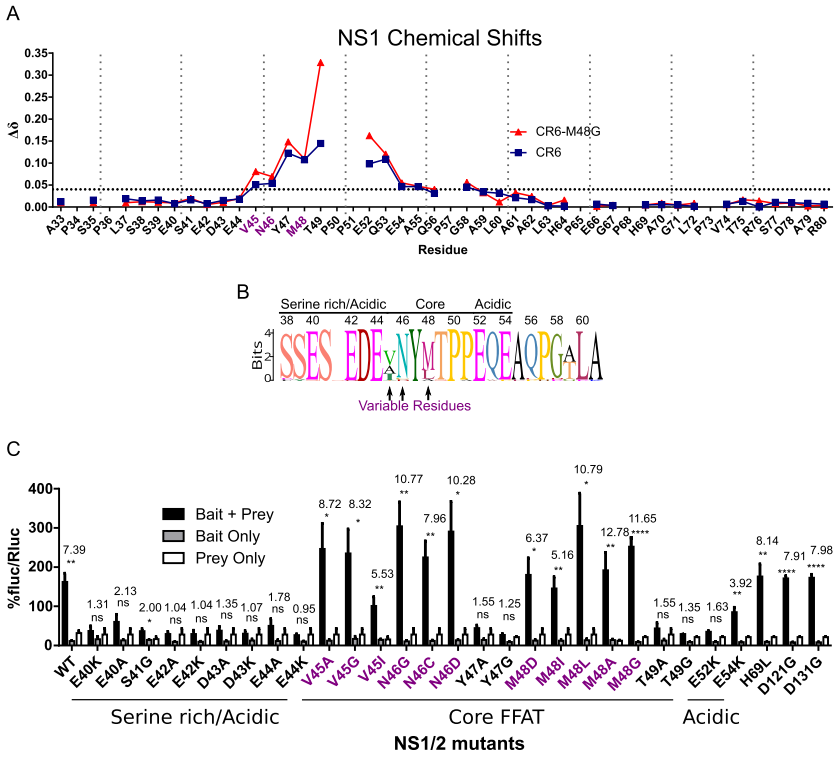

FIG 6 The N-terminal segment of NS1-MNoV interacts with VAPA. (A) Chemical shift perturbations of amide resonances upon titration of unlabeled VAPA into ^{15}N-labeled NS1-CR6 and CR6^{M48G}. The horizontal broken line represents the threshold. Purple residues are indicated as described for panel B. (B) Sequence logo of FFAT-like amino acid sequence of NS1/2 derived from BLAST alignment (Fig. S4C). The font size for each amino acid is proportional to percent conservation at each position. Residues exhibiting greater variability across MNoV strains are highlighted with arrows (colored purple here). (C) M2H interaction with NS1/2 substitutions (NS1/2, bait, VAPA, prey). Residues 69, 121, and 131 are not predicted to interact with VAPA. Purple residues are indicated as described for panel B (one-way ANOVA, Dunnett posttest; fold change data are shown at the top; $n = 3$).

To test which residues within this domain contribute to interaction with VAPA, we introduced single-residue mutations and assessed their effect by M2H analysis. For positions in the N-terminal acidic segment, mutations E40A, E40K, E42A, E42K, D43A, D43K, E44A, and E44K blocked NS1/2-VAPA interactions, while S41G maintained a detectable interaction (Fig. 6C). Within the FFAT-like core segment, Y47A, Y47G, T49A, and T49G ablated NS1/2 interactions with VAPA. Residues at positions 45, 46, and 48 are variable across MNoV strains (Fig. 6B and Fig. S4C). To test the function of amino acids in these positions, we introduced variants observed in other MNoV strains, including V45A, V45I, N46C, N46D, M48A, and M48L, as well as variants not observed in MNoV isolates, including V45G, N46G, M48D, M48I, and M48G. Mutations at these positions did not disrupt interactions, suggesting that the interaction is preserved among variable sequences in these positions across strains (Fig. 6C). For C-terminal acidic residues, E52K mutation disrupted the interaction, but E54K maintained the interaction. Additionally, mutations outside this region, including H69L, D121G, and D131G, did not prevent interaction (Fig. 6C).

In summary, the S40-E54 region of NS1 mimics the host FFAT motif and serves as the basis for interaction with the VAPA MSP domain based on the following findings: (i) the order and chemical nature of the amino acids mimic those of the FFAT motif (acidic, bulky aromatic, and then acidic); (ii) each of those acidic or bulky aromatic amino acids is necessary for binding VAPA; (iii) this NS1 region interacts with the same region of VAPA which binds to FFAT motifs in host proteins; and (iv) these critical amino acids are conserved across norovirus strains.

NS1/2-VAPA interactions are required for recovery of murine norovirus from infectious clones. We used an infectious molecular clone of MNoV to introduce

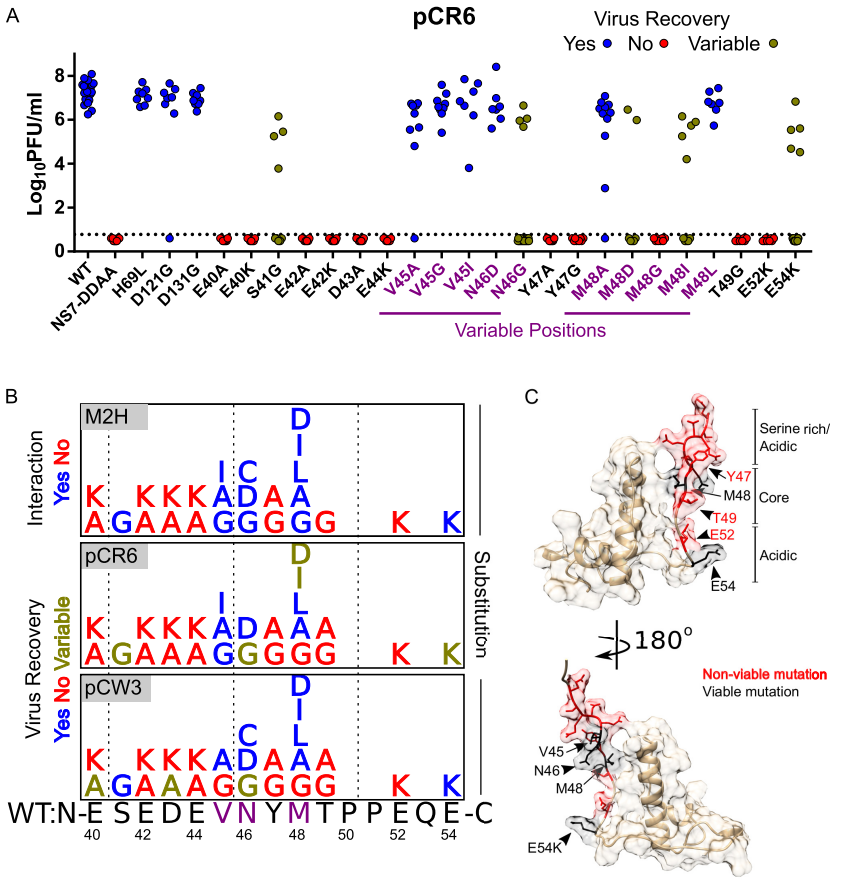

FIG 7 NS1/2 interaction with VAPA enhances recovery of murine norovirus from infectious clones. (A) Recovery titers of mutants of MNoV strain pCR6. Data represent passage 1 titers (n = 7 to 20). (B) Summary of interaction of NS1/2 mutants with VAPA in M2H analysis, and recovery of virus from infectious clones for CW3 and CR6 NS1/2 mutants. (C) Molecular surface-and-ribbon diagram of solution structure of NS1-MNoV (PDB 2MCD [10]) with viable (black) and nonviable (red) mutants.

mutations and to determine the importance of the NS1/2-VAPA interaction and the specific amino acids in the NS1/2 FFAT-like domain required for MNoV growth. Mutations were introduced in a plasmid encoding the CR6 viral genome, and recovery of infectious virus was assessed after transfection of the plasmid into permissive cells. We noticed three patterns of recovery of infectious virus in these experiments (Fig. 7A): (i) some NS1/2 mutations had no discernible effect on virus recovery (V45G, V45A, V45I, N46D, M48A, M48L, H69L, D121G, and D131G); (ii) some NS1/2 mutations resulted in variable recovery (S41G, N46G, M48I, M48D, and E54K); (iii) some NS1/2 mutations completely eliminated virus recovery (E40A, E40K, E42A, E42K, D43A, D43K, E44A, E44K, Y47G, Y47A, M48G, T49G, T49A, and E52K). We saw similar patterns of virus recovery after insertion of mutations into NS1/2 in the CW3 genome, with the following exceptions: NS1/2 mutations S41G, N46C, M48I, M48D, and E54K resulted in consistent recovery of virus; E40A and D43A mutations resulted in variable virus recovery; I45G mutation completely prevented virus recovery (Fig. S5).

Importantly, this mutational analysis of the NS1 domains of two strains of MNoV revealed a strong correlation between mutations that perturbed VAPA interaction (Fig. 7B, top panel) and those which diminished recovery of virus (Fig. 7B, bottom two panels). Side chains for residues that were critical for recovery of virus primarily mapped to a sequence showing highly dynamic behavior in free NS1 and a few N-terminal residues of the NS1 structured domain (10) (Fig. 7C). The specificity of the relationship between side chain and function within this region is strikingly revealed by comparing the role of the tyrosine at position 47, which was important for virus recovery, and the

immediately adjacent methionine at position 48, where multiple amino acid substitutions were tolerated.

DISCUSSION

In this report, we define the importance of the VAPA host protein and its interaction with viral nonstructural protein NS1/2 in replication of MNoV. We confirmed the previously identified interaction between a human norovirus NS1/2 protein and VAPA (12) and found that this interaction is shared with the NS1/2 proteins of two MNoV strains. Using a variety of approaches, including analysis of the interaction of the proteins *in vitro* and in cells, we delineated the structural basis for the interaction between VAPA and NS1/2 and used these data to test for the importance of specific amino acids in NS1/2 for viral replication and for the interaction between VAPA and NS1/2. These studies support the concept that VAPA is a proviral host protein for MNoV infection and that interaction between NS1/2 and VAPA is important for viral replication. Remarkably, the MNoV NS1 domains appear to mimic host VAPA-binding proteins through the conservation of a region that mimics host FFAT domains present in VAPA MSP domain-interacting proteins.

Norovirus mimicry of host FFAT motifs. Mimicry of host molecules and motifs is a pervasive evolutionary theme enabling microbes to hijack host processes (48). While efforts have been made to predict mimicry on a large scale (49), detecting structural and/or functional domain mimics requires validation through detailed studies of individual microbial molecules. Other microbial proteins involved in targeting VAPA mimicry via a FFAT motif have not been reported. It will be interesting to determine whether FFAT domain mimicry is a common strategy for microbial proteins that target VAPA. If so, small molecules that target this interaction surface may have antiviral or antimicrobial properties for multiple microbes that similarly bind VAPA. In this regard, it is important that FFAT motifs tolerate variation at many positions (22, 27), are relatively short, and are unstructured in solution (24), potentially enabling viruses or other organisms to evolve strategies to target VAPA. It is interesting that much of the region of MNoV NS1/2 that contains the FFAT mimic is unstructured in the purified NS1 domain (10). It seems possible that the interaction of these domains with the MSP domain of VAPA is somehow enhanced by the unstructured nature of this region.

The greatest similarity of the MNoV NS1/2 sequences to host FFAT motifs was identified in the N-terminal and C-terminal portions of the motif. The core sequence was less similar, notably lacking a phenylalanine followed by D/E and instead encoding a tyrosine without a flanking acidic residue. The third position of host FFAT motifs (the second of the two F residues, which define the motif in host proteins) tolerates a wide range of residue substitutions without loss of function. Similarly, both NMR experiments and M2H experiments performed with the NS1 M48G mutant have shown consistent tolerance of variability at this site. Nonetheless, at the structural level, the mode of binding mode of NS1/2 to VAPA showed remarkable similarity to the binding of host FFAT motifs to VAPA, for example, by interaction with specific VAPA amino acids in the MSP domain. It is therefore interesting that the core portions of host and norovirus FFAT motifs differ in some regards, suggesting that there may be specific properties of the interaction that are unique to the viral FFAT motif. Future examination of the molecular basis of the interaction between human norovirus NS1/2 and VAPA and of the conservation of relevant amino acids across norovirus genogroups and strains will be useful and interesting.

Role of VAPA in norovirus replication. Importantly, while we studied VAPA in detail, we also found that the related VAPB protein plays a role in MNoV replication and binds NS1/2. It seems possible that these two proteins play similar roles in NoV replication. For VAPA, it is clear that the stages of viral replication after entry and before minus-sense viral RNA synthesis are affected by VAPA. Nevertheless, our work did not reveal the mechanism by which VAPA participates in the viral life cycle. We have considered two possibilities (not mutually exclusive) for the function of the NS1/2-VAPA interaction at this early stage of viral replication. First, the NS1/2-VAPA interaction could

localize NS1/2 to the ER in order to initiate formation of the membranous viral replication compartment. Notably, the advantage afforded by direct interactions of viral proteins with VAPA and VAPB proteins has been reported for hepatitis C virus (28, 29), which also required rearrangements of intracellular membranes to create a replication complex. MNoV NS1/2 is associated with the ER when expressed independently of other viral proteins (46, 50), and VAPA is an ER-resident protein, suggesting the possibility of a role for VAPA in NS1/2 localization. It is notable that the NS1 domain that contains the FFAT motif mimic would be the first portion of the polyprotein synthesized from viral plus-sense RNA and might therefore contribute to coordination of initial steps of viral replication at the ER prior to synthesis and processing of the rest of the viral polyprotein.

Second, it is also conceivable that the interaction of NS1/2 with VAPA alters lipid metabolism through competition for the interactions between VAPA and VAPA client proteins that also have FFAT domains. In this regard, it is not known whether any of the specific processes carried out by VAPA client proteins are important for enhancing or inhibiting norovirus replication. The methods required to address this issue are likely to be complex, since VAPA interacts with multiple client proteins such as OSBP and ceramide transfer protein (CERT) and is involved in a range of processes in the cell, including nonvesicular lipid transfer (20, 23, 51) and lipid metabolism (51, 52), and is present at membrane contact sites (53–57). Nevertheless, the conservation of a structural motif related to the FFAT motifs found in proteins that interact with the MSP domain of VAPA indicates the value of dissecting the possible role of VAPA-dependent functions in the viral life cycle and the impact of NS1/2 function on VAPA-dependent proteins.

MATERIALS AND METHODS

Cells and media. 293T, BV2, and RAW 264.7 cells were maintained in Dulbecco's modified Eagle's medium (DMEM) with 10% fetal calf serum (FBS), 1% penicillin/streptomycin (Pen/Strep), 2 mM L-glutamine, and 10 mM HEPES. All transfections were performed with TransIT-LT1 (Mirus) unless otherwise noted. The Genome Engineering and iPSC Center (St. Louis, MO) engineered *Vapa*$^{-/-}$ RAW 264.7 cell lines 1E6 and 3A11. Briefly, guide RNAs (5′ GGCGAAGCACGAGCAGATCCTGG 3′ and 5′ GATC TGCTCGTGCTTCGCCATGG 3′) targeting *Vapa* were electroporated into RAW 264.7 cells transiently expressing Cas9. Cells were clonally selected and verified for disruption of the endogenous locus via the Cel-1 nuclease assay and were then subjected to deep sequencing to identify frameshift mutations.

Molecular cloning. NS1/2 from strain MNoV CR6 and CW3 infectious clones (11) and GI (NC_001959), as well as VAPA (NM_013933), were cloned into Gateway vector pDONR221 (Life Technologies, Inc.) and subcloned using Gateway destination vectors, including a modified phage-FLAG-hemagglutinin (HA)-attR1-ccdB-attR2-internal ribosome entry site (IRES)-PuroR lentiviral construct. Cloning of mutant MNoV plasmids (58) was done by site-directed mutagenesis using Q5/KLD mix or Phusion (New England Biolabs) as described in reference 59. The MNoV-NS1/2^{FLAG} infectious clone was generated similarly to MNoV-NS4^{FLAG} (45), with FLAG tag nucleotide sequence inserted after nucleotide 383.

Virus reagents and procedures. Stocks were generated as described previously (11). Briefly, infectious clones were transfected into 293T cells to produce infectious virus, which was passaged twice on RAW 264.7 cells. Clarified supernatant was subjected to ultracentrifugation, resuspended in phosphate-buffered saline (PBS), and quantitated by plaque assay. The recovery of infectious FLAG-tagged MNoV was described previously (60). Briefly, infectious clones were transfected in BSRT7 cells infected with fowlpox virus expressing T7 RNA polymerase. BV2 cells were inoculated with the recovered viruses, frozen/thawed upon appearance of cytopathic effects, centrifuged to remove cellular debris, and quantitated by 50% tissue culture infective dose ($TCID_{50}$) analysis. The stability of FLAG tag insertions at passage 3 was verified by RT-PCR and sequencing of the viruses at relevant genomic locations and by immunoblotting against FLAG tags using infected lysates (data not shown). MNoV infectious clones with novel mutations were transfected in 293T cells as described above and passaged once on RAW 264.7 cells, and virus concentrations were assessed using plaque assay. For virus growth analysis, MNoV was inoculated at indicated multiplicities of infection (MOI) into cells in suspension for 30 min on ice and was subsequently washed three times with complete media and harvested at indicated times postinfection. Quantitation of norovirus by plaque assay was performed as described previously (11) except using adherent RAW 264.7 cells. $TCID_{50}$ data were determined on BV2 cells as described previously (61). For viral RNA electroporations, RNA was isolated from norovirus stocks with TRIzol (Thermo Fisher) and transfected by the use of an Amaxa Mouse Macrophage Nucleofector kit (Lonza). Lentivirus was prepared as described previously (62), except transfections were performed with TransIT LT1 (Mirus), and cells were maintained in media with puromycin (5 μg/ml) 48 h after transducing.

Flow cytometry. Cells were infected as described above. At indicated times, supernatant was collected for determinations of viral titers and cells were prepared for fluorescence-activated cell sorter (FACS) analysis as described in reference 62, except using primary antibody anti-NS1/2 rabbit sera (V.

Ward) (1:2,500), and data were acquired on an LSR II or FACSCalibur (BD Biosciences) flow cytometer. Analyses were performed using FlowJo (Treestar, OR).

Confocal microscopy. BV2 cells were seeded on glass coverslips and infected at an MOI of 1 $TCID_{50}$/cell. At 12 hpi, cells were fixed with 4% paraformaldehyde (PFA)–PBS, quenched with 0.1 M glycine–PBS, and permeabilized with 0.2% Triton X-100–PBS. After blocking was performed (using PBS plus 0.1% Tween 20 [PBST] with 1% bovine serum albumin [BSA]–1% normal goat serum [Sigma-Aldrich]), cells were stained with mouse monoclonal anti-FLAG M2 antibodies (Sigma-Aldrich) and rabbit polyclonal anti-NS7 antibodies (1:1,000) at room temperature for 1 h, triply washed (PBST), and then stained with goat anti-mouse IgG Alexa Fluor 488 and goat anti-rabbit IgG Alexa Fluor 546 (1:1,000) at room temperature for 1 h. Coverslips were triply washed and then mounted with Mowiol medium containing DAPI (4′,6-diamidino-2-phenylindole) stain. The confocal images were taken using a Zeiss 510 Meta laser confocal microscope.

Immunoprecipitation. For anti-FLAG immunoprecipitation, BV2 cells were infected at an MOI of 10 $TCID_{50}$/cell and were harvested 8 hpi. Cells were triply washed with cold PBS before lysis was performed with a mixture containing 50 mM Tris-HCl (pH 7.4), 150 mM NaCl, 1 mM EDTA, 2 mM $MgCl_2$, 1% Triton X-100, 1% (vol/vol) protease inhibitor cocktail (Promega), and 0.1% Benzonase (Sigma-Aldrich). The lysates were incubated on ice for 30 min before being spun down for 10 min at 15,000 rpm at 4°C. The supernatants were collected, and the protein concentrations were determined by bicinchoninic acid (BCA) assay (Thermo Fisher). The anti-FLAG M2 affinity agarose gel (Sigma-Aldrich) was prewashed twice with TBS buffer (50 mM Tris-HCl [pH 7.5], 150 mM NaCl). A 2-mg volume of total protein in 1 ml lysis buffer was loaded onto 40 μl anti-FLAG agarose and incubated 4°C overnight with rotation. After removal of unbound protein by centrifugation at 5,000 $\times$ *g* for 30 s at 4°C and three more washes with TBS buffer, the bound proteins were eluted by addition of 50 μl of 2$\times$ SDS-PAGE sample buffer and heating at 95°C for 3 min.

Western blotting. Laemmeli buffer was added to samples and then boiled for 10 to 15 min. Protein was resolved on 10% SDS-PAGE Tris-glycine gels. Protein was transferred semidry to polyvinylidene difluoride (PVDF) membranes, blocked with 5% milk–Tris-buffered saline with Tween 20 (TBST), and then incubated with antibody overnight at 4°C. Membranes were triply washed with TBST and then incubated for an hour with horseradish peroxidase (HRP)-conjugated secondary antibody. Membranes were triply washed and incubated with ECL or ECL2 reagent (Pierce), and then signal was detected on film (MidSci). For densitometry, NS1/2 band density was calculated using ImageJ, normalized to GAPDH band density, and then reported as a ratio to the WT from each respective time point. We used the following antibodies: polyclonal rabbit NS1/2 antisera, a kind gift from Vernon Ward; anti-VAPA clone K-15 (sc-48698; Santa Cruz Biotechnology), anti-FLAG (M2; Sigma-Aldrich), and anti-HA (H9658; Sigma-Aldrich) (conjugated to HRP using a Lightning-Link HRP antibody labeling kit [701-0000; Innova Bioscience]); GAPDH-HRP (G9295-25UL; Sigma-Aldrich); anti-actin (A5316; Sigma-Aldrich); and anti-rabbit HRP (111-035-003), anti-goat HRP (705-035-003), and anti-mouse HRP (115-035-146) (Jackson ImmunoResearch, Inc.).

Strand-specific qPCR. Cells were infected as described above. At each time point postinfection, cells were lysed and total cellular RNA was extracted using a GenElute mammalian total RNA Miniprep kit (Sigma-Aldrich). Quantities of genomic positive/negative RNAs were determined using strand-specific real-time quantitative PCR (RT-qPCR) according to the method described in reference 44 with the following changes: 100-ng total RNA was used in each RT reaction, and 5 μl of cDNA was used for genomic negative qPCR. The mean of $\log_{10}$ genome equivalents (gEq) per nanogram of total RNA of mock-infected cells was used as the limit of detection (LOD). The results were obtained using a ViiA7 real-time PCR system.

Assessment of VAPB in murine norovirus replication. BV2 cells were transduced with lentivirus expressing Cas9 and blasticidin resistance and were maintained in 4 μg/ml blasticidin. Blasticidin-selected cells were then transduced with lentivirus expressing puromycin resistance and either with no single-guide RNA (sgRNA) (empty) or with sgRNA directed against CD300lf, Vapa, or Vapb. Cells were maintained in 4 μg/ml puromycin. Cells were infected at an MOI of 0.1 without washing and were incubated at 37°C for 18 h. Cells were fixed and prepared for FACS analysis as described above. Each point represents an independent MNoV infection; cells were derived from 3 independent transductions of sgRNA-expressing lentivirus. For percent nonhomologous end joining (%NHEJ) estimates, DNA was isolated from cells using QiaAMP (Qiagen), melted and annealed on a thermocycler, treated with T7 endonuclease at 37°C for 1 h, and resolved on 2% agarose gel. Fragment densities were quantified using ImageJ, and percent cleavage was calculated using the following formula: %NHEJ = 100 * [1 − (parental fraction)$^{1/2}$], where parental fraction = (band intensity parental band)/(band intensity parental band + band intensity lower fragments).

Mammalian 2-hybrid assays. Checkmate vectors (Promega) pACT (prey) and pBIND (bait) were converted to Gateway destination vectors, and genes were subcloned using Gateway LR reactions (Life Technology). Subsequent M2H analysis was performed as described in reference 63. In brief, 7.5 fmol bait and prey plasmids were transfected with 100 ng pG5 plasmid into subconfluent 293T cells. At 48 to 51 h posttransfection, cells were lysed and luminescence was measured by the use of a dual-luciferase reporter assay (Promega) using an Opticomp II (MGM Instruments) luminometer. All data shown represent $n = \geq 3$ and were analyzed by one-way analysis of variance (ANOVA) and the Tukey posttest, comparing the greater of the bait-only value and prey-only value to the value corresponding to the combination of the bait data plus the prey data. Fold change was calculated from the value representing the average of the combination of the bait data plus the prey data/the greater of the bait data and the prey data.

Vapa mutant mouse. The Washington University Animal Studies Committee approved all mouse studies performed here. Mice were bred and housed per university guidelines. Day 0.5 B6/J inbred embryos underwent pronuclear microinjection with gRNA and Cas9-mRNA, and then embryos were implanted in surrogate mothers as described previously (64). Mutations in live-born pups were identified by isolation of tail DNA, PCR amplification of the Vapa targeted locus, and Sanger sequencing. Genotypes were verified by TOPO-TA (Life Sciences) cloning of the amplicons and Sanger sequencing. Genotyping was performed as follows. For mutant line 1, primers were designed to amplify the Vapa locus (F-CTGCTGAGCGGACAGGCTG, R-CGCAAGATGGCGGCGGAG) (WT, 500 bp; deletion, 440 bp). For mutant line 2, genotyping to detect single-base-pair insertion was designed as described in reference 65. In brief, primers designed to detect specifically the WT (F-GGCCCCGTCCTAGAGCTCCG, R-ATATGATAGTAACTAT CCAGGATCTGCTCGTGCTACGC) amplified a 180-bp product. Primers detecting the mutant (F-GGCCCCG TCCTAGAGCTCCG, R-AAAAACCAGGATCTGCTCGTGCTTAGG) amplified a 159-bp product. Genotyping was verified by Sanger sequencing.

Protein preparation for NMR experiments. Natural-abundance protein and the ^{15}N-labeled N-terminally His_6-tagged 28–114 domain of MNoV NS1/2 protein were purified as described previously (10). Three fragments of natural-abundance protein and ^{15}N-labeled N-terminally His_6-tagged murine VAPA protein were purified from *Escherichia coli* expression plasmids as follows. (i) The VAPA MSP domain (8–132) gave excellent NMR spectra. (ii) The MSP domain with linker and coiled-coil domain (8–226) gave excellent NMR spectra and formed stable dimers in solution confirmed by size exclusion chromatography and diffusion NMR experiments. (iii) A VAPA fragment (133–226) showed a dimeric size in solution and NMR spectra indicative of contributions from α-helical and disordered segments. Protein samples were concentrated and dialyzed extensively against 10 mM KH_2PO_4–20 mM KCl (pH 7.0). Final concentrations of NS1/2 28–114 (ε_{280} = 13,940 M^{-1} cm^{-1}) and VAPA (ε_{280} = 8,250 M^{-1} cm^{-1}) were 0.4 mM and 1.6 mM, respectively, as determined spectrophotometrically. All samples contained reducing reagent (1 mM dTCEP [deuterated tris(2-carboxyethyl)phosphine]—5% D_2O) for the lock signal and 0.5 mM DSS for chemical shift reference.

Chemical shift perturbation experiments. After 24 h of dialysis against the same buffer solution, protein samples were mixed by stepwise addition of VAPA solution. Each addition was followed by NMR experiments, carried out at 25°C on a Bruker 600-MHz instrument equipped with a cryoprobe. First, for each ^{15}N-labeled NS1/2 protein construct, ^{15}N-^{1}H HSQC spectrum was recorded for an NS1/2 protein only. Following that step, 5 to 6 spectra were recorded after each addition of natural-abundance VAPA, typically at 0.5-fold to 10.0-fold excess over the NS1/2 concentration present. NMR data were processed (Topspin 3.2; Bruker), and the chemical shift perturbations were analyzed using NMRFAM-SPARKY (66). The chemical shift assignments for NS1/2 (BMRB entries 19439 and 19444) and closely related human VAPA (BMRB entry 7025) are available in the Biological Magnetic Resonance Data Bank (BMRB). The specific values of chemical shifts for the buffer conditions and protein constructs used here were verified by acquisition of a standard suite of triple resonance experiments performed on ^{13}C/^{15}N-labeled samples. Chemical shift perturbations on ^{15}N-labeled VAPA were analyzed in analogous fashion, except that the initial concentrations of VAPA and NS1/2 were 0.1 mM and 2.2 mM, respectively, with stepwise addition of NS1/2. Figures show combined differences of ^{1}H and ^{15}N chemical shifts observed between zero and the highest concentration of unlabeled protein used. The combined differences in units (in parts per million) were calculated as $\Delta\delta = \sqrt{\left\{\frac{1}{2}\left[(\Delta\delta_H)^2 + \left(\frac{\Delta\delta_N}{5}\right)^2\right]\right\}}$ and are referred to as chemical shift perturbations. The threshold for perturbations interpreted as specific protein-protein interactions was set at 4 standard deviations above the mean perturbation, excluding the highest perturbations for each data set.

Statistics and software. All statistics were calculated using GraphPad Prism (ns, $P > 0.05$; *, $P \leq 0.05$; **, $P \leq 0.01$; ***, $P \leq 0.001$; ****, $P \leq 0.0001$; all error bars signify standard errors of the means). Sequence alignments and analysis were performed in Geneious 9.1 (67). Molecular graphics were produced using UCSF Chimera (68).

Accession number(s). The chemical shift assignments for NS1/2 (BMRB entries 19439 and 19444) and closely related human VAPA (BMRB entry 7025) are available in the BMRB database.

SUPPLEMENTAL MATERIAL

Supplemental material for this article may be found at https://doi.org/10.1128/mBio.00668-17.

FIG S1, EPS file, 0.9 MB.
FIG S2, EPS file, 0.1 MB.
FIG S3, EPS file, 0.7 MB.
FIG S4, EPS file, 7.9 MB.
FIG S5, EPS file, 0.3 MB.

ACKNOWLEDGMENTS

We thank the Alvin J. Siteman Cancer Center at WUSM and Barnes-Jewish Hospital in St. Louis, MO, for the use of the Genome engineering and iPSC center. Mice were generated using the WUSM Department of Pathology Microinjection Core. We thank Megan Baldridge, Robert Orchard, Craig Wilen, and Donna MacDuff for intellectual

contributions and reviewing the manuscript; Vernon Ward for the generous gift of anti-NS1/2 rabbit sera; and Darren Kreamalmeyer for handling and breeding mice.

The Siteman Cancer Center was supported in part by NCI Cancer Center Support grant P30CA091842. The Washington University School of Medicine (WUSM) Department of Pathology Microinjection Core was supported by P30AR048335. H.W.V. was supported by U19 AI 109725. B.T.M. was supported by NCI-NIH award F31CA177194-01. T.J.N. was supported by NIH training grant 5T32A100716334 and postdoctoral fellowships from the Cancer Research Institute and American Cancer Society. I.G. was supported by funding from the Wellcome Trust (ref: 097997/Z/11/Z) and the Biotechnology and Biological Sciences Research Council (ref: BB/N001176/1). J.B.E. was supported by a Churchill Scholarship.

The funders did not influence study design, data collection or interpretation, or preparation of the manuscript. Neither our views nor those presented in this study represent the official views of the funding agencies.

REFERENCES

1. Atmar RL, Estes MK. 2006. The epidemiologic and clinical importance of norovirus infection. Gastroenterol Clin North Am 35:275–290, viii. https://doi.org/10.1016/j.gtc.2006.03.001.
2. Hall AJ, Lopman BA, Payne DC, Patel MM, Gastañaduy PA, Vinjé J, Parashar UD. 2013. Norovirus disease in the United States. Emerg Infect Dis 19:1198–1205. https://doi.org/10.3201/eid1908.130465.
3. Patel MM, Hall AJ, Vinjé J, Parashar UD. 2009. Noroviruses: a comprehensive review. J Clin Virol 44:1–8. https://doi.org/10.1016/j.jcv.2008.10.009.
4. Zheng DP, Ando T, Fankhauser RL, Beard RS, Glass RI, Monroe SS. 2006. Norovirus classification and proposed strain nomenclature. Virology 346:312–323. https://doi.org/10.1016/j.virol.2005.11.015.
5. Karst SM, Wobus CE, Goodfellow IG, Green KY, Virgin HW. 2014. Advances in norovirus biology. Cell Host Microbe 15:668–680. https://doi.org/10.1016/j.chom.2014.05.015.
6. Thorne LG, Goodfellow IG. 2014. Norovirus gene expression and replication. J Gen Virol 95:278–291. https://doi.org/10.1099/vir.0.059634-0.
7. Sosnovtsev SV, Belliot G, Chang KO, Prikhodko VG, Thackray LB, Wobus CE, Karst SM, Virgin HW, Green KY. 2006. Cleavage map and proteolytic processing of the murine norovirus nonstructural polyprotein in infected cells. J Virol 80:7816–7831. https://doi.org/10.1128/JVI.00532-06.
8. McFadden N, Bailey D, Carrara G, Benson A, Chaudhry Y, Shortland A, Heeney J, Yarovinsky F, Simmonds P, Macdonald A, Goodfellow I. 2011. Norovirus regulation of the innate immune response and apoptosis occurs via the product of the alternative open reading frame 4. PLoS Pathog 7:e1002413. https://doi.org/10.1371/journal.ppat.1002413.
9. Baker ES, Luckner SR, Krause KL, Lambden PR, Clarke IN, Ward VK. 2012. Inherent structural disorder and dimerisation of murine norovirus NS1-2 protein. PLoS One 7:e30534. https://doi.org/10.1371/journal.pone.0030534.
10. Borin BN, Tang W, Nice TJ, McCune BT, Virgin HW, Krezel AM. 2014. Murine norovirus protein NS1/2 aspartate to glutamate mutation, sufficient for persistence, reorients side chain of surface exposed tryptophan within a novel structured domain. Proteins 82:1200–1209. https://doi.org/10.1002/prot.24484.
11. Nice TJ, Strong DW, McCune BT, Pohl CS, Virgin HW. 2013. A single-amino-acid change in murine norovirus NS1/2 is sufficient for colonic tropism and persistence. J Virol 87:327–334. https://doi.org/10.1128/JVI.01864-12.
12. Ettayebi K, Hardy ME. 2003. Norwalk virus nonstructural protein p48 forms a complex with the SNARE regulator VAP-A and prevents cell surface expression of vesicular stomatitis virus G protein. J Virol 77:11790–11797. https://doi.org/10.1128/JVI.77.21.11790-11797.2003.
13. Fernandez-Vega V, Sosnovtsev SV, Belliot G, King AD, Mitra T, Gorbalenya A, Green KY. 2004. Norwalk virus N-terminal nonstructural protein is associated with disassembly of the Golgi complex in transfected cells. J Virol 78:4827–4837. https://doi.org/10.1128/JVI.78.9.4827-4837.2004.
14. Lev S, Ben Halevy D, Peretti D, Dahan N. 2008. The VAP protein family: from cellular functions to motor neuron disease. Trends Cell Biol 18:282–290. https://doi.org/10.1016/j.tcb.2008.03.006.
15. Shi J, Lua S, Tong JS, Song J. 2010. Elimination of the native structure and solubility of the hVAPB MSP domain by the Pro56Ser mutation that causes amyotrophic lateral sclerosis. Biochemistry 49:3887–3897. https://doi.org/10.1021/bi902057a.
16. Skehel PA, Martin KC, Kandel ER, Bartsch D. 1995. A VAMP-binding protein from Aplysia required for neurotransmitter release. Science 269:1580–1583. https://doi.org/10.1126/science.7667638.
17. Weir ML, Klip A, Trimble WS. 1998. Identification of a human homologue of the vesicle-associated membrane protein (VAMP)-associated protein of 33 kDa (VAP-33): a broadly expressed protein that binds to VAMP. Biochem J 333:247–251. https://doi.org/10.1042/bj3330247.
18. Weir ML, Xie H, Klip A, Trimble WS. 2001. VAP-A binds promiscuously to both v- and tSNAREs. Biochem Biophys Res Commun 286:616–621. https://doi.org/10.1006/bbrc.2001.5437.
19. Alpy F, Rousseau A, Schwab Y, Legueux F, Stoll I, Wendling C, Spiegelhalter C, Kessler P, Mathelin C, Rio MC, Levine TP, Tomasetto C. 2013. STARD3 or STARD3NL and VAP form a novel molecular tether between late endosomes and the ER. J Cell Sci 126:5500–5512. https://doi.org/10.1242/jcs.139295.
20. Kawano M, Kumagai K, Nishijima M, Hanada K. 2006. Efficient trafficking of ceramide from the endoplasmic reticulum to the Golgi apparatus requires a VAMP-associated protein-interacting FFAT motif of CERT. J Biol Chem 281:30279–30288. https://doi.org/10.1074/jbc.M605032200.
21. Kumagai K, Kawano M, Shinkai-Ouchi F, Nishijima M, Hanada K. 2007. Interorganelle trafficking of ceramide is regulated by phosphorylation-dependent cooperativity between the PH and START domains of CERT. J Biol Chem 282:17758–17766. https://doi.org/10.1074/jbc.M702291200.
22. Loewen CJ, Roy A, Levine TP. 2003. A conserved ER targeting motif in three families of lipid binding proteins and in Opi1p binds VAP. EMBO J 22:2025–2035. https://doi.org/10.1093/emboj/cdg201.
23. Wyles JP, McMaster CR, Ridgway ND. 2002. Vesicle-associated membrane protein-associated protein-A (VAP-A) interacts with the oxysterol-binding protein to modify export from the endoplasmic reticulum. J Biol Chem 277:29908–29918. https://doi.org/10.1074/jbc.M201191200.
24. Furuita K, Jee J, Fukada H, Mishima M, Kojima C. 2010. Electrostatic interaction between oxysterol-binding protein and VAMP-associated protein A revealed by NMR and mutagenesis studies. J Biol Chem 285:12961–12970. https://doi.org/10.1074/jbc.M109.082602.
25. Kaiser SE, Brickner JH, Reilein AR, Fenn TD, Walter P, Brunger AT. 2005. Structural basis of FFAT motif-mediated ER targeting. Structure 13:1035–1045. https://doi.org/10.1016/j.str.2005.04.010.
26. Loewen CJ, Levine TP. 2005. A highly conserved binding site in vesicle-associated membrane protein-associated protein (VAP) for the FFAT motif of lipid-binding proteins. J Biol Chem 280:14097–14104. https://doi.org/10.1074/jbc.M500147200.
27. Mikitova V, Levine TP. 2012. Analysis of the key elements of FFAT-like motifs identifies new proteins that potentially bind VAP on the ER, including two AKAPs and FAPP2. PLoS One 7:e30455. https://doi.org/10.1371/journal.pone.0030455.
28. Evans MJ, Rice CM, Goff SP. 2004. Phosphorylation of hepatitis C virus nonstructural protein 5A modulates its protein interactions and viral

RNA replication. Proc Natl Acad Sci U S A 101:13038–13043. https://doi.org/10.1073/pnas.0405152101.
29. Tu H, Gao L, Shi ST, Taylor DR, Yang T, Mircheff AK, Wen Y, Gorbalenya AE, Hwang SB, Lai MM. 1999. Hepatitis C virus RNA polymerase and NS5A complex with a snare-like protein. Virology 263:30–41. https://doi.org/10.1006/viro.1999.9893.
30. Roulin PS, Lötzerich M, Torta F, Tanner LB, van Kuppeveld FJ, Wenk MR, Greber UF. 2014. Rhinovirus uses a phosphatidylinositol 4-phosphate/cholesterol counter-current for the formation of replication compartments at the ER-Golgi interface. Cell Host Microbe 16:677–690. https://doi.org/10.1016/j.chom.2014.10.003.
31. Barajas D, Xu K, de Castro Martín IF, Sasvari Z, Brandizzi F, Risco C, Nagy PD. 2014. Co-opted oxysterol-binding ORP and VAP proteins channel sterols to RNA virus replication sites via membrane contact sites. PLoS Pathog 10:e1004388. https://doi.org/10.1371/journal.ppat.1004388.
32. Barajas D, Xu K, Sharma M, Wu CY, Nagy PD. 2014. Tombusviruses upregulate phospholipid biosynthesis via interaction between p33 replication protein and yeast lipid sensor proteins during virus replication in yeast. Virology 471–473:72–80. https://doi.org/10.1016/j.virol.2014.10.005.
33. Derré I, Swiss R, Agaisse H. 2011. The lipid transfer protein CERT interacts with the chlamydia inclusion protein IncD and participates to ER-Chlamydia inclusion membrane contact sites. PLoS Pathog 7:e1002092. https://doi.org/10.1371/journal.ppat.1002092.
34. Elwell CA, Jiang S, Kim JH, Lee A, Wittmann T, Hanada K, Melancon P, Engel JN. 2011. Chlamydia trachomatis co-opts GBF1 and CERT to acquire host sphingomyelin for distinct roles during intracellular development. PLoS Pathog 7:e1002198. https://doi.org/10.1371/journal.ppat.1002198.
35. Berger KL, Randall G. 2009. Potential roles for cellular cofactors in hepatitis C virus replication complex formation. Communicat Integr Biol 2:471–473. https://doi.org/10.4161/cib.2.6.9261.
36. Gao L, Aizaki H, He JW, Lai MM. 2004. Interactions between viral nonstructural proteins and host protein hVAP-33 mediate the formation of hepatitis C virus RNA replication complex on lipid raft. J Virol 78:3480–3488. https://doi.org/10.1128/JVI.78.7.3480-3488.2004.
37. Amini-Bavil-Olyaee S, Choi YJ, Lee JH, Shi M, Huang IC, Farzan M, Jung JU. 2013. The antiviral effector IFITM3 disrupts intracellular cholesterol homeostasis to block viral entry. Cell Host Microbe 13:452–464. https://doi.org/10.1016/j.chom.2013.03.006.
38. Helbig KJ, Eyre NS, Yip E, Narayana S, Li K, Fiches G, McCartney EM, Jangra RK, Lemon SM, Beard MR. 2011. The antiviral protein viperin inhibits hepatitis C virus replication via interaction with nonstructural protein 5A. Hepatology 54:1506–1517. https://doi.org/10.1002/hep.24542.
39. Wang S, Wu X, Pan T, Song W, Wang Y, Zhang F, Yuan Z. 2012. Viperin inhibits hepatitis C virus replication by interfering with binding of NS5A to host protein hVAP-33. J Gen Virol 93:83–92. https://doi.org/10.1099/vir.0.033860-0.
40. Rocha N, Kuijl C, van der Kant R, Janssen L, Houben D, Janssen H, Zwart W, Neefjes J. 2009. Cholesterol sensor ORP1L contacts the ER protein VAP to control Rab7-RILP-p150 glued and late endosome positioning. J Cell Biol 185:1209–1225. https://doi.org/10.1083/jcb.200811005.
41. Gerondopoulos A, Jackson T, Monaghan P, Doyle N, Roberts LO. 2010. Murine norovirus-1 cell entry is mediated through a non-clathrin-, non-caveolae-, dynamin- and cholesterol-dependent pathway. J Gen Virol 91:1428–1438. https://doi.org/10.1099/vir.0.016717-0.
42. Perry JW, Wobus CE. 2010. Endocytosis of murine norovirus 1 into murine macrophages is dependent on dynamin II and cholesterol. J Virol 84:6163–6176. https://doi.org/10.1128/JVI.00331-10.
43. Shivanna V, Kim Y, Chang KO. 2015. Ceramide formation mediated by acid sphingomyelinase facilitates endosomal escape of caliciviruses. Virology 483:218–228. https://doi.org/10.1016/j.virol.2015.04.022.
44. Vashist S, Urena L, Goodfellow I. 2012. Development of a strand specific real-time RT-qPCR assay for the detection and quantitation of murine norovirus RNA. J Virol Methods 184:69–76. https://doi.org/10.1016/j.jviromet.2012.05.012.
45. Thorne L, Bailey D, Goodfellow I. 2012. High-resolution functional profiling of the norovirus genome. J Virol 86:11441–11456. https://doi.org/10.1128/JVI.00439-12.
46. Hyde JL, Sosnovtsev SV, Green KY, Wobus C, Virgin HW, Mackenzie JM. 2009. Mouse norovirus replication is associated with virus-induced vesicle clusters originating from membranes derived from the secretory pathway. J Virol 83:9709–9719. https://doi.org/10.1128/JVI.00600-09.
47. Nishimura Y, Hayashi M, Inada H, Tanaka T. 1999. Molecular cloning and characterization of mammalian homologues of vesicle-associated membrane protein-associated (VAMP-associated) proteins. Biochem Biophys Res Commun 254:21–26. https://doi.org/10.1006/bbrc.1998.9876.
48. Elde NC, Malik HS. 2009. The evolutionary conundrum of pathogen mimicry. Nat Rev Microbiol 7:787–797. https://doi.org/10.1038/nrmicro2222.
49. Hagai T, Azia A, Babu MM, Andino R. 2014. Use of host-like peptide motifs in viral proteins is a prevalent strategy in host-virus interactions. Cell Rep 7:1729–1739. https://doi.org/10.1016/j.celrep.2014.04.052.
50. Hyde JL, Mackenzie JM. 2010. Subcellular localization of the MNV-1 ORF1 proteins and their potential roles in the formation of the MNV-1 replication complex. Virology 406:138–148. https://doi.org/10.1016/j.virol.2010.06.047.
51. Nikawa J, Murakami A, Esumi E, Hosaka K. 1995. Cloning and sequence of the SCS2 gene, which can suppress the defect of INO1 expression in an inositol auxotrophic mutant of Saccharomyces cerevisiae. J Biochem 118:39–45. https://doi.org/10.1093/oxfordjournals.jbchem.a124889.
52. Kagiwada S, Zen R. 2003. Role of the yeast VAP homolog, Scs2p, in INO1 expression and phospholipid metabolism. J Biochem 133:515–522. https://doi.org/10.1093/jb/mvg068.
53. Kumagai K, Kawano-Kawada M, Hanada K. 2014. Phosphoregulation of the ceramide transport protein CERT at serine 315 in the interaction with VAMP-associated protein (VAP) for inter-organelle trafficking of ceramide in mammalian cells. J Biol Chem 289:10748–10760. https://doi.org/10.1074/jbc.M113.528380.
54. Loewen CJ, Young BP, Tavassoli S, Levine TP. 2007. Inheritance of cortical ER in yeast is required for normal septin organization. J Cell Biol 179:467–483. https://doi.org/10.1083/jcb.200708205.
55. Mesmin B, Bigay J, Moser von Filseck J, Lacas-Gervais S, Drin G, Antonny B. 2013. A four-step cycle driven by PI(4)P hydrolysis directs sterol/PI(4)P exchange by the ER-Golgi tether OSBP. Cell 155:830–843. https://doi.org/10.1016/j.cell.2013.09.056.
56. Wakana Y, Kotake R, Oyama N, Murate M, Kobayashi T, Arasaki K, Inoue H, Tagaya M. 2015. CARTS biogenesis requires VAP-lipid transfer protein complexes functioning at the endoplasmic reticulum-Golgi interface. Mol Biol Cell 26:4686–4699. https://doi.org/10.1091/mbc.E15-08-0599.
57. Weber-Boyvat M, Kentala H, Peränen J, Olkkonen VM. 2015. Ligand-dependent localization and function of ORP-VAP complexes at membrane contact sites. Cell Mol Life Sci 72:1967–1987. https://doi.org/10.1007/s00018-014-1786-x.
58. Strong DW, Thackray LB, Smith TJ, Virgin HW. 2012. Protruding domain of capsid protein is necessary and sufficient to determine murine norovirus replication and pathogenesis in vivo. J Virol 86:2950–2958. https://doi.org/10.1128/JVI.07038-11.
59. Liu H, Naismith JH. 2008. An efficient one-step site-directed deletion, insertion, single and multiple-site plasmid mutagenesis protocol. BMC Biotechnol 8:91. https://doi.org/10.1186/1472-6750-8-91.
60. Chaudhry Y, Skinner MA, Goodfellow IG. 2007. Recovery of genetically defined murine norovirus in tissue culture by using a fowlpox virus expressing T7 RNA polymerase. J Gen Virol 88:2091–2100. https://doi.org/10.1099/vir.0.82940-0.
61. Hwang S, Alhatlani B, Arias A, Caddy SL, Christodoulou C, Cunha JB, Emmott E, Gonzalez-Hernandez M, Kolawole A, Lu J, Rippinger C, Sorgeloos F, Thorne L, Vashist S, Goodfellow I, Wobus CE. 2014. Murine norovirus: propagation, quantification, and genetic manipulation. Curr Protoc Microbiol 33:15K.2.1–15K.261. https://doi.org/10.1002/9780471729259.mc15k02s33.
62. Hwang S, Maloney NS, Bruinsma MW, Goel G, Duan E, Zhang L, Shrestha B, Diamond MS, Dani A, Sosnovtsev SV, Green KY, Lopez-Otin C, Xavier RJ, Thackray LB, Virgin HW. 2012. Nondegradative role of Atg5-Atg12/Atg16L1 autophagy protein complex in antiviral activity of interferon gamma. Cell Host Microbe 11:397–409. https://doi.org/10.1016/j.chom.2012.03.002.
63. Greninger AL, Knudsen GM, Betegon M, Burlingame AL, DeRisi JL. 2013. ACBD3 interaction with TBC1 domain 22 protein is differentially affected by enteroviral and kobuviral 3A protein binding. mBio 4:e00098-13. https://doi.org/10.1128/mBio.00098-13.
64. Parikh BA, Beckman DL, Patel SJ, White JM, Yokoyama WM. 2015. Detailed phenotypic and molecular analyses of genetically modified mice generated by CRISPR-Cas9-mediated editing. PLoS One 10:e0116484. https://doi.org/10.1371/journal.pone.0116484.

65. Gaudet M, Fara AG, Beritognolo I, Sabatti M. 2009. Allele-specific PCR in SNP genotyping. Methods Mol Biol 578:415–424. https://doi.org/10.1007/978-1-60327-411-1_26.
66. Lee W, Tonelli M, Markley JL. 2015. NMRFAM-SPARKY: enhanced software for biomolecular NMR spectroscopy. Bioinformatics 31:1325–1327. https://doi.org/10.1093/bioinformatics/btu830.
67. Kearse M, Moir R, Wilson A, Stones-Havas S, Cheung M, Sturrock S, Buxton S, Cooper A, Markowitz S, Duran C, Thierer T, Ashton B, Meintjes P, Drummond A. 2012. Geneious Basic: an integrated and extendable desktop software platform for the organization and analysis of sequence data. Bioinformatics 28:1647–1649. https://doi.org/10.1093/bioinformatics/bts199.
68. Pettersen EF, Goddard TD, Huang CC, Couch GS, Greenblatt DM, Meng EC, Ferrin TE. 2004. UCSF Chimera—a visualization system for exploratory research and analysis. J Comput Chem 25:1605–1612. https://doi.org/10.1002/jcc.20084.